University of Nottingham
UK | CHINA | MALAYSIA

MODELLING FULLY COUPLED MECHANICAL, ECOLOGICAL, AND HYDROLOGICAL FEEDBACK ON PEATLAND DEVELOPMENT

Thesis submitted to the University of Nottingham for the degree of **Doctor of Philosophy, August 2023.**

Adilan Widyawan Mahdiyasa

20206640

Supervised by

Prof. David Large
Dr. Bagus Muljadi
Dr. Matteo Icardi

Abstract

Mathematical models of peatland development have been employed to analyse peatland behaviour. However, the existing models of peatland development ignore the mechanical processes that potentially provide essential feedback on peatland ecology, hydrology, and resilience. This study aimed to develop a fully coupled mechanical, ecological, and hydrological model of peatland development, called MPeat, and examine the consequences of the feedback within the model. MPeat uses poroelasticity theory, which couples fluid flow and solid deformation to model the peat volume changes that lead to variations in peat physical properties, including bulk density, active porosity, and hydraulic conductivity. To validate poroelasticity formulation, the comparisons between numerical and analytical solutions of Terzaghi's and Mandel's problems for one- and two-dimensional test cases are conducted. MPeat in one dimension that models peatland as a vertical column produces shallower water table depth and buffers the effect of climate changes on water balance, leading to greater quantities of carbon than the other peat growth models. Furthermore, by including the influence of vegetation on peat volume changes, MPeat exhibits the possibility of bistability, regime shifts, critical thresholds, and both short- and long-term peatland dynamical behaviour. The expansion of the model into two dimensions by incorporating horizontal space captures the spatial variation of peat thickness, water table depth, plant functional types, and

peat physical properties. The comparison between one-dimensional and two-dimensional versions of MPeat illustrates that the lateral variability of peat physical properties helps peatland to accumulate more water and produces a higher carbon stock. The two-dimensional version of MPeat is employed to analyse the influence of river incisions at the edges and the limits to peatland carbon accumulation due to mechanical instability. River incision, together with the permeable substrate, reduces the water table position, which results in lower peat and carbon accumulation. Moreover, MPeat shows that peatland carbon accumulation in a landscape, consisting of upland, sloping area, and lowland, is limited by mechanical instability. Therefore, the results generated by MPeat highlight the possible importance of mechanical-ecohydrological feedback to the behaviour of peatland.

Acknowledgements

I would like to thank the Directorate General of Higher Education (DIKTI) Indonesia for the funding through the BPPLN scholarship. I thank my supervisors, Prof. David Large, Dr. Bagus Muljadi, and Dr. Matteo Icardi for their help and support. I also would like to thank Dr. Savvas Triantafyllou for the interesting discussions on an earlier version of the model. Finally, I must thank my parents, Mochamad Hatip and Imroatus Sholihah, and my wife, Asrini Chrysanti, for their support and encouragement.

Contents

List of Tables

List of Figures

Chapter 1

Introduction

The purpose of the thesis is to develop a peatland growth model that incorporates the interactions between mechanical, ecological, and hydrological processes and analyse the consequences of potential feedback within the model system on peatland behaviour. In this introductory chapter, the importance of peatlands and approaches to understanding peatland behaviour that could be conducted through field observations, laboratory measurements, and mathematical models, are explained. The significance and limitations of some important mathematical models of peatland development that focus on the ecological, hydrological, or ecohydrological feedback (Ingram, 1982; Clymo, 1984; Hilbert et al., 2000; Frolking et al., 2010; Baird et al., 2012; Morris et al., 2012) are analysed to provide the rationale related to the need for a new conceptual approach to model peatland behaviour. A new model of peatland development is proposed, which involves fully coupled mechanical-ecohydrological feedback. Finally, the aim and specific objectives of the thesis, which are followed by the overall thesis outline, are presented.

1.1 Peatlands

Peatlands are ecosystems characterised by the presence of an accumulated layer of peat at the surface with a minimum thickness ranging from 10 - 100 cm (Cruickshank and Tomlinson, 1990; Lappalainen, 1996; Joosten and Clarke, 2002; Lourenco et al., 2022) (Figure 1.1). Peatlands are found across the world, with the majority located in the boreal and subarctic zone of the northern hemisphere (Armentano and Menges, 1986; Gorham, 1991; Xu et al., 2018). Although the global coverage of peatlands is relatively small, the benefits that peatlands offer for the environment are enormous. Peatlands prevent the environment from floods and drought because peat can maintain the water balance (Gao et al., 2016). The unique characteristics of the peatlands provide suitable habitat for rare species (Rana and Tolvanen, 2021). Peatlands keep essential ecological and archaeological information, for example, pollen records and human artifacts (Speller and Forbes, 2022). Finally, peatlands contain an enormous amount of carbon and significantly influence the global carbon cycle (e.g., Limpens et al., 2008; Loisel et al., 2014; Hugelius et al., 2020; Harris et al., 2022).

Peat formation occurs through the production, partial decomposition, and compaction of organic matter obtained from the dead plant material (Clymo, 1984; Belyea and Clymo, 2001). In the initial process, the coarse organic matter is produced in the surface and rooting area with characteristics of low bulk density and high active porosity and hydraulic conductivity. This condition facilitates the drainage of excess water from the precipitation and the circulation of air, which enables aerobic decay to occur. As more organic matter accumulates and decomposition takes place, the total load becomes more significant and the mechanical rigidity is diminished, resulting in the collapse of the organic matter structure (Fenton, 1980; Clymo,

Figure 1.1: The example of the peatland that is located in Flow Country, Scotland, covers about 4000 km^2 and is the largest blanket bog in Europe.

1984; Whittington and Price, 2006; Waddington et al., 2010). The compaction and decomposition reduce the volume and pore space of the organic matter, particularly as the depth below the surface increases, preventing water discharge and raising the water table position (Clymo, 1984; Quinton et al., 2000; Moore et al., 2005; Mahdiyasa et al., 2022, 2023). The decomposition of organic matter below the water table predominantly occurs under anoxic conditions due to a limited supply of oxygen, leading to a much lower rate of decay than in the oxic conditions above the water table. The accumulation of compacted and incompletely decomposed organic matter due to waterlogged conditions produces peat.

1.2 Peatland carbon stock

Peatland accumulates vast amounts of carbon in the long term over thousands of years because the absorbed carbon through plant photosynthesis is not all released back into the atmosphere as a consequence of incom-

plete decomposition. However, the total estimation of carbon stock from peatland continues to produce uncertainty and variability. Yu et al. (2010) estimated the total carbon stock of the northern peatland was around 547 gigatons of carbon (Gt C) obtained from the historical data that accommodated the area changes of the peatland. The estimated value decreases to 436 Gt C based on the calculation from Loisel et al. (2014), who developed a database from 215 peatland sites in North America and Eurasia. Hugelius et al. (2020) predicted a similar value of northern peatland carbon stock around 415 Gt C and analysed the effect of permafrost thaw, which might change peatland behaviour from net carbon sinks to net carbon sources. In contrast, Nichols and Peteet (2019) estimated a significantly higher value of carbon stock from northern peatland by a factor of two with a value of about 1055 Gt C by combining the Neotoma Paleoecology Database (Williams et al., 2018) for the radiocarbon-dated peat with the peatland characteristics data from Loisel et al. (2014) and Treat et al. (2016).

Significant variations in the peatland carbon stock value occur due to several factors, including the different approximation of peatland area, limited data on peatland characteristics, and the complex feedback mechanism of the peatland. The absence of consensus in the definition of peat (Joosten and Clarke, 2002; Wust et al., 2003; Lourenco et al., 2022) leads to discrepancies in peatland extent and influences the estimation of total peatland carbon stock. The insufficient data on peatland characteristics, including the bulk density, thickness, and carbon accumulation, particularly for peatland in remote areas, produce uncertainties in peatland carbon stock estimation because a single average value is employed to replace the lack of detailed data (Gorham, 1991; Lappalainen, 1996; Turunen et al., 2002). Finally, peatland exhibits complex feedback mechanisms that provide a considerable effect on carbon accumulation. For example, the interactions

between internal and external processes on the peatland produce considerable uncertainty related to the response of the peatland carbon to the changing climate (Loisel et al., 2021). A higher temperature increases the rate of peat decomposition, which results in a more significant carbon release and reduces the peatland carbon stock (Ise et al., 2008; Dorrepaal et al., 2009). Consequently, peatlands might provide positive feedback on global warming because they become a net carbon source. However, the increasing temperature promotes the growth of vegetation and leads to higher peat production from plant litter. Based on the carbon accumulation database of peatland in the northern hemisphere, Charman et al. (2013) found that long-term carbon accumulation shows a strong correlation with the growing season of the vegetation. Furthermore, Charman et al. (2013) suggested that the changes in the net primary productivity are more crucial compared to the variations in decomposition rate for long-term peatland carbon accumulation. Therefore, understanding the behaviour and the complex feedback operating on the peatland are essential in order to analyse the carbon accumulation in this ecosystem.

1.3 Approaches to understanding peatland behaviour

Some approaches, including field observations, laboratory measurements, and mathematical models, can be employed to examine peatland behaviour that incorporates complex feedback mechanisms. Although field observations and laboratory measurements provide data and understanding of some peatland phenomena, the results obtained from these methods are constrained by the timeframe of observation. Contrastingly, mathemati-

cal models offer insight related to the peatland system on long timeframes beyond the capacity of field or laboratory approaches, which is crucial in analysing long-term processes on the peatland.

1.3.1 Field observations

Field observation provides data and information related to peatland behaviour through direct investigation. The data obtained from in-situ measurements encompass essential aspects of peatland ecology, hydrology, and mechanics, including the rate of peat production (Belyea and Clymo, 2001), peat hydraulic conductivity (Baird et al., 2004; Surridge et al., 2005; Hogan et al., 2006), and peat strength (Long, 2005; Boylan et al., 2008). Furthermore, through field observation, the relationship between two or more variables could be analysed and formulated, for example, the relationship between peat production and water table position (Belyea and Clymo, 2001), hydraulic conductivity with depth, degree of humification, and bulk density (Morris et al., 2022), and a critical thickness before the occurrence of mechanical failure with slope gradient (Dykes et al., 2008). However, the data and phenomena observed from this approach are obtained at specific times and areas, which restrict our understanding of general peatland behaviour. As a consequence, a degree of caution is required before implementing the data and analysis of some peatland processes derived from field observation because they might be affected by site-specific characteristics and timeframes of observation.

1.3.2 Laboratory measurements

Laboratory measurements offer controlled conditions to examine peatland characteristics in greater detail, for example, the strength properties of peat that determine the mechanical stability of the peatland. Laboratory testing methods, including triaxial compression, direct shear, direct simple shear, and ring shear, are commonly employed to analyse the strength properties of the peat (Long, 2005; Boylan et al., 2008; Mesri and Ajlouni, 2007; O'Kelly, 2017). Based on these testing methods, triaxial compression produces the highest value of effective friction angle, which influences the value of shear strength, because triaxial compression is affected by the interactions between the orientation of peat fibers with the shearing direction (Boylan et al., 2008). Long (2005) recommended direct simple shear and ring shear methods for laboratory testing of peat strength because they eliminate the effect of fibers orientation and accommodate the large deformations from the peat sample. However, ensuring the samples that accurately represent the peatland conditions with the complex feedback is difficult, which possibly leads to uncertainty in the outputs of laboratory experiments. Furthermore, the laboratory measurement is conducted at a specific time interval, which is unsuitable for some peatland processes that require long-term analysis.

1.3.3 Mathematical models

The main constraint of field observation and laboratory measurement to understanding peatland behaviour is the limited timeframes of observation. Consequently, these approaches are unable to offer insight related to the long-term process that operates on the peatland. The need for understanding peatland behaviour on long timeframes leads to the utilisa-

tion of mathematical models, which allow the simulations of the peatland behaviour that involves complex feedback mechanisms over thousands of years.

The analysis of peatland carbon accumulation and the future impact of climate change on peatland behaviour are examples of processes that require a long timeframe. Alexandrov et al. (2020) employed the Bog Growth Model from Clymo (1984) to estimate the maximum carbon accumulation in the northern peatlands. They found that northern peatlands will act as a carbon sink in the next 5000 years because the current carbon stock estimation is lower than the maximum potential limit. Morris et al. (2015) applied the DigiBog model (Baird et al., 2012; Morris et al., 2012) to investigate the influence of climate change on water table depth and peat remaining mass and examine the ability of peatland to preserve information about climate change. Treat et al. (2021) implemented the Holocene Peat Model from Frolking et al. (2010) to forecast the potential carbon loss due to future climate change and permafrost thaw. The simulation results indicate that the source of carbon is not from newly thawed permafrost but mainly from the active layer of peatland with a depth of about 0.2 - 1 m from the surface.

Another benefit of mathematical models in understanding peatland behaviour is the ability to provide insight into processes that are difficult to observe directly in the field or based on laboratory measurement, for example, bistability conditions and surface energy balance of the peatland. Modelling approach could explain and predict the possibility the bistability conditions of the peatland due to complex feedback and nonlinear behaviour (Hilbert et al., 2000; van der Velde et al., 2021; Mahdiyasa et al., 2023). Consequently, peatland might experience an abrupt shift, known as a tipping point, from one state to another that influences the carbon stock.

The field observation from Lamentowicz et al. (2019) provide the evidence of tipping point phenomenon in a peatland located in northern Poland based on high-resolution multi-proxy method. The mathematical models of energy balance developed by Admiral and Lafleur (2007) described the partition of latent heat flux between vascular plants, hummocks, and hollows and explained the importance of moss on the energy fluxes of the peatland.

Mathematical models, of course, have limitations to understanding peatland behaviour. The modelling approach suffers from the simplification of the processes that occur in the real peatland. Although simplification is necessary for practical reasons, for example, to reduce the computational time, it could affect the accuracy and applicability of the proposed model. Mathematical models also require input data to generate predictions or simulations related to the peatland behaviour. The reliability of model outputs depends on the quality and availability of the input data. Despite these limitations, mathematical models remain an indispensable approach to understanding long-term processes of peatland behaviour that incorporate complex feedback mechanisms (Table 1.1).

This thesis uses a modelling approach, particularly mathematical models of peatland development, to examine the implications of complex feedback on peatland behaviour during the development process. In order to capture the complex feedback mechanism, the model of peatland development needs to incorporate the changes in the peat physical properties, including bulk density, active porosity, and hydraulic conductivity, which are affected by the mechanical, ecological, and hydrological processes (Clymo, 1984; Quinton et al., 2000; Moore et al., 2005; Whittington and Price, 2006; Waddington et al., 2010). However, as explained in the following section, the existing models of peatland development assume constant or partial changes

Table 1.1: The summary of three different approaches, including field observations, laboratory measurements, and mathematical models, for understanding peatland behaviour.

Field observations	**Laboratory measurements**	**Mathematical models**
Field observations provide data and relations of some peatland charateristics through direct investigation.	Laboratory measurements offer controlled conditions that produce a more detailed analysis of peatland characteristics.	Mathematical models allow the simulation of peatland behaviour with a wide range of timeframes.
Field observations are constrained by the space and time of the observed variable and focus on empirical evidence.	Laboratory measurements are conducted at specific time intervals and require sample preparation that represents peatland conditions with complex feedback mechanisms.	Mathematical models provide insight into processes that are difficult to observe directly in the field or based on laboratory measurement.
		Mathematical models can simulate the future response of the peatland with different scenarios.
		Mathematical models suffer from simplifications and assumptions.
		Mathematical models require initial data obtained from field observation or laboratory measurements.

in peat physical properties and ignore the influence of peatland mechanics. These assumptions significantly reduce the understanding of peatland growth and behaviour because, at a fundamental level, the compaction of water-saturated dead organic matter to form peat is a mechanical process. Therefore, a new concept and formulation of peatland development model are required.

1.4 Mathematical models of peatland development

Mathematical models of peatland development have been produced for a range of purposes, including estimating long-term peat and carbon accumulation (Ingram, 1982; Clymo, 1984; Frolking et al., 2001; Swinnen et al., 2019), understanding peatland dynamics (Hilbert et al., 2000; Yu et al., 2001; Frolking et al., 2010; Baird et al., 2012; Morris et al., 2012), and examining the influence of climate change on the peatland carbon stock (Ise et al., 2008; Heinemeyer et al., 2010; Chaudhary et al., 2020; Treat et al., 2021). The existing models focus on ecological, hydrological, or ecohydrological feedback with different assumptions related to the peat physical properties. Some of the most prominent peatland development models (Figure 1.2) are discussed below, including their significance and limitations, to articulate the need for a new generation of peatland development models that contains fully coupled mechanical-ecohydrological feedback and explicitly involves the changes of peat physical properties as internal feedback mechanisms.

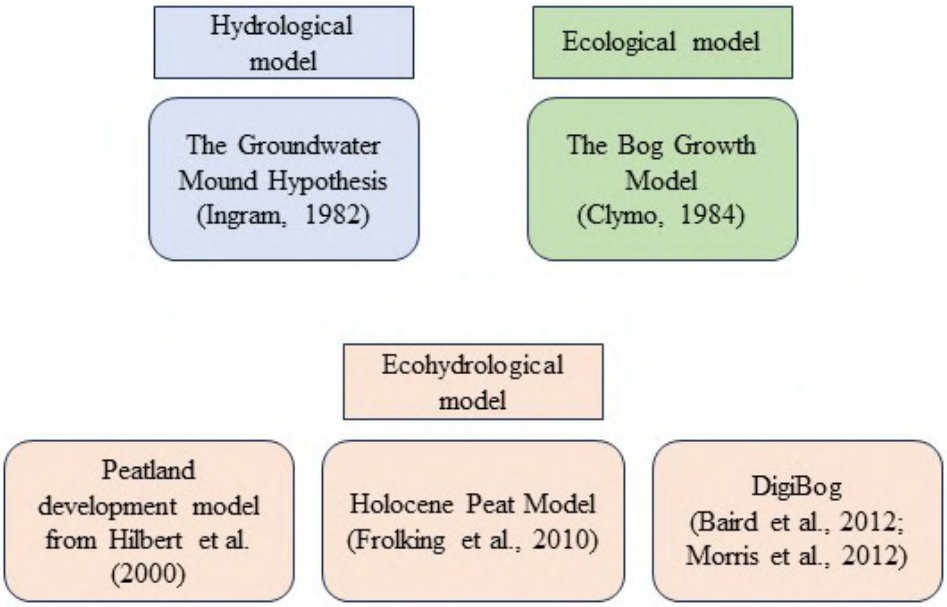

Figure 1.2: Mathematical models of peatland development that provide a substantial impact on the understanding of hydrological, ecological, or ecohydrological processes on the peatland.

1.4.1 The Groundwater Mound Hypothesis

Ingram (1982) proposed a model that analyses the position of the peatland water table in the equilibrium condition, constrained by parallel-sided rivers at the edges with a flat and relatively impermeable substrate (Figure 1.3), which is known as the Groundwater Mound Hypothesis (GMH) (see also Childs (1969)). Because the decomposition rate above the water table with unsaturated conditions is much higher than in the saturated zone below the water table, the peatland shape and thickness are controlled by the position of the water table, which becomes the fundamental idea of GMH. This model assumes that the net precipitation in a drought season is stored in the peatland by flowing steadily through the saturated zone, which is isotropic and has constant hydraulic conductivity.

The GMH is developed based on Darcy's law and the Dupuit-Forchheimer (D-F) approximation, implying that the hydraulic gradient is much smaller

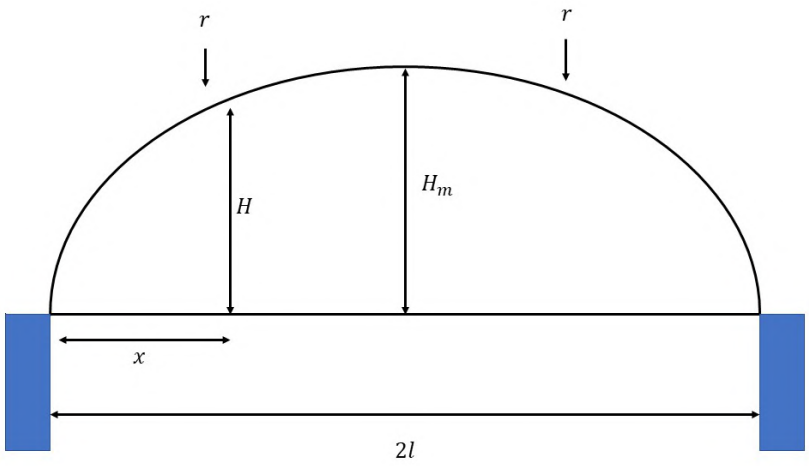

Figure 1.3: Groundwater mound illustration in the peatland with flat substrate and constrained by the river at the edges. The height at the center ($x = l$) is given by H_m and r is the net water recharge to the water table.

in the vertical direction than in the horizontal direction (Strack, 1984). Moreover, the rivers at the edges have negligible depth and static characteristics over time without experiencing a downcutting phenomenon (the effects of rivers incision on the peatland water table and shape are discussed in Chapter 5). As a consequence, GMH predicts the hemi-elliptical shape of the peatland in cross-section through the equation below

$$\frac{r}{\kappa} = \frac{H^2}{2lx - x^2} \tag{1.1}$$

where r is the net recharge (m yr^{-1}), κ is the hydraulic conductivity (m yr^{-1}), H is the peatland height (m), $2l$ is the length of the peatland (m), x is the distance from the end (m). If x equal to L and H equal to H_m or at the center of the peatland, equation 1.1 can be written as

$$\frac{r}{\kappa} = \frac{H_m^2}{l^2} \tag{1.2}$$

The GMH provides a fundamental approach to model the influence of hydrological aspects on peatland development. However, this model ig-

nores the complex feedback and spatial variability of peatlands, including the variations of peat physical properties. Armstrong (1995) modified the GMH by proposing non-uniform hydraulic conductivity that exponentially decreases with depth, showing different predictions of peatland shape and thickness. This model produces a lower hydraulic gradient at the margin and a higher water table compared to the initial GMH from Ingram (1982) due to more impermeable peat layers in the deeper position that supports water accumulation. The difference in the peatland shape and thickness obtained from both models indicates that spatial variability of peat physical properties provides a crucial influence on peatland characteristics.

1.4.2 The Bog Growth Model

Clymo (1984) developed a peat accumulation model based on the rate of addition and rate of decay of organic matter, which is known as the Bog Growth Model (BGM). The two layers of peatland structure are used in this model, consisting of the unsaturated zone above the water table and the saturated zone below the water table. The organic matter accumulation in the unsaturated zone is affected by the mass addition from plant litter on the peatland surface, or around the rooting area for the vascular plant roots, and the mass loss because of aerobic decay. If the rates of mass addition and aerobic decay are constant over time, then the accumulation rate of organic matter in the unsaturated zone is

$$\frac{dM_{un}}{dt} = \psi_{un} - \eta_{un} M_{un} \tag{1.3}$$

The solution of Equation 1.3 gives the amount of organic matter that ac-

cumulated in the unsaturated zone

$$M_{un} = \frac{\psi_{un}}{\eta_{un}}(1 - \exp(-\eta_{un} t_{un})) \tag{1.4}$$

where M_{un} is the cumulative mass of organic matter in the unsaturated zone (kg m^{-2}), ψ_{un} is the rate of addition of mass to the unsaturated zone (kg m^{-2} yr^{-1}), η_{un} is the rate of decay in the unsaturated zone (yr^{-1}), and t is the time (yr).

The process of organic matter accumulation is rapid in the earlier time but gradually declines due to the increasing mass loss. Theoretically, the accumulation process in the unsaturated zone will achieve an asymptotic limit to the value of $\frac{\psi_{un}}{\eta_{un}}$; however, this condition cannot happen for a peatland to continue growing. Consequently, the bottom layer of the unsaturated zone becomes part of the saturated zone and experiences anaerobic decay, which represents the rate of addition of organic matter, or peat in this case, based on the saturated zone point of view. Therefore, the rate of accumulation of peat in the unsaturated zone is affected by the rate at which organic matter is transferred into the saturated zone

$$\frac{dM_{un}}{dt} = \psi_{un} - \eta_{un} M_{un} - \psi_{sa} \tag{1.5}$$

where ψ_{sa} is the rate of addition of mass to the saturated zone (kg m^{-2} yr^{-1}).

In a stable climate, the thickness of the unsaturated zone above the water table will remain constant, and it is not a peat accumulator. The primary function of the unsaturated zone in the peat accumulation model is to

facilitate the decomposition of organic matter before it progresses to the saturated zone, where the actual accumulation of peat takes place. Because in the steady-state condition $\frac{dM_{un}}{dt} = 0$, the rate of input to the saturated zone is

$$\psi_{sa} = \psi_{un} - \eta_{un} M^*_{un} \tag{1.6}$$

where M^*_{un} is the steady-state cumulative mass of organic matter in the unsaturated zone (kg m^{-2}).

The formulation of peat accumulation in the saturated zone is similar to organic matter accumulation in the unsaturated zone but with a much slower decay rate because the process is anaerobic. If the rates of peat addition and anaerobic decay are constant over time, then the rate of peat accumulation in the saturated zone is written as

$$\frac{dM_{sa}}{dt} = \psi_{sa} - \eta_{sa} M_{sa} \tag{1.7}$$

The solution of Equation 1.7 gives the accumulation of peat in the saturated zone

$$M_{sa} = \frac{\psi_{sa}}{\eta_{sa}}(1 - \exp(-\eta_{sa} t_s a)) \tag{1.8}$$

where M_{sa} is the cumulative mass of organic matter in the saturated zone (kg m^{-2}), ψ_{sa} is the rate of addition of mass to the saturated zone (kg m^{-2} yr^{-1}), η_{sa} is the rate of decay in the saturated zone (yr^{-1}), and t is the time (yr).

The accumulation of peat in the saturated zone will converge to $\frac{\psi_{sa}}{\eta_{sa}}$, which becomes the maximum limit of peatland growth, and the graph profile

between age and height is concave.

Clymo et al. (1998) modified the BGM formulation by allowing the rate of decay to decrease linearly and quadratically with the proportion of remaining mass θ. Under the assumption of a linear decline in rate of decay, the rate of peat accumulation in the saturated zone becomes

$$\frac{dM_{sa}}{dt} = \psi_{sa} - \eta_{sa}\theta M_{sa} \tag{1.9}$$

with the solution

$$M_{sa} = \frac{\psi_{sa}}{\eta_{sa}}(\ln(1 + \eta_{sa}t_{sa})) \tag{1.10}$$

Using the assumption of a quadratic decline in rate of decay, the rate of peat accumulation in the saturated zone becomes

$$\frac{dM_{sa}}{dt} = \psi_{sa} - \eta_{sa}\theta^2 M_{sa} \tag{1.11}$$

with the solution

$$M_{sa} = \frac{\psi_{sa}}{\eta_{sa}}(\sqrt{1 + 2\eta_{sa}t_{sa}} - 1) \tag{1.12}$$

where θ is the remaining mass $(-)$, M_{sa} is the cumulative mass of organic matter in the unsaturated zone $(\mathrm{kg\,m^{-2}})$, ψ_{sa} is the rate of addition of mass to the saturated zone $(\mathrm{kg\,m^{-2}\,yr^{-1}})$, η_{sa} is the rate of decay in the saturated zone $(\mathrm{yr^{-1}})$, and t is the time (yr).

There are no asymptotic limits for both cases because the accumulation of peat will increase indefinitely with time. The graph profile between the age and height is concave with approximately logarithmic and parabolic in time

Table 1.2: Bog Growth Model (BGM) with three different rates of decay

Decay rate η	Remaining mass θ	Accumulation rate $\frac{dM_{sa}}{dt}$	Cumulative peat mass M_{sa}
Constant	$\exp(-\eta_{sa}t)$	$\psi_{sa} - \eta_{sa}M_{sa}$	$\frac{\psi_{sa}}{\eta_{sa}}(1 - \exp(-\eta_{sa}t_{sa}))$
Linear	$\frac{1}{1+\eta_{sa}t}$	$\psi_{sa} - \eta_{sa}\theta M_{sa}$	$\frac{\psi_{sa}}{\eta_{sa}}(\ln(1 + \eta_{sa}t_{sa}))$
Quadratic	$\frac{1}{\sqrt{1+2\eta_{sa}t}}$	$\psi_{sa} - \eta_{sa}\theta^2 M_{sa}$	$\frac{\psi_{sa}}{\eta_{sa}}(\sqrt{1 + 2\eta_{sa}t_{sa}} - 1)$

under the assumption of linear and quadratic rates of decay, respectively. Table (1.2) provides the summary of three different assumptions of decay rate employed by BGM.

The BGM predicts the maximum limit of peat accumulation, assuming a constant decomposition rate, without incorporating the possibility of peatland failure due to mass movement (Wilford, 1966; Alexander et al., 1986; Wilson and Hegarty, 1993; Gallart et al., 1994; Dykes and Kirk, 2001; Warburton et al., 2003; Yang and Dykes, 2006; Dykes et al., 2008; Dykes and Warburton, 2008b; Dykes, 2008; Boylan et al., 2008; Dykes and Selkirk-Bell, 2010). The catastrophic failure during the development process prevents the peatland from reaching the asymptotic limit because erosion and drainage, which are the consequences of the mass movement, result in the reduction of peat accumulation (Warburton et al., 2003; Evans and Warburton, 2007; Large et al., 2021). The analysis of peatland failure requires complex feedback from mechanical, ecological, and hydrological processes that are ignored by BGM (see Chapter 6 for a detailed analysis of peatland failure).

In contrast with GMH (Ingram, 1982), which focuses on the hydrological factors through the water table position, BGM emphasises the importance of ecological aspects, including the rate of peat addition and decomposition, to model long-term peatland development. However, two layers of peatland

characteristics that are used by BGM depend on the water table position. Consequently, the assumptions of the steady state in the unsaturated zone and constant rate of peat addition result in significant restrictions on the peatland behaviour (Belyea and Baird, 2006). As peatland grows, the total load from mass accumulation increases, together with the reduced structural integrity due to decomposition, resulting in the collapse of the peat pore structure and affecting the peat physical properties (Fenton, 1980; Waddington et al., 2010; Whittington and Price, 2006). The changes in peat physical properties, for example, bulk density, active porosity, and hydraulic conductivity, influence the peatland carbon accumulation, water storage, and the growth rate of peatland (Whittington and Price, 2006; Waddington et al., 2010; Mahdiyasa et al., 2022, 2023). Therefore, expecting the same rate of peatland growth to coincide with the rise of the water table, in order to fulfill the assumption of BGM, is not reasonable for the developing peatland. The limitations and inconsistencies of ecological or hydrological models of peatland development, for example, BGM (Clymo, 1984) and GMH (Ingram, 1982), become a starting point for developing a coupled ecohydrological approach to analyse peatland as a complex system (Belyea and Baird, 2006).

1.4.3 Ecohydrological models

Hilbert et al. (2000) proposed a one-dimensional model of peatland development that incorporates the interactions between peat production and water table depth. The initial formulation is similar to BGM (Clymo, 1984; Clymo et al., 1998), which assumes a constant unsaturated zone thickness

or water table depth over time

$$\begin{aligned} \frac{dH}{dt} &= \psi - (\eta_{un} - \eta_{sa})z - \eta_{sa}H, \quad z \geq 0 \\ \frac{dH}{dt} &= \psi - \eta_{sa}H, \quad z < 0 \end{aligned} \tag{1.13}$$

where H is the peatland height (m), ψ is the rate of peat production in terms of thickness (m yr^{-1}), η_{un} is the rate of decay in the unsaturated zone ($-$), η_{sa} is the rate of decay in the saturated zone ($-$), and z is the water table depth (m).

To produce a more realistic model, Hilbert et al. (2000) suggested that the water table depth is a function of the hydrological process and peatland height through the following equations

$$\frac{dz}{dt} = \frac{dH}{dt} - \frac{1}{\vartheta_{max}}\frac{dW}{dt}, \quad z \leq 0 \tag{1.14}$$

with

$$\frac{dW}{dt} = P - ET - d \tag{1.15}$$

$$d = P - ET - \vartheta_{max}(\psi - (\eta_{un} - \eta_{sa})z - \eta_{sa}H) \tag{1.16}$$

where ϑ_{max} is the maximum water storage of peat ($-$), W is the water stored in peat (m), P is the rate of precipitation (m yr^{-1}), and ET is the rate of evapotranspiration (m yr^{-1}).

The coupled ecohydrological model is obtained by employing some assumptions related to evapotranspiration, drainage, and rate of peat production.

The rate of evaporation reduces as the depth of the water table increases

$$ET = \frac{e_0}{1 + c_1 z}, \quad z \geq 0 \tag{1.17}$$

where ET is the rate of evapotranspiration (m yr^{-1}), e_0 is the potential evaporation from an open water surface (m yr^{-1}), and c_1 is the coefficient of evaporation (m^{-1}). Based on the assumption of domed shape peatland (Ingram, 1982), the rate of drainage rises with increasing height as follows

$$d = d_0 + c_2 H \tag{1.18}$$

where d is the rate of water draining from peat (m yr^{-1}), d_0 is the drainage rate when peatland height is equal to zero (m yr^{-1}), and c_2 is the coefficient of drainage (yr^{-1}). Finally, because peat production is affected by the position of the water table (Wallén et al., 1988; Waddington and Roulet, 1996), a quadratic function is employed to model this relationship

$$\psi = k(z - z_{min})(z_{max} - z), \quad z_{min} \leq z \leq z_{max} \tag{1.19}$$

$$\psi = 0, \quad z < z_{min} \quad or \quad z > z_{max} \tag{1.20}$$

where ψ is the rate of peat production in term of thickness (m yr^{-1}), k is the parameter controlling maximum growth rate of peat (m yr^{-1}), z is the water table depth (m), z_{max} is the maximum water table depth where ψ becomes zero (m), and z_{min} is the minimum water table depth where ψ becomes zero (m).

Substituting Equation 1.17 and 1.18 to Equation 1.14 and Equation 1.19

to Equation 1.13, the governing equations of the coupled model become

$$\frac{dz}{dt} = \left(\frac{c_2}{\vartheta_{max}} - \eta_{sa}\right) H - (\eta_{un} - \eta_{sa})z + \frac{e_0}{\vartheta_{max}(1 + c_1 z)} + \psi - \frac{P - d_0}{\vartheta_{max}} \tag{1.21}$$

$$\frac{dH}{dt} = k(z - z_{min})(z_{max} - z) - (\eta_{un} - \eta_{sa})z - \eta_{sa} H \tag{1.22}$$

where z is the water table depth (m), c_1 is the coefficient of evaporation (m^{-1}), c_2 is the coefficient of drainage (yr^{-1}), ϑ_{max} is the maximum water storage of peat ($-$), η_{un} is the rate of decay in the unsaturated zone ($-$), η_{sa} is the rate of decay in the saturated zone ($-$), H is the peatland height (m), e_0 is the potential evaporation from an open water surface (m yr^{-1}), P is the rate of precipitation (m yr^{-1}), d_0 is the drainage rate when peatland height is equal to zero (m yr^{-1}), k is the parameter controlling maximum growth rate of peat (m yr^{-1}), z_{max} is the maximum water table depth where ψ becomes zero (m), and z_{min} is the minimum water table depth where ψ becomes zero (m).

The model from Hilbert et al. (2000) indicates that the nonlinear interaction between peat production and water table depth results in the possibility of multiple equilibria. Consequently, the changes in the water balance could shift the equilibrium point of the peatland and lead to unexpected changes in the behavior of the system. The rapid changes from stocking to exporting carbon or vice versa could happen with significant potential hazards because peatlands contain a massive amount of carbon (Yu et al., 2010; Loisel et al., 2014; Nichols and Peteet, 2019; Hugelius et al., 2020). However, this model neglects the influence of the variations in peat physical properties, including the active porosity and hydraulic conductivity, which provide a crucial negative feedback on the peatland water balance (Quinton et al., 2000; Moore et al., 2005; Whittington and Price, 2006; Morris et al.,

2011).

Frolking et al. (2010) proposed a more advanced ecohydrological model called the Holocene Peat Model (HPM), which is the development of Hilbert et al. (2000). The HPM determines vegetation community composition dynamics and annual net primary productivity based on peat thickness and water table depth. Peat accumulation depends on the productivity and decomposability of peatland vegetation, consisting of 12 plant functional types (PFTs). Each PFT has unique characteristics that are used to model the water fluxes, peatland thickness, and annual net carbon balance.

The rate of mass accumulation to the peatland follows the formulation from Frolking et al. (2001)

$$\frac{dM}{dt} = \frac{d}{dt}\sum_i m_i = \sum_i \left(l_i - k_i \left(\frac{m_i}{m_{i,o}} \right) m_i f_n \right) \tag{1.23}$$

where M is the cumulative mass (kg m^{-2}), l_i is the annual litter input (kg m^2 yr^{-1}), k_i is the initial litter decomposition rate (yr^{-1}), $m_{i,o}$ is the total fresh litter input (kg m^{-2}), and f_n is the scalar multiplier for the effect on decomposition rate of litter water content ($-$).

The water balance formulation in the HPM is affected by precipitation, evapotranspiration, and runoff. Annual precipitation is prescribed as an input variable obtained from the climatic data of the observed peatland. The evapotranspiration is formulated as a function of water table depth through the following equation

$$\begin{aligned} ET &= ET_0, \quad z < z_1 \\ ET &= \frac{ET_0}{1 + c_6 c_7 (z - z_1)}, \quad z_1 \leq z \leq z_2 \\ ET &= \frac{ET_0}{1 + c_6}, \quad z_2 < z_{WT} \end{aligned} \tag{1.24}$$

where ET is the evapotranspiration (m yr^{-1}), ET_0 is the maximum annual evapotranspiration (m yr^{-1}), z is the annual water table depth (m) which is defined as the distance between peatland surface and yearly average position of water table, z_1 is the annual water table depth at which annual evapotranspiration begins to decline (m), z_2 is the annual water table depth at which annual evapotranspiration reaches its minimum (m), c_6 is the parameter needed to make a continuous evapotranspiration function between z_1 and z_2 $(-)$, and $c_7 = (z_2 - z_1)^{-1}$ is the inverse different between z_1 and z_2 (m^{-1}).

The formulation of runoff involves the water table depth and peat relative transmissivity as critical variables as follows

$$\begin{aligned} R &= R_1 T(1 - 10z), \quad z \leq 0 \\ R &= R_1 T, \quad z > 0 \end{aligned} \tag{1.25}$$

with

$$R_1 = (P - ET_0 + R_0)(1 + c_8 H) \tag{1.26}$$

where R is the annual the runoff (m yr^{-1}), R_1 is the base runoff (m yr^{-1}), R_0 is the annual runoff adjustment factor (m yr^{-1}), T is the relative transmissivity $(-)$, T_0 is the minimum relative transmissivity for runoff $(-)$, c_8 is the parameter describing the rate of increase in annual runoff (m^{-1}), and H is the peatland height (m). The relative transmissivity model is defined as the ratio between the integrated hydraulic conductivity of the saturated zone below the water table with the integrated hydraulic conductivity from the total peat profile

$$T = T_0 + (1 - T_0) \left(\frac{\sum_{i_{sat}} h_i \kappa_i}{\sum_{i_{all}} h_i \kappa_i} \right) \tag{1.27}$$

where h is the layer thickness (m) and κ is the hydraulic conductivity (m s^{-1}).

The HPM uses empirical relationships to model the changes in peat physical properties, including bulk density, porosity, and hydraulic conductivity. The key variable that controls the bulk density profile is the remaining mass, as written below

$$\rho = \rho_{min} + \Delta\rho \left(1 - 0.5 \left(1 + erfc \left(\frac{c_3\theta}{\sqrt{2}c_4}\right)\right)\right) \tag{1.28}$$

where ρ is the bulk density (kg m^{-3}), ρ_{min} is the minimum bulk density (kg m^{-3}), $\Delta\rho$ is the difference between maximum and minimum bulk density (kg m^{-3}), $erfc$ is the complementary error function, c_3 and c_4 are the parameters that control the bulk density profile ($-$). The changes in the bulk density influence porosity and hydraulic conductivity through the following equations

$$\phi = 1 - \frac{\rho}{\rho_{om}} \tag{1.29}$$

$$log_{10}(\kappa) = 2.14 - 0.043\rho \tag{1.30}$$

where ϕ is the porosity ($-$), ρ is the bulk density (kg m^{-3}), ρ_{om} is the bulk density of organic matter (kg m^{-3}), and κ is the hydraulic conductivity (m s^{-1}).

HPM incorporates the variations of peat physical properties, including bulk density, porosity, and hydraulic conductivity, during the long-term development of the peatland. However, the changes in peat physical properties are mainly obtained from empirical equations that might reduce the ability of HPM to capture important feedback from the peatland. Furthermore, as a one-dimensional model, HPM ignores the spatial heterogeneity of peat-

land characteristics (Rydin and Jeglum, 2006; Baird et al., 2008; Lewis et al., 2012), which provides significant implications for analysing peatland behaviour (see Chapter 5 for detailed analysis).

Baird et al. (2012) and Morris et al. (2012) developed a peatland development model named DigiBog, which comprehensively integrates ecological and hydrological feedback in one, two, or three dimensions. DigiBog is represented by an arrangement of columns of peat with several layers, which allows water to move between the columns and the water table to fluctuate through the layers in each column. However, the vertical movement of the water within the column is not allowed because the hydraulic gradient in the vertical direction is much smaller than in the horizontal direction as a consequence of Dupuit-Forchheimer (D-F) approximation (Strack, 1984). From the ecological aspect point of view, each column could have a different rate of addition or decomposition depending on the location. Through this geometry, the interaction between hydrological and ecological aspects is explicitly simulated.

DigiBog consists of several submodels, including hydrological, plant litter production, decomposition, and hydraulic properties, which control eco-hydrological processes on the peatland. The hydrological submodel is the main component of DigiBog because it influences the plant litter production and decomposition submodels through the water table position. This submodel is developed from the Boussinesq equation (Boussinesq, 1871)

$$\frac{\partial \Gamma}{\partial t} = \frac{\partial}{\partial x}\left(\frac{\kappa(d)}{\phi(d)} d \frac{\partial \Gamma}{\partial x}\right) + \frac{\partial}{\partial y}\left(\frac{\kappa(d)}{\phi(d)} d \frac{\partial \Gamma}{\partial y}\right) + \frac{P(t) - ET(\Gamma, t)}{\phi(d)} \tag{1.31}$$

where Γ is the water table height (m), x and y are the horizontal distances (m), d is the thickness of flow (m), κ is the depth-averaged hydraulic conductivity below the water table (m s^{-1}), ϕ is the drainable porosity ($-$),

P is the rate of rainfall (m yr^{-1}), and ET is the rate of evapotranspiration (m yr^{-1}), and t is the time (yr). The position of the water table influences plant litter production on the peatland through the empirical equation from (Belyea and Clymo, 2001)

$$\psi = \begin{cases} 0.001(9.3 + 133z - 0.022(100z)^2)^2 & \text{for } 0 \leq z \leq 0.668 \\ 0 & \text{for } z > 0.668 \end{cases} \tag{1.32}$$

where ψ is the peat production (kg m^{-2} yr^{-1}) and z is the water table depth (m). The decomposition submodel follows Clymo (1984) with the constant rate of decay

$$\frac{dm}{dt} = -\eta m \tag{1.33}$$

where m is the mass per unit area (kg m^{-2}) and η is the rate of decay (yr^{-1}). The hydraulic properties submodel explains the effect of the decomposition process on the peat hydraulic conductivity through the remaining mass as follows

$$\kappa = \alpha e^{b\theta} \tag{1.34}$$

where κ is the hydraulic conductivity (m s^{-1}), θ is the remaining mass m_t/m_0 $(-)$, and α (m s^{-1}) and b $(-)$ are parameters.

To a certain extent, DigiBog stands as one of the foremost and prominent peatland development models due to its wide range of applications, including the analysis of nonlinear peatland behaviour (Morris et al., 2011), long-term influence of drainage and restoration (Young et al., 2017), peatland carbon accumulation (Young et al., 2019, 2021), and the effect of snow cover on the long-term growth (Ramirez et al., 2023). However, the

main uncertainties related to the DigiBog approach are the assumptions of constant bulk density and active porosity as peatland develops. The decomposition process reduces not only the hydraulic conductivity but also the active porosity due to smaller fragments of organic matter that lead to a decrease in pore space. Quinton et al. (2000) found that active porosity drops by about 40% between the upper surface and 35 cm depth as a consequence of a more decomposed peat in the deeper position. Therefore, the variations of active porosity will affect peat water storage and water table position in the hydrological submodel, which become the foundation of DigiBog.

1.5 Mechanical-ecohydrological feedback on the peatland

The existing ecohydrological models of peatland development exhibit limitations in their ability to appropriately capture the variations of peat physical properties. They assume a constant or employ empirical equations to analyse the peat physical properties, resulting in the constrained analysis of the peatland behaviour. The changes in peat pore structure that influence physical properties, including bulk density, active porosity, and hydraulic conductivity, are determined by decomposition (Moore et al., 2005; Quinton et al., 2000) and mechanical deformation (Kennedy and Price, 2005; Whittington and Price, 2006; Waddington et al., 2010; Rezanezhad et al., 2016). The effect of decay is incorporated through the remaining mass by HPM (Frolking et al., 2010) and DigiBog (Baird et al., 2012; Morris et al., 2012), but the influence of mechanical deformation on the peat physical properties is ignored by the existing ecohydrological models.

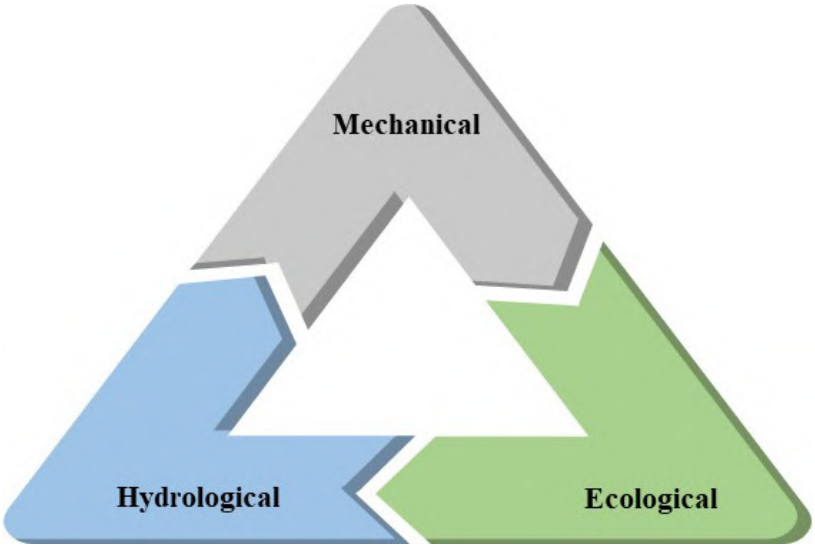

Figure 1.4: The interactions between mechanical, ecological, and hydrological processes produce essential feedback and influence the behaviour of the peatland.

The mechanical deformation is affected by the total load from overlying materials, including surficial peat addition and plant weight, and the position of the water table through the effective stress (Terzaghi, 1943; Price, 2003; Kennedy and Price, 2005). Consequently, during the dry season, peat pore structure experiences a significant deformation effect due to the lower water table position and increasing load from plant weight, reducing active porosity and hydraulic conductivity. This mechanical feedback through the changes of peat physical properties maintains peatland water balance (Whittington and Price, 2006), which in turn, supports the peat accumulation process. Moreover, Waddington et al. (2015) suggested that the peat volume changes from compaction keep the relative distance between the peatland surface and the water table. Therefore, a comprehensive analysis of peatland behaviour requires a mathematical model that incorporates mechanical, ecological, and hydrological processes together with the complex feedback mechanism obtained from the peatland system (Figure 1.4).

Throughout this thesis, the following precise definitions are utilised for the terms compaction, consolidation, and compression. Compaction is the

reduction in volume due to the decrease in void space through the rearrangement of solid particles. If the volume reduction is caused by the expulsion of excess pore water in response to excess pore water pressure, it is called consolidation. The term compression refers to the process of applying inward or compressive forces to the material.

1.6 Thesis aim and objectives

The aim of the thesis is to develop a fully coupled mechanical, ecological, and hydrological model of peatland development, called MPeat, and consider the potential implications of feedback within the model system. MPeat is designed based on the principles of poroelasticity theory, which enables the interaction between fluid flow and solid deformation. Through this approach, the peat physical properties, including bulk density, active porosity, and hydraulic conductivity, are formulated as an integrated process within the overall framework of peatland development, which addresses the limitations of previous models. The specific objectives of this study are presented in the following section.

1. Investigate the influence of mechanical, ecological, and hydrological feedback on the peatland characteristics, including water table depth, thickness, and carbon accumulation.

2. Assess the variations in bulk density, active porosity, and hydraulic conductivity throughout the peatland development process.

3. Analyse peatland dynamics that incorporate the interactions between peat volume changes and plant functional types.

4. Examine the peatland regime shifts and tipping points in a grow-

ing system accounting for fully coupled mechanical, ecological, and hydrological feedback.

5. Investigate the effect of spatial heterogeneity of peatland characteristics and the influence of river incision on the peatland behaviour.

6. Determine the maximum carbon accumulation of peatland in a landscape before the occurrence of failure due to mechanical instability.

1.7 Thesis outlines

Chapter 2 derives the poroelasticity formulation (Biot, 1941), which becomes the essence of MPeat, based on the equation of equilibrium of porous medium and conservation of mass of fluid and solid constituents. The finite element methods are employed to solve the governing equations of poroelasticity, and the results are compared with the analytical solutions from Terzaghi's and Mandel's problems for one- and two-dimensional verification (Terzaghi, 1925, 1943; Mandel, 1953), respectively. The test cases are conducted using a layered porous medium with high contrast in hydraulic conductivity to assess the stability of the proposed algorithm. The test cases are particularly relevant because peatland exhibits significant variations of hydraulic conductivity with depth.

Chapter 3 provides a one-dimensional model of peatland development that couples mechanical, ecological, and hydrological feedback. The changes in peat physical properties obtained from the one-dimensional version of MPeat align with the field observations (Clymo, 1984; Siegel et al., 1995; Hoag and Price, 1997; Quinton et al., 2000; Fraser et al., 2001; Clymo, 2004; Quinton et al., 2008), suggesting plausible outputs of the proposed model. The comparison of MPeat with the other ecohydrological models,

HPM and DigiBog, indicates the importance of mechanical feedback on the peatland characteristics, including water table depth, thickness, and carbon accumulation.

Chapter 4 analyses the consequence of the coupling between plant functional types with peat stiffness on a nonequilibrium model of a peatland by developing the one-dimensional version of MPeat from Chapter 3. In this formulation, the peatland systems exist in two possible states defined by two limit cycles, one corresponding to a wet and the other to a dry attractor. These states can also coexist under the same net rainfall indicating bistability in which a crucial drying threshold leads to a tipping point and associated regime shift from soft-wet to stiff-dry states with related changes in rates of carbon storage. Investigation of the behaviour of these states in response to seasonal variations in water budget suggests that the wet state will display high amplitude and later peak timing of peatland surface when compared to the dry state, a phenomenon that is observed in measures of surface motion (Bradley et al., 2022).

Chapter 5 provides a fully coupled mechanical, ecological, and hydrological model of peatland development MPeat in two dimensions. This model captures spatial variations of peatland characteristics, including peat physical properties, water table depth, and plant functional types composition. The simulation results from the two-dimensional version of MPeat show that hydraulic conductivity is lower at the margin compared to the centre, which is in line with field observation from Baird et al. (2008) and Lewis et al. (2012). The spatial variations of peat physical properties, together with the changes in hydraulic gradient, produce variability in the water table position, which affect peat production and carbon accumulation. Furthermore, river incisions at the boundaries and permeable substrate also lead to variations in the water table position and peat accumulation (Glaser et al.,

2004b), which highlights the effect of these phenomena on understanding peatland behaviour.

Chapter 6 determines the limit to carbon accumulation on the peatland before the occurrence of failure due to mechanical instability by employing a two-dimensional version of MPeat described in Chapter 5. In this simulation, peatland develops across a heterogeneous landscape consisting of upland, lowland, and sloping area with the river at the boundaries based on the theoretical landscape proposed by Winter (2001). The landscape variations, together with the feedback from mechanical, ecological, and hydrological processes, affect the stresses on the peat body that control the occurrence of failure conditions on the peatland. If maximum shear stress is greater than the peat shear strength, then shear failure takes place that is associated with the peat slide phenomenon (Dykes and Kirk, 2001; Dykes and Warburton, 2008b; Dykes et al., 2008; Dykes, 2022). In contrast, tensile failure occurs due to a higher maximum tensile stress than peat tensile strength resulting in a bog burst (Dykes, 2008). Finally, thesis conclusions and recommendations for future work are presented in Chapter 7.

Chapter 2

Modelling peatland mechanics: A poroelasticity approach

2.1 Introduction

In this chapter, I provide the mathematical formulation and numerical verification of the poroelasticity, which couples fluid flow and solid deformation in one and two dimensions to model peatland mechanics. The poroelasticity is developed based on the equation of equilibrium and conservation of mass of fluid and solid constituents. I compare the proposed numerical solver with the benchmark problem from Terzaghi's and Mandel's for the one-dimensional and two-dimensional cases, respectively (Terzaghi, 1925, 1943; Mandel, 1953).

Peat can be viewed as a porous medium because it consists of solid particles from plant litter or organic matter, and the pores are filled with fluid. The mechanical deformation of the peat depends on the stiffness of the peat solid skeleton and the behaviour of the pore fluid. Reeve et al. (2013)

found that a higher value of peat Young's modulus, which represents the stiffness of the porous material, leads to a lower deformation on the peat body. Furthermore, the characteristics of fluid contained in the pore space, including gas content and degree of saturation, also significantly affect the deformation of the peat due to the presence of pore fluid pressure (Boylan et al., 2008; Price and Schlotzhauer, 1999; Price, 2003). The study from Whittington and Price (2006) suggests that a lower water table position produces a more considerable effect of deformation because the peat body cannot withstand loading from overlying material, as the consequence of reducing fluid pressure, which results in the collapse of the pore structure. Therefore, the changes in the pore fluid pressure cause solid deformation on the peat body, and the deformation of the peat solid skeleton influences pore fluid behaviour. This phenomenon is considered as coupled between solid deformation and fluid flow and is denoted as poroelasticity.

The poroelasticity phenomenon was initially analysed by Terzaghi (1925), who considered the uniaxial deformation of soil through the confined compression test which is known as the one-dimensional poroelasticity problem. Terzaghi (1925) assumed that both fluid and solid constituents are incompressible, and the deformation occurs due to the rearrangement of particles. Biot (1941) extended the poroelasticity formulation from Terzaghi (1925) by developing a three-dimensional formulation and removed the incompressible assumption of the constituents. Furthermore, Biot (1955) proposed the formulations that include the anisotropic assumption, and Biot (1973) provided the formulations for the nonlinear case.

The fundamental difference between poroelasticity and classical elasticity is the presence of effective stress. In poroelasticity, the total stresses that act on a porous medium are allocated to pore fluid and the solid skeleton. The first component leads to the pore fluid pressure, and the second component,

termed the effective stress, leads to the displacement of the solid (Terzaghi, 1925, 1943). Therefore, the equation of equilibrium of poroelasticity is presented in terms of effective stress, and the equation of conservation of mass is formulated for both solid and fluid constituents.

In this chapter, I model peatland mechanics through the poroelasticity formulation (Biot, 1941). I provide a strong and weak form for the finite element computation and compare the numerical results from the proposed algorithm with the analytical solution from Terzaghi's and Mandel's problem for one- and two-dimensional verification, respectively (Terzaghi, 1925, 1943; Mandel, 1953). The test case of a layered porous medium in one and two dimensions with high hydraulic conductivity contrast are presented to analyse the stability of the proposed algorithm because peatlands experience a remarkable change in hydraulic conductivity with depth (Clymo, 2004; Fraser et al., 2001; Hoag and Price, 1995).

2.2 Model formulation

2.2.1 Equation of equilibrium

The equation of equilibrium can be formulated by considering the stresses tensor $\boldsymbol{\sigma}$ acting upon the six faces of an elementary volume of a small cuboid material (Figure 2.1). In the presence of body forces $\mathbf{b}$ and taking into account the symmetry of the stress tensor, the equilibrium equation

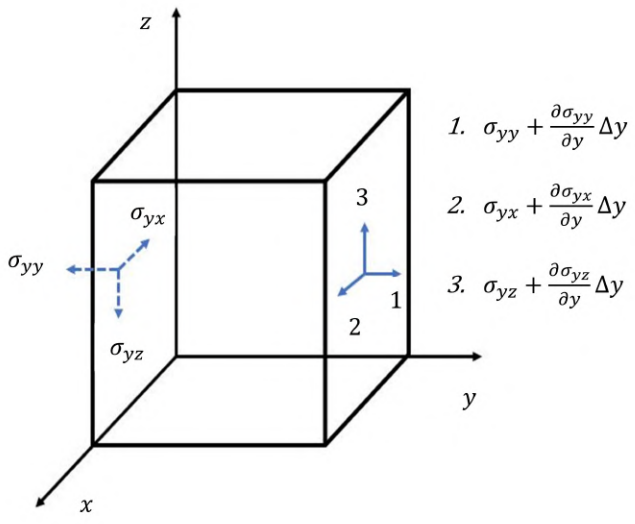

Figure 2.1: Stresses tensor illustration on the right and left faces of a small cuboid material.

becomes

$$\begin{aligned} \frac{\partial \sigma_{xx}}{\partial x} + \frac{\partial \sigma_{xy}}{\partial y} + \frac{\partial \sigma_{zx}}{\partial z} + b_x = 0 \\ \frac{\partial \sigma_{yy}}{\partial y} + \frac{\partial \sigma_{xy}}{\partial x} + \frac{\partial \sigma_{yz}}{\partial z} + b_y = 0 \\ \frac{\partial \sigma_{zz}}{\partial z} + \frac{\partial \sigma_{yz}}{\partial y} + \frac{\partial \sigma_{zx}}{\partial x} + b_z = 0 \end{aligned} \tag{2.1}$$

The Equation (2.1) can be written in the matrix form as

$$\overline{\nabla}^{\boldsymbol{T}} \boldsymbol{\sigma} + \mathbf{b} = \mathbf{0} \tag{2.2}$$

with $\overline{\nabla} = \begin{bmatrix} \partial/\partial x & 0 & 0 \\ 0 & \partial/\partial y & 0 \\ 0 & 0 & \partial/\partial z \\ \partial/\partial y & \partial/\partial x & 0 \\ 0 & \partial/\partial z & \partial/\partial y \\ \partial/\partial z & 0 & \partial/\partial x \end{bmatrix}$, $\boldsymbol{\sigma} = [\sigma_{xx}, \sigma_{yy}, \sigma_{zz}, \sigma_{xy}, \sigma_{yz}, \sigma_{zx}]^T$, and $\mathbf{b} = [0, 0, \rho g]^T$

where $\mathbf{b}$ is the body force and ρ is the average density of the porous medium. The presentation in terms of the matrix form provides convenient notation for the derivation of weak form (Jha and Juanes, 2014). Furthermore, ρ is defined as

$$\rho = \rho_f \phi + \rho_s (1 - \phi) \tag{2.3}$$

where ρ_f is the fluid density (kg m^{-3}), ρ_s is the solid density (kg m^{-3}), and ϕ is the active porosity $(-)$.

The stresses that act to a porous medium will be allocated to the solid skeleton and pore fluid. The first case known as effective stress, and it can be written as

$$\boldsymbol{\sigma} = \boldsymbol{\sigma'} + \alpha \mathbf{m} p \tag{2.4}$$

where $\boldsymbol{\sigma}$ is the total stress tensor (Pa), $\boldsymbol{\sigma'}$ is the effective stress tensor (Pa), α is the Biot's coefficient $(-)$, $\mathbf{m}$ is the vector form of Kronecker's delta $\mathbf{m} = [1 \quad 1 \quad 1 \quad 0 \quad 0 \quad 0]^T$, and p is the pore water pressure (Pa). Biot (1941) defined α as a ratio between drained bulk modulus of the porous material and the poroelastic expansion coefficient. For soil mechanics problems, the value of α is assumed to be one in general (Terzaghi, 1943).

The linear constitutive law gives the relation between effective stress tensor and strain tensor

$$\boldsymbol{\sigma'} = \mathbf{D} \boldsymbol{\epsilon} \tag{2.5}$$

with $\mathbf{D} = \dfrac{E}{(1+\nu)(1-2\nu)} \begin{bmatrix} 1-\nu & \nu & \nu & 0 & 0 & 0 \\ \nu & 1-\nu & \nu & 0 & 0 & 0 \\ \nu & \nu & 1-\nu & 0 & 0 & 0 \\ 0 & 0 & 0 & \dfrac{1-2\nu}{2} & 0 & 0 \\ 0 & 0 & 0 & 0 & \dfrac{1-2\nu}{2} & 0 \\ 0 & 0 & 0 & 0 & 0 & \dfrac{1-2\nu}{2} \end{bmatrix}$ is the stiffness matrix, E is the Young's Modulus (Pa), ν is the Poisson ratio $(-)$ and $\boldsymbol{\epsilon} = [\epsilon_{xx}, \epsilon_{yy}, \epsilon_{zz}, \epsilon_{xy}, \epsilon_{yz}, \epsilon_{zx}]^T$ is the strain tensor $(-)$. The kinematics relations or strain-displacement are

$$\begin{aligned} \epsilon_{xx} &= \frac{\partial u_x}{\partial x},\ \epsilon_{xy} = \frac{1}{2}\left(\frac{\partial u_x}{\partial y} + \frac{\partial u_y}{\partial x}\right) \\ \epsilon_{yy} &= \frac{\partial u_y}{\partial y},\ \epsilon_{yz} = \frac{1}{2}\left(\frac{\partial u_y}{\partial z} + \frac{\partial u_z}{\partial y}\right) \\ \epsilon_{zz} &= \frac{\partial u_z}{\partial z},\ \epsilon_{zx} = \frac{1}{2}\left(\frac{\partial u_z}{\partial x} + \frac{\partial u_x}{\partial z}\right) \end{aligned} \tag{2.6}$$

In the matrix form Equation (2.6) can be written as

$$\boldsymbol{\epsilon} = \overline{\nabla}\mathbf{u} \tag{2.7}$$

where $\mathbf{u} = [u_x, u_y, u_z]^T$ (m) is the displacement.

Putting together (2.2), (2.4), (2.5), and (2.7), the equation of equilibrium can be written in terms of effective stress tensor

$$\overline{\boldsymbol{\nabla}}^{\boldsymbol{T}}\boldsymbol{\sigma'} + \overline{\boldsymbol{\nabla}}^{\boldsymbol{T}}(\alpha \mathbf{m} p) + \mathbf{b} = 0 \tag{2.8}$$

or in terms of displacement

$$\overline{\boldsymbol{\nabla}}^{\boldsymbol{T}}\mathbf{D}\overline{\boldsymbol{\nabla}}\mathbf{u} + \overline{\boldsymbol{\nabla}}^{\boldsymbol{T}}(\alpha \mathbf{m} p) + \mathbf{b} = 0 \tag{2.9}$$

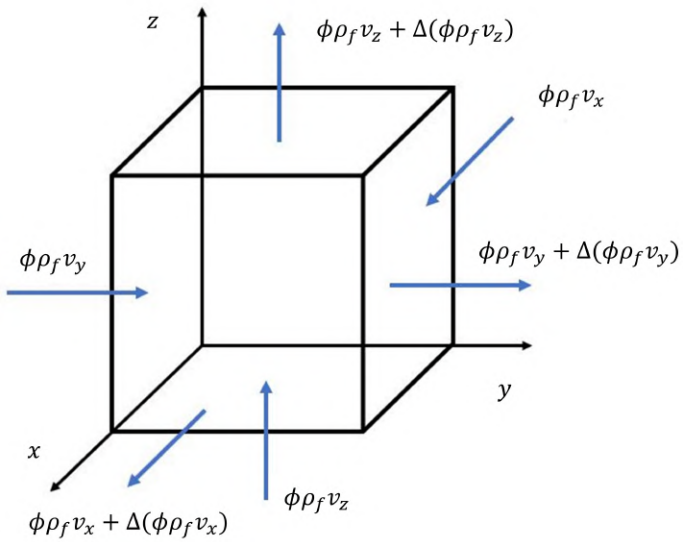

Figure 2.2: Fluid flow illustration through small cuboid material.

2.2.2 Conservation of mass

The law of conservation of mass states that for any system closed to all transfers of matter and energy, the mass of the system must remain constant over time. In my case, the system contains two components, solid and fluid, which must be conserved. The equations of conservation of mass can be constructed by taking into account flow through an elementary volume of a small cuboid material (Figure 2.2).

The fluid mass occupying elementary volume V is $m_f = \rho_f V_f$ where ρ_f is the fluid density and $V_f = \phi V$ is the fluid volume. Using a mass balance equation to the net fluid flux of the elementary volume gives the result

$$\frac{\partial(\phi\rho_f)}{\partial t} + \nabla \cdot (\phi\rho_f \mathbf{v_f}) = 0 \tag{2.10}$$

where ϕ is the active porosity $(-)$, ρ_f is the fluid density $(\mathrm{kg\,m^{-3}})$, $\mathbf{v_f}$ is the average velocity of the fluid $(\mathrm{m\,s^{-1}})$ and t is the time (s). The change

of fluid volume ΔV_f because of loading is

$$\Delta V_f = -\phi C_f \Delta p V \tag{2.11}$$

where C_f is the compressibility of the fluid (Pa^{-1}), ϕ is the active porosity ($-$), p is the pore water pressure (Pa), and V is the total volume (m^3). Mass continuity of the fluid can be written as

$$\rho_{f'} V_{f'} = \rho_f V_f \tag{2.12}$$

where $\rho_{f'}$ and $V_{f'}$ are the density and volume of fluid at reference configuration and ρ_f and V_f are the equivalent variables in the current configuration. Because $\rho_f = \rho_{f'} + \Delta\rho_f$ and $V_f = V_{f'} + \Delta V_f$, Equation (2.12) becomes

$$\frac{\Delta V_f}{V_f} = -\frac{\Delta \rho_f}{\rho_f} \tag{2.13}$$

Based on Equations (2.11) and (2.13), the constitutive equation of the fluid is

$$\frac{\mathrm{d}\rho_f}{\mathrm{d}p} = \rho_f C_f \tag{2.14}$$

where p is the pore water pressure (Pa), C_f is the compressibility of the fluid (Pa^{-1}), and ρ_f is the fluid density ($\mathrm{kg\ m}^{-3}$). Substituting the constitutive equation of the fluid phase (2.14) to mass balance equation (2.10) gives us

$$\frac{\partial \phi}{\partial t} + \phi C_f \frac{\partial p}{\partial t} + \nabla \cdot (\phi \mathbf{v_f}) = 0 \tag{2.15}$$

The mass of the solid skeleton of elementary volume V is $m_s = \rho_s V_s$ where ρ_s is the solid density ($\mathrm{kg\ m}^{-3}$) and $V_s = (1-\phi)V$ is the solid volume (m^3).

The mass balance equation for the solid skeleton can be expressed as

$$\frac{\partial(1-\phi)\rho_s}{\partial t} + \nabla \cdot [(1-\phi)\rho_s \mathbf{v_s}] = 0 \tag{2.16}$$

where $\mathbf{v_s}$ is the average velocity of the solid ($\mathrm{m\,s^{-1}}$), ϕ is the active porosity ($-$), ρ_s is the solid density ($\mathrm{kg\,m^{-3}}$) and t is the time (s). The change of solid volume ΔV_s because of loading, is also influenced by a rearrangement of the solid particles through the average stress increment with value $-\frac{C_s(\Delta\sigma-\Delta p)}{1-\phi}V$; hence it becomes

$$\Delta V_s = -\phi C_s \Delta p V - \frac{C_s(\Delta\sigma - \Delta p)}{1-\phi}V \tag{2.17}$$

where C_s is the compressibility of the solid ($\mathrm{Pa^{-1}}$), σ is the isotropic (average) total stress (Pa), ϕ is the active porosity ($-$), p is the pore water pressure (Pa), V is the total volume ($\mathrm{m^3}$), and t is the time (s). Departing from Equation (2.17) and applying mass continuity (similar to the fluid phase), the constitutive equation of the solid phase can be written as

$$\frac{\partial \rho_s}{\partial t} = \frac{\rho_s C_s}{1-\phi}\left(\frac{\partial \sigma}{\partial t} - \phi\frac{\partial p}{\partial t}\right) \tag{2.18}$$

where p is the pore water pressure (Pa), ρ_s is the solid density ($\mathrm{kg\,m^{-3}}$), ϕ is the active porosity ($-$), C_s is the compressibility of solid ($\mathrm{Pa^{-1}}$), σ is the isotropic (average) total stress (Pa), and t is time (s). Substituting the constitutive equation of the solid phase (2.18) to the mass balance equation (2.16) reads

$$-\frac{\partial \phi}{\partial t} + C_s\left(\frac{\partial \sigma}{\partial t} - \phi\frac{\partial p}{\partial t}\right) + \nabla \cdot [(1-\phi)\mathbf{v_s}] = 0 \tag{2.19}$$

I can eliminate the time derivative of the porosity from Equation (2.15)

and (2.19) by adding these two equations

$$\nabla \cdot \mathbf{v_s} + \nabla \cdot [\phi(\mathbf{v_f} - \mathbf{v_s})] + \phi(C_f - C_s)\frac{\partial p}{\partial t} + C_s\frac{\partial \sigma}{\partial t} = 0 \tag{2.20}$$

The specific discharge $\mathbf{q}$ can be defined as the difference between the average velocity of the fluid $\mathbf{v_f}$ and the average velocity of the solid $\mathbf{v_s}$ multiplied by active porosity ϕ

$$\mathbf{q} = \phi(\mathbf{v_f} - \mathbf{v_s}) \tag{2.21}$$

Substituting Equation (2.21) to (2.20) and knowing that the first term of Equation (2.20) is equal to the time derivative of volumetric strain $\frac{\partial \epsilon}{\partial t} = \nabla \cdot \mathbf{v_s}$, gives us

$$\frac{\partial \epsilon}{\partial t} + \phi(C_f - C_s)\frac{\partial p}{\partial t} + C_s\frac{\partial \sigma}{\partial t} = -\nabla \cdot \mathbf{q} \tag{2.22}$$

The specific discharge $\mathbf{q}$ is given by the Darcy's law

$$\mathbf{q} = -\frac{k}{\mu}(\nabla p - \rho_f \mathbf{g}) \tag{2.23}$$

where k is the intrinsic permeability (m^2), μ is the viscosity of the fluid ($\mathrm{kg\ m^{-1}\ s^{-1}}$), and $\mathbf{g}$ is the gravity vector ($\mathrm{m\ s^2}$) (Bear, 1972). The coefficient in Darcy's law equation (2.23) can be written as a coefficient of permeability or hydraulic conductivity κ that gives us

$$\nabla \cdot \mathbf{q} = \frac{\partial q_x}{\partial x} + \frac{\partial q_y}{\partial y} + \frac{\partial q_z}{\partial z} = -\nabla \cdot (\kappa \nabla p) \tag{2.24}$$

For the isotropic case, there are relations between isotropic total stress σ, isotropic effective stress σ', volumetric strain $\epsilon = \epsilon_{xx} + \epsilon_{yy} + \epsilon_{zz}$, and

compressibility of porous material C

$$\sigma = \sigma' + \alpha p \tag{2.25}$$

$$\sigma' = \frac{\epsilon}{C} \tag{2.26}$$

Finally, making use of Equations (2.22), (2.24), (2.25), (2.26), I can get

$$\alpha \frac{\partial \epsilon}{\partial t} + S_s \frac{\partial p}{\partial t} = \nabla \cdot (\kappa \nabla p) \tag{2.27}$$

where $\alpha = 1 - \frac{C_s}{C}$ is the Biot's coefficient $(-)$, κ is the hydraulic conductivity $(\mathrm{m\ s^{-1}})$, γ_f is the volumetric weight of the fluid $(\mathrm{N\ m^{-3}})$, and S_s is the specific storage $(\mathrm{m^{-1}})$ (Kim et al., 2011; Coussy, 2004; Jha and Juanes, 2014). The interpretation of Equation (2.27), also known as the storage equation, is the compression of porous material consists of the compression of pore fluid and solid particles, plus the amount of fluid expelled from an element by the flow.

2.3 Numerical computation

I summarize the governing equations and complete the model with appropriate boundary conditions. The primary variables are the displacements and the pore water pressure, because of that there are two distinct sets of boundary conditions to produce a strong form of the problem. The first is associated with displacements $\mathbf{u}$ and traction $\mathbf{t}$, and the second is associated with pressure p and flux $\mathbf{q}$. Define a domain Ω and the boundary of

the domain Γ to get

$$\overline{\boldsymbol{\nabla}}^{\boldsymbol{T}}\boldsymbol{\sigma} + \mathbf{b} = \mathbf{0} \tag{2.28}$$

$$\boldsymbol{\sigma'} = \boldsymbol{\sigma} - \alpha \mathbf{m} p \tag{2.29}$$

$$\boldsymbol{\sigma'} = \mathbf{D}\boldsymbol{\epsilon} \tag{2.30}$$

$$\boldsymbol{\epsilon} = \overline{\nabla}\mathbf{u} \tag{2.31}$$

$$\alpha \frac{\partial \epsilon}{\partial t} + S_s \frac{\partial p}{\partial t} = \nabla \cdot (\kappa \nabla p) \tag{2.32}$$

with the boundary conditions

$$\mathbf{u} = \overline{\mathbf{u}} \quad \text{on} \quad \Gamma_u \quad \text{and} \quad \mathbf{t} = \overline{\mathbf{t}} \quad \text{on} \quad \Gamma_t \tag{2.33}$$

$$p = \overline{p} \quad \text{on} \quad \Gamma_p \quad \text{and} \quad \frac{\partial p}{\partial \mathbf{n}} = \overline{\mathbf{q}} \quad \text{on} \quad \Gamma_q \tag{2.34}$$

where $\Gamma = \Gamma_u \cup \Gamma_t$ and $\Gamma = \Gamma_p \cup \Gamma_q$ with $\mathbf{n}$ represents the unit normal vector to Γ.

The weak form of equation of equilibrium can be obtained by multiplying equation (2.28) with an arbitrary function $\delta\mathbf{u}$ such that $\delta\mathbf{u} = 0$ on Γ_u and integrating over Ω reads

$$\int_\Omega \delta\mathbf{u}\overline{\boldsymbol{\nabla}}^{\boldsymbol{T}}\boldsymbol{\sigma}\, d\Omega + \int_\Omega \delta\mathbf{u}\mathbf{b}\, d\Omega = \mathbf{0} \tag{2.35}$$

Integrating by parts the first term of equation (2.35) and applying Gauss divergence theorem results in

$$\int_\Omega (\overline{\nabla}\delta\mathbf{u})^T \sigma\, d\Omega = \int_{\Gamma_t} (\delta\mathbf{u})^T \overline{\mathbf{t}}\, d\Gamma + \int_\Omega (\delta\mathbf{u}\mathbf{b})^T\, d\Omega \tag{2.36}$$

I can rewrite the equation (2.36) to become a function of displacement,

traction, and body force using equation (2.4) and (2.7)

$$\int_\Omega (\overline{\nabla}\delta\mathbf{u})^T\mathbf{D}\overline{\nabla}\delta u\, d\Omega - \int_\Omega (\overline{\nabla}\delta\mathbf{u})^T\alpha\mathbf{m}p\, d\Omega = \int_{\Gamma_t} (\delta\mathbf{u})^T\overline{\mathbf{t}}\, d\Gamma + \int_\Omega (\delta\mathbf{ub})^T\, d\Omega \tag{2.37}$$

The discretization of variables $\mathbf{u}$, $\delta\mathbf{u}$, and p as follows

$$\mathbf{u} = \mathbf{N}\tilde{\mathbf{u}}, \quad \delta\mathbf{u} = \mathbf{N}\delta\tilde{\mathbf{u}}, \quad p = \mathbf{N_p}\tilde{\mathbf{p}} \tag{2.38}$$

where $\mathbf{N}$ and $\mathbf{N_p}$ are the shape function matrices of $\mathbf{u}$ and p, $\tilde{\mathbf{u}}$ and $\tilde{p}$ are the values at the elements nodes. Substituting equation (2.38) to (2.37), I have

$$\mathbf{K}\tilde{\mathbf{u}} - \mathbf{L}\tilde{\mathbf{p}} = \mathbf{F} \tag{2.39}$$

with

$$\mathbf{K} = \int_\Omega (\overline{\nabla}\mathbf{N})^T\mathbf{D}\overline{\nabla}\mathbf{N}\, d\Omega \tag{2.40}$$

$$\mathbf{L} = \int_\Omega (\overline{\nabla}\mathbf{N})^T\alpha\mathbf{m}\mathbf{N_p}\, d\Omega \tag{2.41}$$

$$\mathbf{F} = \int_{\Gamma_t} \mathbf{N}^T\overline{\mathbf{t}}\, d\Gamma + \int_\Omega \mathbf{N}^T\mathbf{b}\, d\Omega \tag{2.42}$$

The weak form formulation of conservation of mass is similar with the equation of equilibrium. Applying the same procedure to equation (2.32) leads to

$$\int_\Omega (\delta p)^T\alpha\mathbf{m}^T\overline{\nabla}\frac{\partial\mathbf{u}}{\partial t}\, d\Omega + \int_\Omega (\delta p)^T S_s\frac{\partial p}{\partial t}\, d\Omega + \int_\Omega (\nabla\delta p)^T\kappa\nabla p\, d\Omega = \int_{\Gamma_q} (\delta p)^T\kappa\overline{q}\, d\Gamma \tag{2.43}$$

Substituting equation (2.38) to (2.43) for discretization process provides us

$$\mathbf{L}^T \dot{\tilde{\mathbf{u}}} + \mathbf{A}\dot{\tilde{\mathbf{p}}} + \mathbf{H}\tilde{\mathbf{p}} = \mathbf{Q} \tag{2.44}$$

with

$$\mathbf{A} = \int_{\Omega} (\nabla \mathbf{N_p})^T S_s \nabla \mathbf{N_p} \, d\Omega \tag{2.45}$$

$$\mathbf{H} = \int_{\Omega} \mathbf{N_p}^T \kappa \nabla \mathbf{N_p} \, d\Omega \tag{2.46}$$

$$\mathbf{Q} = \int_{\Gamma_q} \mathbf{N_p}^T \kappa \bar{q} \, d\Gamma \tag{2.47}$$

$$\dot{\tilde{\mathbf{u}}} = \frac{\partial \tilde{\mathbf{u}}}{\partial t} \tag{2.48}$$

$$\dot{\tilde{\mathbf{p}}} = \frac{\partial \tilde{\mathbf{p}}}{\partial t} \tag{2.49}$$

Finally, equations (2.39) and (2.44) can be written in the following matrix form as a coupled equations

$$\begin{bmatrix} \mathbf{0} & \mathbf{0} \\ \mathbf{L}^T & \mathbf{A} \end{bmatrix} \begin{bmatrix} \dot{\tilde{\mathbf{u}}} \\ \dot{\tilde{\mathbf{p}}} \end{bmatrix} + \begin{bmatrix} \mathbf{K} & -\mathbf{L} \\ \mathbf{0} & \mathbf{H} \end{bmatrix} \begin{bmatrix} \tilde{\mathbf{u}} \\ \tilde{\mathbf{p}} \end{bmatrix} = \begin{bmatrix} \mathbf{F} \\ \mathbf{Q} \end{bmatrix} \tag{2.50}$$

2.4 Results and discussion

2.4.1 One-dimensional verification

In one dimension (y-axis), the governing equations of poroelasticity Equations (2.28), (2.29), (2.30), (2.31), (2.32) can be written as

$$\frac{\partial \sigma}{\partial y} + \rho g = 0 \tag{2.51}$$

$$\sigma' = \sigma - \alpha p \tag{2.52}$$

$$\sigma' = E\epsilon \tag{2.53}$$

$$\epsilon = \frac{\partial u}{\partial y} \tag{2.54}$$

$$\alpha \frac{\partial \epsilon}{\partial t} + S_s \frac{\partial p}{\partial t} = \kappa \frac{\partial^2 p}{\partial y^2} \tag{2.55}$$

where σ is the total stress (Pa), σ' is the effective stress (Pa), ρ is the average density of the porous medium ($\mathrm{kg\,m^{-3}}$), g is the acceleration of gravity ($\mathrm{m\,s^{-2}}$), α is the effective stress coefficient ($-$), p is the pore water pressure (Pa), E is the Young's modulus (Pa), ϵ is the strain ($-$), u is the displacement (m), κ is the hydraulic conductivity ($\mathrm{m\,s^{-1}}$), S_s is the specific storage ($\mathrm{m^{-1}}$), γ_w is the specific weight of water ($\mathrm{N\,m^{-3}}$), and t is the time (s).

To validate the proposed algorithm, I compare the numerical solution in one dimension with the analytical solution of Terzhagi's problem (Terzaghi, 1943). For the one-dimensional test case (Figure 2.3), a uniform vertical load F is applied on the top surface of a fully saturated sample with height

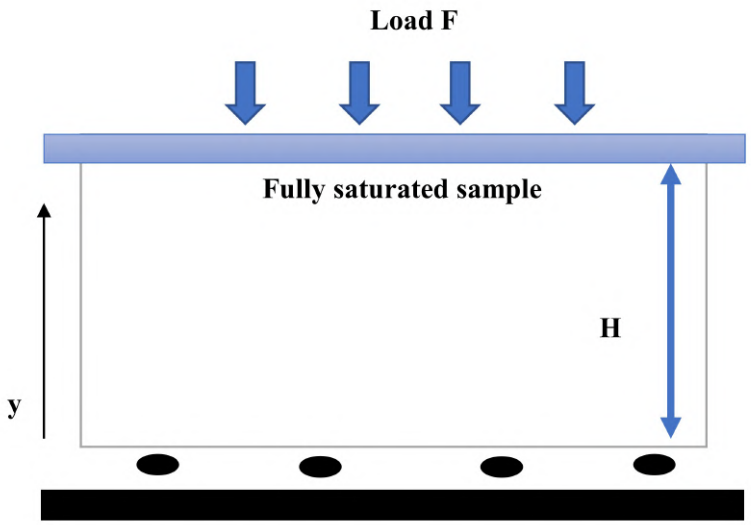

Figure 2.3: Terzaghi's problem illustration with an impermeable and no-displacement lower boundary and fully drained upper boundary.

H. The boundary conditions for this problem are

$$p\left(y, 0^{+}\right) = p_0 \tag{2.56}$$

$$\frac{dp}{dy} = 0 \text{ at } y = 0 \tag{2.57}$$

$$u(0, t) = 0 \tag{2.58}$$

$$p(H, t) = 0 \tag{2.59}$$

where p is the pore water pressure (Pa) and u is the vertical displacement (m). The pore water pressure and vertical displacement are expressed as non-dimensional quantities of normalised pore water pressure P and degree of consolidation U

$$P = \frac{p(y, t)}{p_0} \tag{2.60}$$

$$U = \frac{u(y, t) - u(y, 0^{+})}{u(y, \infty) - u(y, 0^{+})} \tag{2.61}$$

The analytical solutions of Terzaghi's problem are (Biot, 1941; Verruijt,

Table 2.1: Input data for numerical and analytical solutions of Terzaghi's problem.

Name	**Symbol**	**Value**	**Unit**
Load	F	1×10^5	Pa
Initial value of pore water pressure	p_0	1×10^5	Pa
Young's modulus	E	1×10^8	Pa
Bulk modulus	K	5.56×10^7	Pa
Shear modulus	G	4.17×10^7	Pa
Hydraulic conductivity	κ	1×10^{-7}	$\mathrm{m\,s^{-1}}$
Specific storage	S_s	1×10^{-5}	$\mathrm{m^{-1}}$
Biot's coefficient	α	1	$-$
Sample height	H	1	m

2018; Wang, 2000)

$$P = \frac{4}{\pi} \sum_{k=1}^{\infty} \frac{-1^{k-1}}{2k-1} \cos\left[(2k-1)\frac{\pi}{2}\frac{y}{H}\right] exp\left[-(2k-1)^2 \frac{\pi^2}{4}\frac{c_v t}{H^2}\right] \tag{2.62}$$

$$U = 1 - \frac{8}{\pi^2} \sum_{k=1}^{\infty} \frac{1}{(2k-1)^2} exp\left[-(2k-1)^2 \frac{\pi^2}{4}\frac{c_v t}{H^2}\right] \tag{2.63}$$

$$c_v = \frac{\kappa}{S_s + \frac{\alpha^2}{K+(4/3)G}} \tag{2.64}$$

where P is the normalised pore water pressure $(-)$, U is the degree of consolidation $(-)$, c_v is the consolidation coefficient $(\mathrm{m^2\,s^{-1}})$, H is the sample height (m), κ is the hydraulic conductivity $(\mathrm{m\,s^{-1}})$, S_s is the specific storage $(\mathrm{m^{-1}})$, α is the Biot's coefficient $(-)$, K is the bulk modulus (Pa), and G is the shear modulus (Pa).

I use 101 nodes and 100 elements to generate the simulation with the input data stated in Table 2.1. The proposed algorithm shows good performance indicated by a small error between the numerical and analytical solutions (Figure 2.4). Furthermore, the mean absolute error for normalised pore water pressure at the dimensionless time t^* equal to 0.01, 0.1, 0.5, and 1 are 2.5×10^{-3}, 6.3×10^{-4}, 3.3×10^{-5}, and 2.7×10^{-5}, respectively, with $t^* = \frac{(c_v t)}{H^2}$. The mean absolute error for the degree of consolidation also

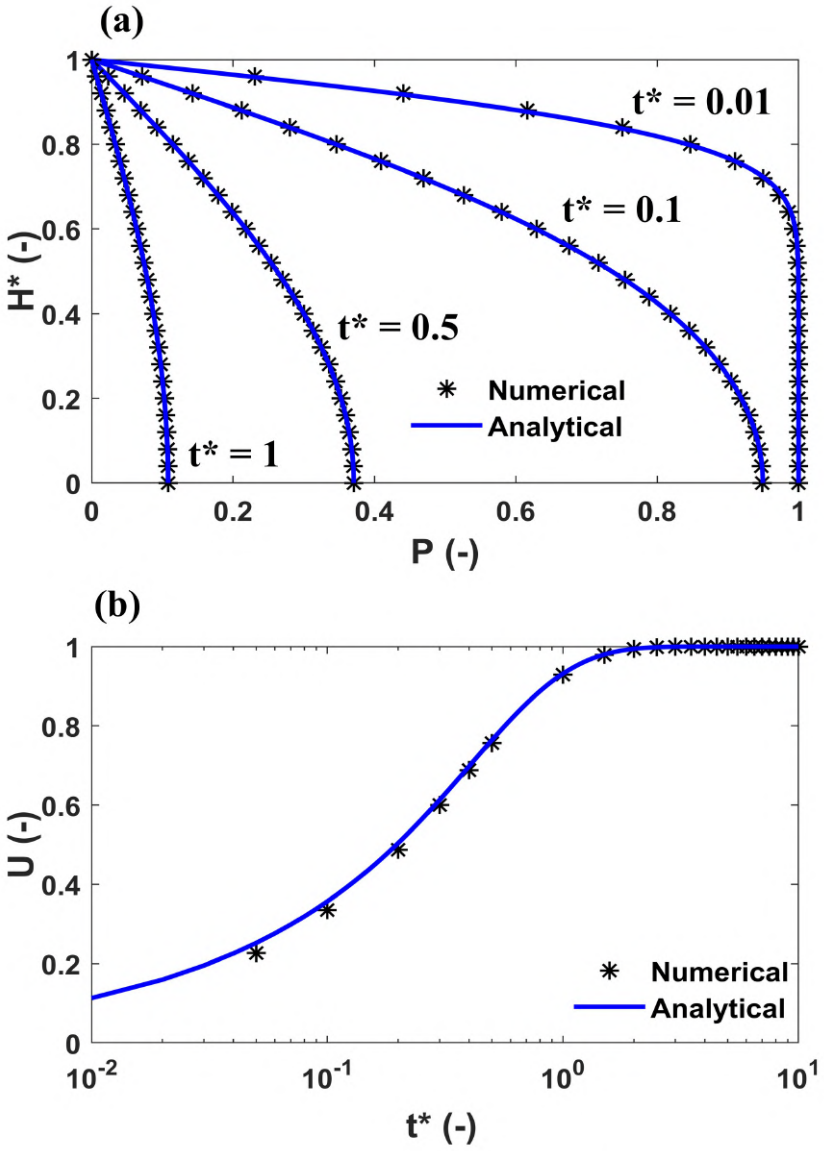

Figure 2.4: The comparison between numerical and analytical solutions of Terzaghi's problem. (a) normalised pore water pressure P with normalised height $H^* = y/H$ at various dimensionless time t^* and (b) degree of consolidation U with dimensionless time t^*.

shows a small value of 3.9×10^{-3}.

2.4.2 Two-dimensional verification

In two dimensions (x- and y-axes) the governing equations of poroelasticity Equations (2.28), (2.29), (2.30), (2.31), (2.32) have the following form

$$\begin{aligned} \frac{\partial \sigma_{xx}}{\partial x} + \frac{\partial \sigma_{xy}}{\partial y} &= 0 \\ \frac{\partial \sigma_{yy}}{\partial y} + \frac{\partial \sigma_{xy}}{\partial x} + \rho g &= 0 \end{aligned} \tag{2.65}$$

$$\begin{aligned} \sigma'_{xx} &= \sigma_{xx} - \alpha p \\ \sigma'_{yy} &= \sigma_{yy} - \alpha p \\ \sigma'_{xy} &= \sigma_{xy} \end{aligned} \tag{2.66}$$

$$\begin{aligned} \sigma'_{xx} &= \frac{E}{(1+\nu)(1-2\nu)}(1-\nu)\epsilon_{xx} + \nu\epsilon_{yy} \\ \sigma'_{yy} &= \frac{E}{(1+\nu)(1-2\nu)}\nu\epsilon_{xx} + (1-\nu)\epsilon_{yy} \\ \sigma'_{xy} &= \frac{E}{(1+\nu)(1-2\nu)}\left(\frac{1-2\nu}{2}\right)\epsilon_{xy} \end{aligned} \tag{2.67}$$

$$\begin{aligned} \epsilon_{xx} &= \frac{\partial u_x}{\partial x} \\ \epsilon_{yy} &= \frac{\partial u_y}{\partial y} \\ \epsilon_{xy} &= \frac{1}{2}\left(\frac{\partial u_x}{\partial y} + \frac{\partial u_y}{\partial x}\right) \end{aligned} \tag{2.68}$$

$$\alpha\frac{\partial \epsilon}{\partial t} + S_s\frac{\partial p}{\partial t} = \nabla \cdot (\kappa \nabla p) \tag{2.69}$$

where σ is the total stress (Pa), σ' is the effective stress (Pa), ρ is the average density of porous medium (kg m^{-3}), g is the acceleration of gravity (m s^{-2}), ν is the Poisson ratio ($-$), α is the effective stress coefficient ($-$), p is the pore water pressure (Pa), E is the Young's modulus (Pa), $\epsilon = \epsilon_{xx} + \epsilon_{yy}$ is the strain ($-$), u is the displacement (m), κ is the hydraulic conductivity (m s^{-1}), S_s is the specific storage (m^{-1}), γ_w is the specific weight of water (N m^{-3}), and t is the time (s).

The verification is conducted by comparing numerical solutions with ana-

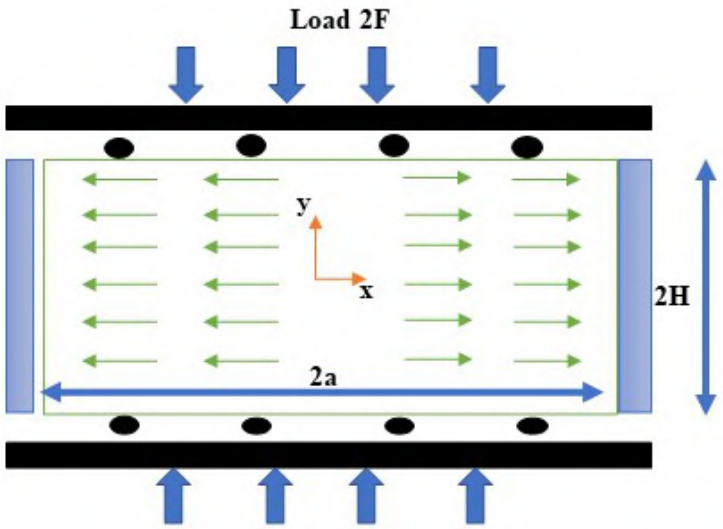

Figure 2.5: Mandel's problem illustration.

lytical solutions from Mandel's problem (Mandel, 1953). Uniform vertical load $2F$ is applied to a rectangular sample through a rigid and frictionless plate of width $2a$ and height $2H$, with drainage to the two sides in lateral condition as shown in Figure 2.5. The deformation of the sample is forced to be an in-plane strain condition, by preventing all deformation in the direction perpendicular to the plane. The pore water pressure distribution will be homogeneous at the instant loading, but when drainage starts, the pore water pressure at two sides, $x = -a$ and $x = a$, is reduced to zero and followed by the pore water pressure in the interior. Because the discharge has only a horizontal component, the pore water pressure, stress and strain are independent of the y-coordinate. Furthermore, $\sigma_{xx} = 0$, $\sigma_{xy} = 0$, u_x is independent of y and u_y is independent of x. Since the problem is symmetric, we solve only the upper right quadrant of the xy plane. I used 441 nodes and 800 elements to generate the simulations. The data for analytical and numerical solutions of this problem are stated in Table 2.2.

The analytical solutions of Mandel's problem for the pore water pressure, horizontal, and vertical displacement are (Cheng and Detournay, 1988;

Table 2.2: Input data for numerical and analytical solutions of Mandel's problem.

Name	**Symbol**	**Value**	**Unit**
Horizontal distance	a	1	m
Consolidation coefficient	c_v	0.17	$\mathrm{m^2\,s^{-1}}$
Force	F	2×10^4	N
Initial value of pore water pressure	p_0	1×10^4	Pa
Bulk modulus	K	1.2×10^8	Pa
Porosity	ϕ	0.375	–
Poisson's ratio	ν	0.2	–
Undrained Poisson's ratio	ν_u	0.5	–
Hydraulic conductivity	κ	1×10^{-5}	$\mathrm{m\,s^{-1}}$
Specific storage	S_s	3.5×10^{-10}	$\mathrm{m^{-1}}$
Skempton's coefficient	B	0.95	–
Shear modulus	G	4×10^7	Pa

Abousleiman et al., 1996)

$$p_0 = \frac{1}{3a} B\,(\,1+\nu_u)\,F \tag{2.70}$$

$$u_{x0} = \frac{F\nu_u x}{2\mu a} \tag{2.71}$$

$$u_{y0} = \frac{F\,(1-\nu_u)\,y}{2\mu a} \tag{2.72}$$

$$p = \frac{2FB(1+\nu_u)}{3a} \sum_{i=1}^{\infty} \frac{\sin\alpha_i}{\alpha_i - \sin\alpha_i\cos\alpha_i} \left(\cos\frac{\alpha_i x}{a} - \cos\alpha_i\right) \exp(-\alpha_i^2 c_v t/a^2) \tag{2.73}$$

$$u_x = \left[\frac{F\nu}{2Ga} - \frac{F\nu_u}{Ga} \sum_{i=1}^{\infty} \frac{\sin\alpha_i\cos\alpha_i}{\alpha_i - \sin\alpha_i\cos\alpha_i} \exp(-\alpha_i^2 c_v t/a^2)\right] x + \frac{F}{G} \sum_{i=1}^{\infty} \frac{\cos\alpha_i}{\alpha_i - \sin\alpha_i\cos\alpha_i} \sin\frac{\alpha_i x}{a} \exp(-\alpha_i^2 c_v t/a^2) \tag{2.74}$$

$$u_y = \left[-\frac{F(1-\nu)}{2Ga} + \frac{F(1-\nu_u)}{Ga} \sum_{i=1}^{\infty} \frac{\sin\alpha_i\cos\alpha_i}{\alpha_i - \sin\alpha_i\cos\alpha_i} \exp(-\alpha_i^2 c_v t/a^2)\right] y \tag{2.75}$$

$$\tan\alpha_i = \frac{1-\nu}{\nu_u - \nu}\alpha_i \tag{2.76}$$

where p is the pore water pressure (Pa), u_x is the horizontal displacement (m), u_y is the vertical displacement (m), F is the force (N), B is the Skempton's coefficient $(-)$, G is the shear modulus (Pa), ν_u is the undrained Poisson's ratio $(-)$, ν is the Poisson's ratio $(-)$, and t is the time (s).

The comparisons between numerical and analytical solutions for Mandel's problem for normalised pore water pressure, normalised horizontal displacement, and normalised vertical displacement are shown in Figure 2.6 at various dimensionless time $t^* = c_v t/a^2$. The mean absolute error for normalised pore water pressure and displacement is small. The first variable, normalised pore water pressure P, has a mean absolute error around 3.8×10^{-3}, 3.8×10^{-4}, and 5.2×10^{-6} at dimensionless time equal to 0.01, 0.1, and 0.5 respectively. For the second variable, normalised horizontal displacement u_x^* , has a mean absolute error around 2.8×10^{-3} and 1.4×10^{-6} at dimensionless time equal to 0.1 and 0.5 respectively. Finally, the mean absolute error of normalised vertical displacement u_y^* is about 1.1×10^{-3} at dimensionless time equal to 0.1 and 5.8×10^{-7} at dimensionless time equal to 0.5.

Mandel's problem has an interesting characteristic, in the centre of the sample the pore water pressure will be higher than the initial pressure for a small time interval. It is shown in Figure 2.6a, the value of normalised pore water pressure at $t^* = 0.01$ and $t^* = 0.1$ is greater than 1. This phenomenon is denoted as the Mandel-Cryer effect, and it occurs due to the deformation and rigid plate conditions producing an additional source term for the pore water pressure distribution (Phillips and Wheeler, 2007; van Duijn and Mikelic, 2021).

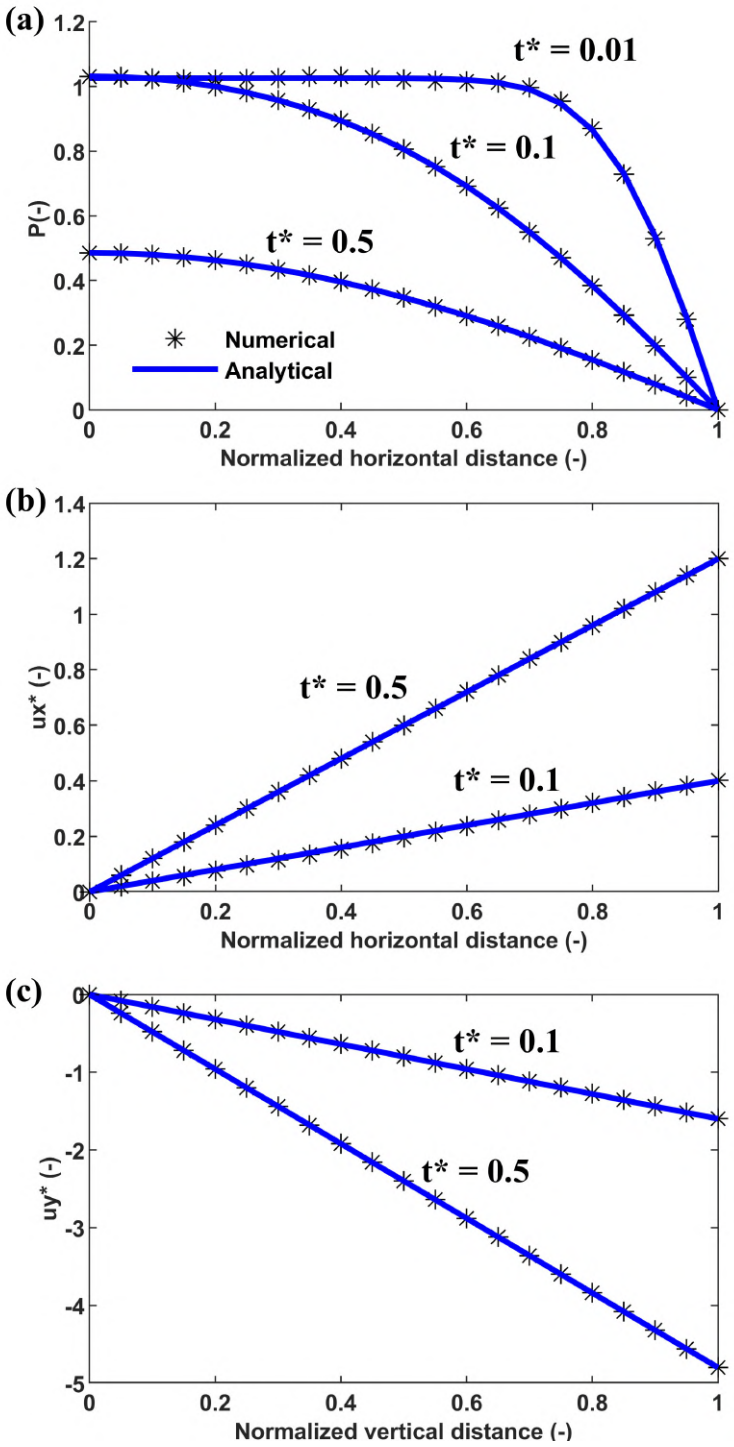

Figure 2.6: Numerical and analytical results of Mandel's problem at various dimensionless times. normalised pore water pressure $P = \frac{p}{p_0}$, normalised horizontal displacement $u_x^* = \frac{u_x}{u_{x0}}$, normalised vertical displacement $u_y^* = \frac{u_y}{u_{y0}}$.

2.4.3 Test case

I simulate the consolidation of a one- and two-dimensional layered porous medium with different physical properties under constant loading. I chose a layered porous medium as the test case because, in general, peatland consists of two layers that have a distinct values of hydraulic conductivity, active porosity, and bulk density (Clymo, 1984; Lewis et al., 2012; Quinton et al., 2000, 2008; Clymo, 2004). Although two layers assumption might be inaccurate representation of the peatland, the simplification offered by this approach is crucial in the early development of the algorithm. The first problem to be considered is the one-dimensional system consisting of two layers with different hydraulic conductivity, active porosity, and Young's modulus, as shown in Table 2.3. The lower boundary is impermeable and rigid, while the upper boundary is fully drained. The boundary conditions at the interface between two layers for the pore water pressure and solid displacement are continuous.

The height of the sample is 1 m, with the first layer starting from 0 m until 0.8 m and the second layer starting from 0.8 m until 1 m (Figure 2.7). I use 101 nodes and 100 elements to generate the simulation with dt equal to 0.1 second. The uniform load with the value of 10 kPa is applied at the top surface, which results in the dissipation of pore water pressure and displacement of solid particles but at a different rate, depending on the layer's physical properties.

At the initial time $t = 0$, the pore water pressure is uniform throughout the sample with the value equal to 1×10^5 Pa. The pore water pressure will start to dissipate at $t = 0^+$ when the load is applied to the top surface and the consolidation process is taking place. The simulation results of the layered sample show a rapid decrease of pore water pressure at the height of 0.8 m

Table 2.3: Input data for one-dimensional layered test case.

Name	**Symbol**	**Value**	**Unit**
Load	F	1×10^4	Pa
Initial value of pore water pressure	p_0	1×10^5	Pa
Hydraulic conductivity first layer	κ_1	1×10^{-7}	$\mathrm{m\,s^{-1}}$
Active porosity first layer	ϕ_1	0.3	–
Young's modulus first layer	E_1	3×10^5	Pa
Specific storage first layer	S_{s1}	1.4×10^{-2}	$\mathrm{m^{-1}}$
Hydraulic conductivity second layer	κ_2	1×10^{-3}	$\mathrm{m\,s^{-1}}$
Active porosity second layer	ϕ_2	0.8	–
Young's modulus second layer	E_2	5×10^5	Pa
Specific storage second layer	S_{s2}	1.4×10^{-2}	$\mathrm{m^{-1}}$

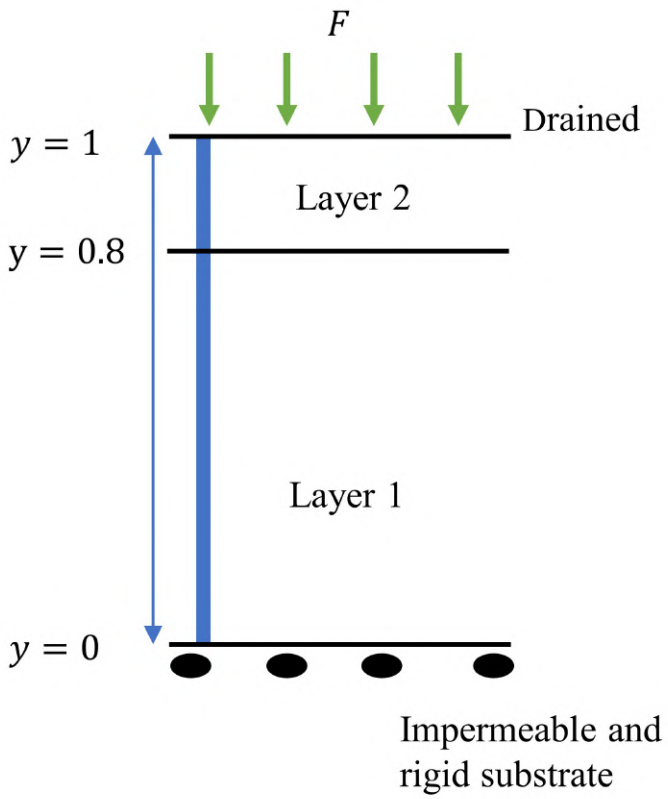

Figure 2.7: The illustration of two layered sample in one dimension. The lower boundary is impermeable and no displacement, while the upper boundary is fully drained. At the height of 0.8 m, which is the transition between first and second layer, the boundary conditions are continuous.

Table 2.4: Input data for two-dimensional layered test case.

Name	**Symbol**	**Value**	**Unit**
Load	F	1×10^4	Pa
Initial value of pore water pressure	p_0	1×10^4	Pa
Hydraulic conductivity first layer	κ_1	1×10^{-7}	$\mathrm{m\,s^{-1}}$
Active porosity first layer	ϕ_1	0.3	–
Young's modulus first layer	E_1	3×10^5	Pa
Specific storage first layer	S_{s1}	1.4×10^{-2}	$\mathrm{m^{-1}}$
Poisson ratio first layer	ν_1	0.2	–
Hydraulic conductivity second layer	κ_2	1×10^{-3}	$\mathrm{m\,s^{-1}}$
Active porosity second layer	ϕ_2	0.8	–
Young's modulus second layer	E_2	5×10^5	Pa
Specific storage second layer	S_{s2}	1.4×10^{-2}	$\mathrm{m^{-1}}$
Poisson ratio second layer	ν_2	0.2	–

due to the transition from the first to the second layer with 10^4 hydraulic conductivity contrast (Figure 2.8). The high hydraulic conductivity value of the second layer leads to more significant water discharge and lower pore water pressure.

In the one-dimensional linear elasticity problem, the solid displacement is only determined by Young's modulus, which represents the stiffness of the material. The material with a higher Young's modulus will experience lower vertical displacement under the same loading. However, in the poroelasticity problem, the changes in pore water pressure provide feedback on the solid displacement through effective stress. My proposed algorithm captures this phenomenon properly. The vertical displacement of the layered sample increases significantly at the height of 0.8 m due to the low pore water pressure, although Young's modulus of the second layer is higher compared to the first layer (Figure 2.8).

The second test case is consolidation in the two-dimensional rectangle system with two layers. Similar to the first test case, I employed different

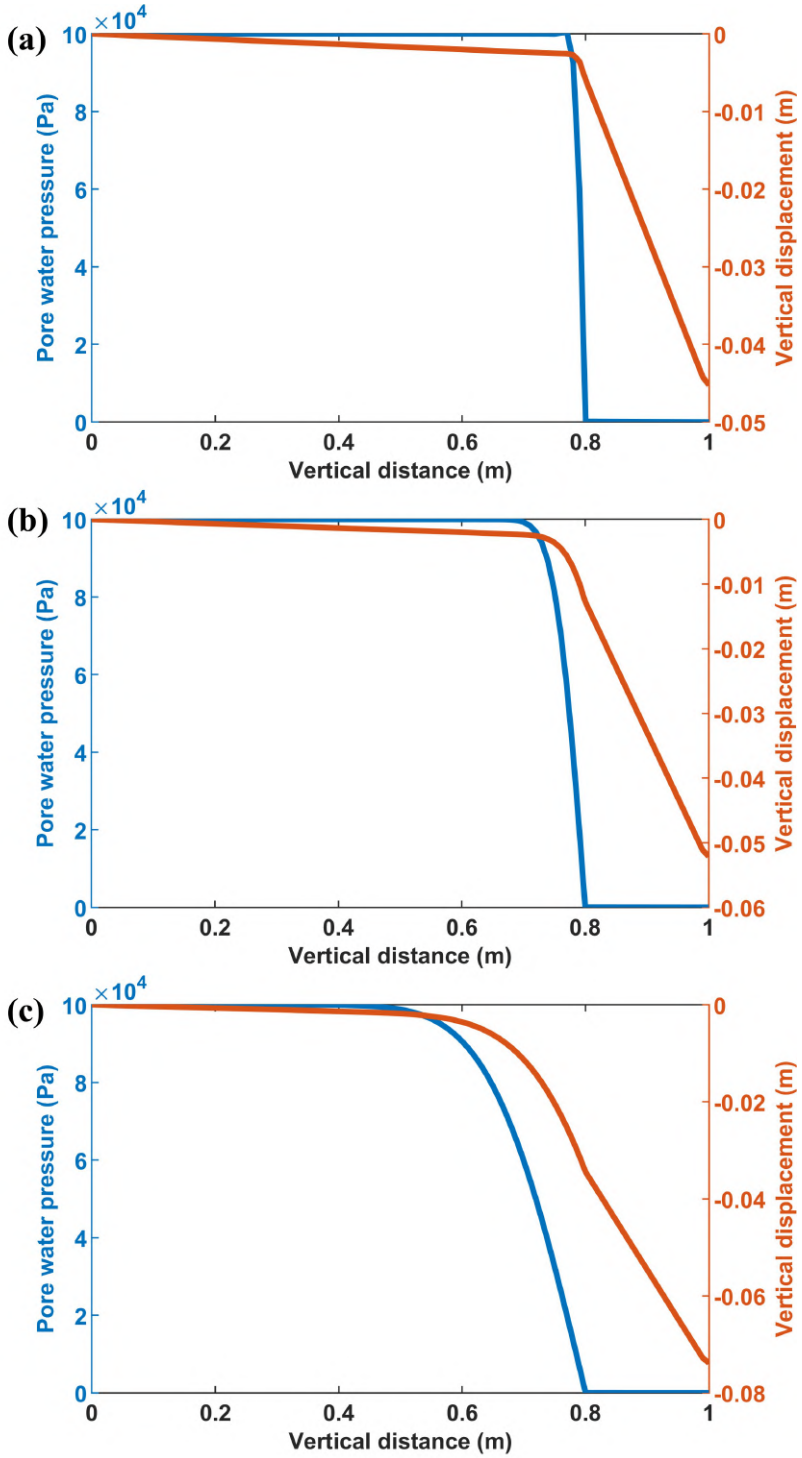

Figure 2.8: The profile of pore water pressure (blue) and vertical displacement (brown) of two layered sample after (a) 100 s, (b) 1000 s, and (c) 10000 s. The layer transition occurs at the height of 0.8 m.

physical properties, including hydraulic conductivity, active porosity, and Young's modulus, summarised in Table 2.4. The system is bounded by an impermeable wall at the bottom, left, and top but fully drained on the

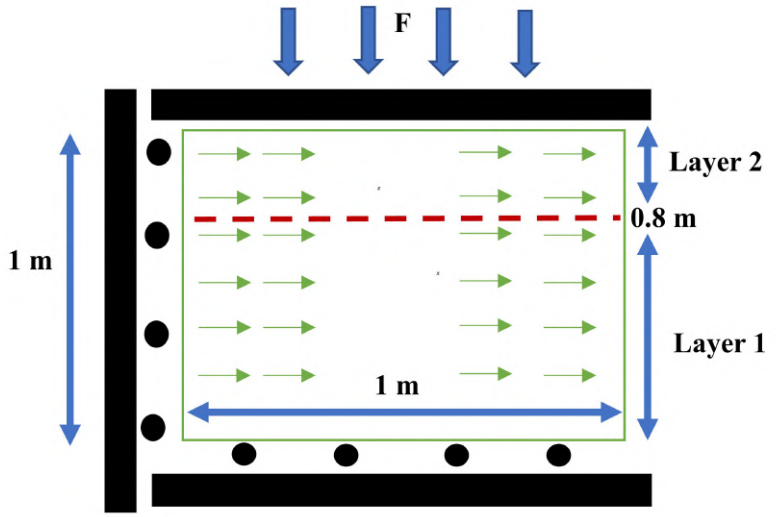

Figure 2.9: The illustration of two layered sample in two dimension. For the fluid boundary, bottom, left and top sides are impermeable, while the right side is fully drained. For the solid boundary, no displacement for the bottom and left, but free to deform at the top and right sides. At the height of 0.8 m, which is the transition between first and second layer, the boundary conditions are continuous. The green arrows indicate the flow of the water.

right side. Therefore, when the load is applied to the top surface, the fluid will start to drain on the right side. The boundary conditions for the solid are no vertical and horizontal displacement at the bottom and left but free to displace at the top and right sides (Figure 2.9).

The sample is 1 $\times$ 1 m, which is divided into 441 nodes and 800 elements with a uniform grid of 0.05 m in the vertical and horizontal direction. Below the height of 0.8 m I used physical properties from the first layer, while above 0.8 m I applied the second layer physical properties. The total time and dt that are used in this simulation are equal to 10000 seconds and 0.1 seconds, respectively. I found that the pore water pressure dropped significantly above 0.8 m due to the high value of hydraulic conductivity of the second layer (Figure 2.10a). Furthermore, the fully drained boundary condition on the right side also produces low pore water pressure in the porous medium. For the solid deformation, the area on the top right side

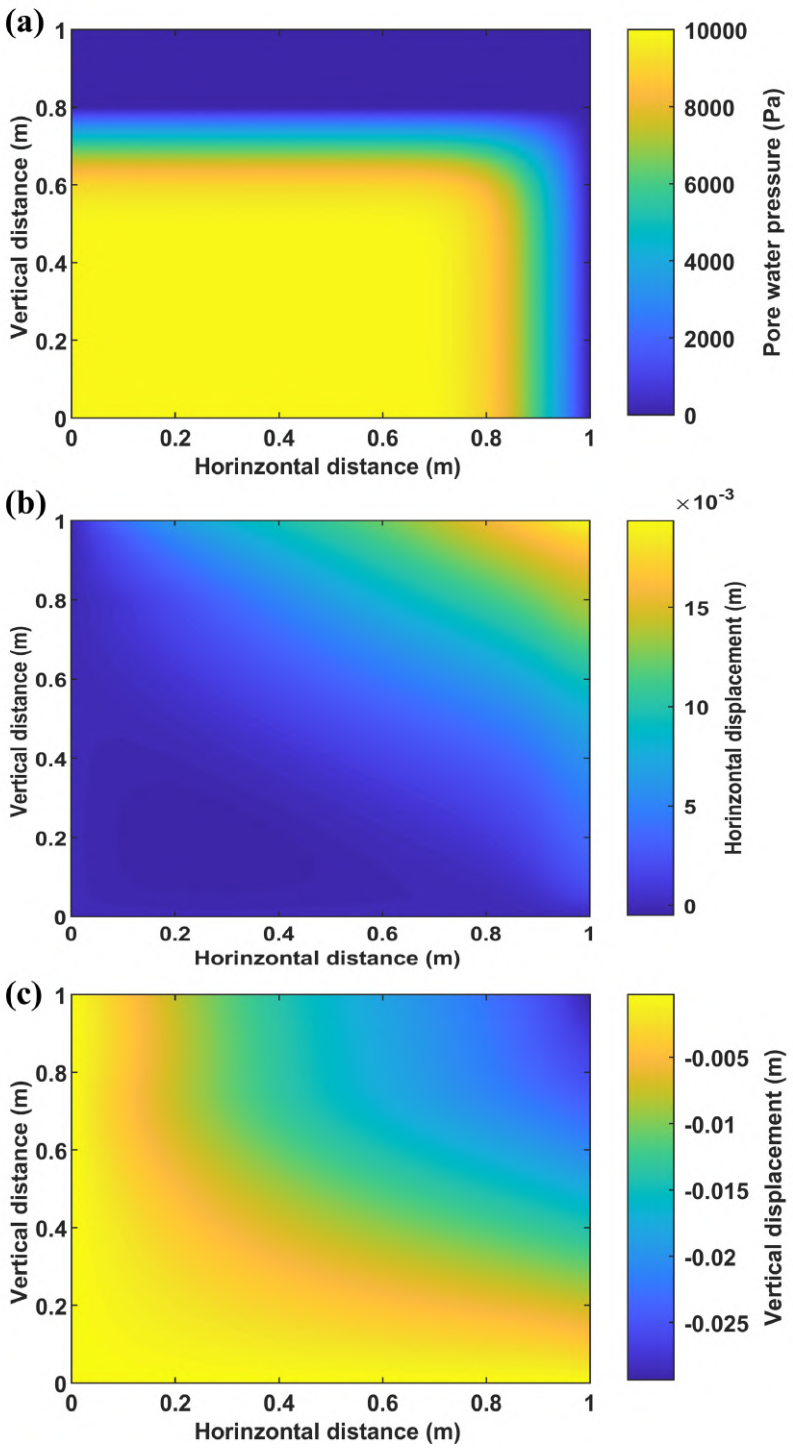

Figure 2.10: (a) The profile of pore water pressure, (b) horizontal displacement, and (c) vertical displacement of the two layered sample after 10000 s. The layer transition occurs at the height of 0.8 m.

experiences maximum deformation in the horizontal (Figure 2.10b) and vertical direction (Figure 2.10c) because of the low pore water pressure together with the boundary conditions of the solid employed in this test case.

The proposed model appropriately solves the consolidation problem of layered systems in one and two dimensions. Although the ratio in hydraulic conductivity between the first and second layers is in order 10^4, the numerical calculation produces stable output for pore water pressure and solid deformation. The small value of mean absolute error between numerical and analytical results in the verification process and the plausible results from numerical test cases under remarkable contrast of hydraulic conductivity confirm the suitability of the proposed model to simulate peatland mechanics.

The mathematical models and numerical solver of poroelasticity explained in this chapter become the essence of the peatland growth model called MPeat, which incorporates fully coupled mechanical, ecological, and hydrological feedback on the peatland. The next chapter provides the formulation of MPeat in one dimension, representing the central column of a peatland.

Chapter 3

A fully coupled mechanical-ecohydrological model of peatland development in one dimension

3.1 Introduction

In this chapter, I propose a model for long-term peatland development incorporating the interactions between mechanical, ecological, and hydrological processes called MPeat in one dimension. The proposed model is formulated via poroelasticity theory, which couples fluid flow and solid deformation, explained in Chapter 2. I employ MPeat to analyse the changes in peat physical properties and to consider the potential implications of mechanical feedback on peatland ecohydrology and carbon stock resilience. The content of this chapter is published in *Ecohydrology* (Mahdiyasa et al., 2022).

Peatlands are complex systems (Belyea, 2009; Belyea and Baird, 2006) with the potential to shift dramatically between equilibrium states in response to environmental change, potentially releasing large quantities of carbon (Jackson et al., 2017; Loisel et al., 2017; Lunt et al., 2019; Yu et al., 2010). One approach to understanding this complex behaviour is through mathematical models that provide insight into the functioning of the peatland system on a wide range of timeframes and particularly beyond the timeframes of direct observation. These mathematical models of peatland development enable us to analyse nonlinear behaviour because of the internal feedback mechanisms (Hilbert et al., 2000; Morris et al., 2011) and the effects of past or future events on peatland carbon storage, for example, climate change (Heinemeyer et al., 2010; Ise et al., 2008; Yu et al., 2001) or drainage (Young et al., 2017).

The most advanced peatland development models are based on ecohydrological processes. For example, the one-dimensional Holocene Peat Model (HPM) (Frolking et al., 2010) groups peatland vegetation into 12 plant functional types (PFTs) based on their characteristics, the quantities of which are determined by the water table depth and nutrient status. Associated with each PFT is a productivity and a decomposition rate, the balance of which determines rates of peat accumulation. The effect of decomposition is tracked for each peat cohort in terms of the remaining mass, which in turn determines the bulk density, hydraulic conductivity, and porosity. DigiBog (Baird et al., 2012; Morris et al., 2012, 2011), a one, two, or three-dimensional peatland development model, is built on a series of coupled ecological and hydrological processes that are divided into plant litter production, decomposition, hydraulic properties, and a hydrological submodel. The hydrological submodel determines water table position and hence litter production and decomposition, which in turn af-

fects hydraulic conductivity. However, bulk density and drainable porosity are held constant. The potential problem with this approach is that HPM, DigiBog, and similar models (e.g., Heinemeyer et al., 2010; Hilbert et al., 2000; Swinnen et al., 2019) ignore the mechanical cause of changes in peat physical properties that have the potential to influence the ecohydrology and peatland resilience. Examples of such mechanical effects that cannot be captured in these models include variable loading of the peat surface as productivity changes, the motion of the peat surface in response to changes in the height of the water table, and mechanical failure of the peat body.

Peat is a mechanically weak, poroelastic material due to its extremely high water content and void ratio with values ranging between 500% - 2000% and 7.5 - 30, respectively (Hanrahan, 1954; Hobbs, 1986, 1987; Mesri and Ajlouni, 2007). As a result, the changes in peat pore structure, which significantly influence hydraulic properties, are not only determined by progressive decomposition (Moore et al., 2005; Quinton et al., 2000) but also compression. Hydraulic conductivity decreases when the water table drops due to the mechanical deformation in the pore structure (Whittington and Price, 2006), an important process that can reduce water discharge from peatland. In a similar way, the enhancement of water input will expand the pore space that leads to an increase in hydraulic conductivity, promoting higher water loss from peatland. Swelling or shrinking of the pore space caused by mechanical deformation leads to the seasonal surface fluctuation, with the magnitude determined by several factors, such as Young's modulus, which is a measure of the stiffness of an elastic material, gas content, and loading effects (Glaser et al., 2004a; Reeve et al., 2013).

The objectives of this chapter are to (1) present a fully coupled mechanical-ecohydrological model of peatland development in one dimension, (2) assess the variations in peat physical properties, including bulk density, active

porosity (pores that actively transmit water (Hoag and Price, 1997)), and hydraulic conductivity, as part of the internal feedback mechanism, (3) analyse the role of mechanical processes on the peatland behaviour.

3.2 Model formulation

MPeat in one dimension is conceptualised as a column of peat at the centre of a peatland with a new layer added every time step. As the peatland develops, its physical properties are affected by the feedback from the mechanical, ecological, and hydrological processes through the coupling between fluid flow and solid deformation, which is known as poroelasticity, and this is the essence of my model (Figure 3.1). Peatland accumulates carbon since peat addition is generally greater than peat decomposition. The rate of decay is high in the unsaturated zone above the water table, while in the saturated zone below the water table, the rate of decay is much lower. Peat that is more decomposed becomes susceptible to deformation because of the decrease in strength and Young's modulus. This deformation affects the structure of pore space, represented by the change in bulk density, active porosity, and hydraulic conductivity. To accommodate this process, I define physical properties functions as follows

$$\rho = \rho(b, u, z) \tag{3.1}$$

$$\phi = \phi(b, u, z) \tag{3.2}$$

$$\kappa = \kappa(\phi) \tag{3.3}$$

$$E = E(\theta) \tag{3.4}$$

where ρ is the bulk density ($\mathrm{kg\,m^{-3}}$), ϕ is the active porosity ($-$), κ is the hydraulic conductivity ($\mathrm{m\,s^{-1}}$), E is the Young's modulus (Pa), b is the

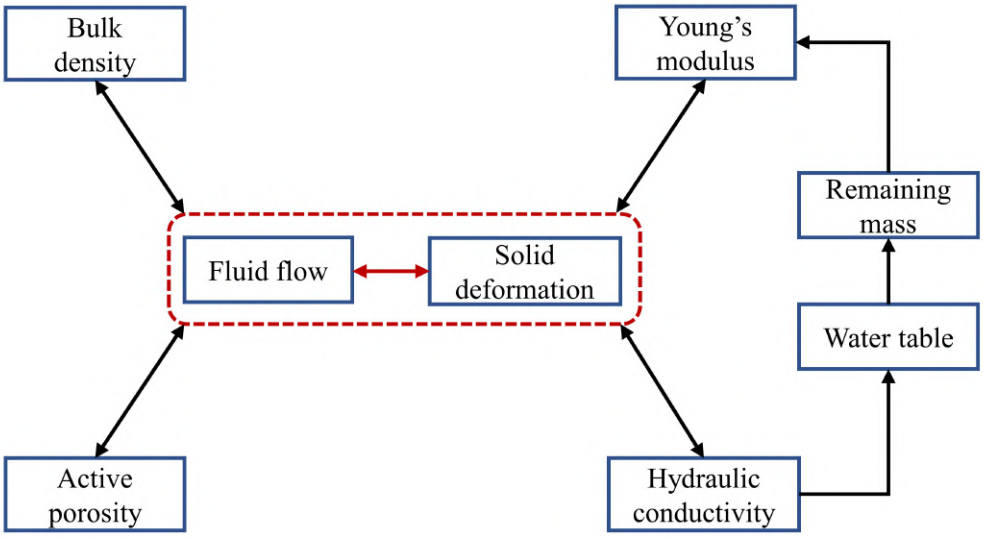

Figure 3.1: Schematic illustration of MPeat explains the interactions between peat physical properties, including bulk density, active porosity, hydraulic conductivity and Young's modulus through the coupling between fluid flow and solid deformation.

peatland height (m), u is the vertical displacement (m), z is the water table depth (m), and θ is the remaining mass ($-$). MPeat is divided into three submodels, mechanical, ecological, and hydrological as explained below.

3.2.1 Mechanical submodel

The mechanical submodel is developed from poroelasticity formulation, which is divided into two categories, i.e., fully saturated and unsaturated, to accommodate the peatland characteristics. The fully saturated poroelasticity is employed to analyse the features of the saturated zone and follows Biot's theory of consolidation (Biot, 1941). For the one-dimensional case and without the influence of body force, the governing equations are summarised as follows

$$\frac{\partial \sigma}{\partial y} = 0 \qquad \text{(2.51 revisited)}$$

$$\sigma' = \sigma - \alpha p \qquad \text{(2.52 revisited)}$$

$$\sigma' = E\epsilon \qquad \text{(2.53 revisited)}$$

$$\epsilon = \frac{\partial u}{\partial y} \qquad \text{(2.54 revisited)}$$

$$\alpha \frac{\partial \epsilon}{\partial t} + S_s \frac{\partial p}{\partial t} = \kappa \frac{\partial^2 p}{\partial y^2} \qquad \text{(2.55 revisited)}$$

where σ is the total stress (Pa), σ' is the effective stress (Pa), ϵ is the strain $(-)$, u is the vertical displacement (m), E is the Young's modulus (Pa), α is the Biot's coefficient $(-)$, p is the pore water pressure (Pa), κ is the hydraulic conductivity ($\mathrm{m\,s^{-1}}$), and S_s is the specific storage ($\mathrm{m^{-1}}$). In this formulation, the vertical head gradient is contained in the pore water pressure, which in turn influences the effective stress. Furthermore, the lower boundary is impermeable and experiences no displacement, while the upper boundary is fully drained.

In the unsaturated zone, water and air occupy the pore space. As the depth of the unsaturated zone is usually less than 0.5 m (Ballard et al., 2011; Ingram, 1982; Swinnen et al., 2019), I assume air pressure equal to atmospheric pressure. By making this assumption, Equation (2.55 revisited) can be extended to represent the unsaturated zone as

$$\alpha_w \frac{\partial \epsilon}{\partial t} + \frac{1}{M_w} \frac{\partial p}{\partial t} = \kappa \frac{\partial^2 p}{\partial y^2} \qquad (3.5)$$

The parameters α_w and M_w depend on the degree of saturation of water

(Cheng, 2020)

$$\alpha_w = S_w \tag{3.6}$$

$$M_w = \frac{\gamma_w(1-\lambda)}{\phi\lambda\mu} S_w^{-1/\lambda} \left(1 - S_w^{1/\lambda}\right)^{\lambda} \tag{3.7}$$

where S_w is the degree of saturation of water $(-)$, γ_w is the specific weight of water $(\mathrm{N\,m^{-3}})$, ϕ is the active porosity $(-)$, λ is the first water retention empirical constant $(-)$, μ is the second water retention empirical constant $(\mathrm{m^{-1}})$, ϵ is the strain $(-)$, p is the pore water pressure (Pa), and κ is the hydraulic conductivity $(\mathrm{m\,s^{-1}})$.

The mechanical submodel is described in terms of a partial differential equation with two independent variables that are space y and time t, while ecological and hydrological submodels only contain time t as an independent variable on their differential equation. To provide a fully coupled model, the space discretisation in the mechanical submodel is obtained from the layer thickness as follows

$$h = \frac{m}{\rho} \tag{3.8}$$

where h is the layer thickness (m), m is the peat mass per unit area $(\mathrm{kg\ m^{-2}})$ and ρ is the bulk density $(\mathrm{kg\ m^{-3}})$.

Mechanical deformation of the peat body cannot be separated from water table depth, peat production, and decomposition. Water table depth determines peat production and plant weight at the top surface (see the Ecological submodel section below), which have a role as load sources. Besides that, water table depth also influences the effective stress because a deeper water table position leads to higher effective stresses and increases deformation. This process reduces the void space and brings the solid par-

ticles into closer contact with one another through vertical displacement, increasing the bulk density and decreasing active porosity

$$\rho_t = \rho_{t-1}\left(\frac{b_{t-1}}{b_{t-1} - u_{t-1}\left(1 + \beta z_{t-1}\right)}\right) \tag{3.9}$$

$$\phi_t = \phi_{t-1}\left(\frac{b_{t-1} - u_{t-1}\left(1 + \beta z_{t-1}\right)}{b_{t-1}}\right) \tag{3.10}$$

where ρ is the bulk density ($\mathrm{kg\,m^{-3}}$), ϕ is the active porosity ($-$), b is the peatland height (m), u is the vertical displacement (m), β is the bulk density and active porosity parameter ($\mathrm{m^{-1}}$), and z is the water table depth (m). The subscripts indicate the updated value of bulk density and active porosity from the previous time. The other factor that affects mechanical deformation significantly is decomposition. Zhu et al. (2020) showed that the decomposition reduces the strength and Young's modulus of dead roots, one of the main constituents of peat fibre. This result leads us to the conclusion that the Young's modulus should decrease as peat decompose. For the initial model, I propose an equation that includes the effect of decomposition on the peat Young's modulus as a linear function

$$E_t = \chi\left(1 + {\theta_t}^{\zeta}\right) \tag{3.11}$$

where E is the Young's modulus (Pa), θ is the remaining mass ($-$), χ is the first Young's modulus parameter (Pa) and ζ is the second Young's modulus parameter ($-$).

3.2.2 Ecological submodel

Peat production follows the equation from Morris et al. (2015), which depends not only on the water table depth but also on the air temperature. This equation is the development of Belyea and Clymo (2001) and can be

written as

$$\psi = \begin{cases} 0.001(9.3 + 133z - 0.022(100z)^2)^2(0.1575Temp + 0.0091) & \text{for } 0 \leq z \leq 0.668 \\ 0 & \text{for } z > 0.668 \end{cases} \tag{3.12}$$

where ψ is the peat production ($\mathrm{kg\,m^{-2}\,yr^{-1}}$), z is the water table depth (m), $Temp$ is the air temperature (°C). Peat production has a strong relationship with above-ground biomass that can be used to model the plant weight at the top surface through the equation and data from Moore et al. (2002). To accommodate the wet condition of the plant that consists of shrub, sedge or herb, and *Sphagnum*, I multiply each type with a constant that is obtained from its water content. Thus, I write the equation for plant weight

$$\Upsilon = c_1 \left(10^{\frac{log_{10}(\psi)+0.409}{0.985}}\right)(1+d_1)\,g + c_2\left(10^{log_{10}(\psi)+0.001}\right)(1+d_2)\,g + (c_3 0.144)(1+d_3)\,g \tag{3.13}$$

where Υ is the plant weight (Pa), ψ is the peat production ($\mathrm{kg\,m^{-2}\,yr^{-1}}$), g is the acceleration of gravity ($\mathrm{m\,s^{-2}}$), c_1, c_2, c_3 are the plant proportions ($-$) and d_1, d_2, d_3 are the constants for plant wet condition ($-$) with the indices 1,2,3 indicating shrub, sedge or herb, and *Sphagnum*, respectively. Besides peat production, the accumulation of mass in the peatland is also influenced by the decomposition process. It occurs in both zones, unsaturated and saturated, but at a different rate. If I assume that the rate of decay is constant at each zone, then the change of mass because of decay can be modelled as (Clymo, 1984)

$$\frac{dm}{dt} = -\eta m \tag{3.14}$$

where m is the mass per unit area ($\mathrm{kg\,m^{-2}}$) and η is the rate of decay ($\mathrm{yr^{-1}}$). Furthermore, the quotient between mass at time t, which has experienced decay, and the initial mass gives us the remaining mass of the peat, or formally

$$\theta_t = \frac{m_t}{m_0} \tag{3.15}$$

where θ is the remaining mass ($-$), m_t is the mass per unit area at time t ($\mathrm{kg\,m^{-2}}$), and m_0 is the initial mass per unit area ($\mathrm{kg\,m^{-2}}$).

3.2.3 Hydrological submodel

The change in active porosity due to compression affects hydraulic conductivity because water cannot move easily as the pore size becomes smaller. Therefore, one of the ways to model the relationship between hydraulic conductivity and active porosity is

$$\kappa_t = \kappa_0 \left(\frac{\phi_t}{\phi_0} \right)^{\xi} \tag{3.16}$$

where κ is the hydraulic conductivity ($\mathrm{m\,s^{-1}}$), κ_0 is the initial value of hydraulic conductivity ($\mathrm{m\,s^{-1}}$), ϕ is the active porosity ($-$), ϕ_0 is the initial value of active porosity ($-$), and ξ is the hydraulic conductivity parameter ($-$). The effect of compression on the peat pore structure depends on Young's modulus, which is a function of decay. Consequently, I can also interpret hydraulic conductivity in Equation (3.16) as an implicit function of decay.

The water table varies over time in response to the internal and external factors, including change in the active porosity, hydraulic conductivity, peatland radius, and net rainfall. I employ the equation from Childs (1969)

(see also Swindles et al. (2012)) to predict the water table height at the centre of the circular peatland

$$\frac{dH}{dt} = \frac{r}{\phi} - \frac{2\kappa H^2}{l^2 \phi} \tag{3.17}$$

where H is the water table height (m), r is the net rainfall (m yr^{-1}), l is the peatland radius (m), ϕ is the active porosity ($-$), and κ is the hydraulic conductivity (m yr^{-1}). The difference between peatland height and water table height at time t result in the water table depth of the peatland, or mathematically

$$z = b - H \tag{3.18}$$

where z is the water table depth (m) and b is the peatland height (m). Water table height cannot exceed peatland height because I assume all the water will flow as surface water over the peatland area.

3.2.4 Numerical formulation and verification

Poroelasticity is used to couple mechanical, ecological, and hydrological submodels through the changes in peat physical properties, including bulk density, active porosity, hydraulic conductivity, and Young's modulus. These changes simultaneously affect the calculations from each submodel. Therefore, in the MPeat, each submodel does not run sequentially to obtain the final results.

I apply the finite element method (e.g., Zienkiewicz et al., 2013) to approximate the solution of the mechanical submodel in which the primary variables are solid displacement and pore water pressure. I compare the numerical solution of a fully saturated case with the analytical solution

of Terzaghi's problem (Terzaghi, 1925, 1943) to validate the finite element algorithm. The proposed algorithm shows good performance indicated by a small error between the numerical and analytical solutions. The highest value of mean absolute error for normalized pore water pressure and degree of consolidation are 2.5×10^{-3} and 3.9×10^{-3}, respectively (see Chapter 2 for the full formulation and verification of the one-dimensional poroelasticity model).

The ecological and hydrological submodels are solved using the finite difference method, which is similar to Morris et al. (2015) but with two main differences. First, the formulation and assumption to calculate the changes in peat physical properties. Second, the influence of air temperature on the decomposition process.

3.3 Model implementation

To illustrate how MPeat works, I simulate peatland vertical growth with a fixed radius and flat substrate for 6000 years using annual time steps. I assume that peat is an elastic material (Waddington et al., 2010), with fluid flow through pore space following Darcy's law. The substrate properties are impermeable and stiff, so at the base layer the peat physical properties are not affected by compression of the substrate. In this model, the load is associated with a surficial peat addition (Equation (3.12)) and plant weight (Equation (3.13)), representing the natural condition of the peatland.

Table 3.1: Symbols and parameter default values for the simulations.

Name	**Symbol**	**Value**	**Unit**	**Reference**
Unsaturated zone decay rate	η_{un}	5×10^{-2}	yr^{-1}	(Clymo, 1984)
Saturated zone decay rate	η_{sa}	8×10^{-5}	yr^{-1}	(Clymo, 1984)
Biot's coefficient	α	1	–	(Terzaghi, 1943)
Bulk density initial value	ρ_0	50	$\mathrm{kg\,m}^{-3}$	(Lewis et al., 2012)
Carbon content	C	0.4	–	(Loisel et al., 2014)
Active porosity initial value	ϕ_0	0.8	–	(Quinton et al., 2000)
Bulk density and active porosity parameter	β	1	m^{-1}	Present study
Hydraulic conductivity initial value	κ_0	1×10^{-2}	$\mathrm{m\,s}^{-1}$	(Hoag and Price, 1995)
Hydraulic conductivity parameter	ξ	15	–	Present study
Degree of saturation of water	S_w	0.4	–	Present study
Water retention empirical constant 1	λ	0.5	–	Present study
Water retention empirical constant 2	μ	0.4	m^{-1}	Present study

Continued on next page

Table 3.1 – *Continued from previous page*

Name	**Symbol**	**Value**	**Unit**	**Reference**
Specific storage	S_s	1.4×10^{-2}	m^{-1}	(Hogan et al., 2006)
Specific weight of water	γ_w	9800	$\mathrm{N\,m}^{-3}$	(Cheng, 2020)
Peatland radius	l	500	m	Present study
Young's modulus parameter 1	χ	2×10^5	Pa	Present study
Young's modulus parameter 2	ζ	0.1	–	Present study
Shrub proportion	c_1	0.61	–	(Moore et al., 2002)
Sedge or herb proportion	c_2	0.09	–	(Moore et al., 2002)
Sphagnum proportion	c_3	0.3	–	(Moore et al., 2002)
Shrub constant	d_1	0.4	–	Present study
Sedge or herb constant	d_2	0.4	–	Present study
Sphagnum constant	d_3	20	–	(McNeil and Waddington, 2003)

I run two groups of simulations based on annual air temperature and net rainfall with the parameter values summarised in Table 3.1. For the first group, I employ constant values for those two variables that are 6 °C and 0.8 $\mathrm{m\,yr}^{-1}$. Although this approach is not realistic, it gives baseline results

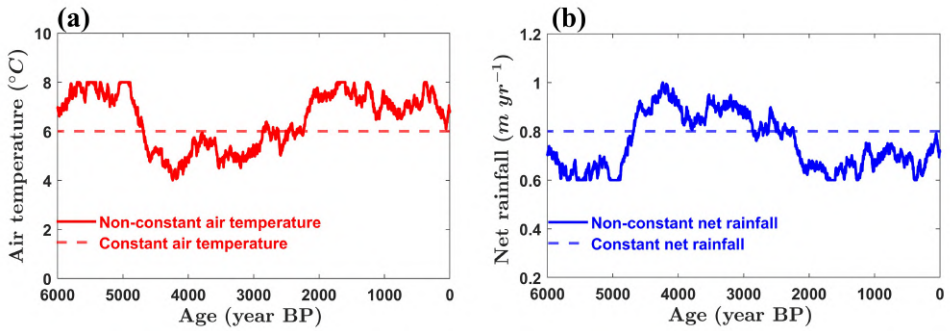

Figure 3.2: The constant and non-constant climate profile over 6,000 years. In the constant case, the value of (a) air temperature and (b) net rainfall are 6 °C and 0.8 m yr^{-1}, while in the non-constant case, the value of air temperature and net rainfall ranging between 4°C−8°C and 0.6m yr^{-1} − 1 m yr^{-1}.

and preliminary information to understand the model. Furthermore, this simplification is crucial for comparison purposes due to the high level of control of the model before proceeding to the next case. In the second group, I simulate the model using a more realistic climate, non-constant annual air temperature and net rainfall, developed from the sinusoidal function with some noise (Figure 3.2). I do not use the climate reconstruction model (e.g., Fischer and Jungclaus, 2011; Mauri et al., 2015; Pauling et al., 2006) because I want to keep it as simple as possible while also maintaining the effect of variable climate on the peatland growth over millennia.

I compare the simulation results of MPeat with DigiBog and HPM for peatland height, cumulative carbon, and water table depth under constant and non-constant climate. DigiBog parameters are obtained from Morris et al. (2015) except for the unsaturated zone decay rate, saturated zone decay rate, and initial bulk density, which are the same as MPeat values. HPM parameters, plant functional types, and formulation, which includes the effect of air temperature, are obtained from Frolking et al. (2010) and Treat et al. (2013), with the potential increase in bulk density $\Delta\rho$ is equal to 50 kg m^{-3}. For all three models, the cumulative carbon is formulated from cumulative organic mass multiplied by 40% of carbon content based

on Loisel et al. (2014).

MPeat sensitivity analysis is conducted by changing the physical properties parameters of the model, i.e., Young's modulus parameters χ and ζ, and hydraulic conductivity parameter ξ. This is because field measurements of the Young's modulus and hydraulic conductivity of peat indicate that they have a wide range of values. I change the value of one parameter and all others remain the same as the baseline value (Table 3.1) for each simulation. Output variables examined from the sensitivity analysis include the value of bulk density, active porosity, hydraulic conductivity, Young's modulus, peatland height, and cumulative carbon.

3.4 Simulation results

3.4.1 Group 1: Constant air temperature and net rainfall

The changes of peat physical properties with respect to depth (Figure 3.3) show that they have similar patterns that are a rapid shift around the depth of the water table, evolving to a relatively constant value in the saturated zone. However, within the saturated zone the trend changes abruptly at depths below 3 m due to the formation of the unsaturated zone about 400 years after peatland initiation (Figure 3.4c, MPeat). In particular, below 3 m the bulk density value decreases dramatically while active porosity, hydraulic conductivity, and Young's modulus values experienced a significant increase.

Comparison of MPeat to DigiBog and HPM (Figure 3.4) illustrates that all models produce similar long-term trends but with a number of key

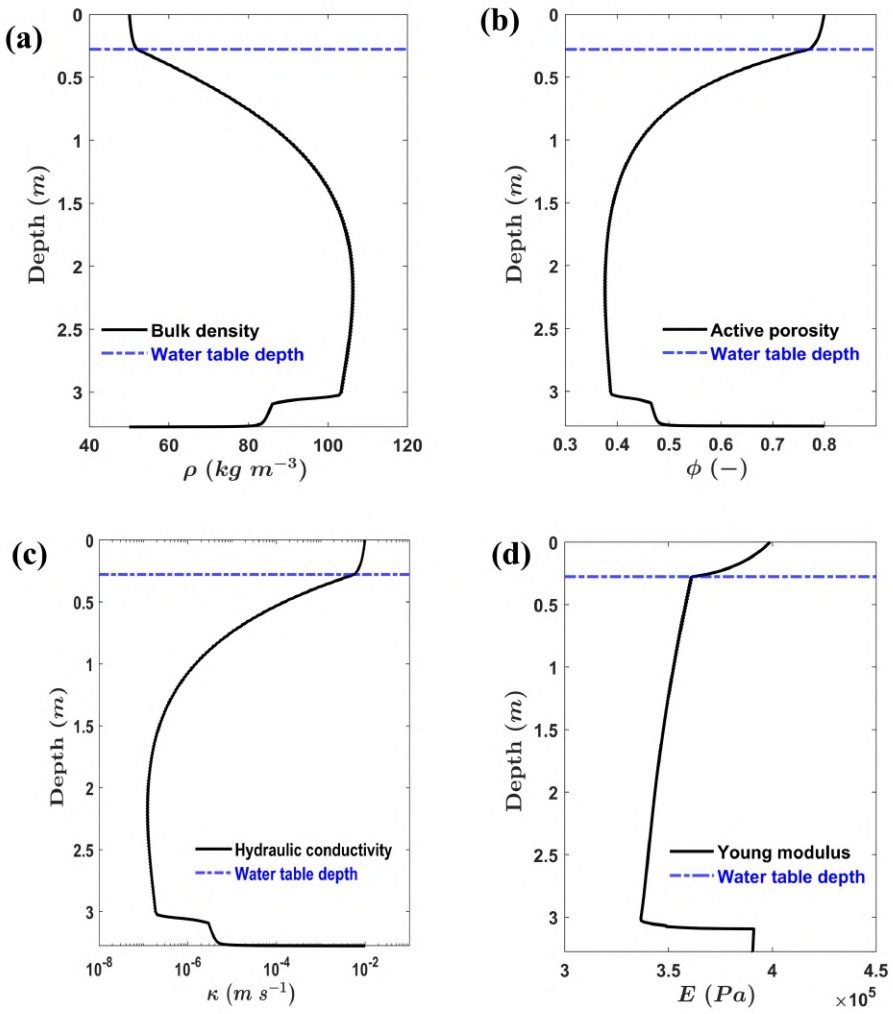

Figure 3.3: The profile of peat physical properties with depth, including (a) bulk density, (b) active porosity, (c) hydraulic conductivity, (d) and Young's modulus after 6,000 simulated years under constant climate.

differences. After 6000 years, peatland height estimated from MPeat (3.27 m) is lower than DigiBog (6.01 m) but relatively similar to HPM (3.25 m). MPeat simulates the highest cumulative carbon (123 kg C m^{-2}) compared to DigiBog (121 kg C m^{-2}) and HPM (120 kg C m^{-2}). MPeat also predicts the water table depth around 0.28 m in the final simulation year, while DigiBog and HPM predict around 0.39 m and 0.29 m, respectively.

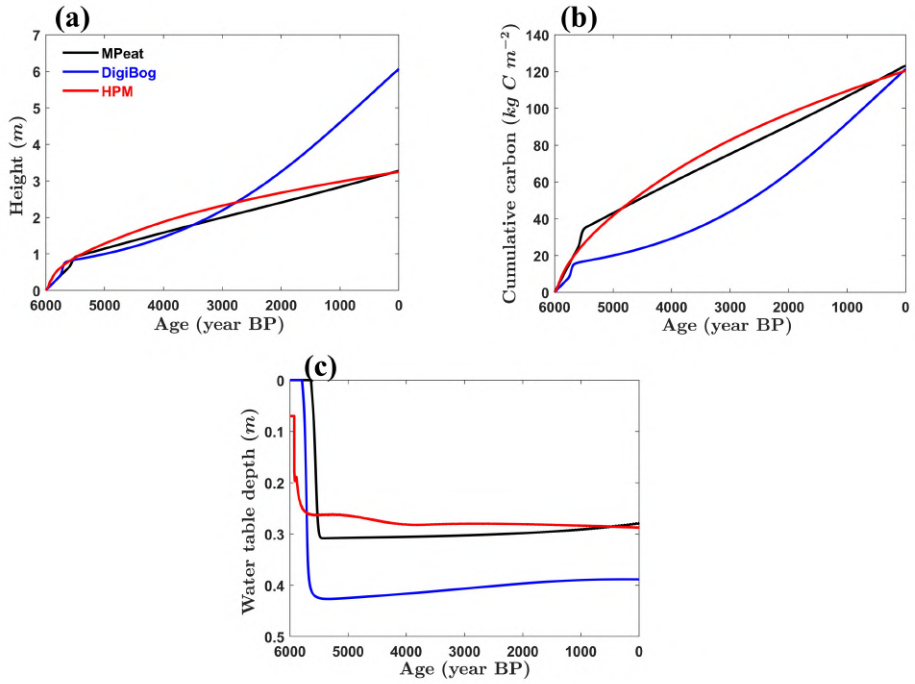

Figure 3.4: The comparison among MPeat, DigiBog, and HPM for (a) peatland height, (b) cumulative carbon, and (c) water table depth under constant climate.

3.4.2 Group 2: Non-constant air temperature and net rainfall

The fluctuations of air temperature and net rainfall provide a significant influence on the peat physical properties in the saturated zone. For example, the decrease in bulk density from 110 to 98 kg m^{-3} at a depth about 2.79 to 2.42 m (Figure 3.5a), and over the same interval, an increase in active porosity (Figure 3.5b) and hydraulic conductivity (Figure 3.5c) from approximately 0.36 to 0.41 and 7.34×10^{-8} to 3.82×10^{-7} m s^{-1} respectively corresponds to an abrupt shift to a cooler and wetter climatic interval around $5000 - 4200$ years BP (Figure 3.2). The opposite patterns of bulk density, active porosity, and hydraulic conductivity occur at a depth about 2.42 to 2.13 m due to a warmer and drier climatic interval around $4200 - 3600$ years BP. The effect of climate change is less pronounced on Young's

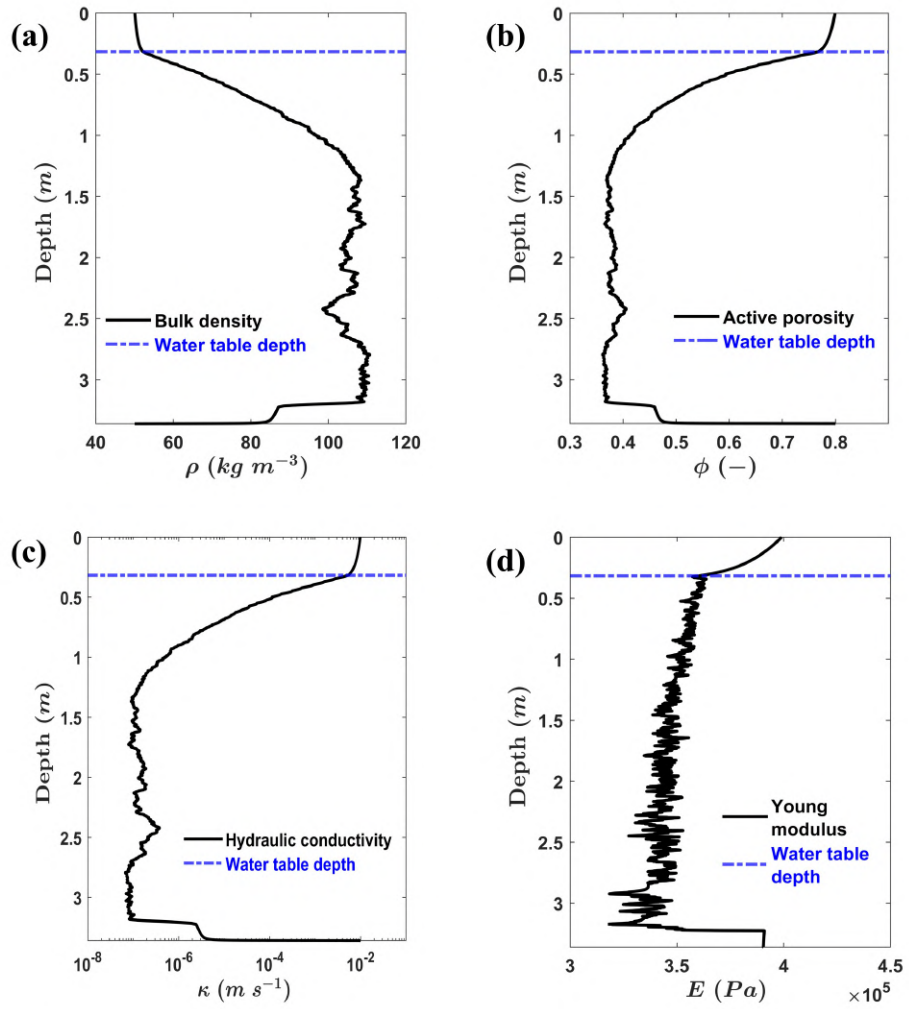

Figure 3.5: The profile of peat physical properties with depth, including (a) bulk density, (b) active porosity, (c) hydraulic conductivity, (d) and Young's modulus after 6,000 simulated years under non-constant climate.

modulus due to its high fluctuations (Figure 3.5d). Young's modulus is controlled solely by the remaining mass, and peatland internal feedback mechanisms are likely to overwrite climate signal preservation contained in the remaining mass.

MPeat estimates lower peatland height than DigiBog (3.36 m vs. 5.99 m) but a greater peatland height than the HPM (3.36 m vs. 2.64 m) after 6000 years (Figure 3.6a). MPeat simulates the highest cumulative carbon (131 kg C m^{-2}), compared to DigiBog (120 kg C m^{-2}) and HPM (98 kg C m^{-2})

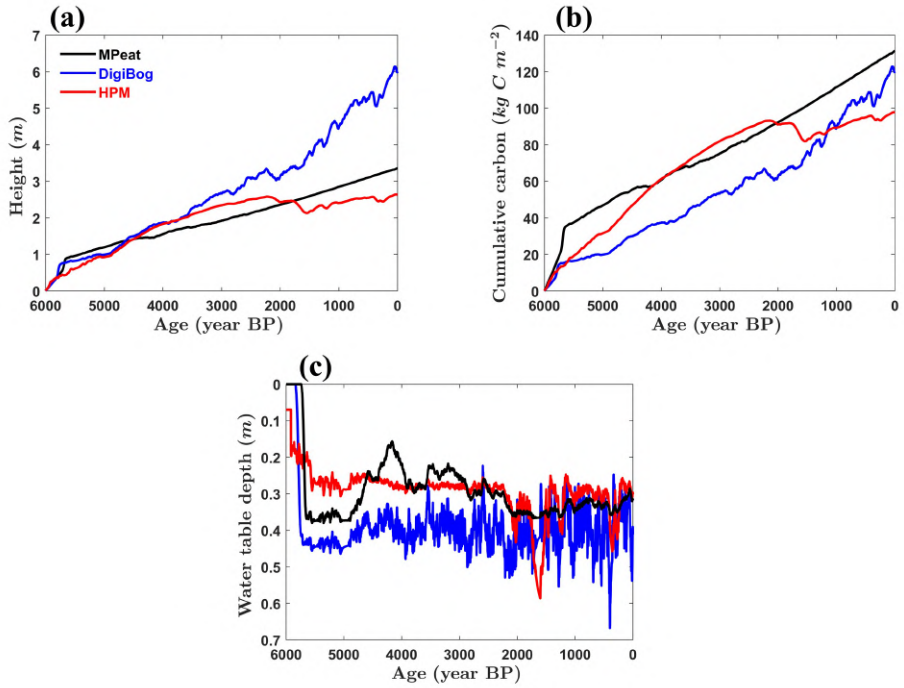

Figure 3.6: The comparison among MPeat, DigiBog, and HPM for (a) peatland height, (b) cumulative carbon, and (c) water table depth under non-constant climate.

(Figure 3.6b), which is similar to those of Group 1. The range of water table depths simulated by MPeat, DigiBog, and HPM are 0.15 to 0.38 m, 0.22 to 0.67 m, and 0.25 to 0.58 m, respectively, without including the initiation time when the unsaturated zone is not well developed (Figure 3.6c). Furthermore, water table depth simulated by DigiBog and HPM experiences sudden increases, particularly in the last 2000 years, increases that are absent from the MPeat simulation. In general, MPeat produces smoother profiles of peatland height, cumulative carbon, and water table depth under non-constant climates.

3.4.3 Sensitivity analysis

Changing Young's modulus parameters (χ and ζ, Equation (3.11)) revealed that the other physical properties as well as peatland height and cumula-

tive carbon, are affected by the initial parameters that determine Young's modulus. Under constant climate (Figure 3.7), increasing the first Young's modulus parameter χ to 3×10^5 Pa resulted in a higher Young's modulus value to the range of $5 \times 10^5 - 6 \times 10^5$ Pa, which in turn reduced the bulk density to $50 - 81$ kg m^{-3} but increased the active porosity and hydraulic conductivity to the interval of $0.49 - 0.8$ and $6.65 \times 10^{-6} - 1 \times 10^{-2}$ m s^{-1}, respectively. A stiffer peat is less affected by compression, which leads to lower water retention due to higher hydraulic conductivity. Therefore, by increasing χ to 3×10^5 Pa, peatland height and cumulative carbon decreased by about 16% and 33% compared to the baseline value after 6000 years (Figure 3.4, MPeat). On the other hand, increasing the second Young's modulus parameter ζ to 0.15 resulted in the lower Young's modulus ($3 \times 10^5 - 4 \times 10^5$ Pa) and consequently higher bulk density ($50 - 111$ kg m^{-3}) but lower active porosity ($0.36 - 0.8$) and hydraulic conductivity ($6.32 \times 10^{-8} - 1 \times 10^{-2}$ m s^{-1}). These conditions increased the peatland height and cumulative carbon by about 2% and 6% in the final simulation year.

Under non-constant climate (Figure 3.8), the influence of parameters χ and ζ on the output variables are similar to the constant climate case. Increasing χ to 3×10^5 Pa resulted in the lower bulk density ($50 - 84$ kg m^{-3}) but higher active porosity ($0.47 - 0.8$) and hydraulic conductivity ($4.04 \times 10^{-6} - 1 \times 10^{-2}$ m s^{-1}). As a consequence, peatland height and cumulative carbon were reduced by about 17% and 34%compared to the baseline value after 6000 years (Figure 3.6, MPeat). Changing ζ to 0.15 increased bulk density ($50 - 115$ kg m^{-3}) but decreased active porosity ($0.35 - 0.8$) and hydraulic conductivity ($3.73 \times 10^{-8} - 1 \times 10^{-2}$ m s^{-1}), which in turn resulted in higher peatland (3.42 m) and cumulative carbon (139 kg C m^{-2}) after 6000 years.

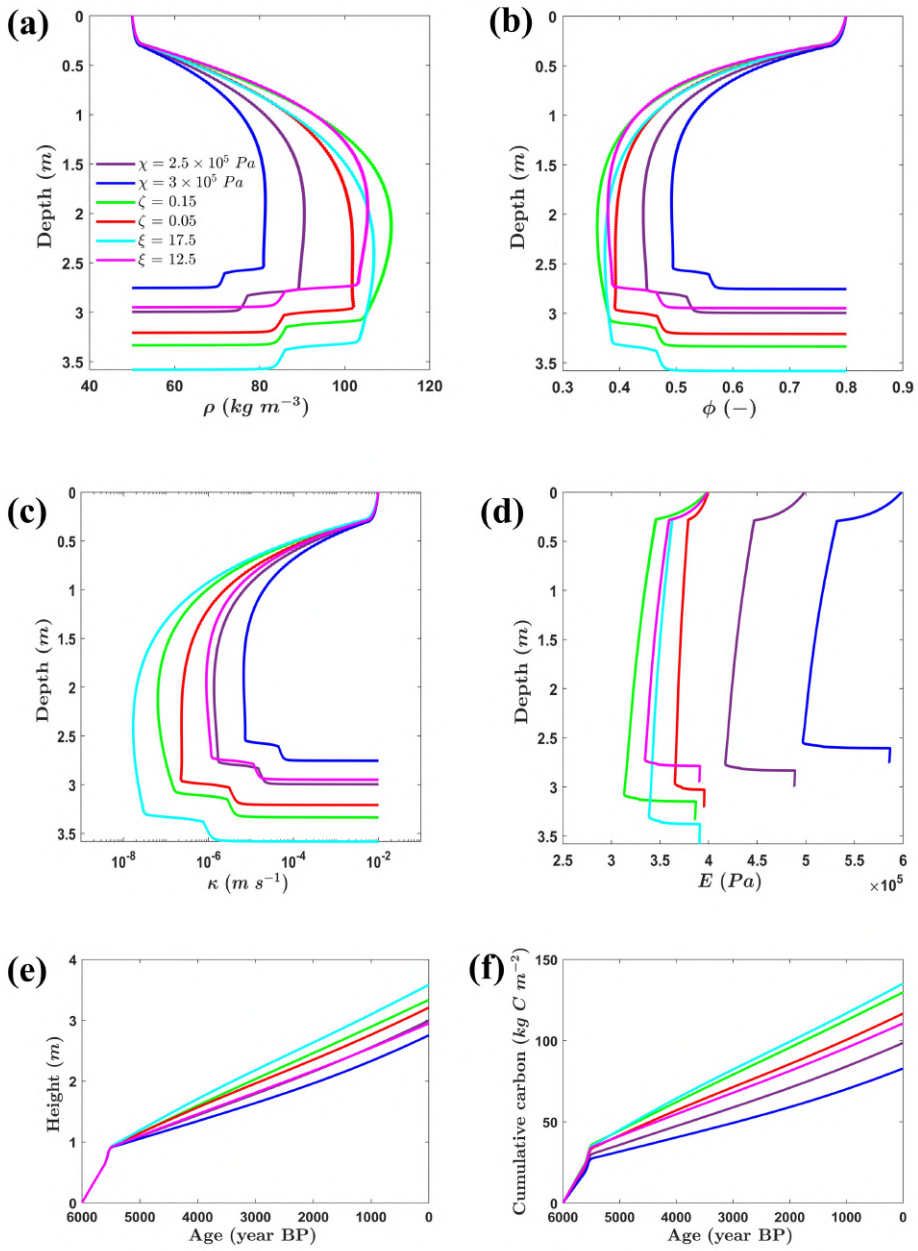

Figure 3.7: MPeat sensitivity analysis with the output variables including (a) bulk density ρ, (b) active porosity ϕ, (c) hydraulic conductivity κ, (d) Young's modulus E , (e) peatland height, and (f) cumulative carbon by changing the values of Young's modulus parameters χ and ζ, and hydraulic conductivity parameter ξ under constant climate. In the base runs (Figure 3.3 and Figure 3.4, MPeat) $\chi = 2 \times 10^5$ Pa, $\zeta = 0.1$, and $\xi = 15$.

The hydraulic conductivity parameter (ξ, Equation (3.16)) controls the decline of the hydraulic conductivity value as the active porosity becomes smaller due to the compression. Under constant climate, decreasing ξ to 12.5, which was associated with an increase in hydraulic conductivity value

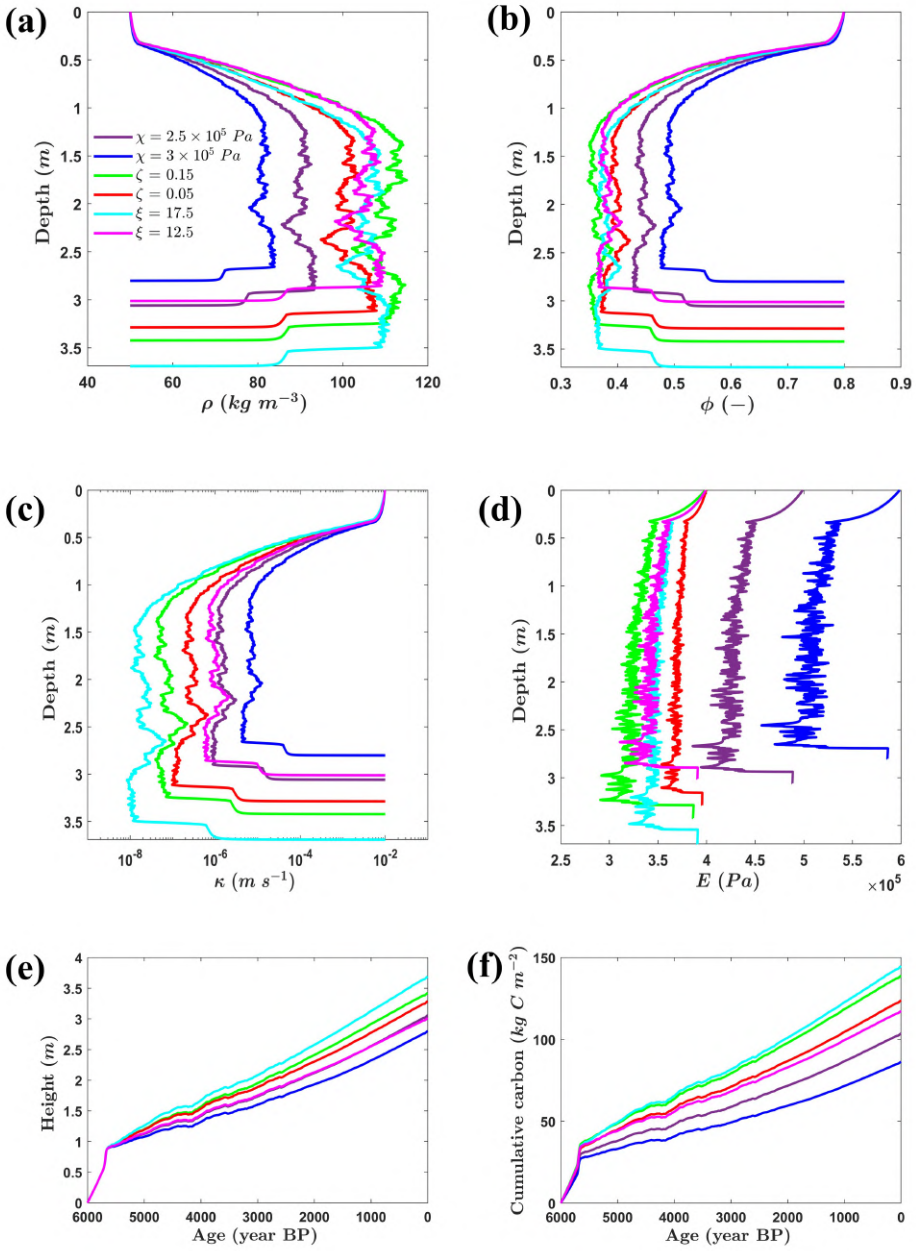

Figure 3.8: MPeat sensitivity analysis with the output variables including (a) bulk density ρ, (b) active porosity ϕ, (c) hydraulic conductivity κ, (d) Young's modulus E , (e) peatland height, and (f) cumulative carbon by changing the values of Young's modulus parameters χ and ζ, and hydraulic conductivity parameter ξ under non-constant climate. In the base runs (Figure 3.6 and Figure 3.7, MPeat) $\chi = 2 \times 10^5$ Pa, $\zeta = 0.1$, and $\xi = 15$.

to the range of $8.80 \times 10^{-7} - 1 \times 10^{-2}$ m s^{-1}, reduced the peatland height by about 0.33 m and resulted in about 13 kg C m^{-2} lower cumulative carbon compared to the baseline value after 6000 years. Under non-constant climate and ξ equal to 12.5, hydraulic conductivity increased to interval

$5.28 \times 10^{-7} - 1 \times 10^{-2}$ m s^{-1}, which reduced peatland height and cumulative carbon by about 0.35 m and 14 kg C m^{-2} in the final simulation year. However, changing ξ had little impact on the other physical properties.

3.5 Discussion

My results illustrate the influence of poroelastic deformation on the ecohydrological processes that lead to peat accumulation. As expected (Fenton, 1980; Quinton et al., 2000; Waddington et al., 2010; Whittington and Price, 2006), the most significant compaction in my model occurs at the transition from the unsaturated to the saturated zone. At this transition, peat experiences high effective stress due to unsaturated conditions. This results in the collapse of the pore structure, increasing bulk density and decreasing active porosity and hydraulic conductivity. The condition is different in the saturated zone where pore water pressure reduces the effective stress generating a relatively stable value of the physical properties (Figure 3.3a, 3.3b, and 3.3c). This finding is in line with expectations and field measurement from Price (2003), who observes that effective stress decreases substantially below the water table.

Because most of the mechanical deformation occurs in the unsaturated zone, MPeat illustrates how water table depth has a considerable impact on the peat physical properties. During warming and drying climatic events, as depth to the water table increases, the value of bulk density increases and active porosity and hydraulic conductivity decline (Figure 3.5a, 3.5b, and 3.5c). As observed in the field (Price et al., 2003), this mechanical behaviour acts to reduce water loss and increase drought resilience. In addition, compression also reduces peat volume, causing the peatland surface

to drop. This drop in the peat surface acts to maintain the relative position of the water table, which in turn helps sustain PFTs associated with wet surface conditions (Schouten, 2002; Waddington et al., 2015). Conversely, a water surplus condition in the cooling and wetting period raises the water table, expands pore space, and decreases effective stress. This condition reduces bulk density and increases active porosity and hydraulic conductivity, leading to lower water retention and raising drainage potential. Such variations in peat physical properties within the saturated zone are routinely observed in cores and measured as dry bulk density. MPeat, therefore, has the capacity to model peat bulk density profiles in a way that can be compared to and complement other paleoclimatic indicators.

3.5.1 Comparison to other ecohydrological models

MPeat, DigiBog, and HPM provide similar long-term trends of peatland development, which indicates they are capable of describing the general evolution of a peatland, including the changes in height, cumulative carbon, and water table depth. However, they have essential differences. The key difference between MPeat and DigiBog is the absence of poroelasticity (Table 3.2). In effect, DigiBog models a stiff peat in which the unsaturated zone cannot deform. This absence of dynamic expansion and compaction have the greatest consequence under a variable climate, with DigiBog sustaining a thicker unsaturated zone and consequently greater peat thickness and less cumulative carbon (Figure 3.6). To some extent, these discrepancies can be reduced by adjusting the parameter and initial values, particularly the bulk density that significantly affects peat thickness and carbon accumulation.

The difference between MPeat and HPM (Table 3.2) primarily occurs due

Table 3.2: The differences in approach for modelling peat physical properties among MPeat, DigiBog and HPM.

MPeat	**DigiBog**	**HPM**
Bulk density is a function of fluid flow and solid deformation.	Bulk density is a constant.	Bulk density is a function of remaining mass.
Active porosity is a function of fluid flow and solid deformation.	Drainable porosity is a constant.	Porosity is a function of peat bulk density and particle bulk density of organic matter.
Hydraulic conductivity is a function of active porosity.	Hydraulic conductivity is a function of remaining mass.	Hydraulic conductivity is a function of peat bulk density.
Young's modulus is a function of remaining mass.	–	–

to the empirical relationship used by HPM to predict the change in bulk density as a function of remaining mass (Frolking et al., 2010). Consequently, the HPM is also an inherently stiffer model and as it evolves under a variable climate, tends to predict similar or deeper water tables and less cumulative carbon than MPeat. The empirical relationships used by HPM, therefore, limit our understanding of mechanical feedback mechanisms.

A final point of difference between the three models is that under variable climate, the outputs from MPeat are smoother than either DigiBog or HPM (Figure 3.6). This smoothness is a consequence of the mechanical buffering inherent to the poroelastic response to changes in excess precipitation and illustrates the potential importance of mechanics in maintaining the resilience of peatland systems. These results are in agreement with a study from Nijp et al. (2017), indicating that the inclusion of moss water storage and peat volume change because of mechanical deformation increase the projection of peatland drought resilience.

It can therefore be concluded that mechanical processes play a vital role

in the peatland carbon stock (Figure 3.9). Compression provides negative feedback to an increasing water table depth (Waddington et al., 2015), which leads to the shorter residence time of organic matter in the unsaturated zone, increasing rates of carbon burial and reducing CO_2 emissions. The experiment from Blodau et al. (2004) corroborates this view and indicates that the production rate of CO_2 rises substantially with an increasing water table depth.

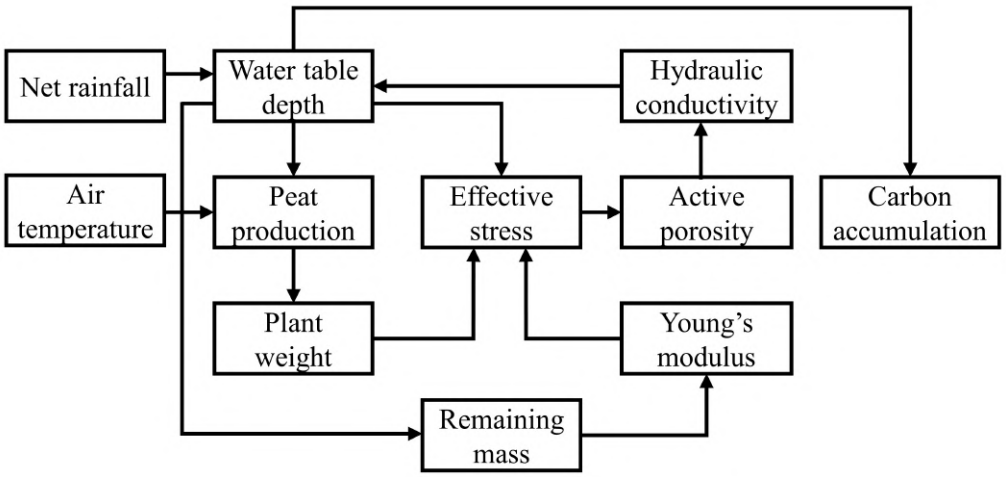

Figure 3.9: Overview of the influence of mechanics on peatland ecohydrology and carbon stock resilience to the external perturbations, including the changes in net rainfall and air temperature.

3.5.2 Comparison with field measurement

A considerable uncertainty in the MPeat model is Young's modulus which in turn has the ability to influence the other physical properties as shown in the sensitivity analysis. Values of Young's modulus of peat are hard to measure in-situ and laboratory determined values are of questionable applicability in the field. For example, Dykes (2008) measured Young's modulus of Irish peat and obtained values ranging from 1.15×10^3 to 3.5×10^3 Pa and concluded that these very low values might be correlated with sample

preparation that affected the strain measurement. As MPeat simulations evolve, Young's modulus values range between 2.9×10^5 and 6×10^5 Pa, far higher than the values provided by Dykes (2008). Nonetheless, according to Mesri and Ajlouni (2007), the ratio between Young's modulus with undrained shear strength lies in the range $20 - 80$, and the reported data for undrained shear strength is in the range of $4 \times 10^3 - 2 \times 10^4$ Pa, depending on the degree of humification and water content (Boylan et al., 2008; Long, 2005). Therefore, the plausible range of peat Young's modulus is $8 \times 10^4 - 1.6 \times 10^6$ Pa, the range value that is used in MPeat. As to the effect of decay on the Young's modulus of peat, this remains unknown beyond the expectation that decay should reduce elasticity within the range of reported values.

Some reassurance that the initial values of Young's modulus chosen in MPeat and subsequent values generated via decay are reasonable come from the comparison of the range of modelled and observed physical properties. Reported measurements of active porosity decrease with depth from as high as 0.8 near the top of the unsaturated zone to as low as 0.1 in the saturated zone (Hoag and Price, 1997; Quinton et al., 2000, 2008; Siegel et al., 1995), similar to the MPeat active porosity pattern and values that range from 0.8 in the unsaturated zone to 0.34 in the saturated zone. Dry bulk density and hydraulic conductivity calculated in MPeat are between $50 - 115$ kg m^{-3} and $8.42 \times 10^{-9} - 1 \times 10^{-2}$ m s^{-1} broadly in line with reported measurements of dry bulk density and hydraulic conductivity around $30 - 120$ kg m^{-3} and $7 \times 10^{-9} - 1.6 \times 10^{-2}$ m s^{-1} (Clymo, 1984, 2004; Fraser et al., 2001; Hoag and Price, 1995; Hogan et al., 2006). Moreover, a considerable increase of hydraulic conductivity at the base of the peat profile obtained from MPeat, corresponding to peat accumulation under fully saturated conditions, is similar to some field observations (Clymo, 2004; Kneale, 1987;

Waddington and Roulet, 1997). However, a notable difference between the modelled and measured peat physical properties is that the range of dry bulk densities generated by MPeat in the saturated zone is narrower than the range typically observed in many peat deposits. The most likely explanation for this is the constant initial value of Young's modulus, which in reality will vary depending on PFT, with woody stemmed shrubs having a greater initial value than moss.

I have discussed the important function of mechanical-ecohydrological feedback in enhancing peatland resilience and sustaining peatland carbon stock in the face of climate change through the MPeat simulations. In the next chapter, MPeat is employed to analyse the consequences of coupling between peat stiffness with vegetation on a nonequilibrium condition of the peatland. This coupling might generate a critical drying threshold below which shrub would become dominant, increasing stiffness in the peat and potentially acting as positive feedback on carbon emissions. Moreover, this condition could be a natural threshold or tipping point in peatland evolution.

Chapter 4

Modelling the influence of mechanical-ecohydrological feedback on the nonlinear dynamics of peatlands

4.1 Introduction

In this chapter, I explore the consequences of coupling between peat stiffness and plant functional types for nonequilibrium models of peatland dynamics in multiple timeframes by developing MPeat in one dimension, described in Chapter 3. Plant functional types are assumed to be a mix of *Sphagnum*, sedge, and shrub, as equations exist to calculate the exact composition of this mixture relative to water table depth. This chapter highlights the possible importance of mechanical-ecohydrological feedback and, in particular, the role of the coupling between the proportion of plant functional types, peat Young's modulus, plant weight, and water table po-

sition in influencing peatland regime shifts, critical thresholds or tipping points, and both short- and long-term peatland dynamical behaviour. The content of this chapter is published in *Ecological Modelling* (Mahdiyasa et al., 2023).

Peatland behaviour is affected by the interplay between positive (destabilising) and negative (stabilising) feedback from internal and external factors. These feedbacks lead to nonlinear dynamics, which in turn create the possibility of peatlands having more than one equilibrium state and experiencing abrupt shifts to alternative states with fundamental differences in characteristics and structures (Belyea, 2009; Belyea and Baird, 2006; Hilbert et al., 2000). Understanding the nonlinear dynamics of peatlands, and in particular tipping points, is important because of the possibility that a sudden shift in behaviour could release a large amount of carbon stored in the peatland (Berg et al., 2009; Jackson et al., 2017; Loisel et al., 2017; Lunt et al., 2019; Yu et al., 2010), or may put the peatland into a less resilient state, with consequences for the global carbon cycle (Chaudhary et al., 2020; Dise, 2009; Kleinen et al., 2012).

Models of nonlinear peatland dynamics (e.g., Baird et al., 2012; Frolking et al., 2010; Heinemeyer et al., 2010; Morris et al., 2012, 2015, 2011; Swindles et al., 2012; Yu et al., 2001) take an ecohydrological approach and assume constant or partial changes of peat physical properties within an equilibrium condition. For example, Hilbert et al. (2000) proposed the bistability of both wet and dry peatland states potentially coexist through the nonlinear interactions between water balance and mass accumulation. Hilbert et al. (2000) also propose a tipping point could arise due to slight variability in water input, which leads to the change in peatland behaviour from carbon sink to carbon source. Similarly, van der Velde et al. (2021) developed a model to analyse regime shifts across biomes, from peatland to

forest, indicating bistability conditions and major release of carbon when the switch occurs. Both Hilbert et al. (2000) and van der Velde et al. (2021) use the peatland water budget as the primary variable to determine the critical threshold before the regime shifts take place. However, peatland internal feedback mechanisms that can maintain the water budget are not considered and are sources of uncertainty in their models. In particular, these models ignore mechanical feedback, and the equilibrium assumption is not realised in peatlands where sustained growth continually changes the ecology, hydrology, and mechanics of the peatland system.

MPeat (Mahdiyasa et al., 2022) is a model of peatland dynamics that incorporates mechanical, ecological, and hydrological feedback through the coupling between fluid flow and solid deformation, which is known as poroelasticity (Biot, 1941; Coussy, 2004; de Boer, 2000; Detournay and Cheng, 1993; Wang, 2000). MPeat simulates the changes in Young's modulus that lead to mechanical deformation as a function of the decomposition process (Chapter 3). However, the effect of mechanical deformation on the peat pore structure is also affected by plant functional types (PFT). Whittington et al. (2007) found that peatland sites dominated by shrub experience limited compressibility, leading to lower hydraulic conductivity reduction when the water table drop. These conditions allow rapid water discharge from the peatland, promoting drier conditions and maintaining the dominance of the shrub. In contrast, sites dominated by sedge or *Sphagnum* have a better ability to expand or shrink, which keeps the relative position of the water table close to the surface and supports the growth of these plant communities. Therefore, stiffer peat dominated by shrubs could become a dry attractor, while softer peat with sedge or *Sphagnum* dominance has the possibility to turn into a wet attractor.

The objectives of this chapter are to (1) present a model of peatland dy-

namics that incorporates the feedback between mechanical processes and plant functional types, (2) investigate the peatland regime shifts and tipping points in a growing system accounting for fully coupled mechanical-ecohydrological feedback, (3) analyse both short- and long-term nonlinear dynamics of the peatland.

4.2 Methods

I based my model on MPeat, explained in Chapter 3, because it includes feedback between mechanical, ecological, and hydrological processes as the peatland develops and adapts it by introducing fundamental changes in the formulation of peat stiffness and plant weight at the top surface. This was necessary as the initial formulation of MPeat does not take into account the influence of plant functional types (PFT) on the peat stiffness and assumes a constant proportion of PFT during the simulation, which significantly affects the total plant weight that acts as the source of loading. By doing this, I am able to use a modified version of MPeat to consider the interactions between Young's modulus, PFT proportion, plant weight, and water table position (Figure 4.1). As most of the MPeat formulations remain unchanged, I only describe the modifications below.

4.2.1 Model formulation

In this model, Young's modulus is determined not only by decomposition (Zhu et al., 2020) but also by PFT. Peat dominated by shrub becomes stiffer and has higher Young's modulus compared to *Sphagnum* peat because the geotechnical behaviour of peat, including Young's modulus, is related to its origin (Farrell, 2012), which shrub produces stiffer plant lit-

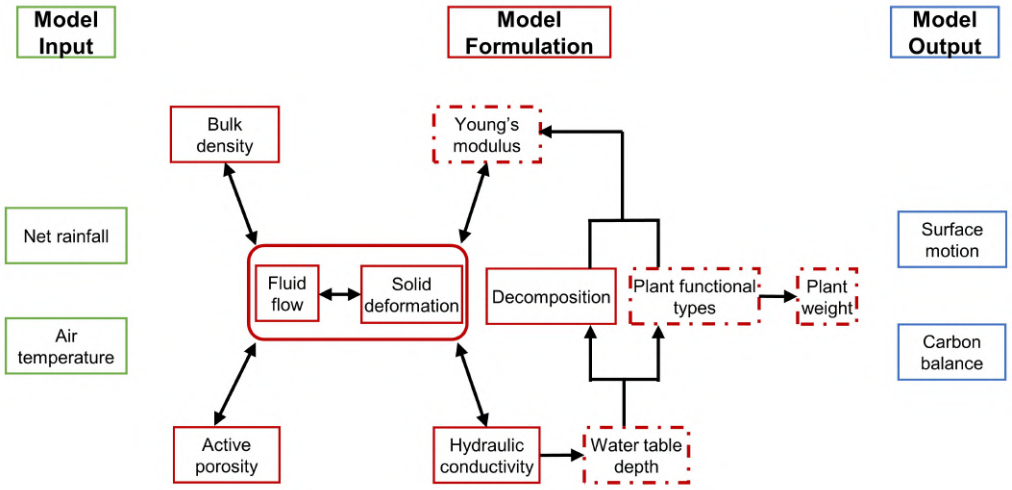

Figure 4.1: Conceptual diagram of the proposed model. The green boxes indicate the climatic input to the proposed model, consisting of net rainfall, which is defined as precipitation minus evapotranspiration, and annual average air temperature. The red boxes explain the model formulation, with the red dashed boxes indicating the changes in formulation from the previously proposed version of MPeat described in Chapter 3. In this formulation, the proportion of plant functional types depends on the water table depth, which in turn influences Young's modulus together with the decomposition process. Through this approach, I can incorporate the influence of the plant functional types on peat stiffness. Furthermore, the proportion of plant functional types also affects the total plant weight at the top surface, which provides loading and compression on the peat pore space. The changes in peat volume due to compression lead to the surface motion and influence carbon balance of the peatland, which are the outputs of the proposed model (blue boxes). Based on these outputs, I analyse regime shifts, tipping points, and both short- and long-term nonlinear dynamics of the peatland.

ter than *Sphagnum* (Ammala and Piltonen, 2019; Wagner et al., 2012). Furthermore, shrub roots provide a supporting matrix in the unsaturated zone, reducing the compression effect (Malmer et al., 1994). To accommodate this behaviour, Young's modulus of all layers in the unsaturated zone increases to a value determined by PFT. In contrast, if the condition is *Sphagnum* dominant, the effect of PFT on Young's modulus only occurs at the top surface (Figure 4.2). I propose an equation that includes the influence of decomposition and PFT on the peat Young's modulus as

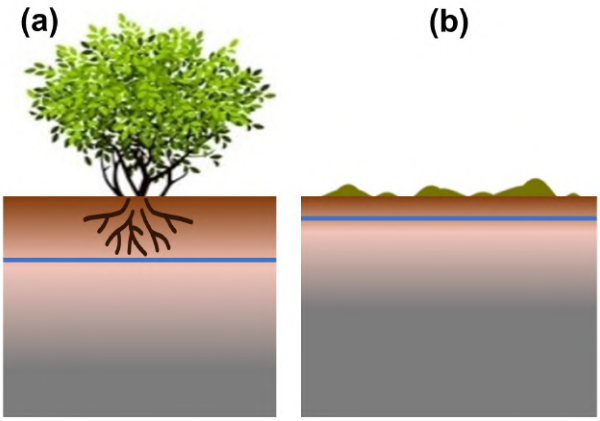

Figure 4.2: The root effect of plant functional types (PFT) on peat Young's modulus. The blue line indicates the position of the water table, which leads to the different compositions of PFT. The lower water table position supports the growth of shrubs, while the higher position of water table increases the proportion of *Sphagnum* in the peatland vegetation communities. (a) If shrub is dominant, Young's modulus value in the unsaturated zone above the water table changes because shrub roots increase the stiffness of the unsaturated zone. (b) If *Sphagnum* is dominant, only Young's modulus value at the top surface is affected due to the absence of root effect on the peat stiffness.

follows

$$E = \chi \left(1 + {\theta_t}^{\zeta}\right) \left(b_1 c_1 + b_2 c_2 + b_3 c_3\right) \tag{4.1}$$

where E is the Young's modulus (Pa), θ is the remaining mass $(-)$, χ is the first Young's modulus parameter (Pa) and ζ is the second Young's modulus parameter $(-)$, b_1, b_2, b_3 are the coefficient to couple PFT with Young's modulus $(-)$, c_1, c_2, c_3 are the PFT proportions $(-)$ with the indices 1, 2, 3 indicating shrub, sedge, and *Sphagnum*, respectively. Due to the uncertainties in the range value of peat Young's modulus (e.g., Dykes, 2008; Price et al., 2005; Reeve et al., 2013), I choose the parameters in Equation 4.1 such that Young's modulus value is in agreement with the data provided by Boylan et al. (2008), Mesri and Ajlouni (2007), and Long (2005) in the range of $8 \times 10^4 - 1.6 \times 10^6$ Pa. Through this range value of Young's modulus, I enable to investigate the effect of mechanical feedback

on the peatland dynamics.

My model formulates the water table position at the centre of a circular domed peatland which is constrained by the rivers based on the equation from Childs (1969) (see also Morris et al., 2015; Swindles et al., 2012). In this formulation, a peatland receives the water from net rainfall that is defined as precipitation minus evapotranspiration and loses water due to lateral discharge towards the rivers, which is affected by the active porosity, hydraulic conductivity, and the distance from the centre to the river or peatland radius

$$\frac{d\Gamma}{dt} = \frac{r}{\phi} - \frac{2\kappa\Gamma^2}{l^2\phi} \qquad \text{(3.17 revisited)}$$

where Γ is the water table height (m), r is the net rainfall ($\mathrm{m\,yr^{-1}}$) that is defined as precipitation minus evapotranspiration, l is the peatland radius (m), ϕ is the active porosity ($-$), and κ is the hydraulic conductivity ($\mathrm{m\,s^{-1}}$). Water table position influences peat production, decomposition rate, and PFT composition. Moore et al. (2002) measured the relationship between the proportion of PFT with the position of the water table and found a strong negative relationship between water table position and shrub proportion. Where the water table was low, PFT composition was dominated by shrub. I apply linear regression to estimate the PFT proportion based on the minimum value of water table depth in each interval from Moore et al. (2002) data, as follows

$$c_1 = 2.23z - 0.28 \tag{4.2}$$

$$c_2 = -1.42z + 0.63 \tag{4.3}$$

$$c_3 = -0.81z + 0.64 \tag{4.4}$$

where c_1, c_2, c_3 are the PFT proportions ($-$) with the indices 1, 2, 3

indicating shrub, sedge, and *Sphagnum*, respectively, and z is the water table depth (m) with the range value between $0.2 - 0.5$ m based on Moore et al. (2002) measurements. I assume the PFT proportion outside the range of the water table depth is equal to the estimated value when the water table depth is located in the limit range. The value of the coefficient of determination R^2 from the linear regression model for shrub, sedge, and *Sphagnum* proportions are 0.95, 0.78, and 0.82, respectively. These values of R^2 indicate that the linear fitting is appropriate to model the relationship between water table depth and PFT proportion.

The dependency of PFT proportion on the water table depth that is formulated in this model provides a more reasonable approach for investigating the influence of PFT on peatland mechanics compared to the constant proportion of PFT in the initial version of MPeat. PFT proportion affects the plant weight at the top surface, which represents the total weight of the living plants that set up the community. Plant weight becomes the source of loading in this system and is calculated through the following equations (Mahdiyasa et al., 2022; Moore et al., 2002)

$$\Upsilon = c_1 \left(10^{\frac{log_{10}(\psi)+0.409}{0.985}}\right)(1+d_1)\,g + c_2\left(10^{log_{10}(\psi)+0.001}\right)(1+d_2)\,g + (c_3 0.144)\,(1+d_3)\,g \tag{3.13 revisited}$$

where Υ is the plant weight (Pa), ψ is the peat production ($\mathrm{kg\,m^{-2}\,yr^{-1}}$), g is the acceleration of gravity ($\mathrm{m\,s^{-2}}$), c_1, c_2, c_3 are the plant proportions $(-)$ and d_1, d_2, d_3 are the constants for plant wet condition $(-)$ with the indices 1, 2, 3 indicating shrub, sedge, and *Sphagnum*, respectively.

4.2.2 Model implementation

I ran two groups of simulations with different time scales. In the first group, I simulated long-term peatland development under a constant radius of 500 m and flat substrate over a period of 6000 years, with the parameter values summarised in Table 4.1. I employed an annual time series of net rainfall (Figure 4.3a), and annual average air temperature (Figure 4.3b) generated from a sinusoidal function with some noise to create variable wet or dry climatic conditions. The range value of net rainfall and average air temperature used in my model are in line with the reported data from Morris et al. (2015), Young et al. (2019), and Young et al. (2021). In this group, the water is added evenly in small increments with timesteps equal to 0.1 years to produce a stable and convergent simulation. The boundary conditions of the model were an impermeable layer with no displacement at the bottom and a fully drained condition of the top layer. The rate of surface motion is obtained from the annual changes in peatland height, which is affected by mechanical, ecological, and hydrological feedback.

In the second group, I decoupled peat production and decomposition processes and focused on the mechanical and hydrological feedback on a shorter time scale. I used peat properties that had been simulated from the first group to model short-term peatland surface motion with weekly timesteps over 150 weeks. I chose peat properties between the ages of $4000 - 3900$ years BP and $2000 - 1900$ years BP to represent the dry and wet conditions of the peatland based on the position of the water table (Figure 4.4b). Unlike the first set of simulations, where peat production and decomposition influence the mechanical deformation through the changes in Young's modulus (Equation (4.1)), the swelling and shrinking in the short-term simulations are affected by the plant weight at the top surface and water

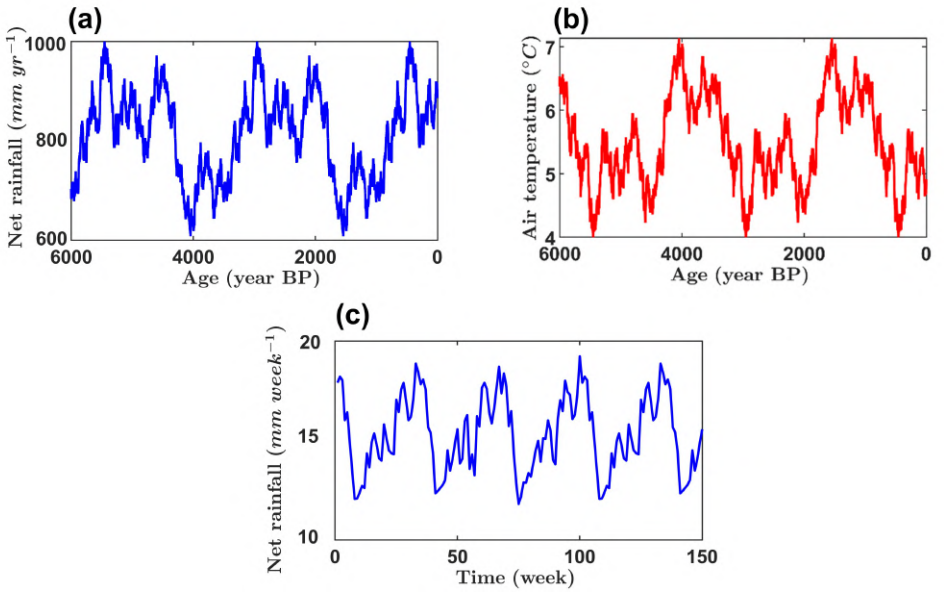

Figure 4.3: The climate profile for long-term and short-term simulations. Long-term simulation is driven by the fluctuations of (a) net rainfall, which is defined as precipitation minus evapotranspiration, and (b) annual average air temperature with the value in the interval of 600-1000 mm yr^{-1} and $4 - 7$ °C, respectively, over 6000 years. (c) Short-term simulation over 150 weeks depends only on net rainfall with the value ranging between $12 - 19$ mm $week^{-1}$ because I exclude peat production and decomposition processes.

Table 4.1: Symbols and parameter default values for the simulations.

Name	**Symbol**	**Value**	**Unit**	**Reference**
Unsaturated zone decay rate	η_{un}	5×10^{-2}	yr^{-1}	(Clymo, 1984)
Saturated zone decay rate	η_{sa}	8×10^{-5}	yr^{-1}	(Clymo, 1984)
Biot's coefficient	α	1	–	(Terzaghi, 1943)
Bulk density initial value	ρ_0	50	$kg\ m^{-3}$	(Lewis et al., 2012)

Continued on next page

Table 4.1 – *Continued from previous page*

Name	**Symbol**	**Value**	**Unit**	**Reference**
Carbon content	C	0.47	–	(Loisel et al., 2014)
Active porosity initial value	ϕ_0	0.8	–	(Quinton et al., 2000)
Bulk density and active porosity parameter	β	2	m^{-1}	Present study
Hydraulic conductivity initial value	κ_0	1×10^{-2}	$\mathrm{m\,s}^{-1}$	(Hoag and Price, 1995)
Hydraulic conductivity parameter	ξ	15	–	(Mahdiyasa et al., 2022)
Degree of saturation of water	S_w	0.4	–	(Mahdiyasa et al., 2022)
Water retention empirical constant 1	λ	0.5	–	(Mahdiyasa et al., 2022)
Water retention empirical constant 2	μ	0.4	m^{-1}	(Mahdiyasa et al., 2022)
Specific storage	S_s	1.4×10^{-2}	m^{-1}	(Hogan et al., 2006)
Specific weight of water	γ_w	9800	$\mathrm{N\,m}^{-3}$	(Cheng, 2020)
Peatland radius	l	500	m	(Mahdiyasa et al., 2022)
Young's modulus parameter 1	χ	2×10^5	Pa	(Mahdiyasa et al., 2022)

Continued on next page

Table 4.1 – *Continued from previous page*

Name	**Symbol**	**Value**	**Unit**	**Reference**
Young's modulus parameter 2	ζ	0.1	–	(Mahdiyasa et al., 2022)
Shrub-Young's modulus parameter	b_1	1.25	–	Present study
Sedge-Young's modulus parameter	b_2	1	–	Present study
Sphagnum-Young's modulus parameter	b_3	0.75	–	Present study
Shrub constant	d_1	0.4	–	(Mahdiyasa et al., 2022)
Sedge constant	d_2	0.4	–	(Mahdiyasa et al., 2022)
Sphagnum constant	d_3	20	–	(McNeil and Waddington, 2003)

table position through the effective stress. Effective stress has an essential role in this model because it can explain the relationship between the total stress received by peat with pore water pressure (Biot, 1941; Price, 2003; Terzaghi, 1943) and the effect of compaction on the peat physical properties (Mahdiyasa et al., 2022; Schlotzhauer and Price, 1999; Whittington and Price, 2006). The model in this group was driven by climatic input in the form of weekly net rainfall only because all variables are not affected by air temperature (Figure 4.3c). Therefore, throughout the year, the water is added unevenly to the peatland in the short-term simulation.

4.2.3 Sensitivity analysis

Model sensitivity to input parameters was evaluated by changing the value of parameters that couple PFT with Young's modulus (Equation (4.1)). I chose to explore the effect of these parameters because of the shortage of information on how significant PFT is on the peat stiffness, which in turn influences the dynamics of the peatland. I increased the value of b_1 to represent the condition that shrubs control the peat stiffness by producing a higher Young's modulus. In contrast, the decreasing value of b_3 simulated the condition that *Sphagnum* was the essential PFT in reducing peat stiffness.

I performed one at a time sensitivity analysis or changed the value of one parameter, and all others remained the same as the baseline value (Table 4.1) for each simulation. The sensitivity analysis outputs consist of the relationship between peat stiffness with the dynamics of surface motion and the peatland carbon balance, including carbon input, carbon output, and net carbon accumulation.

4.3 Simulation results

4.3.1 Long-term dynamical behaviour

Once the unsaturated zone has developed, the PFT proportion fluctuates depending on the water table position, which in turn affects the plant weight at the top surface. For instance, from 5200 - 4302 years BP, water table depth is around 0.24 m (Figure 4.4b), *Sphagnum* is the dominant PFT (44%) compared to the shrub (27%) and sedge (29%) (Figure 4.4a), and the value of plant weight is about 22.14 kg m^{-2} (Figure 4.4c). Contrast-

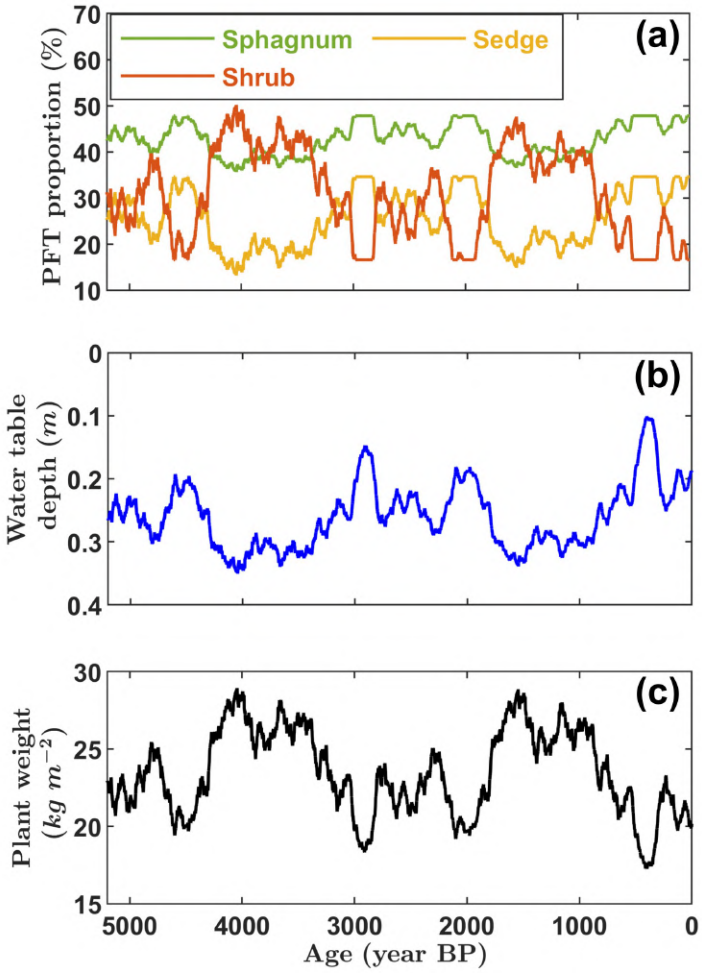

Figure 4.4: (a) The proportion of plant functional types (PFT), including *Sphagnum*, shrub, and sedge, (b) the water table depth, and (c) the plant weight at the top surface over 5200 years or after the unsaturated zone is developed. Between the ages of $3000 - 2850$, $2100 - 1900$, and $500 - 300$ years BP, the simulated water table depth is deeper than 0.2 m, exceeds the limit range of Moore et al. (2002) measurements, which results in a constant proportion of PFT in these periods.

ingly, from $4274 - 3375$ years BP, the water table depth is around 0.32 m, shrub proportion increases to 43%, while *Sphagnum* and sedge decrease to the value of 38% and 19% respectively, and plant weight increases to 26.65 kg m^{-2}. The differences in the PFT composition, water table depth, and plant weight lead to variations in the rate of surface motion (Figures 4.5a and 4.5b).

The rate of surface motion is obtained from the average rate of motion over

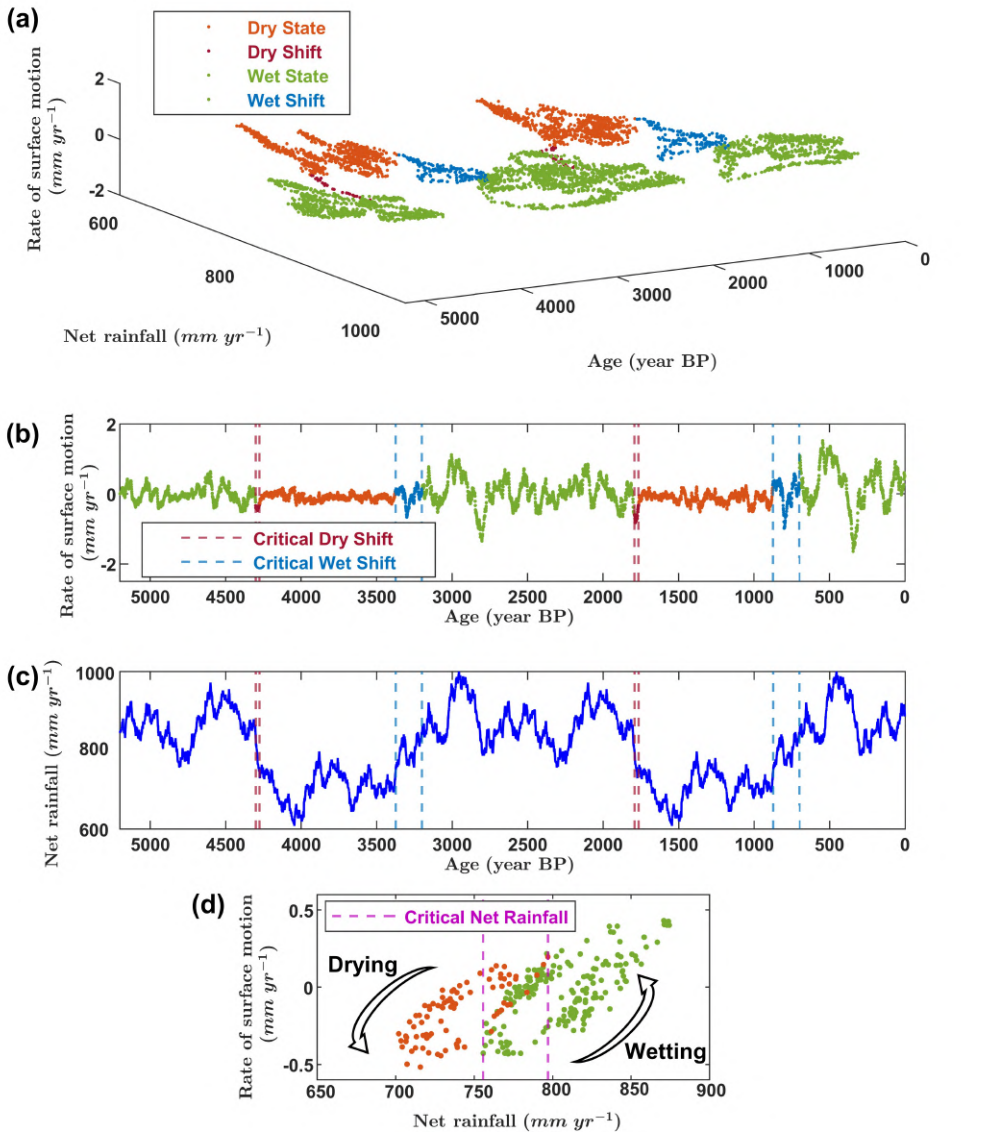

Figure 4.5: (a) The rate of surface motion (positive value indicates the peatland surface is going up while the negative value is going down) with net rainfall and time in three-dimensional space, (b) the projections to two-dimensional space between rate of surface motion with time, (c) the changes in net rainfall that are required to shift peatland from one state to another, and (d) the projections to two-dimensional space between rate of surface motion with net rainfall to show the possibility of bistability conditions because wet and dry attractors could appear under the same range of net rainfall.

an entire year, essentially the net swelling and shrinking of a surface after a complete annual cycle, with positive values indicating that the peatland surface is going up, while the negative values indicate the peatland surface is going down. I use the rate of surface motion to explain the movement

of the peatland surface rather than the absolute position because the reference point will change over time. This approach provides a more robust and efficient calculation process because it can be simulated without specifying some arbitrary datum. As the peatland develops, five distinct clusters of the rate of surface motion are produced, three corresponding to wetter conditions (5200 − 4302, 3199 − 1793, and 699 − 0 years BP), and two corresponding to drier conditions (4274 − 3375 and 1764 − 876 years BP) (Figure 4.5a). The range of the rate of surface motion in the dry state is from -0.51 to 0.23 mm yr^{-1}, with the net rainfall fluctuating around 600 − 790 mm yr^{-1}. Conversely, if the net rainfall varies about 750 − 1000 mm yr^{-1}, the peatland is attracted to the wet state, represented by the high rate of surface motion in the range of -1.64 and 1.52 mm yr^{-1}. The overlap between these two ranges of net rainfall, around 750 − 790 mm yr^{-1}, allows the dry attractor and wet attractor to coexist, which indicates the possibility of bistability (Figure 4.5d). Dry or wet attractors are the oscillatory states of the peatland toward which that peatland system tends to evolve, which have fundamental differences in characteristics and structures. Furthermore, the transition time from dry to wet state (wet shift) persists for around 174 years (Figure 4.5b) and requires 90 mm yr^{-1} change in net rainfall (Figure 4.5c), whereas the transition time from wet to dry (dry shift) is about 26 years, involving about 50 mm yr^{-1} change in net rainfall.

Long-term carbon input, output, and net accumulation are affected significantly by the peatland state. For example, the transition from wet to dry condition that occurs around 4301 to 4275 years BP increases the rate of carbon input from 0.33 to 0.39 kg C m^{-2} yr^{-1} due to the enhancement of productivity (Figure 4.6a). However, this condition also leads to a substantial rise in the rate of peatland carbon release from 0.30 to 0.36

kg C m^{-2} yr^{-1} over the same time interval as the consequence of increasing the depth of the unsaturated zone (Figure 4.6b). In contrast, the transition from dry to wet state about 3374 to 3200 years BP reduces the rate of carbon addition from 0.39 to 0.33 kg C m^{-2} yr^{-1} and carbon output from 0.37 to 0.31 kg C m^{-2} yr^{-1} because of the lower peat production and decomposition process as the water table is closer to the surface, from 0.31 to 0.26 m. The average value of the net rate of carbon accumulation, obtained from the difference between the rate of carbon input and output, is about 0.024 kg C m^{-2} yr^{-1} over the simulation time (Figure 4.6c), which is in line with reported measurements between $0.021 - 0.025$ kg C m^{-2} yr^{-1} (Chaudhary et al., 2020; Loisel et al., 2017, 2014; Treat et al., 2016; Yu et al., 2010).

4.3.2 Short-term dynamical behaviour

Peat that grows in dry conditions has different characteristics, including the physical properties, compared to the wet peat, which results in distinct behaviour of short-term surface motion. During $4000 - 3900$ years BP, shrub proportion increased due to the low net rainfall between $610 - 660$ mm yr^{-1} (Figure 4.3a) which led to the high Young's modulus value in the range of $3.53 \times 10^5 - 3.65 \times 10^5$ Pa (Figure 4.7d). Furthermore, the decrease in water input produced a deep position of the water table ($0.35 - 0.32$ m) from the surface (Figure 4.4b), resulting in a more considerable effect of compaction, which is represented by the high value of bulk density ($115 - 119$ kg m^{-3}) and low value of active porosity ($0.33 - 0.35$) and hydraulic conductivity ($2.3 \times 10^{-8} - 4.9 \times 10^{-8}$ m s^{-1}) in that period (Figures 4.7a-c).

The condition was different during $2000 - 1900$ years BP when peatland experienced high net rainfall ($910 - 950$ mm yr^{-1}), which resulted in a

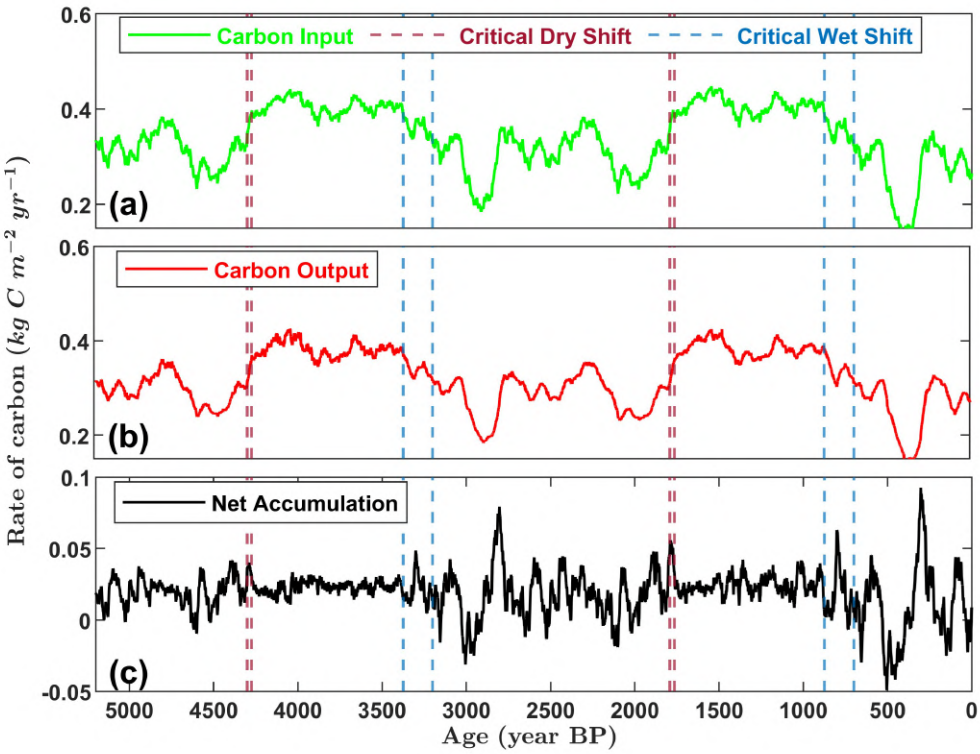

Figure 4.6: Long-term peatland carbon balance over 5200 years. (a) The carbon input is obtained from peat production multiplied by carbon content with a value of 47% based on the data from Loisel et al. (2014). (b) The carbon output is calculated from mass loss due to the decomposition multiplied by the carbon content. (c) The difference between carbon input and carbon output leads to the net carbon accumulation in the peatland. The fluctuation of the net carbon accumulation rate is increasing as the system evolves, particularly in the wet state when subject to the same external forcing.

shallow water table position ($0.18 - 0.20$ m), and consequently led to the *Sphagnum* dominance condition. In this situation, peat stiffness decreased, indicated by the low value of Young's modulus ($3.14 \times 10^5 - 3.22 \times 10^5$ Pa). The high position of the water table reduced the effective stress, which produced peat with lower bulk density ($93 - 95$ kg m^{-3}) and higher active porosity ($0.41 - 0.43$) and hydraulic conductivity ($5.8 \times 10^{-7} - 7.8 \times 10^{-7}$ ms^{-1}). Moreover, the surface loading from plant weight during $4000 - 3900$ years BP (dry period) and $2000 - 1900$ years BP (wet period) was around $26.12 - 28.92$ kg m^{-2} and $19.38 - 20.44$ kg m^{-2}, respectively (Figure 4.4c).

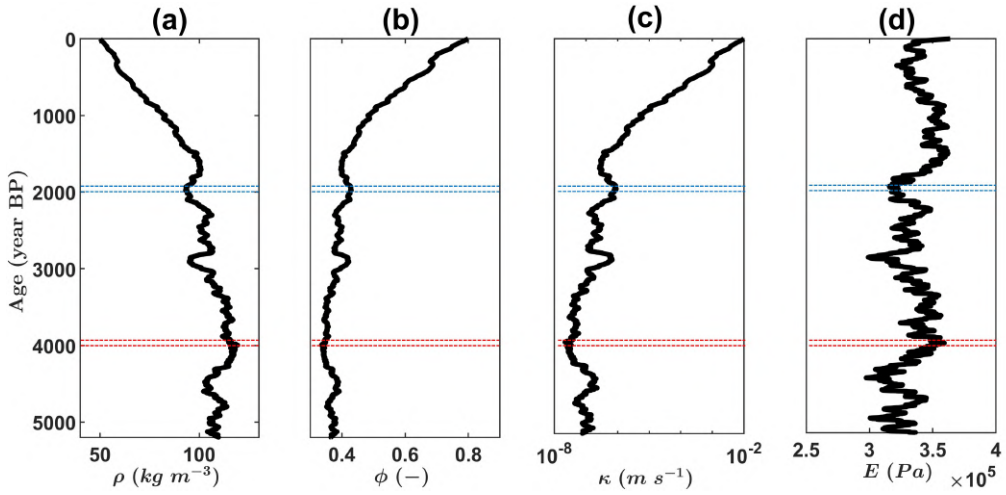

Figure 4.7: The profile of peat physical properties with age-depth, including (a) bulk density ρ, (b) active porosity ϕ, (c) hydraulic conductivity κ, and (d) Young's modulus E over 5200 years. Red and blue dashed lines indicate the dry period $4000 - 3900$ years BP and wet period $2000 - 1900$ years BP, respectively. The range of bulk density calculated in my model between $50 - 119$ kg m^{-3} is in line with the reported value around $30 - 120$ kg m^{-3} (Clymo, 1984; Lewis et al., 2012). The range of active porosity from the simulation about $0.33 - 0.8$ is consistent with the reported measurement between $0.1 - 0.8$ (Hoag and Price, 1997; Quinton et al., 2000, 2008). The simulation result of hydraulic conductivity in the range of $2.2 \times 10^{-8} - 1 \times 10^{-2}$ m s^{-1} align with reported measurements $7 \times 10^{-9} - 1.6 \times 10^{-2}$ m s^{-1} (Clymo, 2004; Fraser et al., 2001; Hoag and Price, 1995). Finally, the simulation result of Young's modulus in my model around $2.9 \times 10^5 - 3.6 \times 10^5$ Pa is in agreement with reported values about $8 \times 10^4 - 1.6 \times 10^6$ Pa (Boylan et al., 2008; Long, 2005; Mesri and Ajlouni, 2007).

Peat characteristics between the ages of $4000 - 3900$ years BP and $2000 - 1900$ years BP, which represent dry and wet periods, were employed to simulate short-term surface motion. The amplitude of surface motion and peak timing varied between dry and wet peat over 150 weeks. Surface displacement ranged from -0.11 to 0.04 m for peat formed in dry condition, while for peat developed in a wet environment it fluctuated between -0.21 and 0.05 m (Figure 4.8a). The negative or positive values indicate shrinkage or swelling of the peat surface from the initial elevation, which was 1.52 m for the dry peat and 2.36 m for the wet peat. Periods of peak timing of surface motion were not synchronized across the two time series, with wet peat experiencing a delay in peak timing relative to the dry peak of

around five weeks. In addition, the hysteresis of surface elevation with the water level also appears for both dry peat (Figure 4.8b) and wet peat (Figure 4.8c). This phenomenon suggests the water level drops faster than the pore structure can collapse and the opposite happens when water is added to the peatland.

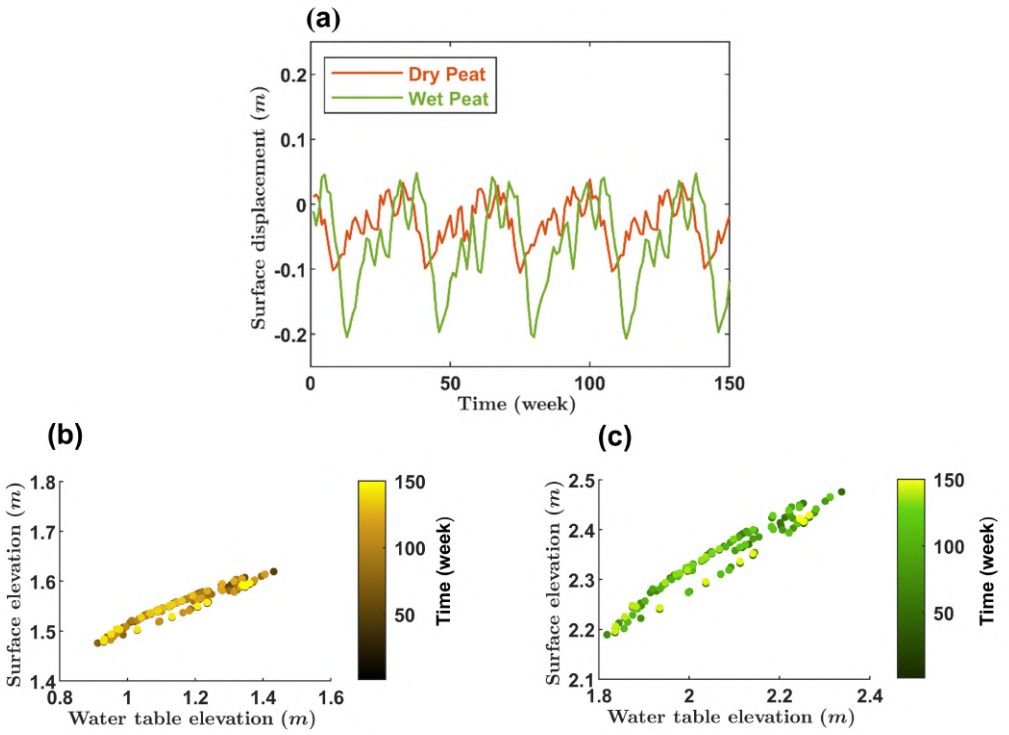

Figure 4.8: (a) The difference in the characteristics of surface motion, including the amplitude and peak timing, between peat that grows in dry and wet conditions over 150 weeks, (b) hysteretic behaviour of surface elevation with water table elevation for dry peat, and (c) wet peat. Water table elevation shows the height of the water table from the base of the peatland. The surface moves with time in the anticlockwise direction.

4.3.3 Sensitivity analysis

The parameter b_1 (Equation (4.1)) controls the effect of the shrub proportion on the peat Young's modulus as the PFT composition changes because of the fluctuation in water table depth. Increasing parameter b_1 to 3.75 (Fig. 9) led to a higher Young's modulus with a value between

$4.07 \times 10^5 - 7.92 \times 10^5$ Pa, which in turn reduced the rate of surface motion to the range of -1.48 until 1.12 mm yr^{-1}. This condition, on average, results in a higher rate of carbon addition and carbon output with a value of about 2.2% and 5.6%, compared to the baseline value. Because the increasing rate of carbon output is higher than carbon input, the net rate of carbon accumulation decreases by around 39%. Moreover, a higher value of Young's modulus leads to a lower amplitude of surface motion for both dry peat (0.07 m) and wet peat (0.17 m), but the shift in peak timing is the same with the short-term baseline simulation, around five weeks.

The changes in Young's modulus value due to the variation in *Sphagnum* proportion are determined by b_3 parameter (Equation (4.1)). Decreasing b_3 parameter to 0.375 resulted in a lower Young's modulus value ($2.43 \times 10^5 - 3.13 \times 10^5$ Pa), and as a consequence, the range of surface motion rate increased to the value between -1.48 and 1.69 mm yr^{-1}. This condition reduced the rate of carbon addition and carbon output by around 1.5% and 3.2% compared to the baseline simulation. The net carbon accumulation rate increased by approximately 19% due to a greater reduction in carbon output than carbon input. Furthermore, a lower Young's modulus value led to a higher amplitude of surface motion for both dry peat and wet peat in the short-term simulation, with the value of about 0.20 m and 0.32 m, respectively, and produced a more extended shift in peak timing about six weeks.

4.4 Discussion

The most significant observation arising from this model is the apparent bistability of the peatland with respect to net rainfall (Figure 4.5d), with

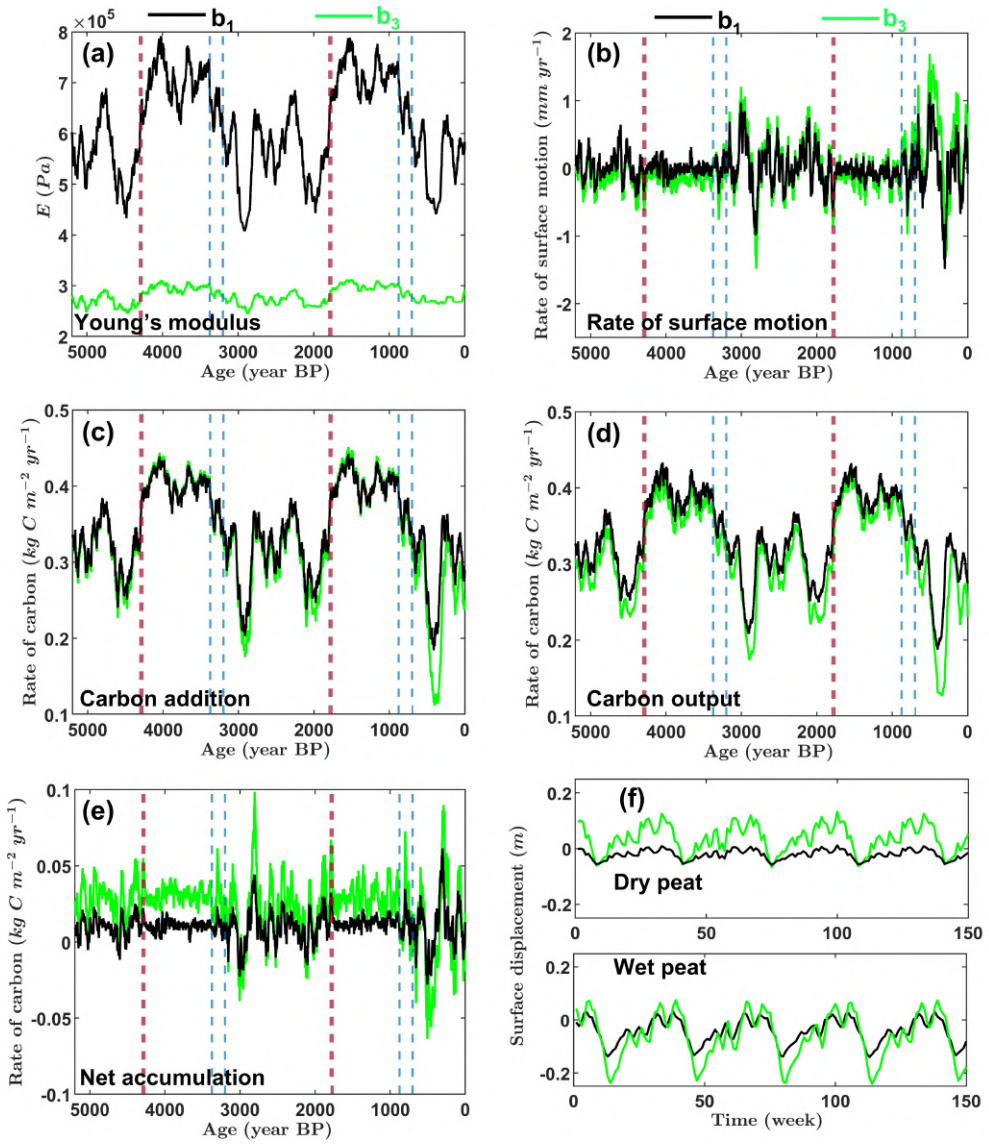

Figure 4.9: The sensitivity analysis by changing the value of parameter b_1 to 3.75 (black line) or b_3 to 0.375 (green line) with the output variables are (a) Young's modulus E, (b) rate of surface motion, (c) rate of carbon addition, (d) rate of carbon output, (e) net rate of carbon accumulation, and (f) short-term surface motion. The parallel dashed red and blue lines indicate a critical dry and wet shift, respectively.

both wet and dry states being possible for the same net rainfall, but at different times. Another view of this is that as net rainfall varies over time, the peatland jumps between attractors characterised by two limit cycles. In comparison to the bistability predicted by Hilbert et al. (2000), who consider equilibrium states, my model is more complex because the system is continually evolving. By definition, an equilibrium state can be

achieved if the state variable does not change with time. However, interactions between internal and external feedback mechanisms will prevent the peatland from reaching that condition because the peat physical properties, including bulk density, active porosity, hydraulic conductivity, and Young's modulus, change in time and space (Boylan et al., 2008; Fraser et al., 2001; Hogan et al., 2006; Lewis et al., 2012). This dynamic view of an evolving system is potentially more useful as there is no indication that Holocene peatlands are close to an equilibrium state. It can also be seen (Figures. 4.5b and 4.6c) that as the model peatland grows, the amplitude of oscillations, particularly in the wet state, increases. This is not surprising as growth between the fixed lateral boundaries in the model will steepen hydrological gradients over time, generating increasing extreme responses to the same changes in net rainfall. It should also, in the long term, favour the dry state, assuming that the processes of decay do not impose an earlier limit. If these modelled results have a bearing on reality, then some caution should also be exercised when interpreting the response of the peat to palaeoclimatic change, as the same climate forcing could generate quite different outcomes in the evolving peatland system. The inference of a permanent state of disequilibrium also raises the important question as to whether it would ever be possible for an observer on the surface of a peatland to determine if the system was tending to a long-term stable carbon balance as might be expected if they were to assume a constant decay rate.

Another key observation that operates on different time frames is the hysteretic behaviour of surface elevation with the water level. Short-term hysteresis is a well known consequence of the filling and draining of porous matter and is obtained from field measurement. The data from Fritz et al. (2008) showed that delayed response of the surface motion to the changes

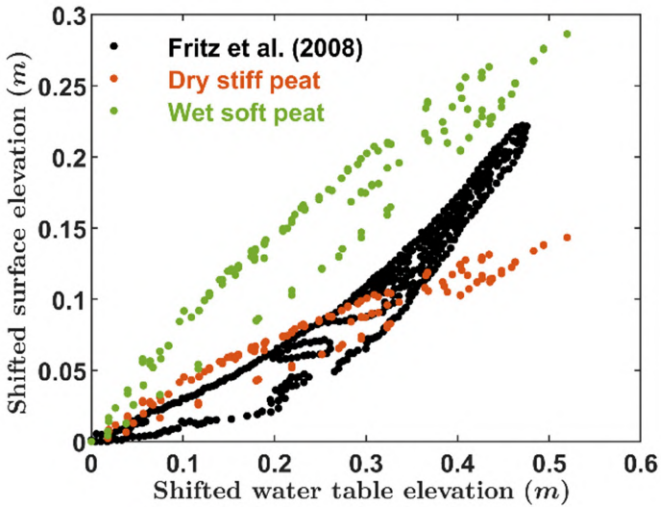

Figure 4.10: Comparison with Figure. 4 Fritz et al. (2008) related to the hysteretic response of surface elevation with water table elevation. Shifted water table elevation is obtained from the water table elevation minus its minimum value, and shifted surface elevation is obtained from the surface elevation minus its minimum value.

in water level results in a hysteresis loop, with a positive relationship between these two variables, and this observation is in agreement with my simulation results (Figure 4.10). The slope of surface elevation with water level decreases in the dry period, which may indicate that peat is stiffer at depth in the study area measured by Fritz et al. (2008), because the enhancement of peat stiffness will produce lower surface displacement and results in a flatter curve. In my simulations, stiffer peat that formed in dry conditions has a smaller slope of surface elevation with water level (0.3) compared to the wet peat (0.6), while Fritz et al. (2008) data show that the slope in the dry and wet conditions are around 0.2 and 0.8, respectively. The more pronounced difference between dry and wet conditions in the Fritz et al. (2008) data might be related to the peat characteristics in that specific site, including the restiad PFT composition compared to my model and possibly the influence of this on the microporosity (Rezanezhad et al., 2010; Silins and Rothwell, 1998). However, the main reason for comparison with Fritz et al. (2008) data is to demonstrate how the model

provides an interpretative framework for analysing their observation of a peatland which in other respects (e.g., uniform surface loading and reduction in elasticity with decay) can be considered comparable to my model. Furthermore, this comparison also indicates the ability of my model to capture the heterogeneity and nonlinearity of peatland behaviour, provide a context for interpreting field data, and suggest that my chosen physical properties appear to be reasonable for the purpose of analysing peatland behaviour.

The long-term nonlinear hysteretic response to oscillatory changes in net precipitation may reflect fundamental differences in the behaviour of the wetting and drying system that result from a change in the state of the peatland (Figure 4.5d). Intuitively, differences in the response of peatland to wetting and drying are reasonable as it should be easier to lose potential energy by lowering a water table than to build potential energy. This result may also indicate that the production of peat by compaction is a nonlinear process on multiannual timescales, with periods of either net growth (accumulation) or subsidence (compaction) of the peat occurring in response to longer terms changes in weather or climate. Some evidence of such longer-term oscillatory mechanical behaviour can be observed in the field observations of Howie and Hebda (2018), whose data, when plotted on an appropriate scale, appears to display evidence of multiannual oscillations in surface motion.

4.4.1 Peatland regime shifts and tipping points

I found that a more substantial change in net rainfall is required to move the peatland from a dry state to wet state, than the other way around (Figure 4.5a and 4.5c). A significant increase in water input is necessary

to produce higher pore water pressure and expand the pore space, leading to more substantial peat water storage, which is the requirement for the regime shift from dry to wet states. However, as the dry state develops, the flow of water on the near-surface will be more favourable because the compaction effect is less significant for the stiffer material. Consequently, near-surface hydraulic conductivity will remain high, preventing the peatland from accumulating more water. This condition supports a dry state to turn into a more dominant attractor that can accommodate greater perturbations and potentially becomes a preferable state in the long-term as the peatland grows.

It is notably difficult to predict when the regime shifts will appear in complex dynamical systems (Scheffer et al., 2009; Scheffer and Carpenter, 2003), including peatlands (Belyea, 2009; Belyea and Baird, 2006), because they involve heterogeneous processes and nonlinear feedbacks. However, as the system approaches a tipping point, the variability of state behaviour changes (Carpenter and Brock, 2006; Kleinen et al., 2003; Oborny et al., 2005; van Nes and Scheffer, 2003), in my case is the rate of surface motion, that can be used as an early warning signal. For instance, before the regime shift around 3200 years BP, the standard deviation in the rate of surface motion increased from 0.07 to 0.27 $\mathrm{mm\,yr^{-1}}$ (Figure 4.11), indicating the upcoming major transition from dry state to wet state. This is because the ability of the system to recover from perturbations and track fluctuations is decreasing near the critical threshold (Berglund and Gentz, 2002).

The proposed model shows how the feedback between internal and external factors affects peatland states and regime shifts under uniform landscape conditions. However, the state behaviour is also influenced by the spatial topography of the peatland. Assuming a sufficiently complex landscape (e.g., blanket bog with variable slopes, drainage lines, and local hydrol-

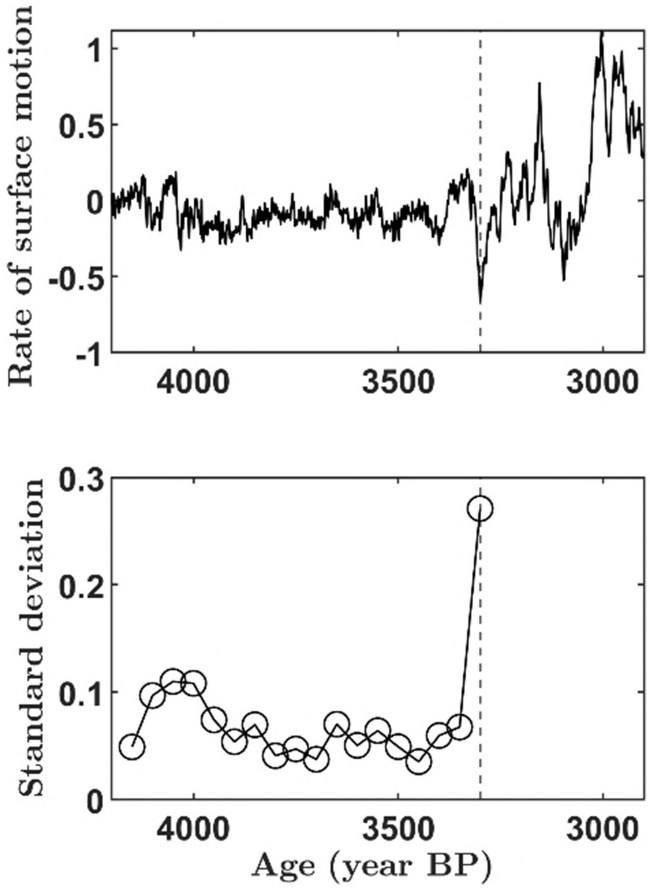

Figure 4.11: The standard deviation of the rate of surface motion (mm yr^{-1}) increases significantly before the regime shift from dry state to wet state around 3200 years BP.

ogy), and then on account of lateral flow with variations in the net water budget, it appears to be quite likely that wet and dry states could coexist in a landscape, and particularly, if the net rainfall were to fall within the region of bistability. This conclusion is supported by satellite observation of surface motion that indicates the bimodal wet state or dry state behaviour in such landscapes (Bradley et al., 2022) with a mean annual net rainfall of around 800 mm yr^{-1} a value that is remarkably close to the 760 to 790 mm yr^{-1} annual net rainfall range in which bistability occurs within my model. However, in practice the situation is potentially far more complex, for example, microtopography of hummocks and hollows also exerts an influence on peatland mechanical behaviour (Marshall et al., 2022) at a

much smaller scale ($1 - 10$ m) than the 90 m scale observations of Bradley et al. (2022).

A complex landscape, together with the variability of the peat physical properties throughout the peatland area, may also promote one state to be more stable than the other. Slope variabilities in a complex landscape have a major impact on the peatland hydrology (Holden, 2005; Holden and Burt, 2003), where the areas with a steeper slope experiences a higher rate of water discharge. This condition results in a smaller decrease in net rainfall required to shift from wet state to dry state than would be the case if the substrate was flat. Moreover, higher bulk density and lower hydraulic conductivity at mesotope margins (Baird et al., 2008; Lapen et al., 2005; Lewis et al., 2012) suggest smaller peat water storage in that location, which supports the dry state becoming more stable. Conversely, lower hydraulic gradients at mesotope centres will promote the accumulation of water, resulting in the wet condition becoming a dominant state. The state should change rapidly at a transition region between these two areas (margin and centre), and this is consistent with satellite observations (Bradley et al., 2022).

4.4.2 Peatland characteristics in different states

my simulation results show apparent differences in the characteristics of peatland surface motion between the wet state and dry state over long-term and short-term periods. In the long-term simulations, the rate of surface motion of dry peat is lower compared to wet peat (Figures 4.5a and 4.5b). The plant community composition in the dry state is dominated by shrub (Alshammari et al., 2020; Moore et al., 2002; Sottocornola et al., 2009; Wierda et al., 1997), which increases peat stiffness (Figure 4.7d) and

loading from plant weight at the top surface (Figure 4.4c). The presence of shrub roots provides a supporting matrix (Malmer et al., 1994), particularly in the unsaturated zone where mechanical deformation mainly occurs (Fenton, 1980; Mahdiyasa et al., 2022; Quinton et al., 2000; Waddington et al., 2010; Whittington and Price, 2006), which limits the expansion and contraction of peat volume and prevents the peatland surface from oscillating with a higher amplitude.

In the short-term simulation, the differences between wet and dry states are not only the magnitude but also the peak timing of surface motion. Generally, if I exclude the effect of peat addition and decomposition, the main drivers in short-term surface motion are the interactions between effective stress, pore water pressure, and peat physical properties. The peat physical properties of short-term simulations are obtained between the ages of $4000 - 3900$ BP and $2000 - 1900$ BP to represent the dry and wet states, respectively (Figure 4.7). The different values of Young's modulus between the two states result in a considerable distinction in the amplitude of surface motion, which corroborates the result from Reeve et al. (2013), indicating that lower Young's modulus produces more substantial changes in elevation of peat surface. Moreover, the wet peat has a lower bulk density and higher active porosity (Waddington et al., 2010; Whittington and Price, 2006), which lead to more significant water storage due to the larger pore size. These characteristics delay the effect of effective stresses on the reduction or expansion of peat volume because the process of expulsion or infiltration of water requires more time, resulting in a shift in the peak timing of surface motion. Another possible explanation for this is that the variation in hydraulic conductivity between wet and dry peat leads to the difference in time for pore water pressure to reach equilibrium (Biot, 1941; Ferronato et al., 2010; Moradi et al., 2019; Terzaghi, 1943), producing the

delayed effect of compression.

my short-term simulation result, which is developed from the coupling between mechanical and hydrological feedbacks, agrees in general with the satellite measurements from Bradley et al. (2022), who found that wet peat dominated by *Sphagnum* tends to experience a delay in peak timing. As opposed to that characteristic, peat in the dry state, typically dominated by shrub, undergoes earlier time to reach the peak of surface elevation. These distinct behaviours of surface motion, including amplitude and peak timing, between wet and dry peat could be used as a reliable indicator to assess peatland conditions. However, the shifts in peak timing are more evident in the satellite observations compared to my simulation, with a difference of about ten weeks. This discrepancy could be attributed to the seasonal growth and dieback of plants that are not included in my short-term simulation, peat physical properties variation between model simulation and the study location, and possibly the accuracy of signal processing undertaken by Bradley et al. (2022).

4.4.3 Peatland carbon balance and resilience

my simulations show that the peatland accumulates carbon more effectively in the drier states, with the water table depth fluctuating in the range of $0.3 - 0.35$ m, because at that interval, peat production reaches the maximum value, as shown by Belyea and Clymo (2001) from observational studies, and Morris et al. (2012) from the theoretical model DigiBog (Figure 4.6). Therefore, the significant increase in peat production cancels out the effect of a considerable rise in peat decomposition. Furthermore, this result indicates the important contribution of vascular plants, as the unsaturated zone thickness increases, to peat production that provides a significant

amount of above-ground biomass and root biomass (Moore et al., 2002; Wallén, 1986; Wallèn, 1987; Wallén et al., 1988). Charman et al. (2013) support my results and found that peatlands become stronger carbon sinks under a warming climate because the net primary productivity is a more critical variable than decomposition for determining long-term peatland carbon accumulation. However, as the peatland in the stiffer, drier state is less able to adjust its surface height to a falling water table, it is more susceptible to periods of drought and fire damage and becomes less resilient.

Conversely, although peatlands in the wetter state will accumulate less carbon, it is more resilient to further changes in the climate, as the peatland surface experiences more oscillation in the wetter state and can adjust more effectively to the fluctuations of water input (Alshammari et al., 2020; Bradley et al., 2022). The drop in water input will be accompanied by a decrease in surface elevation due to the compaction, which maintains the relative position of the water table from the surface (Mahdiyasa et al., 2022; Whittington and Price, 2006).

I have demonstrated the application of MPeat to explain the bistability, regime shift, tipping point, and nonlinear dynamics of the peatland in multiple timeframes by incorporating the influence of vegetation on peat volume changes. However, in one dimension, MPeat cannot capture the spatial variability of peatland characteristics, including peat physical properties, thickness, and water table depth. To understand the influence of spatial heterogeneity on peatland behaviour, it should be possible to extend MPeat into two dimensions, as explained in Chapter 5.

Chapter 5

A fully coupled mechanical-ecohydrological model of peatland development in two dimensions

5.1 Introduction

The influence of mechanical, ecological, and hydrological feedback in one dimension to analyse peatland behaviour has been presented in Chapters 3 and 4. However, a one-dimensional model, which represents peatland as a vertical column of peat at the centre area, ignores the spatial variability of peatland characteristics, such as peat thickness, water table depth, and physical properties that have the potential to provide essential feedback mechanisms (Rydin and Jeglum, 2006; Baird et al., 2008; Lewis et al., 2012). Moreover, the effect of natural boundary conditions, such as the river at the edges, is neglected in the one-dimensional analysis. As a result,

a higher dimensional model is required to overcome the limitations of the one-dimensional model.

Previous studies (e.g., Clymo, 1984; Hoag and Price, 1995, 1997; Quinton et al., 2000; Fraser et al., 2001; Clymo, 2004; Lapen et al., 2005; Quinton et al., 2008; Baird et al., 2008; Lewis et al., 2012) have explored spatial variability in the horizontal and vertical directions of peat physical properties, including bulk density, active porosity, and hydraulic conductivity. The horizontal variation of hydraulic conductivity was observed by Lapen et al. (2005), who found that hydraulic conductivity in the blanket peatland is lower at the margin than at the centre based on the field measurements and analysis of a peatland groundwater flow model. Field observations from Baird et al. (2008) and Lewis et al. (2012), who measured lateral variability of the hydraulic conductivity in a raised and a blanket peatland, respectively, support Lapen et al. (2005) finding by obtaining the same pattern of horizontal changes in hydraulic conductivity. Lewis et al. (2012) also observed the variability in the lateral direction of bulk density with the increasing value from the centre toward the margin. In the vertical direction, deeper peat exhibits a higher value of bulk density and a lower value of active porosity and hydraulic conductivity, with abrupt changes occurring between the unsaturated and saturated zone (Clymo, 1984; Hoag and Price, 1995, 1997; Quinton et al., 2000; Fraser et al., 2001; Clymo, 2004; Quinton et al., 2008).

The spatial variations of peat physical properties occur as a consequence of mechanical-ecohydrological processes on the peatland. As a porous medium with a low value of Young's modulus (Long, 2005; Mesri and Ajlouni, 2007; Boylan et al., 2008; Dykes, 2008), the peat body is susceptible to deformation. The deformation is non-uniform throughout the peatland area due to the spatial variations of water table depth that influence the effective stress.

A more significant deformation effect because of the increase in water table depth at the margin leads to higher bulk density and lower active porosity and hydraulic conductivity, preventing greater water discharge from the peatland. Lapen et al. (2005) posited that a lower hydraulic conductivity at the margin has a significant influence on maintaining the wet condition at the centre, which affects peat accumulation. Therefore, the spatial variations of peat physical properties potentially provide essential feedback as the peatland develops.

Higher dimensional models of peatland development assume constant or limited spatial variations of peat physical properties and ignore mechanical feedback (e.g., Ingram, 1982; Winston, 1994; Armstrong, 1995; Korhola et al., 1996; Borren and Bleuten, 2006; Baird et al., 2012; Morris et al., 2012; Swinnen et al., 2019). For example, Borren and Bleuten (2006) proposed a three-dimensional model of peatland development based on the groundwater flow model (Strack, 1984) and focused on the ecohydrological feedback between water table position with peat production and decomposition following the Clymo (1984) model. The mechanical compaction is assumed to be negligible, and the spatial variations in the bulk density and hydraulic conductivity are obtained based on the empirical relationship between different peatland types, consisting of bog, throughflow fen, and fen. DigiBog (Baird et al., 2012; Morris et al., 2012) is a one-, two-, or three-dimensional model of peatland development that accommodates the spatial changes in hydraulic conductivity through the differences in remaining mass that are affected by water table position and decomposition processes (Moore et al., 2005; Quinton et al., 2000). Although DigiBog captures more complex feedback between ecological and hydrological processes than the model from Borren and Bleuten (2006), the omission of mechanical feedback leads to the assumption of constant active porosity

and bulk density as the peatland grows. Cobb et al. (2017) developed a tropical peatland growth model in two dimensions to analyse the influence of climate, particularly the rainfall pattern, on carbon storage. This model simulates the dynamics of the water table and peat accumulation through the groundwater flow model (Strack, 1984) and the difference between peat production and decomposition. The carbon storage is estimated from the stable peat surface Laplacian that is affected by the rate of peat production and decomposition. The peat surface Laplacian indicates the curvature of the peat surface, calculated as the sum of second derivatives of surface elevation. Although the surface Laplacian provides information related to the peatland morphology, this model ignores the mechanical feedback and assumes a constant value of hydraulic conductivity that becomes the source of uncertainty in estimating the peatland carbon storage.

Another phenomenon that requires a higher dimensional model is the influence of non-constant river elevation at the boundary. The majority of the peatland growth models, including DigiBog (Baird et al., 2012; Morris et al., 2012), the models from Borren and Bleuten (2006), and (Cobb et al., 2017), are developed based on the assumption of the negligible depth of rivers or a constant river elevation at the edges over the simulation time. However, Glaser et al. (2004b) suggested that river incision provides a substantial effect on the water table position, which in turn determines the thickness and shape of the peatland. As a consequence, the downcutting river also affects peatland mechanics through the changes in effective stress that leads to the different compaction effects on the peat pore structure. The feedback generated from the river behaviour at the edges would indicate the importance of boundary conditions on the peatland interior.

This chapter, therefore, set out to (1) provide a fully coupled mechanical-ecohydrological model of peatland development in two dimensions, (2) anal-

yse the feedback from spatial variability of peatland characteristics on the long-term behaviour, (3) investigate the influence of river incision at the boundary on the peatland characteristics.

5.2 Model formulation

MPeat in two dimensions is a fully coupled mechanical, ecological, and hydrological model of long-term peatland growth that accommodate the spatial variability of peat characteristics. This model is developed based on the continuum models (Irgens, 2008; Jog, 2015), which assume that peatland constituents, both solid and fluid particles, entirely fill the peatland body. Through this concept, the conservation of mass can be appropriately defined to formulate mechanical processes on the peatland obtained from the coupling between solid deformation and fluid flow or poroelasticity (Biot, 1941; Detournay and Cheng, 1993; de Boer, 2000; Wang, 2000; Coussy, 2004). The mechanical deformation of peat pores affects physical properties, including bulk density, active porosity, and hydraulic conductivity, resulting in different peatland behaviour (Figure 5.1). For example, the changes in hydraulic conductivity influence the water table position, which in turn, affects the peat production and decomposition processes. Furthermore, the proportion of plant functional types (PFT) and the plant weight are also affected because they are a function of the water table depth (Moore et al., 2002; Munir et al., 2015; Peltoniemi et al., 2016; Kokkonen et al., 2019; Laine et al., 2021). The two-dimensional version of MPeat is designed to model these complex feedbacks, together with the spatial variations in the horizontal and vertical directions from the peatland. As explained below, the formulation of the proposed model is divided into mechanical, ecological, and hydrological submodels.

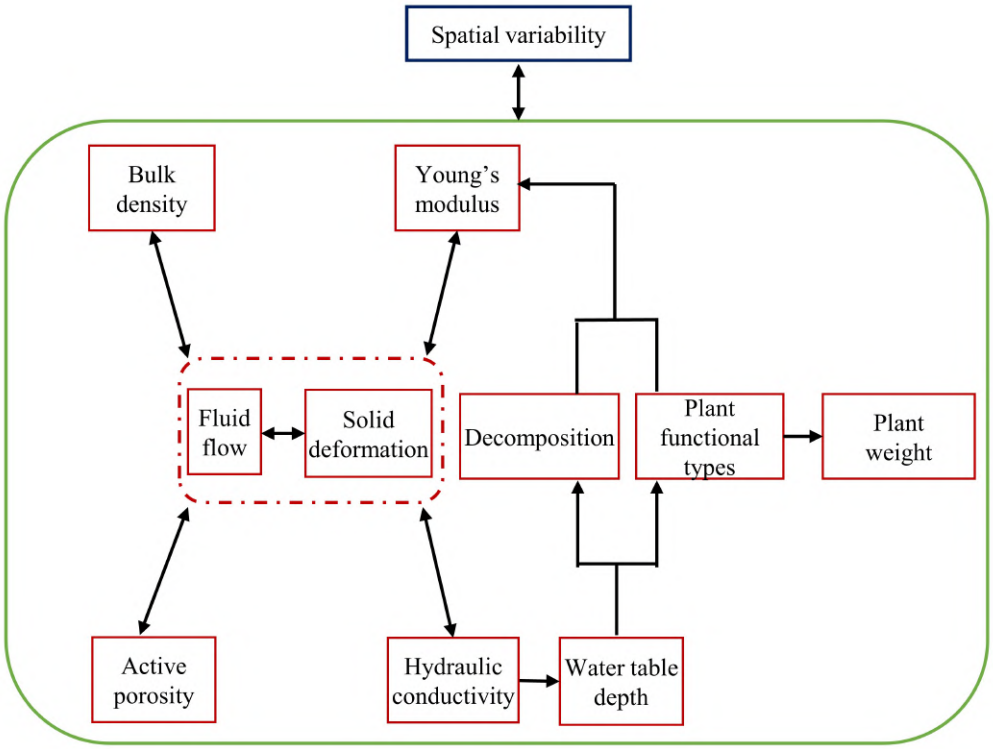

Figure 5.1: Illustrative formulation of the two-dimensional version of MPeat that model the feedback between mechanical, ecological, and hydrological processes together with the spatial variability of peatland characteristics in two dimensions. This model captures the changes of peat physical properties in both vertical and horizontal directions appropriately to analyse peatland behaviour.

5.2.1 Mechanical submodel

The mechanical submodel is developed from the two-dimensional poroelasticity theory for both fully saturated and unsaturated cases. Below the water table, I employed a fully saturated poroelasticity (Biot, 1941) where

the governing equations are

$$\overline{\nabla}^{T}\boldsymbol{\sigma} + \mathbf{b} = \mathbf{0} \tag{2.65 revisited}$$

$$\boldsymbol{\sigma'} = \boldsymbol{\sigma} - \alpha \mathbf{m} p \tag{2.66 revisited}$$

$$\boldsymbol{\sigma'} = \mathbf{D}\boldsymbol{\epsilon} \tag{2.67 revisited}$$

$$\boldsymbol{\epsilon} = \overline{\nabla}\mathbf{u} \tag{2.68 revisited}$$

$$\alpha \frac{\partial \epsilon}{\partial t} + S_s \frac{\partial p}{\partial t} = \nabla \cdot (\kappa \nabla p) \tag{2.69 revisited}$$

with $\overline{\nabla} = \begin{bmatrix} \partial/\partial x & 0 \\ 0 & \partial/\partial y \\ \partial/\partial y & \partial/\partial x \end{bmatrix}$, $\boldsymbol{\sigma} = [\sigma_{xx}, \sigma_{yy}, \sigma_{xy}]^T$, $\mathbf{b} = [0, \rho g]^T$, $\mathbf{m} = [1 \quad 1 \quad 0]^T$, $\mathbf{D} = \frac{E}{(1+\nu)(1-2\nu)} \begin{bmatrix} 1-\nu & \nu & 0 \\ \nu & 1-\nu & 0 \\ 0 & 0 & \frac{1-2\nu}{2} \end{bmatrix}$, $\boldsymbol{\epsilon} = [\epsilon_{xx}, \epsilon_{yy}, \epsilon_{xy}]^T$, $\mathbf{u} = [u_x, u_y]^T$.

Above the water table, I use the same assumption as the one-dimensional model related to air pressure (air pressure is equal to atmospheric pressure). Therefore, the unsaturated zone can be modelled as (Cheng, 2020)

$$\alpha_w \frac{\partial \epsilon}{\partial t} + \frac{1}{M_w} \frac{\partial p}{\partial t} = \nabla \cdot (\kappa \nabla p) \tag{5.1}$$

with the parameters

$$\alpha_w = S_w \tag{5.2}$$

$$M_w = \frac{\gamma_w (1-\lambda)}{\phi \lambda \mu} S_w^{-1/\lambda} \left(1 - S_w^{1/\lambda}\right)^{\lambda} \tag{5.3}$$

where $\boldsymbol{\sigma}$ is the total stress tensor (Pa), $\boldsymbol{\sigma'}$ is the effective stress tensor (Pa), α is the Biot's coefficient $(-)$, $\boldsymbol{\epsilon}$ is the strain tensor $(-)$, $\mathbf{u}$ is the displacement (m), p is the pore water pressure (Pa), $\mathbf{b}$ is the body force

($\mathrm{N\,m^{-3}}$), S_w is the degree of saturation of water ($-$), γ_w is the specific weight of water ($\mathrm{N\,m^{-3}}$) , ϕ is the active porosity ($-$), λ is the first water retention empirical constant ($-$), μ is the second water retention empirical constant (m^{-1}), ϵ is the strain ($-$), p_w is the pore water pressure (Pa), and κ is the hydraulic conductivity ($\mathrm{m\,s^{-1}}$).

The discretisation is required in order to solve the partial differential equations from poroelasticity formulation. In one dimension, the discretisation is relatively simple because it is only a vertical line, which represents the peatland height. However, in two dimensions, the discretisation becomes more complex and significantly affects the stability of the model (George, 2000; Edelsbrunner, 2001; Zhu et al., 2006). Persson and Strang (2004) proposed a mesh generator code to discretise the two- or three-dimensional domain based on the signed distance function. The code is straightforward that can be used for a finite element or finite volume discretisation, geometry modelling, and computer graphics. However, the algorithm requires a predetermined equation for domain descriptions that cannot be obtained from my problem. The internal and external feedback mechanism changes the domain and shape of the peatland as it grows with time. Therefore, I implemented the Delaunay triangulation, which provides an optimal and non-overlapping connection between the neighboring triangles from a data sets of points to create a two-dimensional mesh (Shewchuk, 2002).

The load from plant weight, new layer addition, and body force results in the deformation of the peat pore structure represented by vertical and horizontal displacement of the solid particle. I proposed the influence of two-dimensional deformation on the peat bulk density and active porosity

as follows

$$\rho_t = \frac{\rho_{t-1}}{1 + \beta_\rho \nabla \cdot \mathbf{u}} \tag{5.4}$$

$$\phi_t = \frac{\phi_{t-1} + \beta_\phi \nabla \cdot \mathbf{u}}{1 + \nabla \cdot \mathbf{u}} \tag{5.5}$$

where ρ is the bulk density (kg m^{-3}), β_ρ is the bulk density parameter ($-$), ϕ is the active porosity ($-$), β_ϕ is the active porosity parameter ($-$), $\mathbf{u}$ is the displacement (m).

The formulation of Young's modulus is similar to Equation (4.1) from the one-dimensional model, which is a function of remaining mass and the proportion of plant functional types. Therefore, peat becomes stiffer and has a higher Young's modulus if the shrub is dominant, while peat becomes softer with a lower Young's modulus if *Sphagnum* dominates the plant functional type. However, in order to reduce the computational time, I used the average value of the remaining mass for the peat located below the water table in Young's modulus calculation.

5.2.2 Ecological submodel

Peat production is calculated through Equation (3.12), which depends on the water table position and air temperature. Peat production together with the proportion of plant functional types are employed to model the plant weight at the top surface as stated in the Equation (3.13). The decomposition model is obtained from Equation (3.14) and the remaining mass is calculated from the ratio between mass at time t, which has experienced decay, and the initial mass (Equation (3.15)).

I used a similar linear regression model to estimate the proportion of PFT

based on the water table positions Equation (4.2), (4.3), (4.4). The main difference is the relaxation of the minimum and maximum values of PFT proportion. In this model, PFT proportion is not limited by the range value of the water table position that is available from Moore et al. (2002) measurements. However, through this approach, there is a possibility that the PFT proportion is negative or the total proportion is greater than one. Therefore, I assigned the minimum value of each PFT proportion equal to zero if the value is negative and normalised the total proportion.

5.2.3 Hydrological submodel

I model the peatland groundwater flows in two dimensions using the Boussinesq equation (Boussinesq, 1871) subject to net rainfall that acts as a source term (Cobb et al., 2017; Baird et al., 2012; Morris et al., 2012)

$$S_y \frac{\partial H}{\partial t} = \nabla \cdot (T \nabla H) + r \tag{5.6}$$

where H is the water table height (m), S_y is the specific yield ($-$), T is the transmissivity ($\mathrm{m^2\,yr^{-1}}$), and r is the net rainfall (precipitation minus evapotranspiration) ($\mathrm{m\,yr^{-1}}$). Boussinesq equation is developed based on the Dupuit and Forchheimer (D-F) assumption (Dupuit, 1863; Forchheimer, 1930), which states that groundwater flows horizontally in unconfined aquifers. The D-F assumption is appropriate to model the peatland groundwater because the peatland lateral distance is much wider than the thickness, which leads to the dominant horizontal flow.

MODFLOW from U.S. Geological Survey (McDonald and Harbaugh, 2003) and DigiBog (Baird et al., 2012; Morris et al., 2012) use the finite difference method to solve the Equation (5.6). However, the grid characteristics,

including the size and shape, are crucial in the finite difference method to satisfy the conservation of mass principle, resulting in higher computational time, error, and instability in solving the complex boundaries and system. I applied the finite volume method (Eymard et al., 2000; Moukalled et al., 2016) that provides flexibility in discretisation, and the conservation of mass principle can be adequately accommodated within each control volume.

In the finite volume form, the continuity equation that explains the balance of flow can be obtained by integrating Equation (5.6) over arbitrary control volume V to give

$$\int_V S_y \frac{\partial H}{\partial t} dV = \int_V \nabla \cdot (T \nabla H)\, dV + \int_V r dV \tag{5.7}$$

The Gauss divergence theorem is used to simplify the Equation (5.7), thus

$$\int_V S_y \frac{\partial H}{\partial t} dV = \int_S T \nabla H \cdot \boldsymbol{n} dS + \int_V r dV \tag{5.8}$$

where S is the surface of the control volume and $\boldsymbol{n}$ represents the outward unit normal to the surface.

The changes in the active porosity due to the deformation of peat pore structure influence hydraulic conductivity through the Equation (3.16). Although the formulation of hydraulic conductivity is the same as the one-dimensional model, the input to the formulation is different because active porosity is affected by vertical and horizontal deformation. Therefore, hydraulic conductivity also varies in the two-dimensional space. I assume that the height of the water table cannot surpass the height of the peatland because the water will flow as surface water, which is the same assumption employed in a one-dimensional model. Furthermore, the water table depth

is obtained from the difference between peatland height and water table height.

5.2.4 Numerical verification

The numerical verification is focused on the mechanical submodel developed based on two-dimensional poroelasticity. I compare the proposed algorithm for the fully saturated case with the analytical solution from Mandel's problem (Mandel, 1953). I employ 441 nodes and 800 elements to discretise the domain with a horizontal and vertical distance of 1 m. The numerical calculation shows a good agreement with the analytical solution indicated by a relatively small mean absolute error for normalized pore water pressure and solid displacement (see Chapter 2 for the full formulation and verification of two-dimensional poroelasticity). The first variable, normalized pore water pressure P, has the highest mean absolute error around 3.8×10^{-3}. For the second variable, normalized horizontal displacement u_x^*, has the highest mean absolute error around 2.8×10^{-3}. Finally, the highest mean absolute error of normalized vertical displacement u_y^* is about 1.1×10^{-3}.

5.3 Model implementation

I simulate long-term peatland development over 5000 years with flat and rigid substrates which are constrained by parallel rivers (Ingram, 1982) to demonstrate the proposed model. I modelled half of the domain from the central vertical axis to the one river with a distance of 500 m, which is discretised by a 10 m uniform horizontal grid, because I assumed that the peatland grows symmetrically (Baird et al., 2012; Morris et al., 2012). The

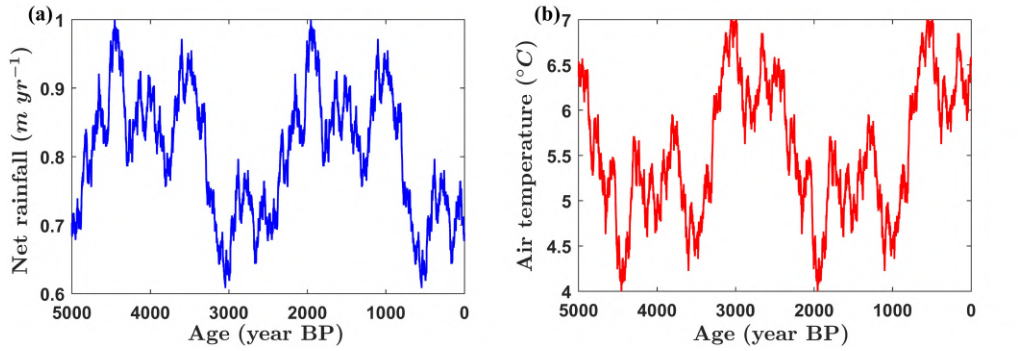

Figure 5.2: The climate profile over 5000 years, consisting of (a) net rainfall, which is defined as precipitation minus evapotranspiration, with the range value of 0.6 m yr^{-1} − 1 m yr^{-1}, and (b) annual average air temperature with the range value of 4 °C − 7 °C.

boundary conditions for the central axis are impermeable, and no horizontal displacement. I employed non-constant net rainfall (precipitation minus evapotranspiration) (Figure 5.2a) and annual average air temperature (Figure 5.2b) obtained from a sinusoidal function with some noise under the range value of 0.6 m yr^{-1} − 1 m yr^{-1} and 4 °C − 7 °C, respectively (Morris et al., 2015; Young et al., 2019, 2021). The total load on this system is associated with the surficial peat addition, plant weight, and body force. The surficial peat addition and plant weight were applied at the top surface, while the body force acted throughout the peatland area. In general, the simulations can be divided into two groups, with the parameter values summarised in Table 5.1.

In the first group, I focused on the addition of the horizontal dimension on peatland behaviour, including the thickness, physical properties, water table depth, PFT proportion, and plant weight. The simulations were conducted under the conditions of an impermeable substrate and constant river elevation. I assumed that the elevation of the substrate and river was the same, with a value equal to zero over the simulation time. Therefore, at the boundary between the peatland and the river, the peatland water table height was equal to zero. In general, the analysis in this group is conducted

Table 5.1: Symbols and parameter default values for the simulations.

Name	**Symbol**	**Value**	**Unit**	**Reference**
Unsaturated zone decay rate	η_{un}	5×10^{-2}	yr^{-1}	(Clymo, 1984)
Saturated zone decay rate	η_{sa}	8×10^{-5}	yr^{-1}	(Clymo, 1984)
Biot's coefficient	α	1	–	(Terzaghi, 1943)
Poisson ratio	ν	0.2	–	Present study
Bulk density initial value	ρ_0	50	$\mathrm{kg\,m}^{-3}$	(Lewis et al., 2012)
Carbon content	C	0.47	–	(Loisel et al., 2014)
Active porosity initial value	ϕ_0	0.8	–	(Quinton et al., 2000)
Bulk density parameter	β_ρ	3	–	Present study
Active porosity parameter	β_ϕ	2	–	Present study
Hydraulic conductivity initial value	κ_0	1×10^{-2}	$\mathrm{m\,s}^{-1}$	(Hoag and Price, 1995)
Hydraulic conductivity parameter	ξ	15	–	(Mahdiyasa et al., 2022)
Specific yield	S_y	1.4×10^{-2}	–	(Bourgault et al., 2017)
Degree of saturation of water	S_w	0.4	–	(Mahdiyasa et al., 2022)

Continued on next page

Table 5.1 – *Continued from previous page*

Name	**Symbol**	**Value**	**Unit**	**Reference**
Water retention empirical constant 1	λ	0.5	–	(Mahdiyasa et al., 2022)
Water retention empirical constant 2	μ	0.4	m^{-1}	(Mahdiyasa et al., 2022)
Specific storage	S_s	1.4×10^{-2}	m^{-1}	(Hogan et al., 2006)
Young's modulus parameter 1	χ	4×10^5	Pa	(Mahdiyasa et al., 2022)
Young's modulus parameter 2	ζ	0.1	–	(Mahdiyasa et al., 2022)
Shrub-Young's modulus parameter	b_1	1.25	–	(Mahdiyasa et al., 2023)
Sedge-Young's modulus parameter	b_2	1	–	(Mahdiyasa et al., 2023)
Sphagnum -Young's modulus parameter	b_3	0.75	–	(Mahdiyasa et al., 2023)
Shrub constant	d_1	0.4	–	(Mahdiyasa et al., 2022)
Sedge constant	d_2	0.4	–	(Mahdiyasa et al., 2022)
Sphagnum constant	d_3	20	–	(McNeil and Waddington, 2003)

under variable climates (Figure 5.2) to capture the effect of dry and wet conditions on peatland growth. However, only for the comparison with DigiBog (see Subsection 5.5.3), I employ constant net rainfall (0.8 m yr^{-1}) and air temperature (6 °C) in order to provide similar and comparable conditions.

In the second group, I analysed the effect of river incision on the peatland characteristics. I assumed that a peatland developed above a permeable substrate with decreasing river elevation at the edges due to the river incision. I explored the influence of a permeable substrate by allowing the water to flow in the substrate through the domain addition, with stiff and constant hydraulic conductivity characteristics. By including the permeable substrate, I aimed to simulate the water outflow through this area as the river decreases due to the incision phenomenon. Furthermore, the river incision effect was adapted by setting the peatland water table height equal to the lowered river elevation at the boundary. The river incision rate together with the hydraulic conductivity of the substrate, affect the peatland drainage and water table position, which in turn determines the peat production, decomposition and compaction through the changes in loading and effective stress. In this group, I employed two combinations of river incision rate Ω and substrate hydraulic conductivity κ_{subs}. The first combination indicates that the peatland experiences a significant decrease in river elevation during the development process, represented by the higher value of the river incision rate. In contrast, the change in river elevation is reduced in the second combination, indicated by the lower value of river incision rate.

$$\Omega = 5 \times 10^{-3}\,\mathrm{m\,yr^{-1}}\,, \kappa_{subs} = 1 \times 10^{-8}\,\mathrm{m\,s^{-1}}$$

$$\Omega = 5 \times 10^{-6}\,\mathrm{m\,yr^{-1}}\,, \kappa_{subs} = 1 \times 10^{-8}\,\mathrm{m\,s^{-1}}$$

To simplify the difference in the modelled peatland, I denote Peatland 1 as the peatland that grows in the constant river elevation and impermeable substrate, while Peatland 2 and 3 indicate a peatland that develops under the condition of non-constant river elevation and permeable substrate with Peatland 2 having the higher value of river incision rate than Peatland 3.

5.4 Simulation results

5.4.1 Peatland 1: Constant river elevation and impermeable substrate

The Peatland 1 simulation produces a dome shape peatland with the maximum thickness obtained at the centre (2.63 m) and decreases toward the margin. The peat physical properties, including bulk density (Figure 5.3), active porosity (Figure 5.4), and hydraulic conductivity (Figure 5.5), show spatial variability in the vertical and horizontal directions with the range value between 50 - 103 $\mathrm{kg\,m^{-3}}$, 0.47 - 0.8, and 1×10^{-2} - 3.7×10^{-6} $\mathrm{m\,s^{-1}}$, respectively, over 5000 years. They experience substantial changes in the transition between unsaturated and saturated zones but with different rates because the contrast becomes more significant at the margin compared to the centre.

After the unsaturated zone is developed, around 150 years since peatland initiation, water table depth experiences fluctuations depending on the net rainfall, hydraulic conductivity, and hydraulic gradient (Figure 5.6a). The spatial variability appears in the peatland water table depth, which is lower at the centre compared to the margin, especially after 2000 years BP, as the difference in the hydraulic gradient becomes more significant. Conse-

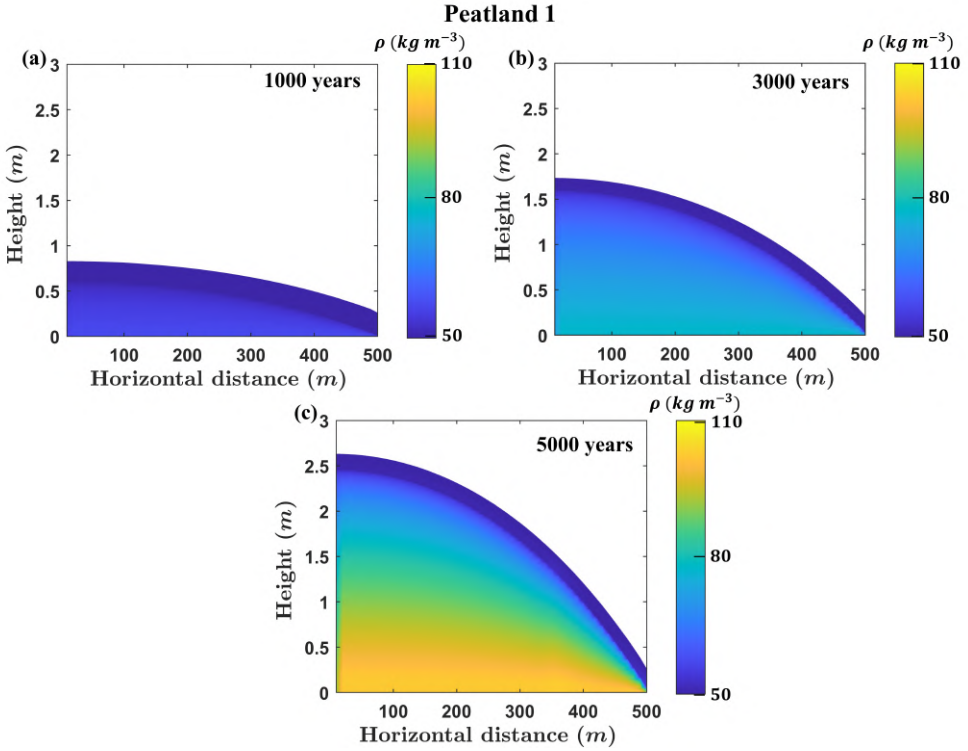

Figure 5.3: The two-dimensional profile of bulk density after (a) 1000 years, (b) 3000 years, and (c) 5000 years from Peatland 1.

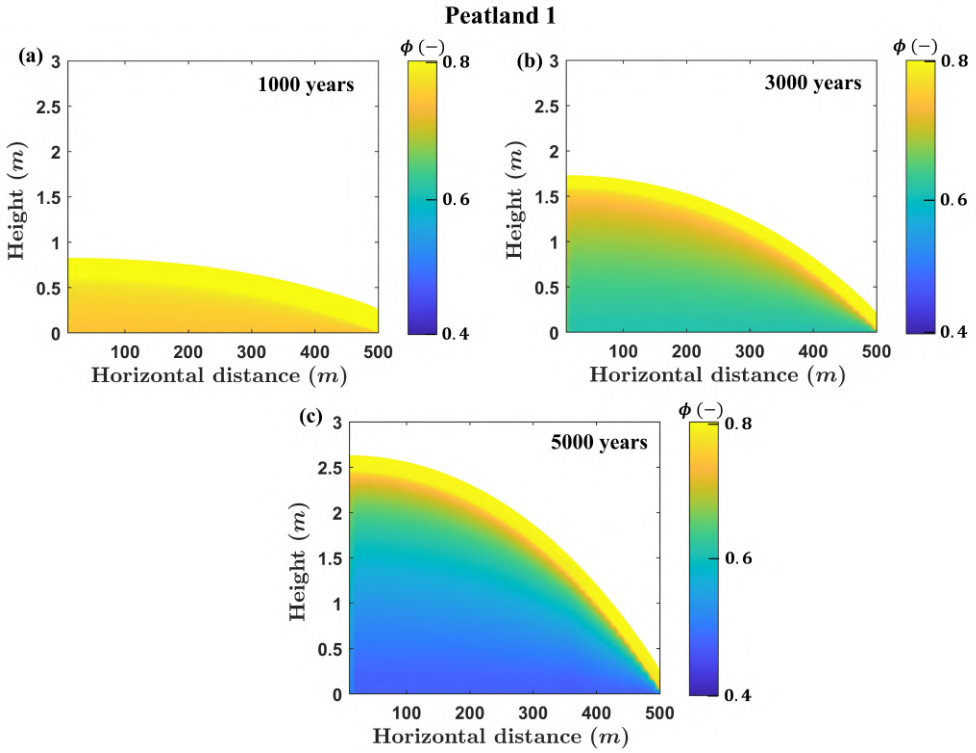

Figure 5.4: The two-dimensional profile of active porosity after (a) 1000 years, (b) 3000 years, and (c) 5000 years from Peatland 1.

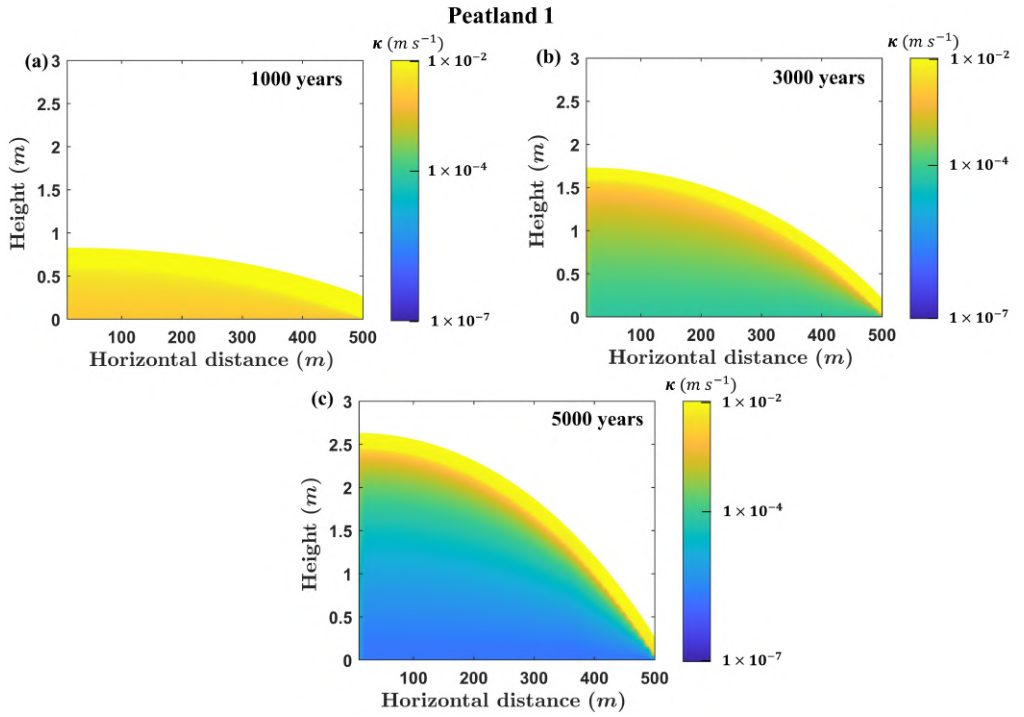

Figure 5.5: The two-dimensional profile of hydraulic conductivity after (a) 1000 years, (b) 3000 years, and (c) 5000 years from Peatland 1.

quently, the increasing variation in hydraulic gradient during the development processes potentially leads to drier conditions of the margins. Moreover, the differences in water table depth between the margin and centre increase in the wet season because of the disparity in the water storage. The water table depth fluctuates from 0 m until 0.34 m at the centre, and from 0.08 m until 0.35 m at the margin, with a maximum discrepancy of about 0.17 m.

The lateral variability in the water table depth influences PFT proportions and plant weight. For example, around 500 years BP, water table depth at the centre and margin are about 0.20 and 0.28 m, respectively. As a result, the *Sphagnum* proportion is higher at the centre (48%) compared to the margin (41%), while the shrub proportion becomes less dominant at the centre (18%) than at the margin (35%) (Figure 5.6b). Moreover, the variation of PFT proportion at 500 years BP leads to a different plant weight

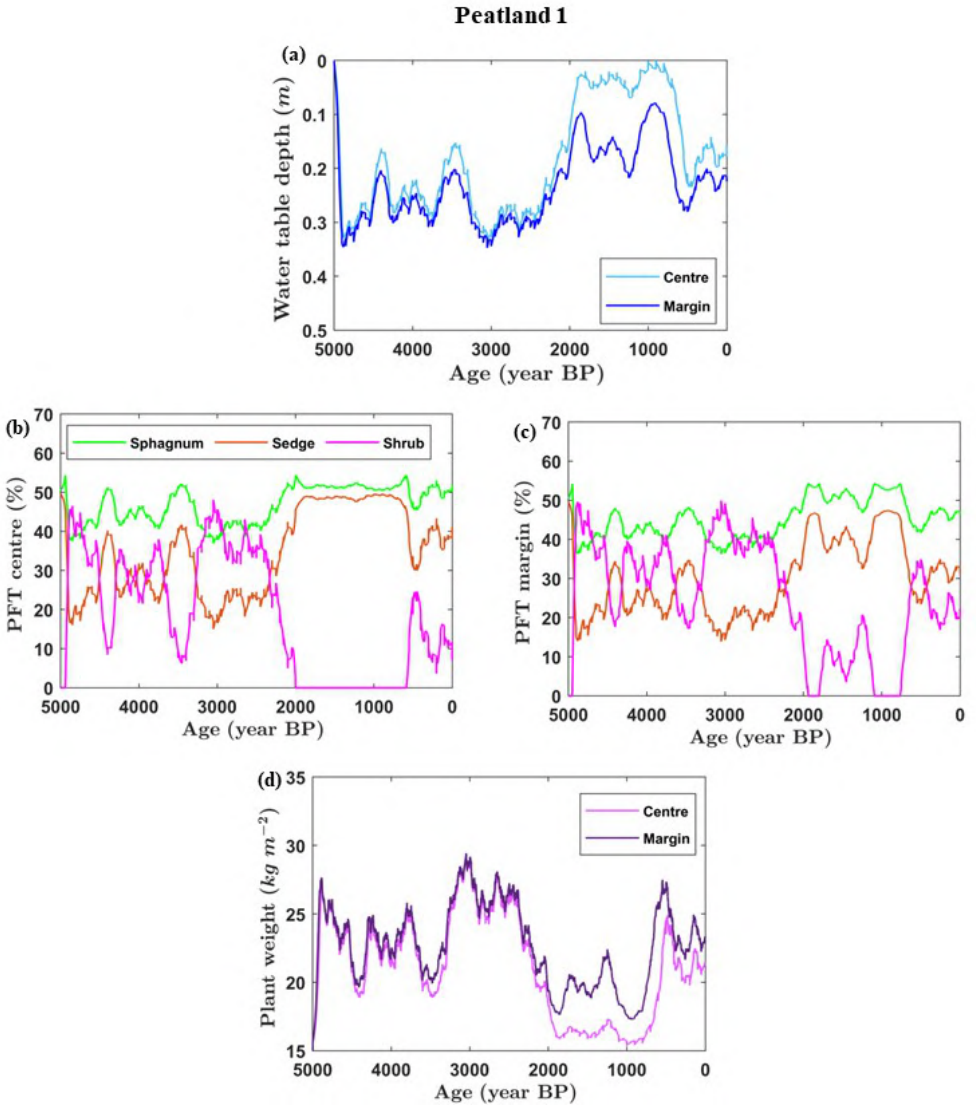

Figure 5.6: The profile of (a) water table depth, (b) plant functional types (PFT) proportion at the centre, (c) PFT proportion at the margin, and (d) plant weigh over 5000 years from Peatland 1. The water table depth is higher at the margin, which supports the shrub growth and produces a higher plant weight at the margin compared to the centre.

between the centre and margin, about 24.57 kg m^{-2} and 26.71 kg m^{-2}, respectively (Figure 5.6c).

5.4.2 Peatland 2 and 3: Non-constant river elevation and permeable substrate

The difference in the boundary conditions behaviour, represented by the changes in the river elevation at the edges, substantially affects the peatland interior. After 5000 years, the maximum thickness obtained from the Peatlands 2 and 3 are 1.51 m and 2.24 m, respectively. Peatland 2 experiences a more significant propagation effect than Peatland 3 as a consequence of a higher river incision rate, as shown in the Figures 5.7, 5.8, and 5.9. The range of water table depth obtained from Peatland 2 is about 0.03 - 0.34 m at the centre and 0.08 - 0.35 m at the margin, with the highest variation between these two areas around 0.09 m (Figure 5.10a). Conversely, Peatland 3 produces a minimum and maximum values of water table depth from 0.008 m to 0.34 m (at the centre) and from 0.07 m to 0.35 m (at the margin), with the highest difference about 0.15 m (Figure 5.10d) after the appearance of unsaturated zone.

The difference in the range of water table depth obtained from Peatlands 2 and 3 affect PFT proportion, plant weight, and mechanical compaction. In Peatland 2, PFT proportion (Figure 5.10b) fluctuates between the centre and margin with the maximum variation of about 8% (*Sphagnum*), 13% (sedge), and 21% (shrub) that leads to the most considerable difference in the plant weight of about 4.20 kg m^{-2} (Figure 5.10c). In contrast, Peatland 3 provides variation of PFT proportion in the lateral direction (Figure 5.10e) with the greatest difference between the margin and the centre around 11%, 18%, and 29% for *Sphagnum*, sedge, and shrub, respectively.

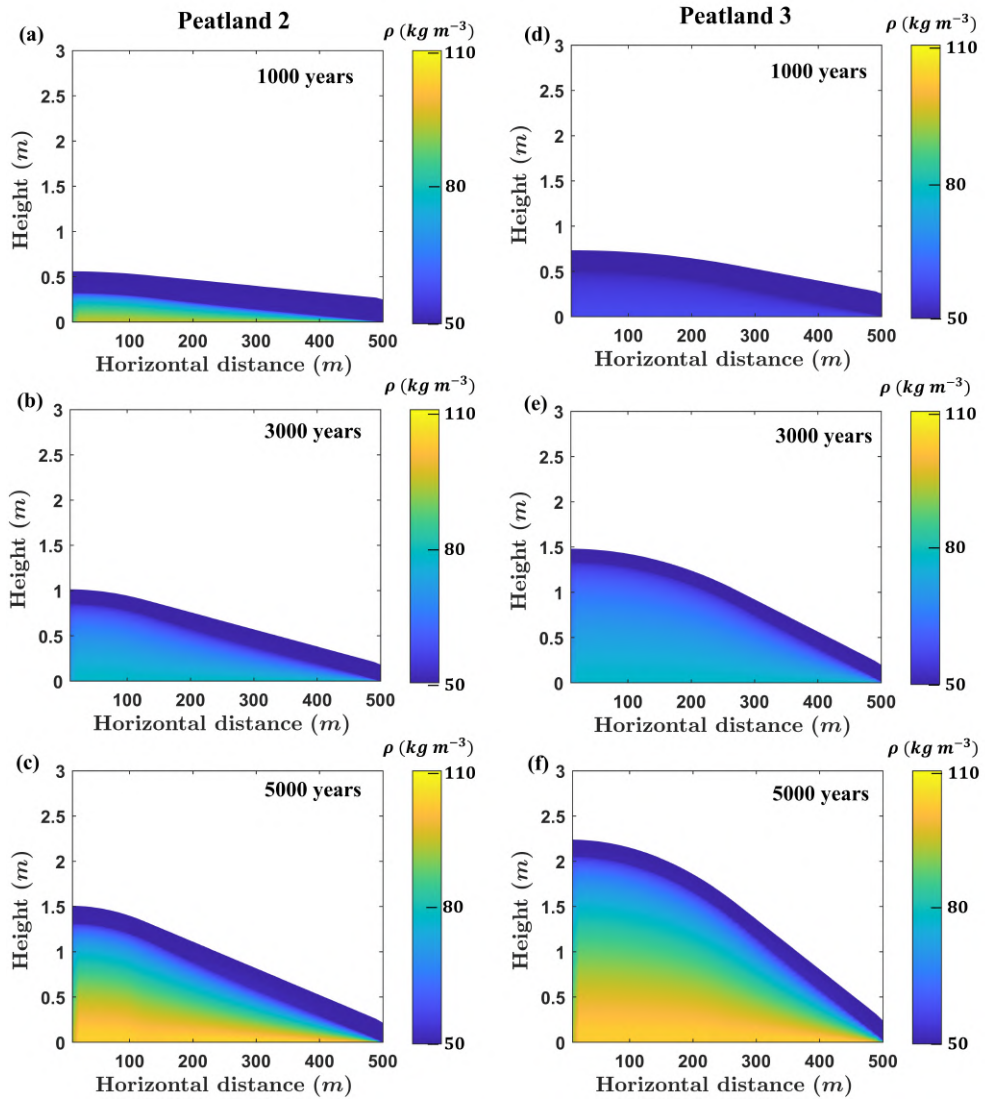

Figure 5.7: The two-dimensional profile of bulk density after 1000, 3000, 5000 years (a), (b), (c) from Peatland 2 and (d), (e), (f) from Peatland 3, respectively.

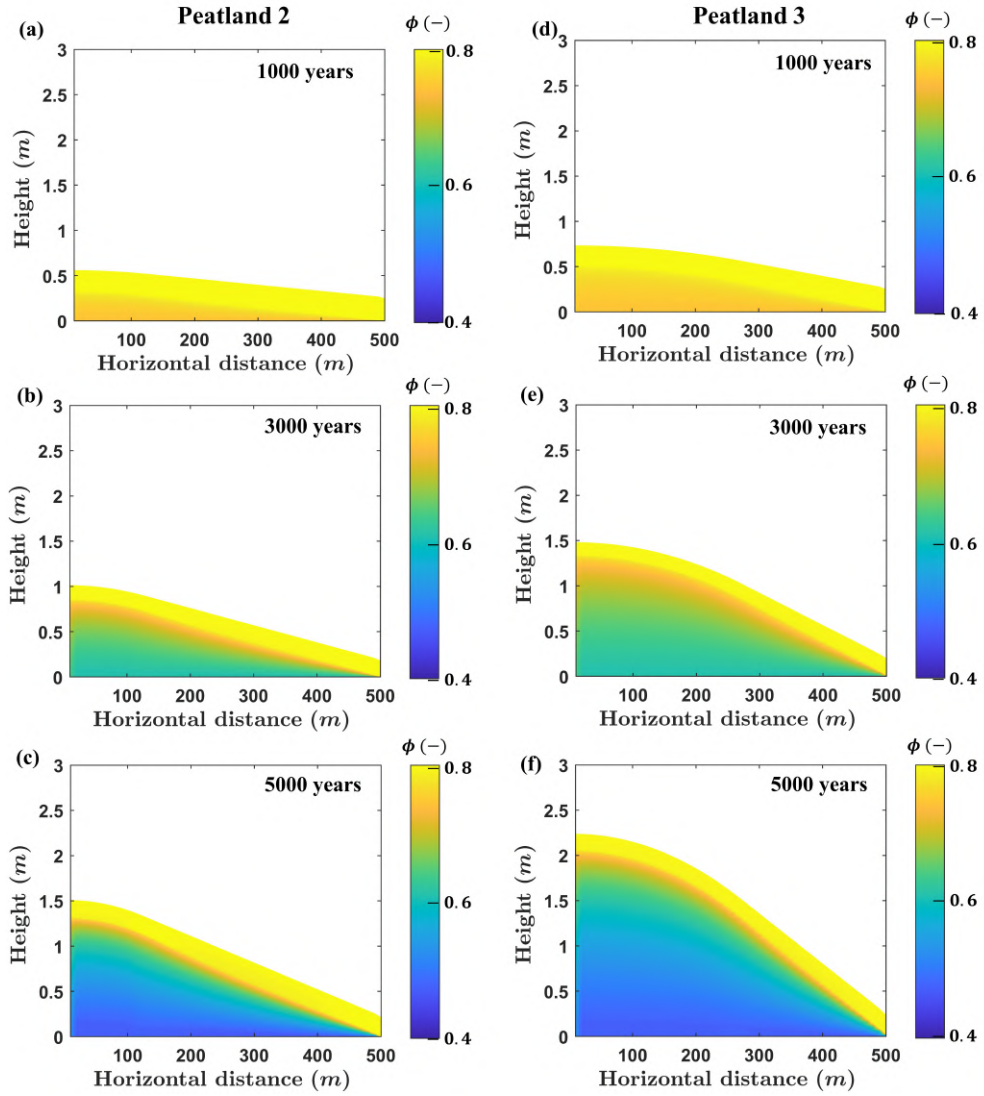

Figure 5.8: The two-dimensional profile of active porosity after 1000, 3000, 5000 years (a), (b), (c) from Peatland 2 and (d), (e), (f) from Peatland 3, respectively.

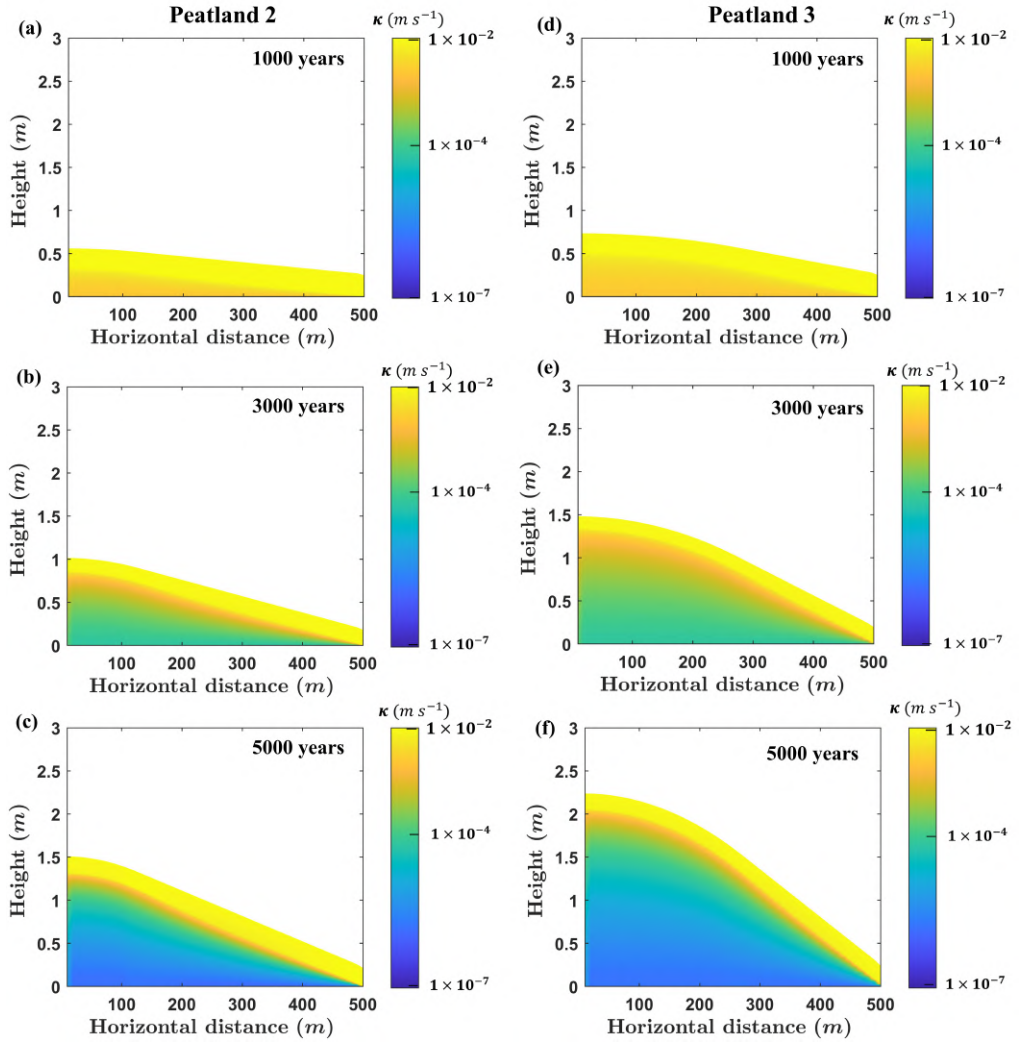

Figure 5.9: The two-dimensional profile of hydraulic conductivity after 1000, 3000, 5000 years (a), (b), (c) from Peatland 2 and (d), (e), (f) from Peatland 3, respectively.

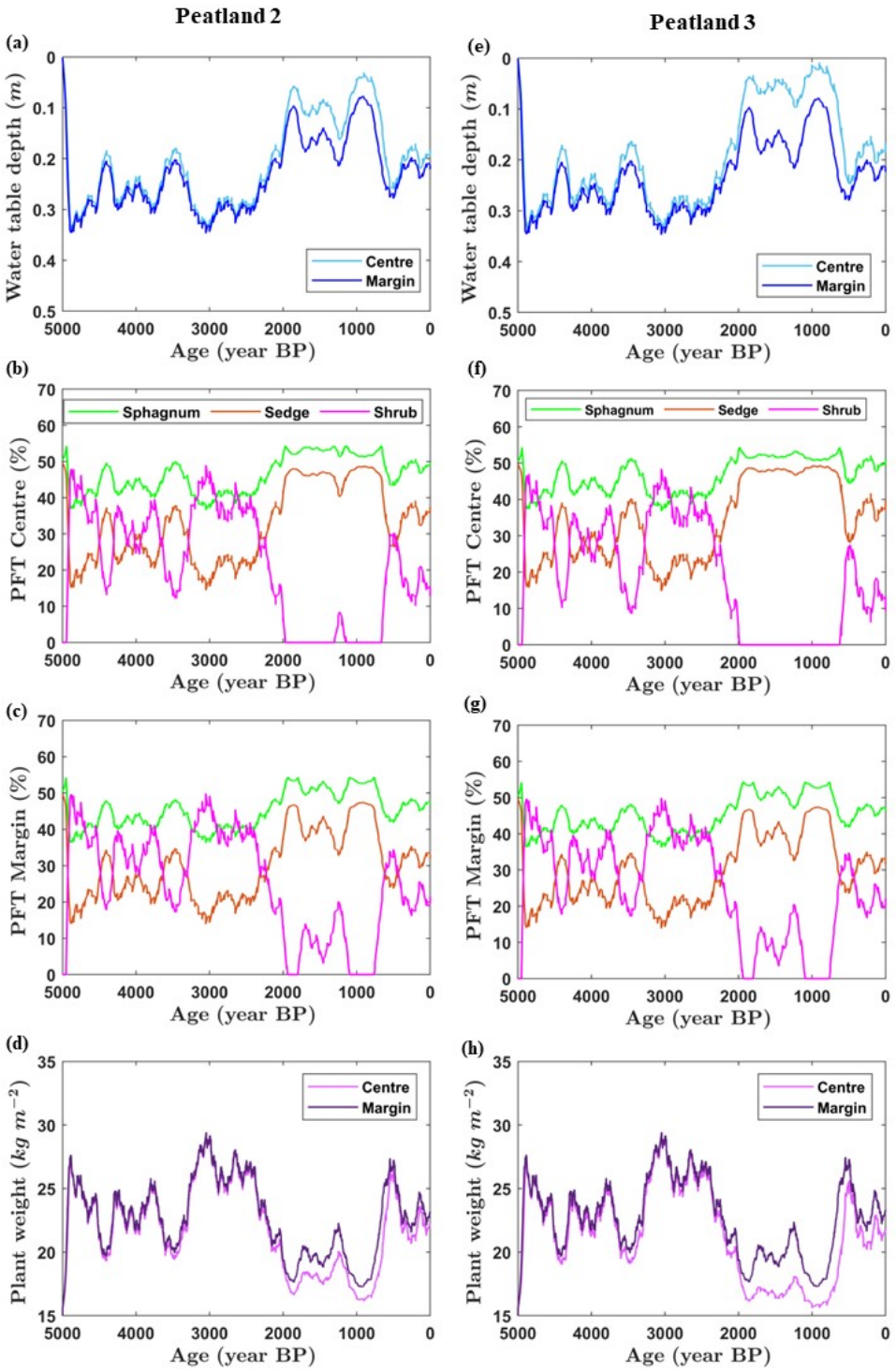

Figure 5.10: The profile of water table depth, plant functional types (PFT) proportion at the centre, PFT proportion at the margin, and plant weight over 5000 years (a), (b), (c), (d) from Peatland 2 and (e), (f), (g), (h) from Peatland 3, respectively.

The variations of PFT proportion obtained from Peatland 3 result in the maximum discrepancy for the plant weight around 6.06 $\mathrm{kg\,m^{-2}}$ (Figure 5.10f). Furthermore, Peatland 2 provides a more considerable effect of compaction than Peatland 3 due to the deeper position of water table, that leads to the higher maximum bulk density (105 $\mathrm{kg\,m^{-3}}$ vs. 103 $\mathrm{kg\,m^{-3}}$), lower minimum active porosity (0.46 vs. 0.47) and hydraulic conductivity (2.8×10^{-6} $\mathrm{m\,s^{-1}}$ vs. 3.7×10^{-6} $\mathrm{m\,s^{-1}}$) in the final simulation year (Figures 5.7, 5.8, and 5.9).

5.5 Discussion

The most important result from the two-dimensional version of MPeat is the ability to model the influence of spatial variability on long-term peatland behaviour. The addition of the second dimension provides a significant impact on the peat physical properties because they change in the vertical and horizontal directions. I found that the active porosity (Figure 5.4) and hydraulic conductivity (Figure 5.5) decrease systematically from the centre to the margin, while the bulk density (Figure 5.3) experiences an opposite pattern with the increasing value from the peatland interior to the edges. These horizontal variations in the peat physical properties obtained from MPeat are in agreement with previous modelling- and field-based studies (Armstrong, 1995; Whittington and Price, 2006; Lapen et al., 2005; Baird et al., 2008; Lewis et al., 2012).

The horizontal variability of the peat physical properties occurs because the peatland experiences not only different effects of decomposition (Lapen et al., 2005) but also compaction between the margin and the centre. The steeper hydraulic gradient at the margin promotes water release and re-

duces the position of the water table (Reeve et al., 2006; Lewis et al., 2012; Kværner and Snilsberg, 2011; Regan et al., 2019), which results in higher loading from plant weight and effective stress. In contrast, peatland topography at the centre is mainly flat, leading to the shallow water table position (Figure 5.6a), which in turn, limits the deformation of the peat pore space. At smaller scales of a few meters, another possible factor affecting the horizontal variance of peat physical properties is the peatland microform. The measurement from Whittington and Price (2006) showed that bulk density and hydraulic conductivity differ substantially in the lateral direction over distances of a few metres between hummocks, lawns, and hollows. Moreover, Baird et al. (2016) showed that the difference in the hydraulic conductivity between contiguous microform could vary by more than an order of magnitude. The variation in the water table position and plant functional types in the peatland microform (Eppinga et al., 2008; Malhotra et al., 2016; Moore et al., 2019), which significantly affect the loading, effective stress, and compaction on the peat pore space, might become a reasonable explanation for this behaviour. However, Baird et al. (2016) found that the change in hydraulic conductivity is less evident at a deeper location between adjacent hummocks and hollows, which suggests that the lateral variability of hydraulic conductivity at the small scale between the microhabitat types beyond the uppermost peat is questionable.

The changes of peat physical properties in the vertical direction, from the top surface to the bottom layer, obtained from the proposed model show an increasing value of bulk density and a decreasing value of active porosity and hydraulic conductivity (Clymo, 1984; Hoag and Price, 1995, 1997; Quinton et al., 2000; Fraser et al., 2001; Clymo, 2004; Quinton et al., 2008). The rapid changes occur at the transition between the unsaturated and saturated zone, indicating significant compaction on the peat pore space

due to the substantial increase of effective stress (Mahdiyasa et al., 2022, 2023). The fluctuations of peat physical properties become gradual in the saturated zone because pore water pressure reduces the effective stress that limits the deformation of the peat solid skeleton. Price (2003) found the decreasing value of effective stress below the water table that leads to smaller changes in peat volume, which supports my simulation results.

5.5.1 Comparison with field measurements

I compare the spatial variability of peat physical properties in the vertical and horizontal directions obtained from Peatland 1 with field observations. In the vertical direction, the changes in bulk density simulated from Peatland 1 are in the range of 50 - 103 $\mathrm{kg\,m^{-3}}$, consistent with the reported measurements of bulk density about 30 - 120 $\mathrm{kg\,m^{-3}}$ (Lunt et al., 2019; Loisel et al., 2014; Clymo, 1984). Furthermore, the simulation results of active porosity and hydraulic conductivity fluctuate between 0.47 - 0.8 and 3.7×10^{-6} - 1×10^{-2} $\mathrm{m\,s^{-1}}$, which are in accord with the field observations of active porosity and hydraulic conductivity about 0.1 - 0.8 and 7×10^{-9} - 1.6×10^{-2} $\mathrm{m\,s^{-1}}$, respectively (Quinton et al., 2008; Clymo, 2004; Fraser et al., 2001; Quinton et al., 2000; Hoag and Price, 1997, 1995). In the horizontal direction, I use the data from Lewis et al. (2012), who measured the lateral variabilities of hydraulic conductivity and bulk density at a depth of 30 to 40 cm from a blanket peatland in Ireland as a comparison. Although the peatland type from Lewis et al. (2012) is different from my simulations, the main reason for the comparison is to demonstrate the ability of the model to produce reasonable outputs of the lateral variability on peat physical properties that are empirically proven to occur in the real peatland. Lewis et al. (2012) found that the average values of

hydraulic conductivity at the margin and the centre are around 10^{-6} and 10^{-4} m s^{-1}, respectively. Peatland 1 produces hydraulic conductivity with a similar value at the margin (6.4×10^{-6} m s^{-1}) but higher at the centre (1.3×10^{-3} m s^{-1}) compared to the Lewis et al. (2012) observations. Moreover, the bulk density values obtained from Lewis et al. (2012) are around 55 and 110 kg m^{-3}, while my simulation provides the value of about 59 and 101 kg m^{-3} at the centre and margin, respectively. Although there are some discrepancies between simulation results with the field measurement, which are related to the differences in the peat stiffness, PFT composition, and substrate topography that result in the variations of compaction effect (Mahdiyasa et al., 2023, 2022; Whittington et al., 2007; Malmer et al., 1994), MPeat can model the spatial variability of peat physical properties reasonably well.

The thickness and carbon accumulation rate of Peatland 1 obtained from the simulation appear to be realistic. Peatland 1 produces an average growth rate of about 0.53 mm yr^{-1}, which leads to the maximum height of 2.63 m after 5000 years. Charman (2002) found that the average peat accumulation rate of the blanket and raised peatland are about 0.65 and 1 mm yr^{-1}, respectively, based on the relation between peatland carbon accumulation with age-depth curves. Aaby and Tauber (1975) analysed the correlation between the rate of peat accumulation with the degree of humification and found the growth rate of raised peatland in the range of 0.16 - 0.80 mm yr^{-1} with the average value of 0.44 mm yr^{-1}. Aaby and Tauber (1975) suggested that the relationship between the degree of humification and the growth rate is affected significantly by mechanical compaction. A more decomposed peat experiences a higher compaction effect due to the reduction in Young's modulus and strength (Mahdiyasa et al., 2023), which results in a lower peat thickness. Furthermore, the av-

erage value of the net rate of carbon accumulation obtained from Peatland 1 is about 0.0183 kg C m^{-2} yr^{-1}, which is in agreement with the reported measurements of northern peatlands during the Holocene with an average value around 0.0186 kg C m^{-2} yr^{-1} (Yu et al., 2009, 2010).

5.5.2 Comparison to a one-dimensional peatland growth model

I compare the water table depth, peatland height, and cumulative carbon obtained from the centre of the two-dimensional version of MPeat (MPeat2D) Peatland 1 with a one-dimensional version MPeat (MPeat1D) using the same climatic input as shown in Figure 5.2 and parameter values summarised in Table 5.1. MPeat2D predicts a shallower water table compared to the MPeat1D with the range value of 0 – 0.34 m and 0.16 – 0.36 m, respectively, after the appearance of the unsaturated zone (Figure 5.11a). The difference in the water table depth occurs because MPeat2D incorporates the spatial variability of the peat physical properties and a non-uniform hydraulic gradient, including the lower hydraulic conductivity at the margin and nearly flat topography at the centre (Baird et al., 2008; Lewis et al., 2012), which cannot be captured by MPeat1D. Moreover, the emergence of the unsaturated zone, represented by non-zero values of water table depth, is faster in the MPeat2D than MPeat1D with the difference of about 650 years. Consequently, MPeat2D undergoes a shorter time of fully saturated condition in the earlier time of development process, which prevents substantial changes in the peat physical properties near the substrate, as experienced by MPeat1D (Figures 3.3 and 3.5).

The discrepancy in the water table position at the centre between MPeat2D and MPeat1D leads to the variation in peatland height and cumulative car-

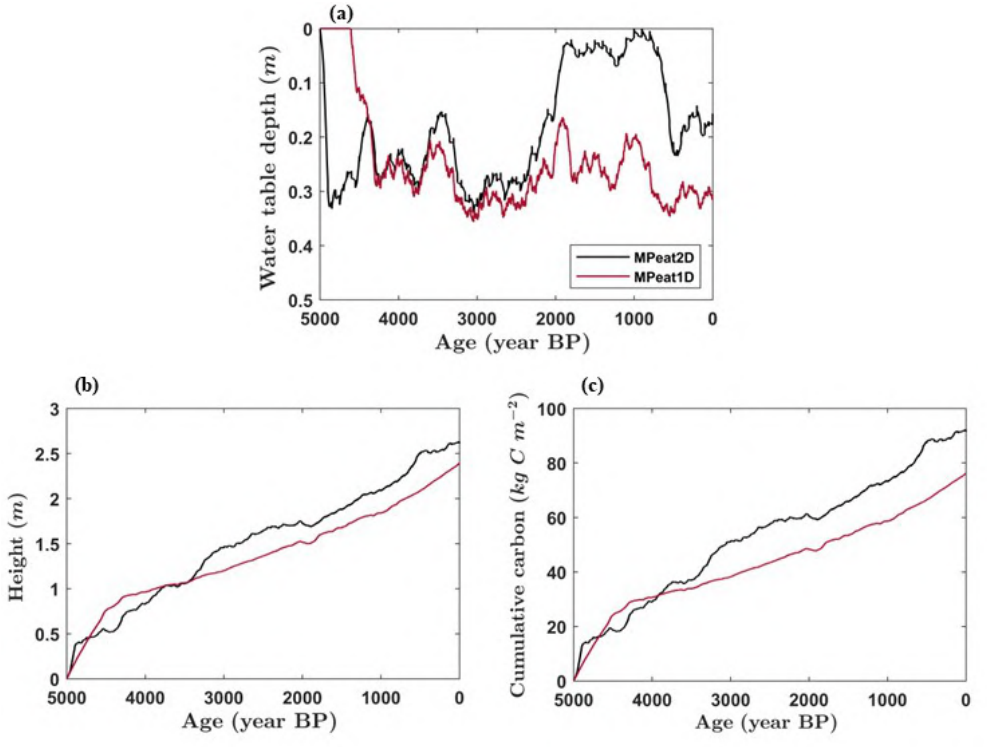

Figure 5.11: The comparison between the two-dimensional version of MPeat (MPeat2D) Peatland 1 with the one-dimensional version of MPeat (MPeat1D) for (a) water table depth, (b) peatland height, and (c) cumulative carbon at the centre over 5000 years. Both models use the same input for the climate and parameters, as shown in the Figure 5.2 and Table 5.1

bon (Figures 5.11b and 5.11c). The maximum height of the peatland after 5000 years obtained from MPeat2D (2.63 m) is greater than MPeat1D (2.39 m) due to the reduction of the compaction effect as the water table is closer to the surface (Whittington and Price, 2006; Waddington et al., 2010; Mahdiyasa et al., 2022, 2023). MPeat2D produces a higher cumulative carbon compared to MPeat1D in the final simulation year, with values of about 91 kg C m^{-2} and 76 kg C m^{-2}, respectively, because the shallow water table position results in a lower unsaturated zone thickness that experiences high rates of decay. Although the increasing peat production as the water table drops could compensate for an increment in the decomposition process, the studies from Evans et al. (2021), Huang et al. (2021), and Ma et al. (2022) indicate the positive feedback of wet conditions on

carbon accumulation.

The comparison between MPeat2D and MPeat1D shows the importance of spatial variability of water table position and peat physical properties, including bulk density, active porosity, and hydraulic conductivity, on the thickness and carbon stock of the peatland. These results are in agreement with Lapen et al. (2005), who found that lateral variations of hydraulic conductivity, lower at the margin than at the centre, encourage water accumulation that leads to more significant peat thickness. However, the analysis of Lapen et al. (2005) is based on the sensitivity analysis of the groundwater flow model at steady-state conditions, which omits the complex feedback from the peatland and only applies in specific situations. In contrast, MPeat provides a comprehensive approach that incorporates mechanical, ecological, and hydrological feedback to highlight the influence of spatial variations in the peatland characteristics during the development process.

5.5.3 Comparison to the other two-dimensional peatland growth model

In general, some results obtained from MPeat to analyse the influence of spatial variability on peatland behaviour align with DigiBog (Baird et al., 2012; Morris et al., 2012). Using the same assumption of the impermeable substrate with static river elevation at the edges and constant climate, both models produce dome shapes of the peatland in two dimensions over 5000 years (Figure 5.12a). However, the inclusion of mechanical processes on MPeat provides a plausible profile of bulk density and active porosity that are assumed to be a constant by DigiBog. The changes in peat physical properties and the discrepancy in the hydraulic gradient obtained from

MPeat lead to the spatial variation of water table depth which is inline with the field observation from Lewis et al. (2012) (Figure 5.12b). In contrast, DigiBog produces a relatively uniform hydraulic gradient that results in the constant water table depth between the centre and the margin. This condition limits the capabilities of DigiBog to simulate the lateral variation in peat production, decomposition, and PFT proportion because they depend on the water table depth (Clymo, 1984; Belyea and Clymo, 2001; Moore et al., 2002; Kokkonen et al., 2019; Laine et al., 2021). Although MPeat also suffers from the appearance of a cliff at the margin as DigiBog, the cliff height from MPeat (around 0.27 m) is lower than DigiBog (around 1.15 m) in the final simulation year due to the influence of mechanical compaction. A significant amount of effective stress is produced at the margin because of the higher water table depth, which decreases the peatland thickness in that area. This phenomenon also supports the importance of mechanical feedback to simulate a plausible shape of the peatland in two dimensions because the peat cliff at the margin does not appear in the natural condition, except due to extraction or erosion (Morris et al., 2012; Tuukkanen et al., 2017; Tarvainen et al., 2022).

The two-dimensional version of MPeat is developed based on the continuum concept (Irgens, 2008; Jog, 2015), while DigiBog uses linked vertical column to simulate a peatland. As a consequence, MPeat produces a smoother profile of peatland shape, especially near the margin compared to DigiBog. This is because, through the continuum concept, the deformation of peat pore structure due to the loading from a new surficial peat addition, plant weight, and body force is distributed continuously throughout the peatland. The continuum concept is also employed by Cobb et al. (2017) to model the development of tropical peatland in two dimensions and analyse the stable condition of the peatland shape and topography.

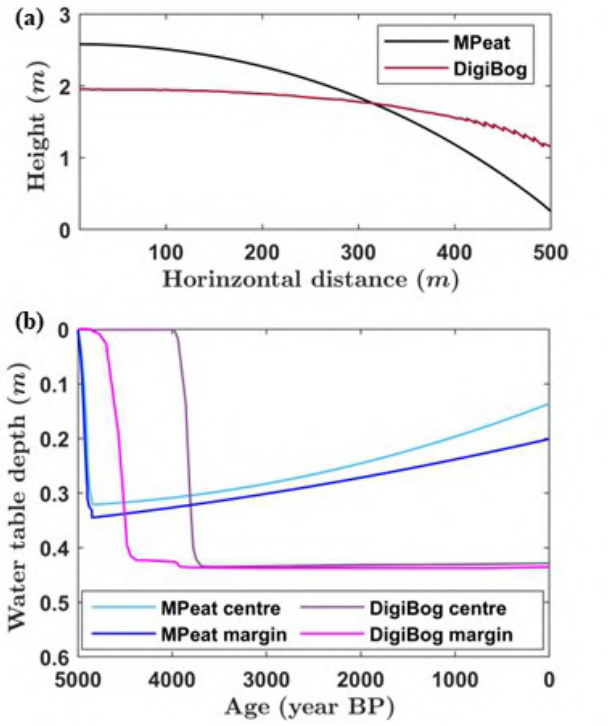

Figure 5.12: The comparison between (a) peatland shape and (b) water table depth from MPeat Peatland 1 and DigiBog Bog 2 (Morris et al., 2012) over 5000 years. Both models assume that the peatland develops above impermeable substrate with static river elevation at the edges and constant climate.

The current two-dimensional version of MPeat is unable to model the lateral expansion of peatland growth, as shown by DigiBog, and it might become a feature that could be enhanced. MPeat assumes a fixed horizontal domain where peat is uniformly distributed in the initial stages of development. Lateral expansion is crucial to model the paludification process that influences peatland behaviour because the transition process from forest to peatland involves changes in vegetation, nutrient availability, and peat physical properties (Charman, 2002; Anderson et al., 2003; Rydin and Jeglum, 2006). Another two-dimensional peatland growth model that provides lateral expansion is developed by Winston (1994). However, this model ignores the spatial variability of peat physical properties and internal feedback mechanisms, which limits our understanding of peatland behaviour as a complex system (Belyea and Baird, 2006; Belyea, 2009).

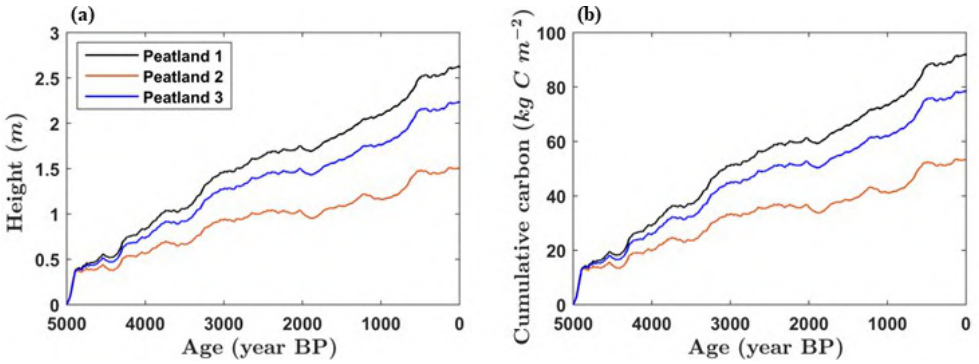

Figure 5.13: The profile of (a) peatland height and (b) cumulative carbon from Peatland 1 (without river incision and impermeable substrate), Peatland 2 (high rate of river incision and permeable substrate), and Peatland 3 (low rate of river incision and permeable substrate) at the centre over 5000 years.

5.5.4 The influence of river incision at the edges

The inclusion of river incision and permeable substrate on the MPeat leads to the different peatland shapes and thicknesses under the same climatic influence. A higher river incision rate produces a significant deviation from the dome shape, as shown by Peatland 2 (Figure 5.7, 5.8, and 5.9). The shape becomes more linear under a greater drop in river elevation, which reduces the variations in the hydraulic gradient and supports the water flow from the centre to the margin. Therefore, the spatial variability of water table depth, PFT proportion, and plant weight decrease as the river elevation experiences further drops (Figure 5.10). The variation in the peatland shape is reasonable due to the fact that the dome shape of the peatland is proposed based on the groundwater mound hypothesis, which assumes that the river and the substrate are at the same elevation all the time (Ingram, 1982).

The decreasing river elevation due to the incision phenomenon leads to higher water discharge from the peatland, which in turn reduces the peatland water table and the thickness, starting from the margin and propa-

gating towards the centre. The thicknesses of Peatlands 2 and 3 are lower, about 43% and 15% at the centre, compared to Peatland 1 that grows under constant river elevation and impermeable substrate after 5000 years, which is equivalent to the carbon loss of around 39 kg C m^{-2} and 13 kg C m^{-2}, respectively (Figure 5.13). This result is consistent with the study from Glaser et al. (2004b), who found that river incision reduces the water table height and thickness of the peatland. Furthermore, MPeat shows that river incision affects the peat physical properties by producing a higher value of bulk density (Figure 5.7) and a lower value of active porosity (Figure 5.8) and hydraulic conductivity (Figure 5.9). In general, the river incision is similar to the drainage process because it reduces the water table position, which leads to the enhancement of the effective stress and compaction effect on the peat pore space (Ballard et al., 2012; Regan et al., 2019; Word et al., 2022).

In order to generalise the results obtained from MPeat for the influence of the dynamics behaviour of the river at the boundary, I proposed a dimensionless quantity ω. This quantity is a function of river incision rate, substrate hydraulic conductivity, and the distance from the peatland centre to the margin or peatland radius. I include the peatland radius because the lateral discharge of water is reduced with the increasing distance between the centre and margin (Childs, 1969; Ingram, 1982; Armstrong, 1995), which results in a lower drop of the water table under the same value of river incision (Glaser et al., 2004b). Therefore, ω can be writen as

$$\omega = \frac{\Omega \kappa_{subs}}{lg} \tag{5.9}$$

where ω is the dimensionless quantity to represent the influence of river incision $(-)$, Ω is the river incision rate $(\mathrm{m\,yr^{-1}})$, κ_{subs} is the substrate

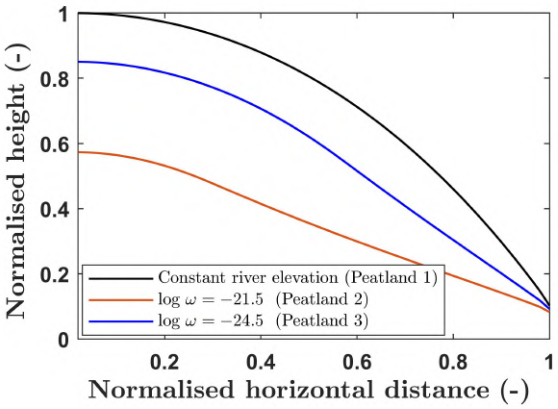

Figure 5.14: The effect of downcutting river at the boundaries on the peatland shape and thickness over 5000 years with different values of dimensionless constant ω, which is a function of river incision rate, substrate hydraulic conductivity, and peatland radius. Peatland 2 experiences a more significant influence of river incision than Peatland 3 indicated by a higher value of ω. Normalised height and normalised horizontal distance are obtained from peatland height divided by maximum height and peatland horizontal distance divided by maximum horizontal distance or peatland radius, respectively.

hydraulic conductivity ($\mathrm{m\,s^{-1}}$), l is the peatland radius (m), and g is the acceleration of gravity ($\mathrm{m\,s^{-2}}$).

Figure 5.14 shows the shapes of Peatlands 2 and 3 in terms of ω after 5000 years. A higher value of ω indicates that the effect of boundary conditions is more prominent in influencing the peatland interior, while a lower value of ω shows that the dynamics of the boundary conditions might be less critical on the peatland behaviour. Therefore, through this approach, the comparison between MPeat and field measurements is likely to become more appropriate because I have reduced the uncertainty of some variables.

I have shown the importance of spatial heterogeneity of peatland characteristics including peat thickness, water table depth, PFT composition, and peat physical properties, on the peatland behaviour through the two-dimensional version of MPeat. In the next chapter, MPeat is employed to analyse the limits to peatland carbon accumulation because of the me-

chanical instability that leads to peatland failure. The failure condition is determined by the interactions between stresses on the peat body and the peat strengths. I analyse the shear and tensile failure that lead to the peat slide and bog burst phenomena, respectively (Dykes and Kirk, 2001; Dykes and Warburton, 2008b; Dykes, 2008; Dykes et al., 2008; Dykes, 2022).

Chapter 6

Modelling the influence of mechanical instability on the limits to peatland carbon accumulation

6.1 Introduction

The two-dimensional model of peatland growth presented in Chapter 5 explains the influence of a higher dimension for understanding peatland behaviour. MPeat in two dimensions captures the spatial variations of water table depth, peat thickness, plant functional type composition, and peat physical properties, including bulk density, active porosity, and hydraulic conductivity as a peatland grows, which is beyond the ability of a one-dimensional model. Another phenomenon that requires analysis in the higher dimension is the mechanism of peatland failure due to mechanical instability in the long-term development. The peatland failure is a complex

process involving internal and external feedback mechanisms, particularly the interactions between stresses on the peat body and peat strength, which is affected by the peatland landscape.

Peatland failure involving a mass movement of peat is reported to occur throughout the world (Wilford, 1966; Wilson and Hegarty, 1993; Gallart et al., 1994; Dykes and Kirk, 2001; Warburton et al., 2003; Dykes et al., 2008; Dykes and Warburton, 2008b; Dykes, 2022) and provides several implications. This phenomenon affects peatland carbon stock because it supports peat erosion and drainage, reducing the carbon accumulation process (Warburton et al., 2003; Evans and Warburton, 2007) and possibly converting the peatland from net carbon sinks to carbon sources. The mass movement results in the loss of habitats not only for animals and plants in the failure location but also for aquatic life if the movement of peat mass reaches the main rivers or watercourses (McCahon et al., 1987). Furthermore, the recorded data of devastating peat mass movement events in Ireland resulted in extensive damage to property and infrastructure, with considerable economic loss (Long and Jennings, 2006; Dykes and Warburton, 2007).

The previous studies of the peatland failure mechanism indicate that the peat strength and the slope inclination are primary factors controlling peat mass movement, including peat slides and bog bursts. Dykes and Warburton (2008b) employed a slope stability model to analyse the mass movement in the Dooncarton Mountain in Ireland and found that the occurrence of peat slides is significantly influenced by the shear strength and the slope angle. Moreover, the studies of mass movement in terms of bog bursts in Maghera Mountain, Ireland, provided quantitative evidence that tensile strength is potentially a crucial factor in the occurrence of this type of peatland failure (Dykes, 2008). The recorded data of peatland failure

shows that a higher slope angle leads to lower peat thickness because peat growth is constrained by mechanical instability (Wilford, 1966; Alexander et al., 1986; Wilson and Hegarty, 1993; Gallart et al., 1994; Dykes and Kirk, 2001; Warburton et al., 2003; Yang and Dykes, 2006; Dykes et al., 2008; Dykes and Warburton, 2008b; Dykes, 2008; Boylan et al., 2008; Dykes and Selkirk-Bell, 2010). Therefore, the variations in the slope angle, and the interactions between stresses on the peat body and peat strength determine the maximum limit of peat and carbon accumulation before the failure takes place.

The existing models to analyse long-term peat and carbon accumulation focus on the water supply and the balance between peat production and decomposition (e.g., Yu et al., 2001; Frolking et al., 2010; Heinemeyer et al., 2010; Baird et al., 2012; Morris et al., 2012), with the basic concept proposed by Ingram (1982) and Clymo (1984) through the Groundwater Mound Hypothesis and Bog Growth Model, respectively (see Chapter 1). However, these models ignore the possibility of peatland failure due to the mechanical instability that affects the carbon accumulation process. MPeat is a fully coupled mechanical-ecohydrological model of long-term peatland growth, formulated based on poroelasticity theory. The two-dimensional version of MPeat includes the spatial variations of water table position, plant functional types (PFT) composition, and peat physical properties, including bulk density, active porosity, and hydraulic conductivity, leading to the differences in the peat production and stresses experienced by the peat body (see Chapter 5). This model incorporates the possibility of failure conditions during development processes, which could change the estimation of the long-term peat and carbon accumulation. Therefore, the two-dimensional version of MPeat provides a conceptual framework that is suitable for analysing the maximum carbon accumulation of the peatland

in a given landscape.

The objectives of this chapter are to (1) examine the influence of a landscape, consisting of upland, sloping area, and lowland, which is constrained by the river on the peatland behaviour, (2) analyse the mechanical instability that leads to the peatland failure, (3) estimate the limits to carbon accumulation of a peatland before the occurrence of failure.

6.2 Methods

I modify the two-dimensional formulation of MPeat to investigate the peatland failure through the stresses on the peat body that are affected by feedback from mechanical, ecological, and hydrological processes. The shear failure that leads to the peat slide (Dykes and Kirk, 2001; Dykes and Warburton, 2008b; Dykes et al., 2008; Dykes, 2022) appears if the maximum shear stress is greater than the peat shear strength. In contrast, if the maximum tensile stress surpasses the peat tensile strength, then the peatland experiences a tensile failure that is related to the bog burst phenomenon (Dykes, 2008).

6.2.1 Model formulation

The mechanical submodel from MPeat, which is developed based on poroelasticity theory (Biot, 1941; Detournay and Cheng, 1993; de Boer, 2000; Wang, 2000; Coussy, 2004), produces pore water pressure and displacement of the solid particles, both in the vertical and horizontal directions, as the main outputs. I performed back calculations to obtain the stresses on the peat body through the kinematics relation and linear constitutive law that

provide a formulation between displacement and stresses (Equations 2.65 - 2.68). The mechanical failure occurs if the maximum stresses exceed the strengths of the material (e.g., Puzrin et al., 2014; Elsoufiev, 2007; Collins, 1993). Therefore, I calculate the principal stresses that provide maximum value of normal stresses, including tensile and compressive, as written below

$$\sigma_{1,2} = \frac{\sigma_{xx} + \sigma_{yy}}{2} \pm \sqrt{\left(\frac{\sigma_{xx} - \sigma_{yy}}{2}\right)^2 + {\sigma_{xy}}^2} \tag{6.1}$$

Furthermore, the maximum shear stress can be written as

$$\tau_{max} = \frac{\sigma_1 - \sigma_2}{2} = \sqrt{\left(\frac{\sigma_{xx} - \sigma_{yy}}{2}\right)^2 + {\sigma_{xy}}^2} \tag{6.2}$$

where σ_1 is the maximum principal stress (Pa), σ_2 is the minimum principal stress (Pa), σ_{xx} is the horizontal component of stress (Pa), σ_{yy} is the vertical component of stress (Pa), σ_{xy} is the shear stress (Pa), and τ_{max} is the maximum shear stress (Pa).

6.2.2 Model implementation and setup

I simulate the peatland development above rigid, impermeable, and non-flat substrate constrained by the two parallel rivers at the edges. I assume that substrate topography and peatland properties are symmetric toward the central vertical axis, with impermeable and no horizontal displacement characteristics. Through this assumption, I reduce the model domain and only simulate peatland from the centre to the one river with a distance of 500 m that is discretised by a 10 m uniform horizontal grid. Furthermore, the river at the boundaries is assumed to be static with negligible depth because I omit the downcutting phenomenon as the peatland grows. The substrate topography consists of the upland and lowland, which is separated

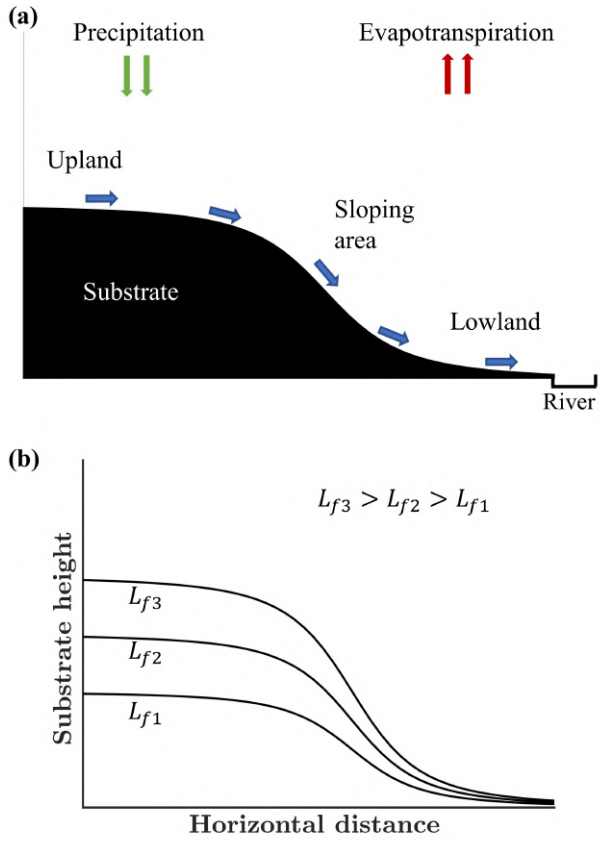

Figure 6.1: (a) The illustration of the proposed landscape that consists of the upland, lowland, and sloping area based on Winter (2001). Peatland receives water from net rainfall, which is defined as the precipitation (green arrows) minus evapotranspiration (red arrows). The blue arrows indicate the direction of water flow. (b) The illustration of landscape factor L_f which is defined as the ratio between the maximum height of the substrate with the horizontal distance from the centre to the edges $\left(\frac{H_s}{l}\right)$ to quantify the landscape characteristics. A higher value of landscape factor L_f indicates that the landscape contains a steeper slope.

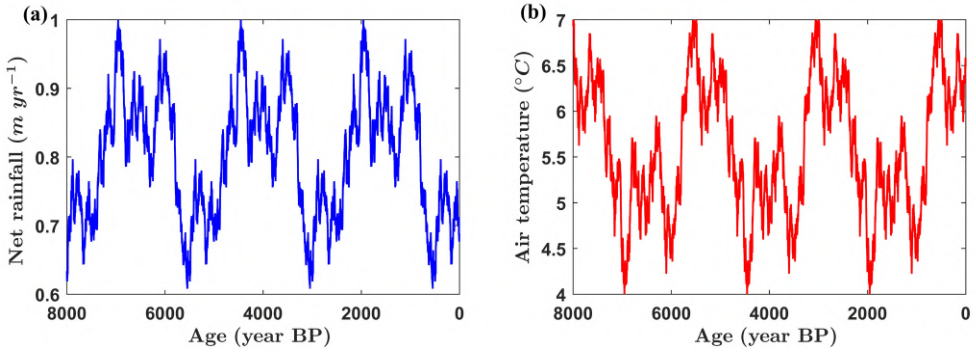

Figure 6.2: The climate profile over 8000 years, consisting of (a) net rainfall, which is defined as precipitation minus evapotranspiration, with the range value of $0.6\,\mathrm{m\,yr^{-1}} - 1\,\mathrm{m\,yr^{-1}}$, and (b) annual average air temperature with the range value of $4\,^{\circ}\mathrm{C}\ -\ 7\,^{\circ}\mathrm{C}$.

by the sloping area following the conceptual landscape from Winter (2001), as shown in Figure 6.1. I proposed a dimensionless constant landscape factor L_f, which is defined as

$$L_f = \frac{H_s}{l} \tag{6.3}$$

where H_s is the maximum height of the substrate (m) and l is the horizontal distance from the centre to the edges (m).

I varied the landscape factor of the proposed model from 0.01 to 0.03 over 8000 years with the input parameters and initial values summarised in Table 6.1. The detailed assessment is provided for peatland with a landscape factor of 0.01 because it serves as the baseline simulation. In order to reduce the repetition of information, the analysis is focused on failure conditions and accumulated carbon for higher landscape factors. The simulations employ climatic inputs of net rainfall (precipitation minus evapotranspiration) and air temperature between the range of $0.6 - 1$ m yr^{-1} and $4 - 7$ °C, respectively, generated from the sinusoidal function with some noise, as shown in Figure 6.2 (Morris et al., 2015; Young et al., 2019, 2021).

As the peatland grows, the complex interactions between mechanical, ecological, and hydrological processes occur in the proposed landscape. The flow of water is affected by the landscape topography, which leads to variations in the water table position, peat thickness, and carbon accumulation obtained from cumulative peat mass multiplied by 47% of carbon content (Loisel et al., 2014). The upland, lowland, and sloping areas, together with the total load that the peatland received from surficial peat addition, plant weight at the top surface, and peat self-weight that produces body force, lead to the different stresses on the peat body. Furthermore, these

Table 6.1: Symbols and parameter default values for the simulations.

Name	**Symbol**	**Value**	**Unit**	**Reference**
Unsaturated zone decay rate	η_{un}	5×10^{-2}	yr^{-1}	(Clymo, 1984)
Saturated zone decay rate	η_{sa}	8×10^{-5}	yr^{-1}	(Clymo, 1984)
Biot's coefficient	α	1	–	(Terzaghi, 1943)
Poisson ratio	ν	0.2	–	Present study
Bulk density initial value	ρ_0	50	$\mathrm{kg\,m}^{-3}$	(Lewis et al., 2012)
Bulk density parameter	β_ρ	2	–	Present study
Carbon content	C	0.47	–	(Loisel et al., 2014)
Active porosity initial value	ϕ_0	0.8	–	(Quinton et al., 2000)
Active porosity minimum value	ϕ_{min}	0.1	–	(Siegel et al., 1995)
Active porosity parameter	β_ϕ	2	–	Present study
Hydraulic conductivity initial value	κ_0	1×10^{-2}	$\mathrm{m\,s}^{-1}$	(Hoag and Price, 1995)
Hydraulic conductivity minimum value	κ_{min}	1×10^{-10}	$\mathrm{m\,s}^{-1}$	(Morris et al., 2022)
Hydraulic conductivity parameter	ξ	15	–	(Mahdiyasa et al., 2022)

Continued on next page

Table 6.1 – *Continued from previous page*

Name	**Symbol**	**Value**	**Unit**	**Reference**
Specific yield	S_y	1.4×10^{-2}	–	(Bourgault et al., 2017)
Degree of saturation of water	S_w	0.4	–	(Mahdiyasa et al., 2022)
Water retention empirical constant 1	λ	0.5	–	(Mahdiyasa et al., 2022)
Water retention empirical constant 2	μ	0.4	m^{-1}	(Mahdiyasa et al., 2022)
Specific storage	S_s	1.4×10^{-2}	m^{-1}	(Hogan et al., 2006)
Young's modulus parameter 1	χ	4×10^5	Pa	(Mahdiyasa et al., 2022)
Young's modulus parameter 2	ζ	0.1	–	(Mahdiyasa et al., 2022)
Shrub-Young's modulus parameter	b_1	1.25	–	(Mahdiyasa et al., 2023)
Sedge-Young's modulus parameter	b_2	1	–	(Mahdiyasa et al., 2023)
Sphagnum-Young's modulus parameter	b_3	0.75	–	(Mahdiyasa et al., 2023)
Shrub constant	d_1	0.4	–	(Mahdiyasa et al., 2022)
Sedge constant	d_2	0.4	–	(Mahdiyasa et al., 2022)

Continued on next page

Table 6.1 – *Continued from previous page*

Name	Symbol	Value	Unit	Reference
Sphagnum constant	d_3	20	–	(McNeil and Waddington, 2003)

interactions might result in peatland failure if the values of stresses exceed the shear or tensile strength of the peat in the range of 4000 – 35330 Pa and 2900 - 11300 Pa, respectively (Long, 2005; Boylan et al., 2008; Dykes, 2008; Dykes and Warburton, 2008b; Hendry et al., 2012; O'Kelly, 2015, 2017; Wang and Li, 2023).

6.3 Simulation results

6.3.1 The influence of substrate topography on the peatland characteristics

Peatland with a landscape factor of 0.01 shows spatial distribution of peat physical properties, including bulk density (Figure 6.3), active porosity (Figure 6.4), and hydraulic conductivity (Figure 6.4) in the range of 50 - 122 kg m^{-3}, 0.12 - 0.8, and 1×10^{-10} - 1×10^{-2} m s^{-1}, respectively, after 8000 years. The topography of the landscape affects peat physical properties, indicated by the difference in the bulk density, active porosity, and hydraulic conductivity values between the upland, sloping area, and lowland. The sloping area provides the highest bulk density (122 kg m^{-3})

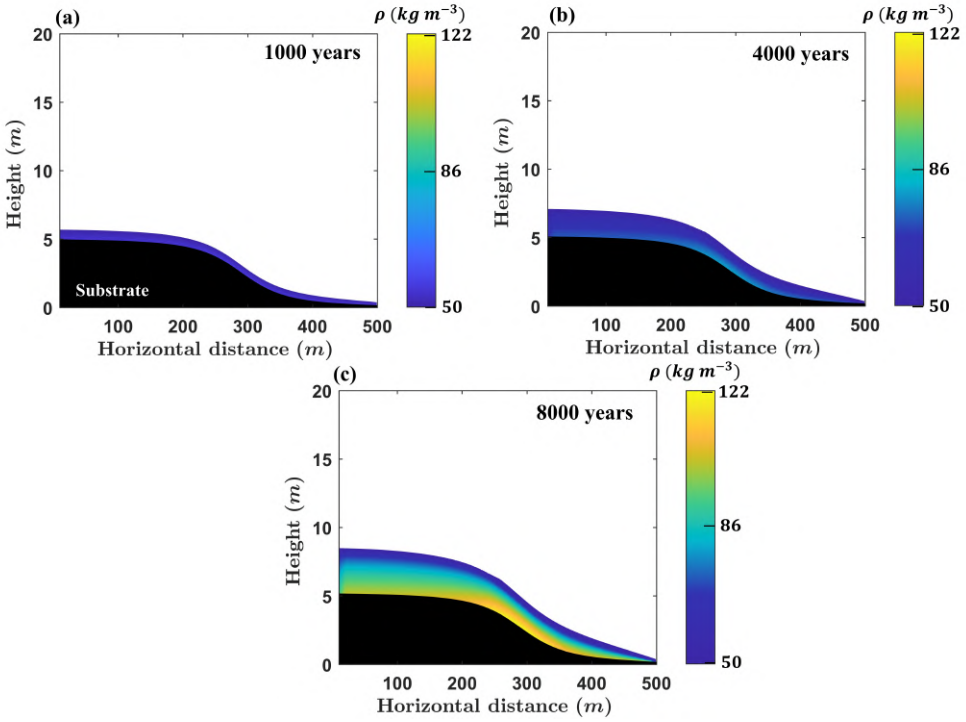

Figure 6.3: The two-dimensional profile of bulk density after (a) 1000 years, (b) 4000 years, and (c) 8000 years with the landscape factor of 0.01.

and the lowest active porosity (0.12) and hydraulic conductivity (1×10^{-10} m s^{-1}), suggesting a more significant compaction effect compared to the upland and lowland.

The fluctuations of the water table depth after the emergence of the unsaturated zone, 150 years since peatland initiation, are between 0 – 0.37 m at the centre, 0.02 – 0.36 m at the intermediate, and 0.05 – 0.37 m at the margin (Figure 6.6a). The centre, intermediate, and margin denote the location with the horizontal distance of 0 m, 300 m, and 500 m, representing upland, sloping area, and lowland, respectively. Furthermore, as peatland develops, the water table depth decreases, producing a wetter peatland under the same climatic influence. This condition occurs due to the compaction on the peat pore space from the increasing load provides a more significant effect on reducing water discharge, resulting in greater water accumulation.

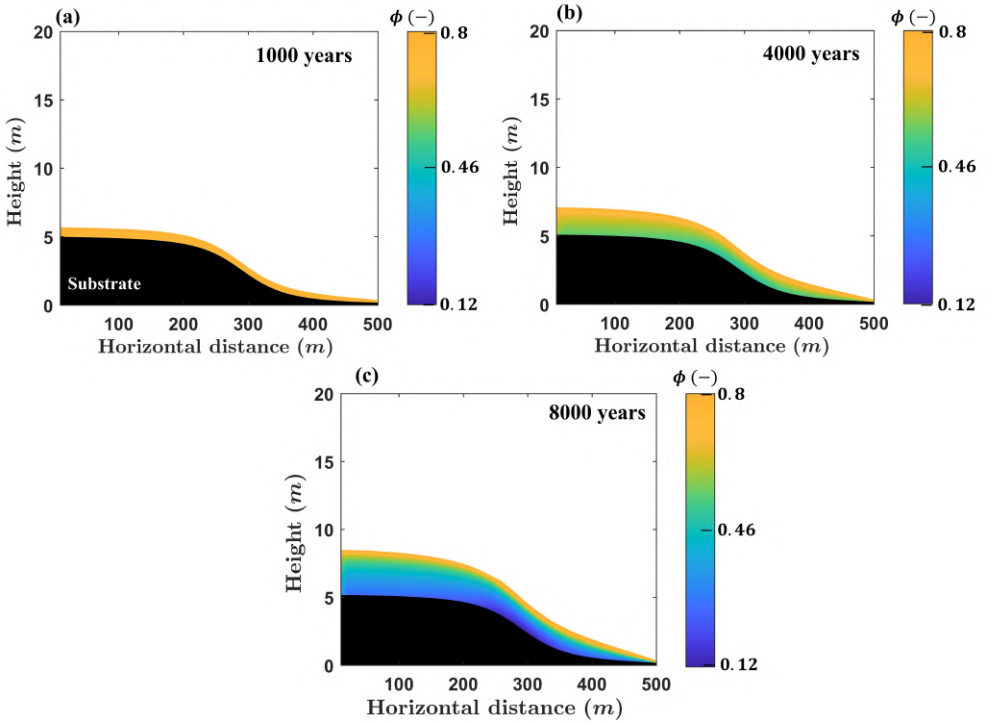

Figure 6.4: The two-dimensional profile of active porosity after (a) 1000 years, (b) 4000 years, and (c) 8000 years with the landscape factor of 0.01.

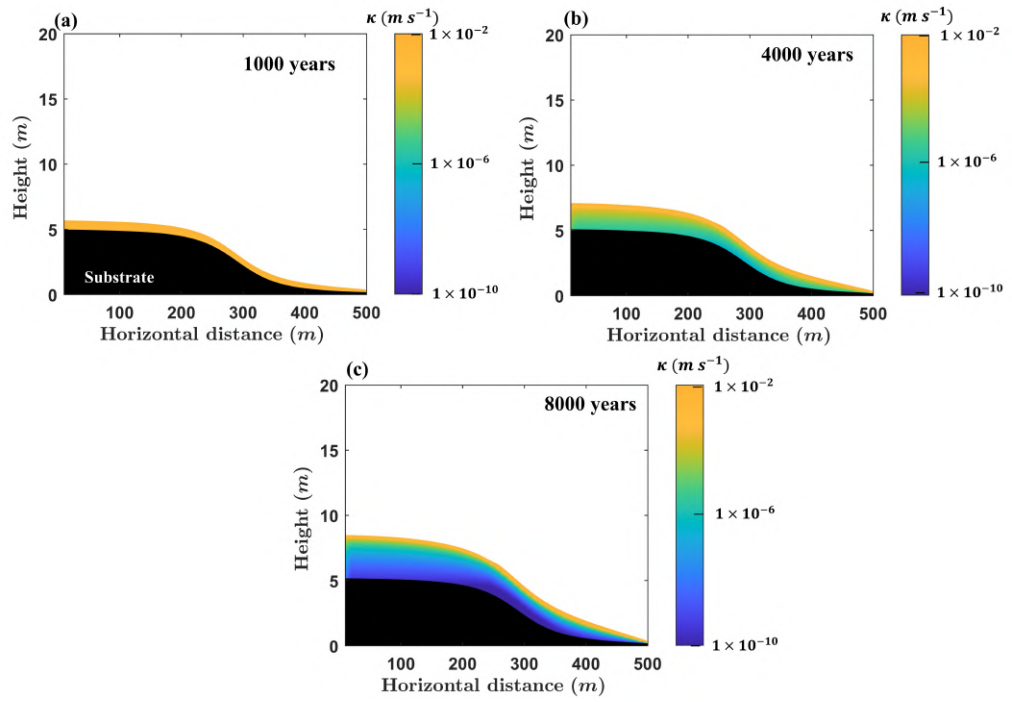

Figure 6.5: The two-dimensional profile of hydraulic conductivity after (a) 1000 years, (b) 4000 years, and (c) 8000 years with the landscape factor of 0.01.

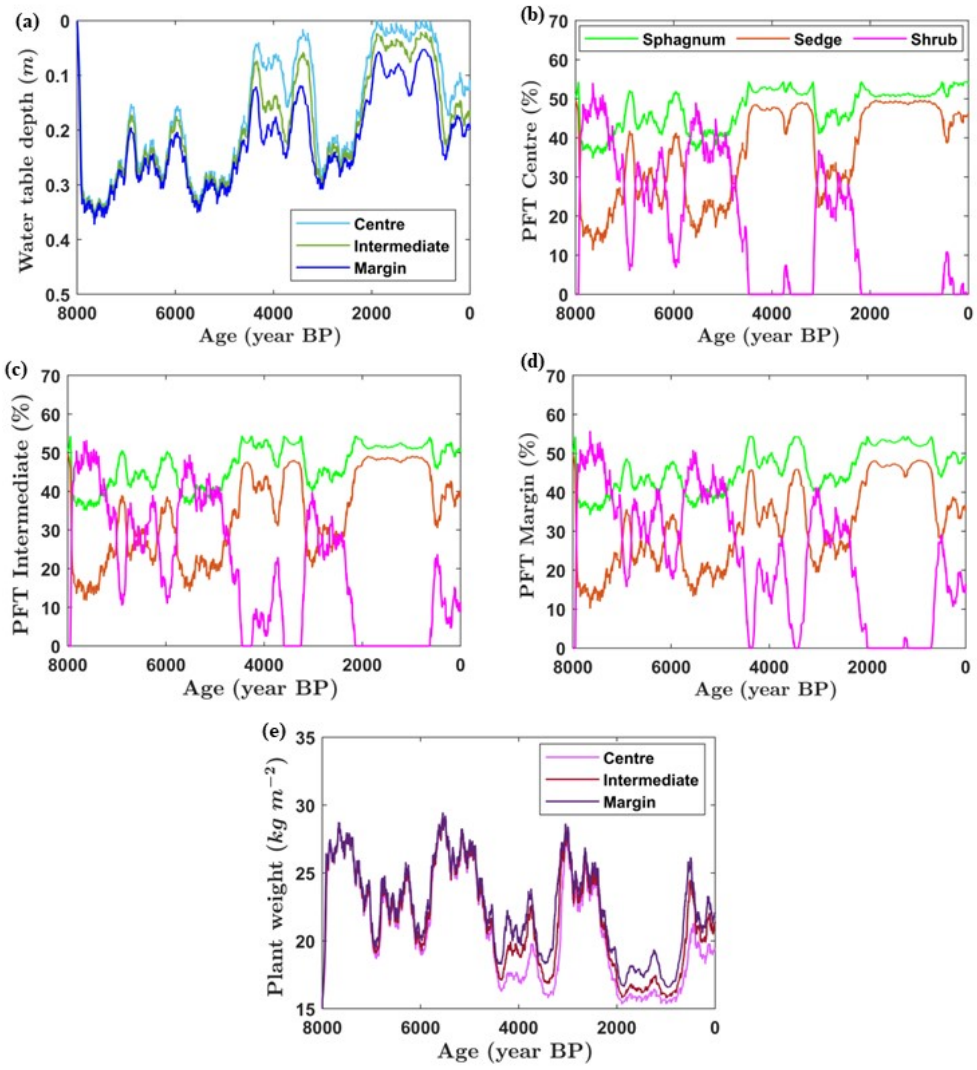

Figure 6.6: The profile of (a) water table depth, (b) plant functional types (PFT) proportion at the centre, (c) PFT proportion at the intermediate, (d) PFT proportion at the margin, and (e) plant weigh over 8000 years. The centre, intermediate, and margin denote the location with the horizontal distance of 0 m, 300 m, and 500 m, which represent upland, sloping area, and lowland, respectively.

The spatial distribution of water table depth leads to variations in PFT composition and plant weight at the top surface. For example, between the ages of 4400 - 3400 years BP when peatland experiences high net rainfall, *Sphagnum* becomes dominant compared to sedge and shrub with the proportions of 50 - 54% (*Sphagnum*), 40 - 49% (sedge), 0 - 7% (shrub) at the centre, 46 - 54% (*Sphagnum*), 31 - 48% (sedge), 0 - 22% (shrub) at the intermediate, and 44 - 54% (*Sphagnum*), 27 - 46% (sedge), 0 - 28% (shrub) at the margin (Figures 6.6b-d). Furthermore, plant weight at the top surface, which is a function of PFT composition, also indicates variability between the centre (15.77 - 19.82 kg m^{-2}), intermediate (16.48 - 22.16 kg m^{-2}), and margin (18.24 - 23.85 kg m^{-2}) at the same time interval (Figure 6.6e).

6.3.2 Peatland stresses and cumulative carbon

The simulated peatland with a landscape factor of 0.01 exhibits the range values of shear stress from 100 Pa until 10320 Pa after 8000 years (Figure 6.7). The sloping area produces higher shear stress with a maximum value of 10320 Pa, compared to the upland and lowland, which provides the maximum shear stress of 7824 Pa and 9722 Pa, respectively. Moreover, the greatest value of tensile or compressive stresses (4140 Pa) appears in the transition between the sloping area and the lowland with a horizontal distance of around 350 – 370 m from the centre (Figure 6.8). Over 8000 years of development, the cumulative carbon estimated from the peatland centre is around 129 kg C m^{-2}, which is higher than the cumulative carbon calculated based on the total average of peatland area, including upland, sloping area, and lowland, with a value of around 88 kg C m^{-2} (Figure 6.9).

The maximum shear and tensile stresses exceed the lower limit of shear and tensile strength around 5200 and 2500 years BP, respectively. The

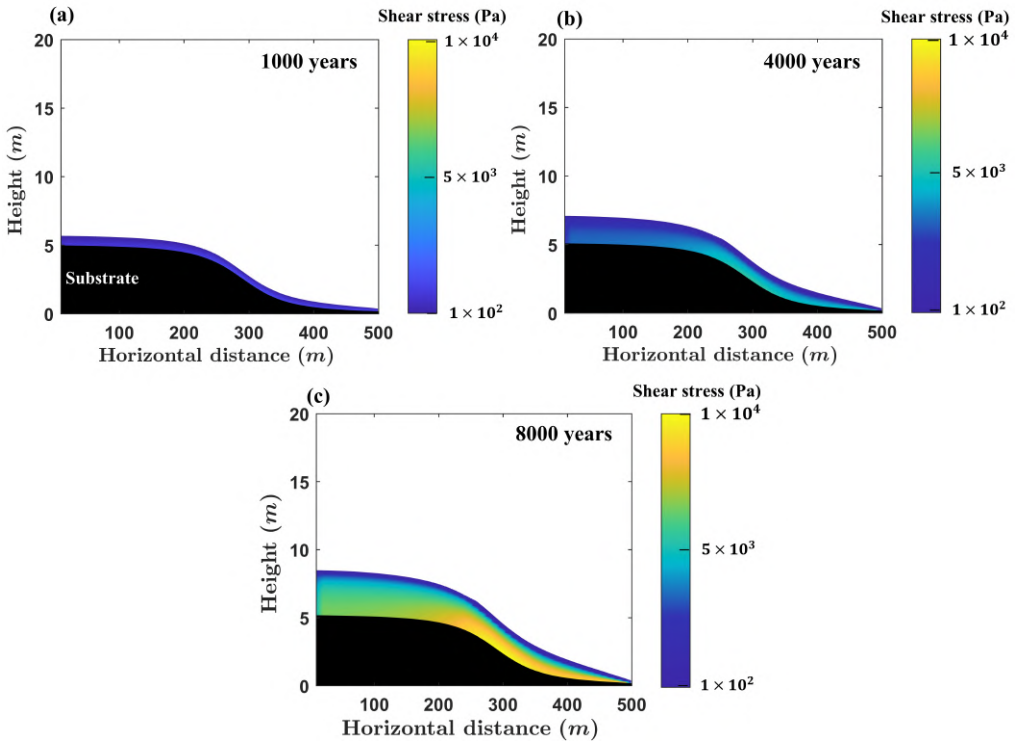

Figure 6.7: The two-dimensional profile of shear stress after (a) 1000 years, (b) 4000 years, and (c) 8000 years, respectively

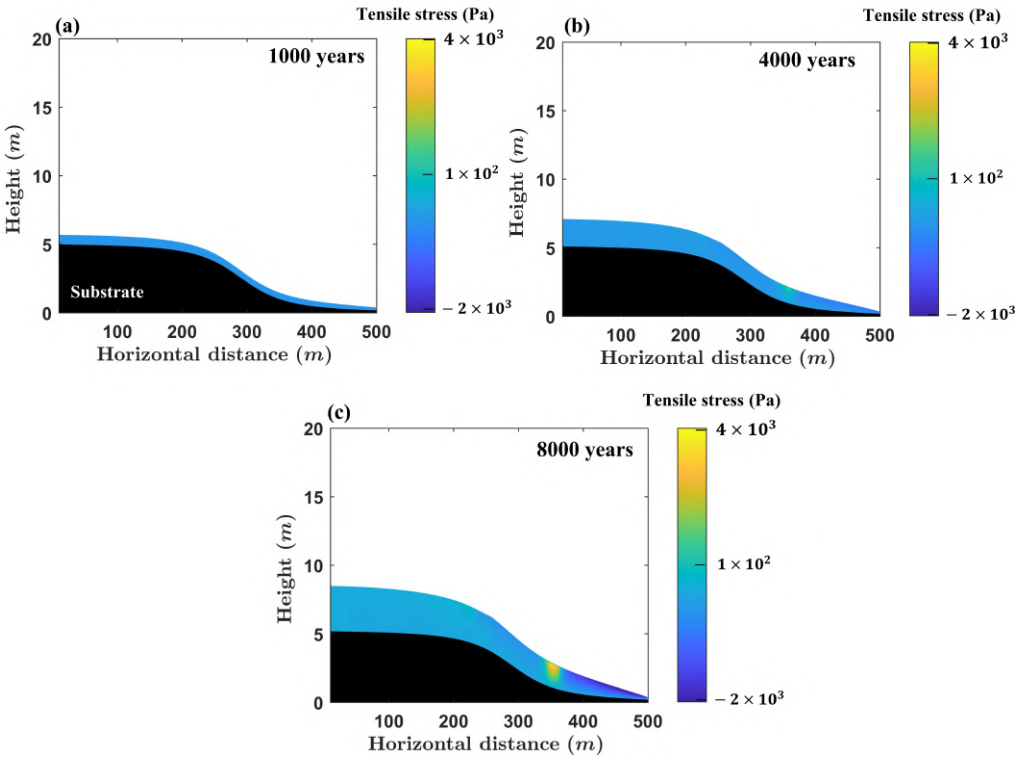

Figure 6.8: The two-dimensional profile of tensile stress after (a) 1000 years, (b) 4000 years, and (c) 8000 years, respectively

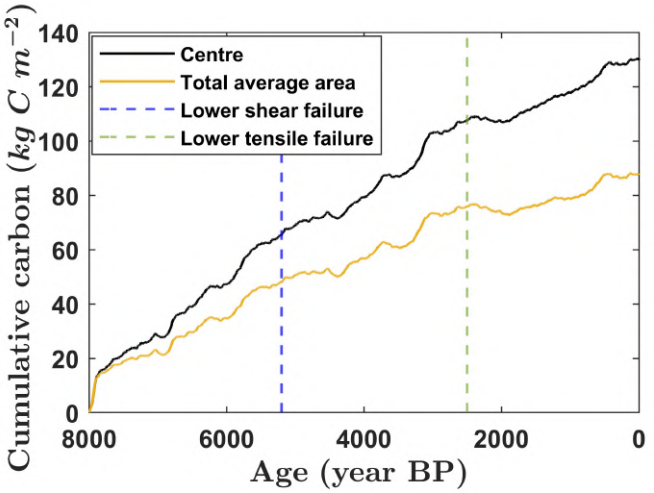

Figure 6.9: The cumulative carbon estimated from the centre and total average of the peatland area with the landscape factor of 0.01 over 8000 years. The blue and green dashed lines indicate the time when the lower limit of shear and tensile strengths are exceeded, around 5200 and 2500 years BP, respectively.

cumulative carbon, when the maximum shear stress is higher than the lower limit of shear strength, is about 65 kg C m^{-2} (obtained from the centre area) and 48 kg C m^{-2} (obtained from the total average of the peatland area). In contrast, at the time the maximum tensile stress surpasses the lower limit of tensile strength, the peatland has accumulated carbon around 107 kg C m^{-2} and 76 kg C m^{-2}, based on the centre and the total average of the peatland area, respectively. However, in this landscape, the stresses never exceed the upper limit of peat strengths within a simulation time of 8000 years.

6.3.3 The influence of landscape factor on peatland shear failure

The maximum shear stress increases with a higher value of the landscape factor, which affects the occurrence of the shear failure condition (Figure 6.10). For example, to surpass the lower limit of shear strength, the peat-

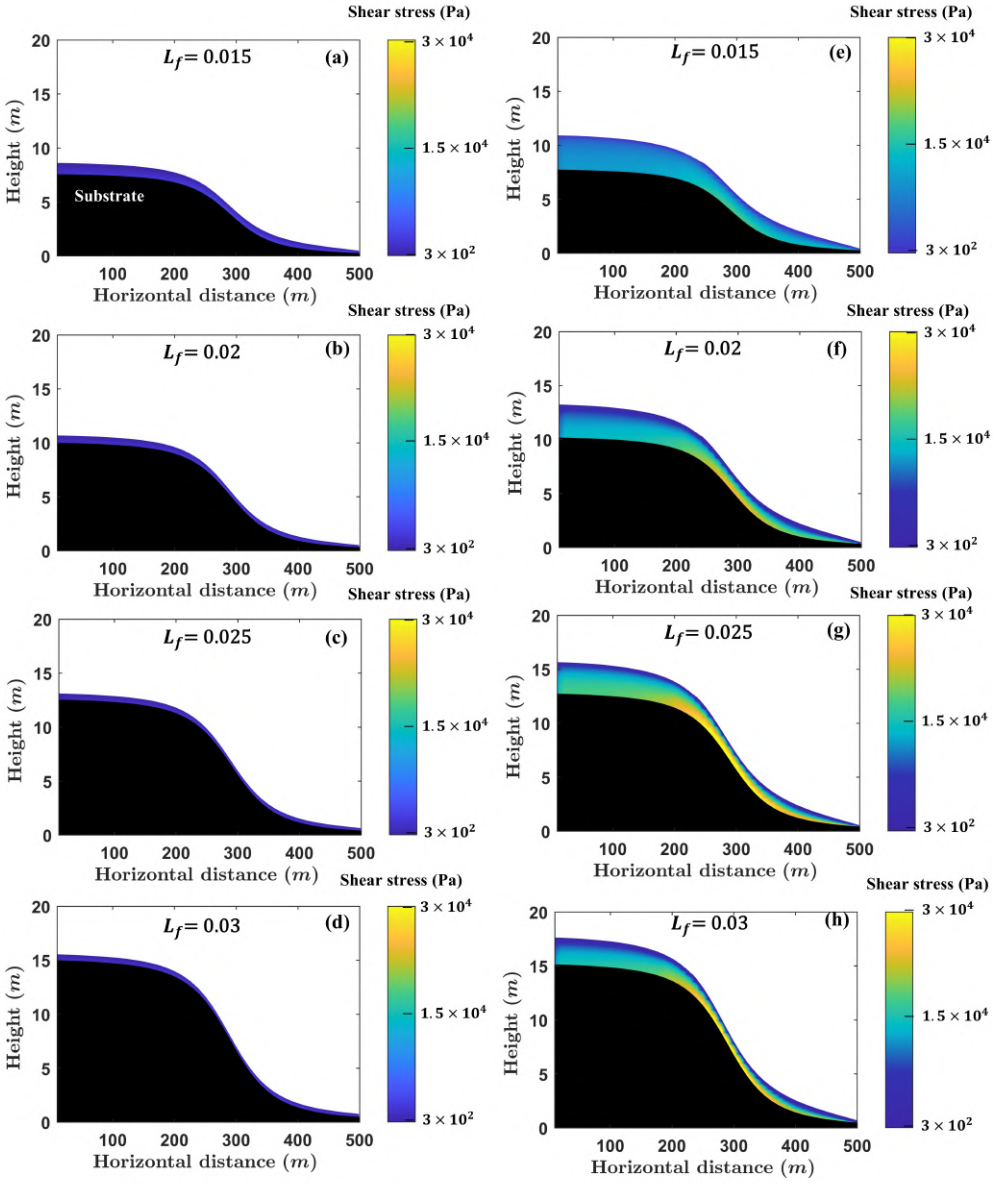

Figure 6.10: The peatland profile when the value of shear stress exceeds the lower limit of shear strength with landscape factors of (a) $L_f = 0.015$, (b) $L_f = 0.02$, (c) $L_f = 0.025$, and (d) $L_f = 0.03$. The peatland profile in the final simulation year for landscape factors of (e) $L_f = 0.015$ and (f) $L_f = 0.02$ because the values of maximum shear stresses are lower than the upper limit of shear strength within 8000 years of simulation. The peatland profile when the value of shear stress exceeds the upper limit of shear strength with landscape factors of (g) $L_f = 0.025$ and (h) $L_f = 0.03$.

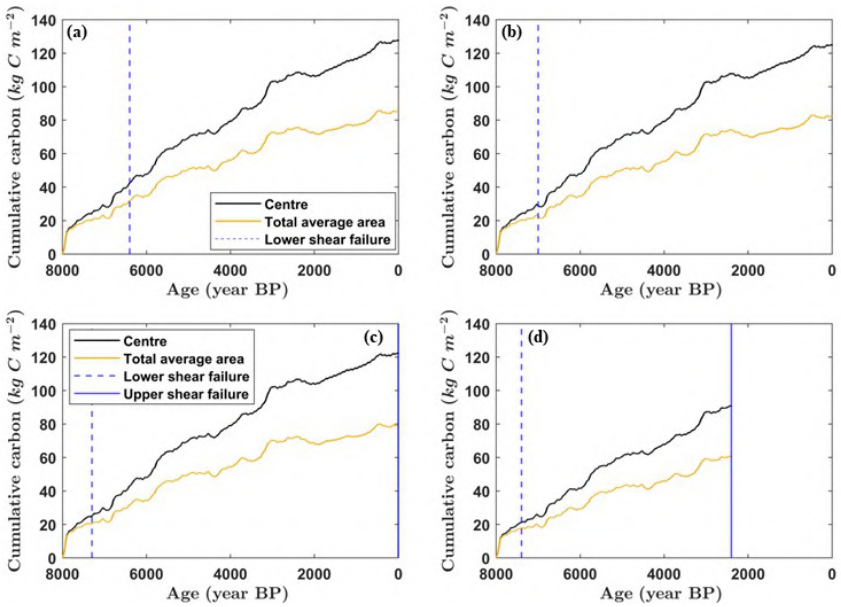

Figure 6.11: The cumulative carbon on the peatland that is affected by shear failure for landscape factors of (a) $L_f = 0.015$, (b) $L_f = 0.02$, (c) $L_f = 0.025$, and (d) $L_f = 0.03$ obtained from the centre and total average of peatland area.

land with a landscape factor of 0.015 took about 1600 years, while a higher landscape factor of 0.02 required a shorter time, around 1000 years since peatland initiation. Furthermore, the maximum shear stresses were lower than the upper limit of shear strength over 8000 years of simulation for the peatland with landscape factors of 0.015 and 0.02. In contrast, the landscape factors of 0.025 and 0.03 produce maximum shear stresses that are greater than the upper limit of shear strength after around 8000 and 5600 years of development or around 0 and 2400 years BP, respectively.

The maximum carbon accumulation on the peatland due to shear failure is obtained when the maximum shear stress has exceeded the upper limit of shear strength. In this condition, the cumulative carbon obtained from the centre of the peatland was about 122 and 90 kg C m^{-2} for the landscape factors of 0.025 and 0.03, respectively (Figures 6.11c and d). These estimated cumulative carbon decreased to the value of 79 kg C m^{-2} for the landscape factors of 0.025 and to the value of 60 kg C m^{-2} for the land-

scape factors of 0.03 if the calculation was based on the total average of peatland area.

6.3.4 The influence of landscape factor on peatland tensile failure

The higher landscape factor leads to an increase in maximum tensile stress that affects the occurrence of the tensile failure condition (Figure 6.12). Peatland with landscape factors of 0.015 and 0.02 required about 4500 and 3900 years to produce tensile stresses that are greater than the lower limit of tensile strength. Moreover, the maximum tensile stresses were lower than the upper limit of the tensile strength within the simulation time of 8000 years under these landscape factors. Contrastingly, the upper limit of tensile strength was surpassed after about 6500 and 6400 years of the development process, or about 1500 and 1600 years BP, by the peatland with landscape factors of 0.025 and 0.03, respectively

The maximum carbon accumulation due to tensile failure is obtained when the maximum tensile stress is greater than the upper limit of tensile strength. This condition appeared in the peatland with landscape factors of 0.025 and 0.03, which produced cumulative carbon of about 99 and 98 kg C m^{-2}, respectively, estimated from the centre of the peatland (Figure 6.13c and d). These values were higher compared to the estimated cumulative carbon based on the total average peatland area around 65 kg C m^{-2} for the landscape factor of 0.025 and 63 kg C m^{-2} for the landscape factor of 0.03.

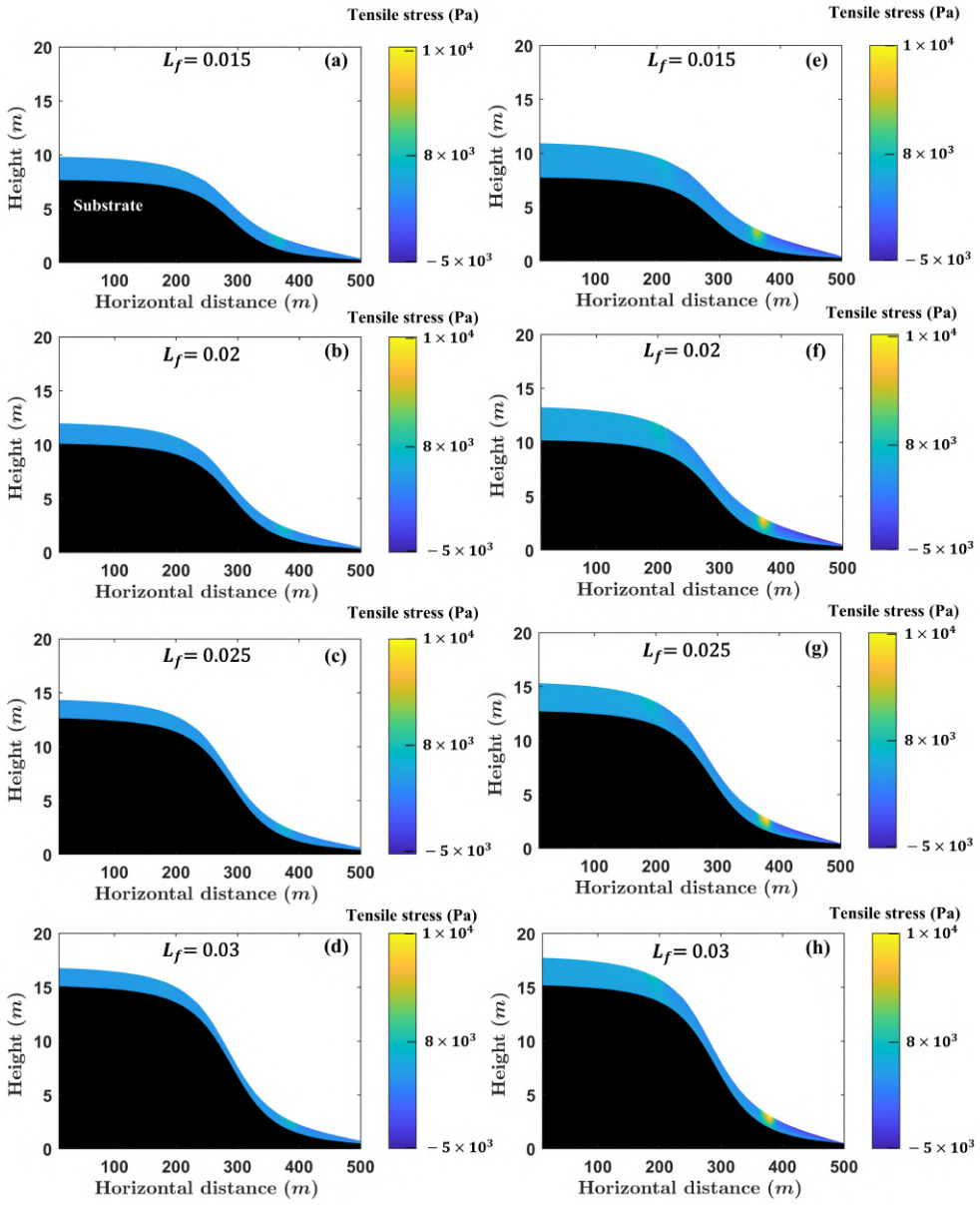

Figure 6.12: The peatland profile when the value of tensile stress exceeds the lower limit of tensile strength with landscape factors of (a) $L_f = 0.015$, (b) $L_f = 0.02$, (c) $L_f = 0.025$, and (d) $L_f = 0.03$. The peatland profile in the final simulation year for landscape factors of (e) $L_f = 0.015$ and (f) $L_f = 0.02$ because the values of maximum tensile stresses are lower than the upper limit of tensile strength within 8000 years of simulation. The peatland profile when the value of tensile stress exceeds the upper limit of tensile strength with landscape factors of (g) $L_f = 0.025$ and (h) $L_f = 0.03$.

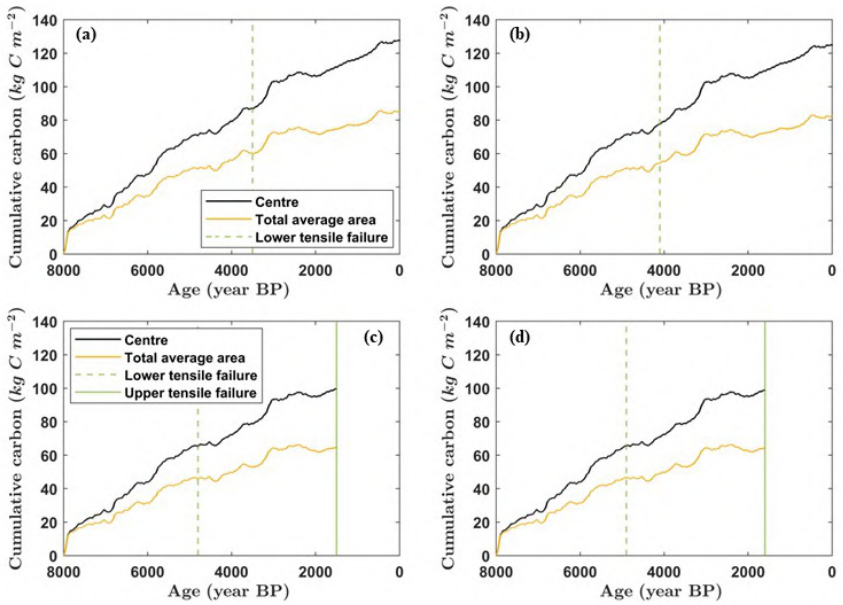

Figure 6.13: The cumulative carbon on the peatland that is affected by tensile failure for landscape factors of (a) $L_f = 0.015$, (b) $L_f = 0.02$, (c) $L_f = 0.025$, and (d) $L_f = 0.03$ obtained from the centre and total average of peatland area.

6.4 Discussion

My simulations show that peatland carbon accumulation in the proposed landscape, with the river at the edges as a natural boundary condition, is limited by mechanical instability (Figures 6.11 and 6.13). The enhancement of total load and the deficiency of space that can accommodate the lateral expansion as the peatland develops result in higher stresses on the peat body. Moreover, peat has relatively low shear and tensile strength (Long, 2005; Boylan et al., 2008; Dykes, 2008; Dykes and Warburton, 2008b; Hendry et al., 2012; O'Kelly, 2015, 2017; Wang and Li, 2023), which supports the emergence of mechanical instability, including peat slide and bog bursts (Dykes and Kirk, 2001; Dykes and Warburton, 2008b; Dykes et al., 2008; Dykes, 2008, 2022). Peat slides occur because the peatland undergoes shear failure, resulting in the depletion of peat mass and carbon stock (Figure 6.10). Bog bursts that lead to wrinkles on the peatland surface

appear as a consequence of a higher maximum tensile stress than the peat tensile strength (Dykes, 2008), which is supported by the changing pattern of tensile and compressive stresses (Briggs et al., 2007; Large et al., 2021) (Figure 6.12). The peatland failure due to mechanical instability, including peat slides and bog bursts, might produce water channels that lead to erosion, drainage and oxidation, which influence the carbon accumulation process (Warburton et al., 2003; Evans and Warburton, 2007; Large et al., 2021).

The variations of slope angle, which are represented by the different values of landscape factor in the proposed model, provide a significant influence on the occurrence of peatland failure (Dykes and Warburton, 2007; Boylan et al., 2008; Dykes and Selkirk-Bell, 2010; Dykes, 2022). Peatlands with a steeper slope are more vulnerable to mechanical instability due to higher shear and tensile stresses (Figure 6.10 and 6.12). Another factor that might affect the failure conditions on the peatland is substrate roughness. The increase in substrate roughness might provide a higher shearing resistance between the base of the peat with the substrate surface, potentially leading to a lower possibility of shear failure. However, the substrate with high roughness conditions could support the occurrence of cracks that produce bog bursts.

The potential occurrence of peatland failure prior to reaching hydrological or ecological limits of the carbon accumulation provides crucial implications not only for the estimation of total carbon stock (Nichols and Peteet, 2019; Alexandrov et al., 2020) but also for the peatland management. The main objective of the management strategy should be to minimise the risk of failure rather than to expect maximum growth from the peatland with a steep slope angle. In terms of the peatland restoration, it is essential to maintain the total loads and stresses that the peatland receives during the

restoration process are less than the upper limit of shear or tensile strength to prevent catastrophic failure.

6.4.1 Peatland mechanical conditions and carbon accumulation

The peat strengths, which determine the mechanical condition of the peatland, exhibit a wide range of values due to several factors. The reported data from Long (2005) and Dykes (2008) suggested that peat shear and tensile strength vary significantly with the degree of humification. The reinforcement effect on the peat body from a fibrous structure of organic matter is reduced as the peat undergoes decomposition because it breaks down the peat constituents into smaller fragments. Furthermore, the considerable range in the peat strengths is also related to the difficulties in the measurement process. Field measurement that employs back analysis from actual failure provides limited data and is possibly affected by the site-specific characteristics. In contrast, measuring the stresses and strains of the peat sample that represents the in-situ and actual failure conditions in the laboratory is complicated (Boylan et al., 2008; Dykes, 2008).

I divide the peatland mechanical condition into three categories based on reported data from in-situ and laboratory measurements of peat shear and tensile strengths between 4000 – 35330 Pa and 2900 - 11300 Pa, respectively (Long, 2005; Boylan et al., 2008; Dykes, 2008; Dykes and Warburton, 2008b; Hendry et al., 2012; O'Kelly, 2015, 2017; Wang and Li, 2023). In the first condition, the maximum shear or tensile stress is less than the lower limit of shear or tensile strength that produces mechanically stable peatland. The cumulative carbon in this state represents the total carbon per area accumulated by the peatland with the minimum possibility of failure. The

first condition appears in the early stage of peatland development because the load that peatland receives, especially from its self-weight or body force, is not significant.

As the peatland grows, the mass contained in the peatland increases, which produces higher loading and stresses on the peat body. If the maximum stresses are between the lower and upper limits of peat strengths, then the peatland is classified into the second condition. In this state, the mechanical stability reduces because of a higher possibility of the peatland experiencing mechanical failure. Although the peatland could accumulate more carbon, the second condition provides an early warning signal before the emergence of catastrophic failure with significant potential risks (Long and Jennings, 2006; Dykes and Warburton, 2007). Finally, in the third condition, the maximum shear or tensile stress exceeds the upper limit of shear or tensile strength, which indicates that the peatland is almost certain to undergo mechanical instability. Consequently, in the last state, the carbon accumulation process on the peatland ceases because mass movement and erosion reduce the peatland carbon stock (Warburton et al., 2003; Evans and Warburton, 2007).

The cumulative carbon with different landscape factors for peatland in the first, second, or third condition is summarised in Figure 6.14. The nonlinear response of cumulative carbon with landscape factor obtained from the proposed model is intriguing because it might provide theoretical and practical implications of long-term peatland carbon accumulation in the landscape. The maximum carbon that can be stored by the peatland before the occurrence of failure condition decreases substantially with the increasing landscape factor. As a consequence, models to estimate the peatland carbon stock, which are developed on the flat and uniform substrate (e.g., Clymo, 1984; Frolking et al., 2010) should be interpreted with caution and

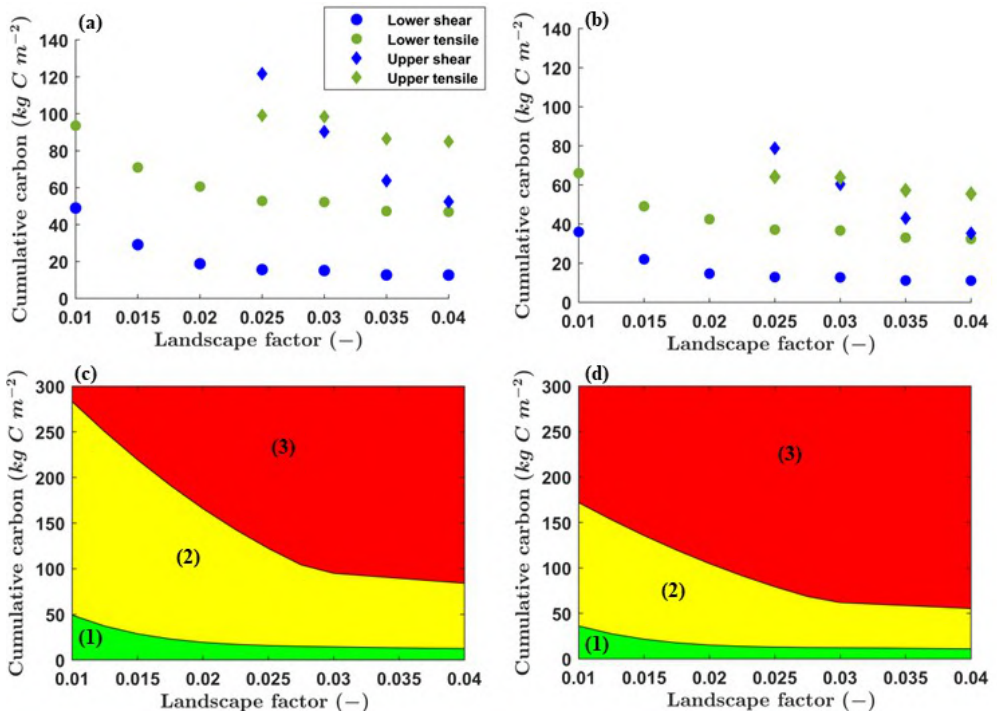

Figure 6.14: The critical values of peatland cumulative carbon with different landscape factors at the time the stresses exceed the lower or upper limit of peat strength estimated from (a) the centre area and (b) the total average of the peatland area. Based on these critical values, the relation between cumulative carbon and landscape factor is grouped into three distinct regions, i.e., the stable condition in the green region, possible failure condition in the yellow region, and failure condition in the red region, estimated from (c) the centre area and (d) the total average of the peatland area.

requires further modification to account for the landscape variations before they can be applied on the global scale.

Across all peatland mechanical conditions, the estimated cumulative carbon from the centre provides a more significant result compared to the cumulative carbon based on the total average of the peatland area. This condition is related to the variation in peatland characteristics, including water table position, PFT composition, and peat physical properties between upland, sloping area, and lowland (Kremenetski et al., 2003; Holden and Connolly, 2011). The sloping area experiences a greater water discharge, which results in lower peat thickness (Tipping, 2008; Parry et al.,

2012) and reduces carbon accumulation, while the peatland centre located at the upland provides the optimal position for carbon accumulation due to the lower water table depth (Figure 6.6a). Therefore, if the predicted cumulative carbon from the model is potentially relevant to reality, then a degree of caution may be required when interpreting the peatland carbon accumulation data from the field. The measurement conducted at the centre area tends to overestimate and requires further calibration in order to represent the cumulative carbon of the peatland.

6.4.2 Comparison with actual peatland mechanical failure

Based on the reported data, peatland mechanical failure occurs over distinct ranges of slope angle and peat thickness. For the blanket peatland in the British Isles and subantarctic islands, the slope angle that leads to mechanical failure is between 2° – 55°, with the associated peat thickness starting from 0.5 m to 3 m (Wilford, 1966; Alexander et al., 1986; Wilson and Hegarty, 1993; Gallart et al., 1994; Dykes and Kirk, 2001; Warburton et al., 2003; Yang and Dykes, 2006; Dykes et al., 2008; Dykes and Warburton, 2008b; Dykes, 2008; Boylan et al., 2008; Dykes and Selkirk-Bell, 2010). My simulation with the landscape factor of 0.03, which is related to the slope angle around 4°, produces the peat thickness at the time of failure (peatland in the third condition) about 1.4 m due to shear failure and about 1.5 m due to tensile failure, located at the horizontal distance of 300 m and 360 m from the centre, respectively. These results are in agreement with the field observations that indicate peatlands with a thickness between 1.4 – 2.5 m encounter peat slides and 1.6 – 3 m experience bog bursts when subjected to a slope angle of approximately 4°. Moreover,

based on my simulations, a higher landscape factor results in an occurrence of shear failure faster than tensile failure. This condition indicates that shear failure becomes more dominant with an increasing slope angle, which is in agreement with the data from Dykes (2022).

The shear failure is predicted to appear at the base layer of the peat along the sloping area according to the proposed model (Figure 6.10), which aligns with the previous field observations of the peat slides (Dykes and Kirk, 2001; Warburton et al., 2003; Dykes and Warburton, 2008b; Dykes et al., 2008). This area is prone to shear failure due to a substantial increase in the shear stress from the slope inclination and a low peat shear strength as a consequence of the more decomposed peat at the base layer. Furthermore, the observed shear failure in the field demonstrates a strong relationship between rainfall and peat slides (Dykes and Kirk, 2001; Long and Jennings, 2006; Dykes and Warburton, 2007, 2008a). A high-intensity or prolonged rainfall increases the total load on the peatland through the enhancement of the body force (Warburton et al., 2004), resulting in a considerable rise of the stresses. In addition, a more significant pore water pressure generated by a higher rainfall rate could reduce the shearing resistance between peat and the substrate, which increases the susceptibility to peat slides (Dykes and Warburton, 2007, 2008b; Dykes and Selkirk-Bell, 2010).

The model estimates the emergence of tensile failure at the surface between the sloping area and the lowland (Figure 6.12). In this location, peat undergoes the transition from tensile to compressive stress because the lateral force from the sloping area is restricted by the river at the edges. This condition results in the bog burst and leads to the cracking of the surface, potentially creating wrinkled patterns on the peatland (Briggs et al., 2007; Large et al., 2021). Dykes (2008) reported the phenomenon of surface rup-

turing due to tensile failure appears on Maghera Mountain, Co. Clare, Ireland.

The analysis of peatland failure that affects long-term carbon accumulation indicates the usefulness of MPeat in two dimensions to understanding peatland behaviour. Possibilities for future research with MPeat appear to be abundant due to its capability to provide fully coupled mechanical, ecological, and hydrological processes on the peatland. Moreover, the modularity of the MPeat algorithm allows for the modification and addition of submodels for future development. Some opportunities for future research involving MPeat are discussed in Chapter 7.

Chapter 7

Conclusions and future research

7.1 Thesis conclusions

The most significant outcome of this thesis is the inclusion of fully coupled mechanical-ecohydrological feedback on the model of peatland development. The coupling between mechanical and ecohydrological processes was conducted through the poroelasticity concept (Biot, 1941; Detournay and Cheng, 1993; de Boer, 2000; Wang, 2000; Coussy, 2004) that models the mechanical deformation of peat pore space (Chapter 2). Consequently, the peat physical properties, including bulk density, active porosity, and hydraulic conductivity, are obtained as internal feedback mechanisms without employing empirical relationships or constant assumptions. This new approach becomes a key improvement compared to the existing models to provide a more comprehensive understanding of peatland behaviour.

MPeat illustrates the critical function of mechanical-ecohydrological feed-

back in maintaining the relative position of the water table, which enhances peatland carbon accumulation and resilience. MPeat produced a relatively stable water table depth and a higher value of cumulative carbon compared to the other ecohydrological models, HPM and DigiBog, which are in agreement with the analysis from Waddington et al. (2015) and Nijp et al. (2017) (Chapter 3). Furthermore, by considering the interactions between plant functional types and mechanical feedback on the nonequilibrium condition of peatland, MPeat shows that the limit cycles of wet and dry attractors could coexist under the same net rainfall, which potentially provides a more realistic approach to understanding bistability compared to the model from Hilbert et al. (2000) who predicted bistability in the equilibrium states (Chapter 4). The condition of a continuously evolving system, indicated by the increasing oscillation rate of surface motion, carbon balance, and water table depth over time under the same climatic influence, also suggests that caution might be needed to interpret the palaeo-record data from the peatland. Finally, I successfully demonstrated how the application of a one-dimensional version of MPeat could help explain the regime shift, tipping point, and nonlinear dynamics of the peatland in multiple timeframes.

The simplification in modelling the influence of vegetation on peat stiffness through Young's modulus might produce uncertainty in MPeat. The formulation of Young's modulus is straightforward and developed based on the empirical relationship, in which decomposition reduces the peat stiffness and shrubs produce stiffer peat compared to *Sphagnum* (Whittington et al., 2007; Zhu et al., 2020). This simplicity, combined with a scarcity of Young's modulus data, might affect the simulation results, particularly related to the outputs in peat physical properties. However, despite these limitations, the range value and the profile of peat physical properties ob-

tained from MPeat are in agreement with the field observations (Clymo, 1984; Hoag and Price, 1995, 1997; Quinton et al., 2000; Fraser et al., 2001; Clymo, 2004; Quinton et al., 2008; Lewis et al., 2012). As better data on Young'modulus become available, the inputs to the model can be modified to improve the accuracy of the results.

MPeat captures the spatial variations of peatland characteristics, including water table depth, peat thickness, plant functional type composition, and peat physical properties, due to the implications of mechanical-ecohydrological feedback during the development process (Chapter 5). A higher bulk density and lower hydraulic conductivity at the margin compared to the centre obtained from MPeat are in accord with field observations from Baird et al. (2008) and Lewis et al. (2012). The comparison between one-dimensional and two-dimensional versions of MPeat indicates that the lateral variations of peat physical properties support water retention and produce greater carbon accumulation, particularly at the centre, corroborating the finding from Lapen et al. (2005). Moreover, MPeat shows that the inclusion of river incision at the boundaries and permeable substrate characteristics decrease the water table position, leading to the reduction of peatland thickness under the same climatic condition, which is in agreement with the simulation from Glaser et al. (2004b). However, the lack of data, for example, the rate of river incision on the peatland that becomes the primary factor in this process, reduces the reliability of model outputs. To overcome this limitation, I represented the simulation results related to the influence of river incision and permeable substrate as dimensionless quantities.

The two-dimensional version of MPeat was implemented to examine peatland failure due to mechanical instability, which determines the limits to carbon accumulation in the landscape, consisting of upland, a sloping area, and lowland (Chapter 6). The estimated peatland thickness and slope an-

gle when the failure takes place are consistent between simulation results and the observation of actual peatland failure (Wilford, 1966; Alexander et al., 1986; Wilson and Hegarty, 1993; Gallart et al., 1994; Dykes and Kirk, 2001; Warburton et al., 2003; Yang and Dykes, 2006; Dykes et al., 2008; Dykes and Warburton, 2008b; Dykes, 2008; Boylan et al., 2008; Dykes and Selkirk-Bell, 2010), which reflects the success of the proposed model. Based on the simulation results, a higher slope angle increases the susceptibility of peatland failure, particularly in the sloping area for shear failure and in the transition between the sloping area with lowland for tensile failure. The possibility of failure conditions during the development process influences the estimation of carbon accumulation on the peatland because the mass movement might result in the formation of water channels that facilitate the drainage and oxidation processes (Warburton et al., 2003; Evans and Warburton, 2007). Moreover, the simulation results show that the cumulative carbon obtained from the centre is more significant compared to the estimation based on the total average of the peatland area. The spatial variations of water table position, which affect peat production and decomposition, are the main factor that leads to the discrepancies in the estimated cumulative carbon. Therefore, a degree of caution might be required when interpreting the result from the field measurement because the centre tends to overestimate the cumulative carbon per area of the peatland.

The uncertainties in the peat strengths, indicated by a wide range of values for both shear and tensile strengths (Long, 2005; Boylan et al., 2008; Dykes, 2008; Dykes and Warburton, 2008b; Hendry et al., 2012; O'Kelly, 2015, 2017; Wang and Li, 2023), critically affect the prediction of peatland failure. The variations in peatland characteristics, including peat physical properties, water content, and degree of humification, become factors that

influence the variability in peat strength (Long, 2005; Boylan et al., 2008; Dykes, 2022). The uncertainties could be minimised by employing the appropriate peatland data that align with the specific value of peat strengths. However, obtaining high-quality data, which is suitable for the proposed model, is challenging. Another approach is to utilise a probabilistic or stochastic model to estimate the failure condition of the peatland, which allows for the quantification of uncertainties involved in the process (see Subsection 7.2 future research related to the stochastics model of peatland failure).

7.2 Future research

7.2.1 Stochastics model of peatland failure

The peatland mechanical condition is classified into three classes based on the comparison between maximum stresses on the peat body and peat strengths, as explained in Chapter 6. In the first condition, the peatland is mechanically stable because the maximum stresses on the peat body are less than the lower limit of peat strengths. Contrastingly, in the third condition, the peatland experiences mechanical instability that leads to the failure condition because the maximum stresses exceed the upper limit of peat strengths. The difficulties in determining the peatland mechanical condition increase in the second condition. The peatland has the possibility to experience mechanical failure because the maximum stresses are between the lower and upper limits of peat strengths. To quantify the possibility of mechanical failure, stochastic models based on the probability of failure methods might offer appropriate approaches (Brown, 2012; Phoon et al., 2022). In this stochastic model, the stresses and strengths are considered

as random variables with a specific probability distribution. The difference between these two random variables determines the failure condition of the peatland

$$Z = X_h - X_s \tag{7.1}$$

where Z is the failure conditions due to mechanical instability, X_h is the random variable of peat strength, and X_s is the random variable of stress on the peat body. Because the failure condition occurs when the stresses are greater than the strengths, the probability of failure is modelled as

$$P(Z < 0) = P(X_h - X_s < 0) \tag{7.2}$$

This stochastic model allows us to calculate and quantify the occurrence of peatland failure due to mechanical instability in terms of probability value, which incorporates uncertainties of some variables.

7.2.2 Modelling the influence of drainage and rewetting

The decrease in water table position due to drainage reduces peatland carbon accumulation through the oxidation process (Warburton et al., 2003; Evans and Warburton, 2007) and the loss of dissolved organic carbon that accompanies the outflow of water from the peatland (Hooijer et al., 2010; Xu et al., 2021). The deeper water table also affects vegetation communities and peat production (Belyea and Clymo, 2001; Moore et al., 2002), which determines the rate of carbon input to the peatland. Drainage leads to the dry condition of the peatland, reducing peatland resilience and increasing the susceptibility to peat fire that could release significant amounts of car-

bon into the atmosphere (Hooijer et al., 2010; Nelson et al., 2021; Ohkubo et al., 2021). Consequently, to prevent the negative impacts of drainage and restore the peatland condition, a rewetting is used. However, measuring the long-term success of restoration programmes requires a considerable amount of resources, particularly if it focuses on field observation. Mathematical models of peatland development provide an alternative approach to understanding the long-term effect of drainage and rewetting on peatland behaviour, which involves complex feedback mechanisms.

The two-dimensional version of MPeat has the ability to capture the influence of river incision on the peatland behaviour (described in Chapter 5), which could be used as the starting point to analyse the drainage effect. To some extent, the river incision phenomenon and the drainage provide similar implications to the peatland behaviour because they support the water discharge and reduce the water table position, affecting peat production, decomposition, plant functional types composition, and carbon accumulation. However, the rate of water table drop in the drainage process is much faster than the rate of river incision, which might produce instability in the model. Therefore, the proposed model in Chapter 5 requires further extensions, mainly in the area around ditch drainage, to improve the numerical stability.

7.2.3 Modelling tropical peatland behaviour

Tropical peatlands cover around 465555 km^2, with an estimated carbon storage of about 103.6 Gt C (Crezee et al., 2022). Tropical peatland provides vital ecosystem services and becomes a habitat for many rare species, in addition to the globally significant carbon storage. The existing models of tropical peatlands focus on ecohydrological feedback mechanisms to

analyse the carbon balance and behaviour of this system (Kurnianto et al., 2015; Cobb et al., 2017; Cobb and Harvey, 2019). However, these models ignore mechanical processes despite the fact that compaction and deformation are crucial physical processes determining peat formation, hydrology, and stability.

Modifications of some processes are required before applying MPeat to model tropical peatland. MPeat uses the empirical relationship between peat production and water table depth, which is formulated based on the data from Ellergower Moss, Scotland (Belyea and Clymo, 2001). The rate of peat production in the tropical peatland should be different from the northern temperate peatland due to the variations in the vegetation composition. This condition leads to the variations in peat composition and susceptibility for decay (Young et al., 2023). The hydraulic conductivity of tropical peatlands is relatively high compared to the northern temperate peatland, which affects the water table position (Baird et al., 2017). Finally, the compaction from trees and the influence of roots for maintaining mechanical stability are significant processes in tropical peatlands, which requires an additional formulation in the MPeat mechanical submodel.

7.2.4 Modelling peatland growth in three dimensions

The development of MPeat into a three-dimensional model provides opportunities to understand phenomena that require explicit spatial interactions and more complex feedback mechanisms, such as surface patterning and lateral expansion. The peatland surface patterning is highly directional and affected by spatial characteristics, which indicates a three-dimensional model is preferred. The analysis of peatland surface patterning is typically developed based on ecohydrological feedback, which encompasses the in-

teractions between water table position, vegetation communities, nutrient availability, and peat hydraulic properties (Eppinga et al., 2009; Morris et al., 2013; Béguin et al., 2019). However, as a porous medium with relatively low shear and tensile strength (Long, 2005; Boylan et al., 2008; Dykes, 2008; Dykes and Warburton, 2008b; Hendry et al., 2012; O'Kelly, 2015, 2017; Wang and Li, 2023), mechanical instability also determines the process of surface patterning on the peatland. The simulation from Briggs et al. (2007) indicates that the peatland surface might experience wrinkles due to the changing pattern between tensile and compressive stresses. Furthermore, the three-dimensional model takes into account the intricate characteristics of the substrate that is crucial to simulate the peatland lateral expansion. The analysis of a nonuniform rate and direction of peatland expansion is allowed in a three-dimensional model, resulting in a more accurate representation of the actual process.

The extension into three dimensions is challenging because it increases the model complexities and becomes computationally expensive in terms of model run times. The lateral expansion of the peatland also involves a moving boundary problem (Tezduyar, 2001; Gawlik and Lew, 2015), which requires different formulations from the current MPeat boundary conditions. To achieve this, simplifying assumptions may be necessary, including turning off component parts of the model and exploring the mechanical behaviour of different bilayer peatland geometries.

7.2.5 Microscale modelling

Another aspect that could be developed to produce a more plausible peatland growth model is microscale modelling. This approach focuses on the analysis of small-scale processes which provide a global impact on the peat-

land behaviour, for instance, the presence of gas bubbles and capillary forces. The entrapped gas bubbles block the pore space and affect the water flow, thus decreasing hydraulic conductivity (Baird and Waldron, 2003; Beckwith and Baird, 2001; Reynolds et al., 1992). Besides that, they have been shown to provide a noticeable effect on pore water pressure (Kellner et al., 2004), which in turn influence effective stress. Introducing this aspect into the model requires a deep understanding of a complex peat pore structure, including the effect of dual-porosity, to determine the area where bubbles get trapped. Moreover, another small-scale process that could enhance MPeat capability to analyse peatland behaviour is the inclusion of capillary forces. This process determines the water storage in the peat pore space and creates the capillary fringe. As a consequence, the water table might rise significantly with a small addition of water input (Gillham, 1984), which affects the deformation of peat pore space (Shantz and Price, 2006; O'Kelly, 2013).

Bibliography

Aaby, B. and Tauber, H. (1975). Rates of peat formation in relation to degree of humification and local environment, as shown by studies of a raised bog in deninark. *Boreas*, 4(1):1–17.

Abousleiman, Y., Cheng, A. H., Cui, L., Detournay, E., and Roegiers, J.-C. (1996). Mandel's problem revisited. *Géotechnique*, 46(2):187–195.

Admiral, S. W. and Lafleur, P. M. (2007). Modelling of latent heat partitioning at a bog peatland. *Agricultural and Forest Meteorology*, 144(3):213–229.

Alexander, R. W., Coxon, P., and Thorn, R. H. (1986). A bog flow at straduff townland, county sligo. *Proceedings of the Royal Irish Academy. Section B: Biological, Geological, and Chemical Science*, 86B:107–119.

Alexandrov, G. A., Brovkin, V. A., Kleinen, T., and Yu, Z. (2020). The capacity of northern peatlands for long-term carbon sequestration. *Biogeosciences*, 17(1):47–54.

Alshammari, L., Boyd, D. S., Sowter, A., Marshall, C., Andersen, R., Gilbert, P., Marsh, S., and Large, D. J. (2020). Use of surface motion characteristics determined by insar to assess peatland condition. *Journal of Geophysical Research: Biogeosciences*, 125(1):e2018JG004953.

Ammala, A. and Piltonen, P. (2019). Sphagnum moss as a functional reinforcement agent in castor oil-based biopolyurethane composites. *Mires and Peat*, 24(28):1–11.

Anderson, R. L., Foster, D. R., and Motzkin, G. (2003). Integrating lateral expansion into models of peatland development in temperate new england. *Journal of Ecology*, 91(1):68–76.

Armentano, T. V. and Menges, E. S. (1986). Patterns of change in the carbon balance of organic soil-wetlands of the temperate zone. *Journal of Ecology*, 74:755–774.

Armstrong, A. C. (1995). Hydrological model of peat-mound form with vertically varying hydraulic conductivity. *Earth Surface Processes and Landforms*, 20(5):473–477.

Baird, A. J., Eades, P. A., and Surridge, B. W. J. (2008). The hydraulic structure of a raised bog and its implications for ecohydrological modelling of bog development. *Ecohydrology*, 1(4):289–298.

Baird, A. J., Low, R., Young, D., Swindles, G. T., Lopez, O. R., and Page, S. (2017). High permeability explains the vulnerability of the carbon store in drained tropical peatlands. *Geophysical Research Letters*, 44(3):1333–1339.

Baird, A. J., Milner, A. M., Blundell, A., Swindles, G. T., and Morris, P. J. (2016). Microform-scale variations in peatland permeability and their ecohydrological implications. *Journal of Ecology*, 104(2):531–544.

Baird, A. J., Morris, P. J., and Belyea, L. R. (2012). The digibog peatland development model 1: rationale, conceptual model, and hydrological basis. *Ecohydrology*, 5(3):242–255.

Baird, A. J., Surridge, B. W. J., and Money, R. P. (2004). An assessment of the piezometer method for measuring the hydraulic conductivity of a cladium mariscus—phragmites australis root mat in a norfolk (uk) fen. *Hydrological Processes*, 18(2):275–291.

Baird, A. J. and Waldron, S. (2003). Shallow horizontal groundwater flow in peatlands is reduced by bacteriogenic gas production. *Geophysical Research Letters*, 30(20).

Ballard, C. E., McIntyre, N., and Wheater, H. S. (2012). Effects of peatland drainage management on peak flows. *Hydrol. Earth Syst. Sci.*, 16(7):2299–2310.

Ballard, C. E., McIntyre, N., Wheater, H. S., Holden, J., and Wallage, Z. E. (2011). Hydrological modelling of drained blanket peatland. *Journal of Hydrology*, 407(1):81–93.

Bear, J. (1972). *Dynamics of Fluids in Porous Media*. John Wiley, New York.

Beckwith, C. W. and Baird, A. J. (2001). Effect of biogenic gas bubbles on water flow through poorly decomposed blanket peat. *Water Resources Research*, 37(3):551–558.

Belyea, L. R. (2009). *Nonlinear dynamics of peatlands and potential feedbacks on the climate system*, pages 5–18. Geophysical Monograph Series. American Geophysical Union, Washington DC, United States.

Belyea, L. R. and Baird, A. J. (2006). Beyond the "limits to peat bog growth": cross-scale feedback in peatland development. *Ecological Monographs*, 76(3):299–322.

Belyea, L. R. and Clymo, R. S. (2001). Feedback control of the rate of

peat formation. *Proceedings of the Royal Society of London. Series B: Biological Sciences*, 268(1473):1315–1321.

Berg, E. E., Hillman, K. M., Dial, R., and DeRuwe, A. (2009). Recent woody invasion of wetlands on the kenai peninsula lowlands, south-central alaska: a major regime shift after 18 000 years of wet sphagnum–sedge peat recruitment. *Canadian Journal of Forest Research*, 39(11):2033–2046.

Berglund, N. and Gentz, B. (2002). Metastability in simple climate models: pathwise analysis of slowly driven langevin equations. *Stochastics and Dynamics*, 02(03):327–356.

Biot, M. (1955). Theory of elasticity and consolidation for a porous anisotropic solid. *Journal of Applied Physics*, 26(2).

Biot, M. (1973). Nonlinear and semilinear rheology of porous solids. *Journal of Geophysical Research*, 78.

Biot, M. A. (1941). General theory of three-dimensional consolidation. *Journal of Applied Physics*, 12(2):155–164.

Blodau, C., Basiliko, N., and Moore, T. R. (2004). Carbon turnover in peatland mesocosms exposed to different water table levels. *Biogeochemistry*, 67(3):331–351.

Borren, W. and Bleuten, W. (2006). Simulating holocene carbon accumulation in a western siberian watershed mire using a three-dimensional dynamic modeling approach. *Water Resources Research*, 42(12).

Bourgault, M.-A., Larocque, M., and Garneau, M. (2017). Quantification of peatland water storage capacity using the water table fluctuation method. *Hydrological Processes*, 31(5):1184–1195.

Boussinesq, J. (1871). Théorie de l'intumescence liquide, applelée onde solitaire ou de translation, se propageant dans un canal rectangulaire. *Comptes Rendus de l'Académie des Sciences.*, 72.

Boylan, N., Jennings, P., and Long, M. (2008). Peat slope failure in ireland. *Quarterly Journal of Engineering Geology and Hydrogeology*, 41(1):93–108.

Bradley, A. V., Andersen, R., Marshall, C., Sowter, A., and Large, D. J. (2022). Identification of typical ecohydrological behaviours using insar allows landscape-scale mapping of peatland condition. *Earth Surf. Dynam.*, 10(2):261–277.

Briggs, J., Large, D. J., Snape, C., Drage, T., Whittles, D., Cooper, M., Macquaker, J. H., and Spiro, B. F. (2007). Influence of climate and hydrology on carbon in an early miocene peatland. *Earth and Planetary Science Letters*, 253(3):445–454.

Brown, E. T. (2012). Risk assessment and management in underground rock engineering—an overview. *Journal of Rock Mechanics and Geotechnical Engineering*, 4(3):193–204.

Béguin, C., Brunetti, M., and Kasparian, J. (2019). Quantitative analysis of self-organized patterns in ombrotrophic peatlands. *Scientific Reports*, 9(1499).

Carpenter, S. R. and Brock, W. A. (2006). Rising variance: a leading indicator of ecological transition. *Ecology Letters*, 9(3):311–318.

Charman, D. (2002). *Peatlands and Environmental Change*. John Wiley and Sons Ltd., Chichester.

Charman, D. J., Beilman, D. W., Blaauw, M., Booth, R. K., Brewer, S., Chambers, F. M., Christen, J. A., Gallego-Sala, A., Harrison, S. P.,

Hughes, P. D. M., Jackson, S. T., Korhola, A., Mauquoy, D., Mitchell, F. J. G., Prentice, I. C., van der Linden, M., De Vleeschouwer, F., Yu, Z. C., Alm, J., Bauer, I. E., Corish, Y. M. C., Garneau, M., Hohl, V., Huang, Y., Karofeld, E., Le Roux, G., Loisel, J., Moschen, R., Nichols, J. E., Nieminen, T. M., MacDonald, G. M., Phadtare, N. R., Rausch, N., Sillasoo, U., Swindles, G. T., Tuittila, E. S., Ukonmaanaho, L., Väliranta, M., van Bellen, S., van Geel, B., Vitt, D. H., and Zhao, Y. (2013). Climate-related changes in peatland carbon accumulation during the last millennium. *Biogeosciences*, 10(2):929–944.

Chaudhary, N., Westermann, S., Lamba, S., Shurpali, N., Sannel, A. B. K., Schurgers, G., Miller, P. A., and Smith, B. (2020). Modelling past and future peatland carbon dynamics across the pan-arctic. *Global Change Biology*, 26(7):4119–4133.

Cheng, A. H. (2020). A linear constitutive model for unsaturated poroelasticity by micromechanical analysis. *International Journal for Numerical and Analytical Methods in Geomechanics*, 44(4):455–483.

Cheng, A. H. and Detournay, E. (1988). A direct boundary element method for plane strain poroelasticity. *International Journal for Numerical and Analytical Methods in Geomechanics*, 12(5):551–572.

Childs, E. C. (1969). *An introduction to the physical basis of soil water phenomena*. John Wiley and Sons Ltd.

Clymo, R. S. (1984). The limits to peat bog growth. *Philosophical Transactions of the Royal Society of London. B, Biological Sciences*, 303(1117):605–654.

Clymo, R. S. (2004). Hydraulic conductivity of peat at ellergower moss, scotland. *Hydrological Processes*, 18(2):261–274.

Clymo, R. S., Turunen, J., and Tolonen, K. (1998). Carbon accumulation in peatland. *Oikos*, 81(2):368–388.

Cobb, A. R. and Harvey, C. F. (2019). Scalar simulation and parameterization of water table dynamics in tropical peatlands. *Water Resources Research*, 55(11):9351–9377.

Cobb, A. R., Hoyt, A. M., Gandois, L., Eri, J., Dommain, R., Abu Salim, K., Kai, F. M., Haji Su'ut, N. S., and Harvey, C. F. (2017). How temporal patterns in rainfall determine the geomorphology and carbon fluxes of tropical peatlands. *Proceedings of the National Academy of Sciences*, 114(26):E5187–E5196.

Collins, J. A. (1993). *Failure of Materials in Mechanical Design: Analysis, Prediction, Prevention*. Wiley-Interscience, 2nd edition.

Coussy, O. (2004). *Poromechanics*. John Wiley and Sons Ltd, Chichester, UK.

Crezee, B., Dargie, G., Ewango, C., Mitchard, E., Emba, O., Kanyama, J., Bola, P., Ndjango, B., Girkin, N., Bocko, Y., Ifo, S., Hubau, W., Seidensticker, D., Batumike, R., Imani, G., Cuní-Sanchez, A., Kiahtipes, C., Lebamba, J., Wotzka, P., Bean, H., Baker, T., Baird, A., Boom, A., Morris, P., Page, S., Lawson, I., and Lewis, S. (2022). Mapping peat thickness and carbon stocks of the central congo basin using field data. *Nature Geoscience*, 15:639–644.

Cruickshank, M. M. and Tomlinson, R. W. (1990). Peatland in northern ireland: inventory and prospect. *Irish Geography*, 23(1):17–30.

de Boer, R. (2000). *Theory of Porous Media*. Springer, Berlin, Heidelberg, Germany.

Detournay, E. and Cheng, A. H. D. (1993). *Fundamentals of Poroelasticity*, pages 113–171. Pergamon, Oxford.

Dise, N. B. (2009). Peatland response to global change. *Science*, 326(5954):810–811.

Dorrepaal, E., Toet, S., Van Logtestijn, R. S., Swart, E., Van De Weg, M. J., Callaghan, T. V., and Aerts, R. (2009). Carbon respiration from subsurface peat accelerated by climate warming in the subarctic. *Nature*, 460(7255):616–619.

Dupuit, J. (1863). *Etudes theoriques et pratiques sur le mouvement des eaux dans les canaux decouverts et a travers les terrains permeabls: avec des considerations relatives au regime des grandes eaux, au debouche a leur donner, et a la marche des alluvions dans les rivie'res a fond mobile.* Dunod, Paris, France.

Dykes, A. and Warburton, J. (2008a). Characteristics of the shetland islands (uk) peat slides of 19 september 2003. *Landslides*, 5:213–226.

Dykes, A. P. (2008). Tensile strength of peat: laboratory measurement and role in irish blanket bog failures. *Landslides*, 5(4):417–429.

Dykes, A. P. (2022). Recent peat slide in co. antrim extends the known range of weak basal peat across ireland. *Environmental Geotechnics*, 9(1):22–35.

Dykes, A. P., Gunn, J., and Convery, K. J. (2008). Landslides in blanket peat on cuilcagh mountain, northwest ireland. *Geomorphology*, 102(3):325–340.

Dykes, A. P. and Kirk, K. J. (2001). Initiation of a multiple peat slide on cuilcagh mountain, northern ireland. *Earth Surface Processes and Landforms*, 26(4):395–408.

Dykes, A. P. and Selkirk-Bell, J. M. (2010). Landslides in blanket peat on subantarctic islands: causes, characteristics and global significance. *Geomorphology*, 124(3):215–228.

Dykes, A. P. and Warburton, J. (2007). Significance of geomorphological and subsurface drainage controls on failures of peat-covered hillslopes triggered by extreme rainfall. *Earth Surface Processes and Landforms*, 32(12):1841–1862.

Dykes, A. P. and Warburton, J. (2008b). Failure of peat-covered hillslopes at dooncarton mountain, co. mayo, ireland: Analysis of topographic and geotechnical factors. *CATENA*, 72(1):129–145.

Edelsbrunner, H. (2001). *Geometry and Topology for Mesh Generation*. Cambridge University Press,, Cambridge, United Kingdom.

Elsoufiev, S. A. (2007). *Strength Analysis in Geomechanics*. Springer.

Eppinga, M. B., Rietkerk, M., Borren, W., Lapshina, E. D., Bleuten, W., and Wassen, M. J. (2008). Regular surface patterning of peatlands: Confronting theory with field data. *Ecosystems*, 11(4):520–536.

Eppinga, M. B., Rietkerk, M., Wassen, M. J., and Ruiter, P. C. D. (2009). Linking habitat modification to catastrophic shifts and vegetation patterns in bogs. *Plant Ecology*, 200:53–68.

Evans, C. D., Peacock, M., Baird, A. J., Artz, R. R. E., Burden, A., Callaghan, N., Chapman, P. J., Cooper, H. M., Coyle, M., Craig, E., Cumming, A., Dixon, S., Gauci, V., Grayson, R. P., Helfter, C., Heppell, C. M., Holden, J., Jones, D. L., Kaduk, J., Levy, P., Matthews, R., McNamara, N. P., Misselbrook, T., Oakley, S., Page, S. E., Rayment, M., Ridley, L. M., Stanley, K. M., Williamson, J. L., Worrall, F.,

and Morrison, R. (2021). Overriding water table control on managed peatland greenhouse gas emissions. *Nature*, 593(7860):548–552.

Evans, M. and Warburton, J. (2007). *Geomorphology of Upland Peat: Erosion, Form and Landscape Change*. John Wiley and Sons.

Eymard, R., Gallouët, T., and Herbin, R. (2000). *Finite volume methods*, volume 7, pages 713–1018. Elsevier.

Farrell, E. R. (2012). *Organics/peat soils*, pages 463–479. ch 35. ICE Publishing, London.

Fenton, J. H. C. (1980). The rate of peat accumulation in antarctic moss banks. *Journal of Ecology*, 68(1):211–228.

Ferronato, M., Castelletto, N., and Gambolati, G. (2010). A fully coupled 3-d mixed finite element model of biot consolidation. *Journal of Computational Physics*, 229(12):4813–4830.

Fischer, N. and Jungclaus, J. H. (2011). Evolution of the seasonal temperature cycle in a transient holocene simulation: orbital forcing and sea-ice. *Clim. Past*, 7(4):1139–1148.

Forchheimer, P. (1930). *Hydraulik (3 auflage)*. B. G. Teubner, Berlin.

Fraser, C. J. D., Roulet, N. T., and Moore, T. R. (2001). Hydrology and dissolved organic carbon biogeochemistry in an ombrotrophic bog. *Hydrological Processes*, 15(16):3151–3166.

Fritz, C., Campbell, D. I., and Schipper, L. A. (2008). Oscillating peat surface levels in a restiad peatland, new zealand—magnitude and spatiotemporal variability. *Hydrological Processes*, 22(17):3264–3274.

Frolking, S., Roulet, N. T., Moore, T. R., Richard, P. J. H., Lavoie, M., and Muller, S. D. (2001). Modeling northern peatland decomposition and peat accumulation. *Ecosystems*, 4(5):479–498.

Frolking, S., Roulet, N. T., Tuittila, E., Bubier, J. L., Quillet, A., Talbot, J., and Richard, P. J. H. (2010). A new model of holocene peatland net primary production, decomposition, water balance, and peat accumulation. *Earth Syst. Dynam.*, 1(1):1–21.

Gallart, F., Clotet-Perarnau, N., Bianciotto, O., and PuigdefÃ bregas, J. (1994). Peat soil flows in bahÃa del buen suceso, tierra del fuego (argentina). *Geomorphology*, 9(3):235–241.

Gao, J., Holden, J., and Kirkby, M. (2016). The impact of land-cover change on flood peaks in peatland basins. *Water Resources Research*, 52(5):3477–3492.

Gawlik, E. S. and Lew, A. J. (2015). Unified analysis of finite element methods for problems with moving boundaries. *SIAM Journal on Numerical Analysis*, 53(6):2822–2846.

George, P.-L. (2000). *Mesh Generation – Application to Finite Elements*. Hermes Science Publishing, Paris.

Gillham, R. (1984). The capillary fringe and its effect on water-table response. *Journal of Hydrology*, 67(1):307–324.

Glaser, P. H., Chanton, J. P., Morin, P., Rosenberry, D. O., Siegel, D. I., Ruud, O., Chasar, L. I., and Reeve, A. S. (2004a). Surface deformations as indicators of deep ebullition fluxes in a large northern peatland. *Global Biogeochemical Cycles*, 18(1).

Glaser, P. H., Hansen, B. C., Siegel, D. I., Reeve, A. S., and Morin, P. J. (2004b). Rates, pathways and drivers for peatland development in the

hudson bay lowlands, northern ontario, canada. *Journal of Ecology*, 92(6):1036–1053.

Gorham, E. (1991). Northern peatlands: Role in the carbon cycle and probable responses to climatic warming. *Ecological Applications*, 1(2):182–195.

Hanrahan, E. T. (1954). An investigation of some physical properties of peat. *Géotechnique*, 4(3):108–123.

Harris, L. I., Richardson, K., Bona, K. A., Davidson, S. J., Finkelstein, S. A., Garneau, M., McLaughlin, J., Nwaishi, F., Olefeldt, D., Packalen, M., Roulet, N. T., Southee, F. M., Strack, M., Webster, K. L., Wilkinson, S. L., and Ray, J. C. (2022). The essential carbon service provided by northern peatlands. *Frontiers in Ecology and the Environment*, 20(4):222–230.

Heinemeyer, A., Croft, S., Garnett, M. H., Gloor, E., Holden, J., Lomas, M. R., and Ineson, P. (2010). The millennia peat cohort model, predicting past, present and future soil carbon budgets and fluxes under changing climates in peatlands. *Climate Research*, 45(1):207–226.

Hendry, M. T., Sharma, J. S., Martin, C. D., and Barbour, S. L. (2012). Effect of fibre content and structure on anisotropic elastic stiffness and shear strength of peat. *Canadian Geotechnical Journal*, 49(4):403–415.

Hilbert, D. W., Roulet, N., and Moore, T. (2000). Modelling and analysis of peatlands as dynamical systems. *Journal of Ecology*, 88(2):230–242.

Hoag, R. S. and Price, J. S. (1995). A field-scale, natural gradient solute transport experiment in peat at a newfoundland blanket bog. *Journal of Hydrology*, 172(1):171–184.

Hoag, R. S. and Price, J. S. (1997). The effects of matrix diffusion on solute transport and retardation in undisturbed peat in laboratory columns. *Journal of Contaminant Hydrology*, 28(3):193–205.

Hobbs, N. B. (1986). Mire morphology and the properties and behaviour of some british and foreign peats. *Quarterly Journal of Engineering Geology and Hydrogeology*, 19(1):7–80.

Hobbs, N. B. (1987). A note on the classification of peat. *Géotechnique*, 37(3):405–407.

Hogan, J. M., van der Kamp, G., Barbour, S. L., and Schmidt, R. (2006). Field methods for measuring hydraulic properties of peat deposits. *Hydrological Processes*, 20(17):3635–3649.

Holden, J. (2005). Controls of soil pipe frequency in upland blanket peat. *Journal of Geophysical Research: Earth Surface*, 110(F1).

Holden, J. and Burt, T. P. (2003). Runoff production in blanket peat covered catchments. *Water Resources Research*, 39(7).

Holden, N. M. and Connolly, J. (2011). Estimating the carbon stock of a blanket peat region using a peat depth inference model. *CATENA*, 86(2):75–85.

Hooijer, A., Page, S., Canadell, J. G., Silvius, M., Kwadijk, J., Wösten, H., and Jauhiainen, J. (2010). Current and future co_2 emissions from drained peatlands in southeast asia. *Biogeosciences*, 7(5):1505–1514.

Howie, S. A. and Hebda, R. J. (2018). Bog surface oscillation (mire breathing): A useful measure in raised bog restoration. *Hydrological Processes*, 32(11):1518–1530.

Huang, Y., Ciais, P., Luo, Y., Zhu, D., Wang, Y., Qiu, C., Goll, D. S., Guenet, B., Makowski, D., De Graaf, I., Leifeld, J., Kwon, M. J., Hu, J., and Qu, L. (2021). Tradeoff of co2 and ch4 emissions from global peatlands under water-table drawdown. *Nature Climate Change*, 11(7):618–622.

Hugelius, G., Loisel, J., Chadburn, S., Jackson, R. B., Jones, M., MacDonald, G., Marushchak, M., Olefeldt, D., Packalen, M., Siewert, M. B., Treat, C., Turetsky, M., Voigt, C., and Yu, Z. (2020). Large stocks of peatland carbon and nitrogen are vulnerable to permafrost thaw. *Proceedings of the National Academy of Sciences*, 117(34):20438–20446.

Ingram, H. A. P. (1982). Size and shape in raised mire ecosystems: a geophysical model. *Nature*, 297(5864):300–303.

Irgens, F. (2008). *Continuum Mechanics*. Springer-Verlag Berlin, Heidelberg.

Ise, T., Dunn, A. L., Wofsy, S. C., and Moorcroft, P. R. (2008). High sensitivity of peat decomposition to climate change through water-table feedback. *Nature Geoscience*, 1(11):763–766.

Jackson, R. B., Lajtha, K., Crow, S. E., Hugelius, G., Kramer, M. G., and Piñeiro, G. (2017). The ecology of soil carbon: pools, vulnerabilities, and biotic and abiotic controls. *Annual Review of Ecology, Evolution, and Systematics*, 48(1):419–445.

Jha, B. and Juanes, R. (2014). Coupled multiphase flow and poromechanics: A computational model of pore pressure effects on fault slip and earthquake triggering. *Water Resources Research*, 50(5):3776–3808.

Jog, C. S. (2015). *Continuum Mechanics: Volume 1: Foundations and*

Applications of Mechanics. Cambridge University Press, Cambridge, 3rd edition.

Joosten, H. and Clarke, D. (2002). *Wise use of mires and peatlands - Background and principles including a framework for decision-making*. International Mire Conservation Group and International Peat Society.

Kellner, E., Price, J. S., and Waddington, J. M. (2004). Pressure variations in peat as a result of gas bubble dynamics. *Hydrological Processes*, 18(13):2599–2605.

Kennedy, G. and Price, J. (2005). A conceptual model of volume-change controls on the hydrology of cutover peats. *Journal of Hydrology*, 302(1):13–27.

Kim, J., Tchelepi, H. A., and Juanes, R. (2011). Stability and convergence of sequential methods for coupled flow and geomechanics: Fixed-stress and fixed-strain splits. *Computer Methods in Applied Mechanics and Engineering*, 200(13):1591–1606.

Kleinen, T., Brovkin, V., and Schuldt, R. J. (2012). A dynamic model of wetland extent and peat accumulation: results for the holocene. *Biogeosciences*, 9(1):235–248.

Kleinen, T., Held, H., and Petschel-Held, G. (2003). The potential role of spectral properties in detecting thresholds in the earth system: application to the thermohaline circulation. *Ocean Dynamics*, 53(2):53–63.

Kneale, P. E. (1987). Sensitivity of the groundwater mound model for predicting mire topography. *Hydrology Research*, 18(4-5):193–202.

Kokkonen, N. A. K., Laine, A. M., Laine, J., Vasander, H., Kurki, K., Gong, J., and Tuittila, E.-S. (2019). Responses of peatland vegetation

to 15-year water level drawdown as mediated by fertility level. *Journal of Vegetation Science*, 30(6):1206–1216.

Korhola, A., Alm, J., Tolonen, K., Turunen, J., and Jungner, H. (1996). Three-dimensional reconstruction of carbon accumulation and ch4 emission during nine millennia in a raised mire. *Journal of Quaternary Science*, 11(2).

Kremenetski, K., Velichko, A., Borisova, O., MacDonald, G., Smith, L., Frey, K., and Orlova, L. (2003). Peatlands of the western siberian lowlands: current knowledge on zonation, carbon content and late quaternary history. *Quaternary Science Reviews*, 22(5):703–723.

Kurnianto, S., Warren, M., Talbot, J., Kauffman, B., Murdiyarso, D., and Frolking, S. (2015). Carbon accumulation of tropical peatlands over millennia: a modeling approach. *Global Change Biology*, 21(1):431–444.

Kværner, J. and Snilsberg, P. (2011). Groundwater hydrology of boreal peatlands above a bedrock tunnel – drainage impacts and surface water groundwater interactions. *Journal of Hydrology*, 403(3):278–291.

Laine, A. M., Korrensalo, A., Kokkonen, N. A. K., and Tuittila, E.-S. (2021). Impact of long-term water level drawdown on functional plant trait composition of northern peatlands. *Functional Ecology*, 35(10):2342–2357.

Lamentowicz, M., Kołaczek, P., Mauquoy, D., Kittel, P., Łokas, E., Słowiński, M., Jassey, V., Niedziółka, K., Kajukało-Drygalska, K., and Marcisz, K. (2019). Always on the tipping point – a search for signals of past societies and related peatland ecosystem critical transitions during the last 6500 years in n poland. *Quaternary Science Reviews*, 225:105954.

Lapen, D. R., Price, J. S., and Gilbert, R. (2005). Modelling two-dimensional steady-state groundwater flow and flow sensitivity to boundary conditions in blanket peat complexes. *Hydrological Processes*, 19(2):371–386.

Lappalainen, E. (1996). Global peat resources.

Large, D. J., Marshall, C., Jochmann, M., Jensen, M., Spiro, B. F., and Olaussen, S. (2021). Time, hydrologic landscape, and the long-term storage of peatland carbon in sedimentary basins. *Journal of Geophysical Research: Earth Surface*, 126(3):e2020JF005762.

Lewis, C., Albertson, J., Xu, X., and Kiely, G. (2012). Spatial variability of hydraulic conductivity and bulk density along a blanket peatland hillslope. *Hydrological Processes*, 26(10):1527–1537.

Limpens, J., Berendse, F., Blodau, C., Canadell, J. G., Freeman, C., Holden, J., Roulet, N., Rydin, H., and Schaepman-Strub, G. (2008). Peatlands and the carbon cycle: from local processes to global implications - a synthesis. *Biogeosciences*, 5(5):1475–1491.

Loisel, J., Gallego-Sala, A. V., Amesbury, M. J., Magnan, G., Anshari, G., Beilman, D. W., Benavides, J. C., Blewett, J., Camill, P., Charman, D. J., Chawchai, S., Hedgpeth, A., Kleinen, T., Korhola, A., Large, D., Mansilla, C. A., Müller, J., van Bellen, S.and West, J. B., Yu, Z., Bubier, J. L., Garneau, M., Moore, T., Sannel, A. B. K., Page, S., Väliranta, M., Bechtold, M., Brovkin, V., Cole, L. E., Chanton, J. P.and Christensen, T. R., Davies, M. A.and Deand Vleeschouwer, F., Finkelstein, S. A., Frolking, S., Gałka, M., Gandois, L., Girkin, N., Harris, L. I., Heinemeyer, A., Hoyt, A. M., Jones, M. C., Joos, F., Juutinen, S., Kaiser, K., Lacourse, T.and Lamentowicz, M., Larmola, T., Leifeld, J., Lohila, A., Milner, A. M., Minkkinen, K., Moss,

P., Naafs, B. D., Nichols, J., O'Donnell, J., Payne, R., Philben, M., Piilo, S., Quillet, A., Ratnayake, A. S., Roland, T. P., Sjögersten, S., Sonnentag, O., Swindles, G. T., Swinnen, W., Talbot, J., Treat, C., and Valach, A. C.and Wu, J. (2021). Expert assessment of future vulnerability of the global peatland carbon sink. *Nature Climate Change*, 11:70–77.

Loisel, J., van Bellen, S., Pelletier, L., Talbot, J., Hugelius, G., Karran, D., Yu, Z., Nichols, J., and Holmquist, J. (2017). Insights and issues with estimating northern peatland carbon stocks and fluxes since the last glacial maximum. *Earth-Science Reviews*, 165:59–80.

Loisel, J., Yu, Z., Beilman, D. W., Camill, P., Alm, J., Amesbury, M. J., Anderson, D., Andersson, S., Bochicchio, C., Barber, K., Belyea, L. R., Bunbury, J., Chambers, F. M., Charman, D. J., De Vleeschouwer, F., Fiałkiewicz-Kozieł, B., Finkelstein, S. A., Gałka, M., Garneau, M., Hammarlund, D., Hinchcliffe, W., Holmquist, J., Hughes, P., Jones, M. C., Klein, E. S., Kokfelt, U., Korhola, A., Kuhry, P., Lamarre, A., Lamentowicz, M., Large, D., Lavoie, M., MacDonald, G., Magnan, G., Mäkilä, M., Mallon, G., Mathijssen, P., Mauquoy, D., McCarroll, J., Moore, T. R., Nichols, J., O'Reilly, B., Oksanen, P., Packalen, M., Peteet, D., Richard, P. J., Robinson, S., Ronkainen, T., Rundgren, M., Sannel, A. B. K., Tarnocai, C., Thom, T., Tuittila, E.-S., Turetsky, M., Väliranta, M., van der Linden, M., van Geel, B., van Bellen, S., Vitt, D., Zhao, Y., and Zhou, W. (2014). A database and synthesis of northern peatland soil properties and holocene carbon and nitrogen accumulation. *The Holocene*, 24(9):1028–1042.

Long, M. (2005). Review of peat strength, peat characterisation and constitutive modelling of peat with reference to landslides. *Studia Geotechnica et Mechanica*, 27(3-4):67–90.

Long, M. and Jennings, P. (2006). Analysis of the peat slide at pollatomish, county mayo, ireland. *Landslides*, 3:51–61.

Lourenco, M., Fitchett, J. M., and Woodborne, S. (2022). Peat definitions: A critical review. *Progress in Physical Geography: Earth and Environment*, 0(0):1–15.

Lunt, P. H., Fyfe, R. M., and Tappin, A. D. (2019). Role of recent climate change on carbon sequestration in peatland systems. *Science of The Total Environment*, 667:348–358.

Ma, L., Zhu, G., Chen, B., Zhang, K., Niu, S., Wang, J., Ciais, P., and Zuo, H. (2022). A globally robust relationship between water table decline, subsidence rate, and carbon release from peatlands. *Communications Earth & Environment*, 3(1):254.

Mahdiyasa, A. W., Large, D. J., Muljadi, B. P., and Icardi, M. (2023). Modelling the influence of mechanical-ecohydrological feedback on the nonlinear dynamics of peatlands. *Ecological Modelling*, 478:110299.

Mahdiyasa, A. W., Large, D. J., Muljadi, B. P., Icardi, M., and Triantafyllou, S. (2022). Mpeat—a fully coupled mechanical-ecohydrological model of peatland development. *Ecohydrology*, 15(1):e2361.

Malhotra, A., Roulet, N. T., Wilson, P., Giroux-Bougard, X., and Harris, L. I. (2016). Ecohydrological feedbacks in peatlands: an empirical test of the relationship among vegetation, microtopography and water table. *Ecohydrology*, 9(7):1346–1357.

Malmer, N., Svensson, B. M., and Wallén, B. (1994). Interactions between sphagnum mosses and field layer vascular plants in the development of peat-forming systems. *Folia Geobotanica and Phytotaxonomica*, 29(4):483–496.

Mandel, J. (1953). Consolidation des sols (Étude mathématique). *Géotechnique*, 3(7):287–299.

Marshall, C., Sterk, H. P., Gilbert, P. J., Andersen, R., Bradley, A. V., Sowter, A., Marsh, S., and Large, D. J. (2022). Multiscale variability and the comparison of ground and satellite radar based measures of peatland surface motion for peatland monitoring. *Remote Sensing*, 14(2):336.

Mauri, A., Davis, B. A. S., Collins, P. M., and Kaplan, J. O. (2015). The climate of europe during the holocene: a gridded pollen-based reconstruction and its multi-proxy evaluation. *Quaternary Science Reviews*, 112:109–127.

McCahon, C. P., Carling, P. A., and Pascoe, D. (1987). Chemical and ecological effects of a pennine peat-slide. *Environmental Pollution*, 45(4):275–289.

McDonald, M. G. and Harbaugh, A. W. (2003). The history of modflow. *Groundwater*, 41(2):280–283.

McNeil, P. and Waddington, J. M. (2003). Moisture controls on sphagnum growth and co2 exchange on a cutover bog. *Journal of Applied Ecology*, 40(2):354–367.

Mesri, G. and Ajlouni, M. (2007). Engineering properties of fibrous peats. *Journal of Geotechnical and Geoenvironmental Engineering*, 133(7):850–866.

Moore, P. A., Lukenbach, M. C., Thompson, D. K., Kettridge, N., Granath, G., and Waddington, J. M. (2019). Assessing the peatland hummock–hollow classification framework using high-resolution elevation

models: implications for appropriate complexity ecosystem modeling. *Biogeosciences*, 16(18):3491–3506.

Moore, T. R., Bubier, J. L., Frolking, S. E., Lafleur, P. M., and Roulet, N. T. (2002). Plant biomass and production and co2 exchange in an ombrotrophic bog. *Journal of Ecology*, 90(1):25–36.

Moore, T. R., Trofymow, J. A., Siltanen, M., Prescott, C., and Group, C. W. (2005). Patterns of decomposition and carbon, nitrogen, and phosphorus dynamics of litter in upland forest and peatland sites in central canada. *Canadian Journal of Forest Research*, 35(1):133–142.

Moradi, M., Keshavarz, A., and Fazeli, A. (2019). One dimensional consolidation of multi-layered unsaturated soil under partially permeable boundary conditions and time-dependent loading. *Computers and Geotechnics*, 107:45–54.

Morris, P. J., Baird, A. J., and Belyea, L. R. (2012). The digibog peatland development model 2: ecohydrological simulations in 2d. *Ecohydrology*, 5(3):256–268.

Morris, P. J., Baird, A. J., and Belyea, L. R. (2013). The role of hydrological transience in peatland pattern formation. *Earth Surface Dynamics*, 1(1):29–43.

Morris, P. J., Baird, A. J., Young, D. M., and Swindles, G. T. (2015). Untangling climate signals from autogenic changes in long-term peatland development. *Geophysical Research Letters*, 42(24):10,788–10,797.

Morris, P. J., Belyea, L. R., and Baird, A. J. (2011). Ecohydrological feedbacks in peatland development: a theoretical modelling study. *Journal of Ecology*, 99(5):1190–1201.

Morris, P. J., Davies, M. L., Baird, A. J., Balliston, N., Bourgault, M.-A., Clymo, R. S., Fewster, R. E., Furukawa, A. K., Holden, J., Kessel, E., Ketcheson, S. J., Kløve, B., Larocque, M., Marttila, H., Menberu, M. W., Moore, P. A., Price, J. S., Ronkanen, A.-K., Rosa, E., Strack, M., Surridge, B. W. J., Waddington, J. M., Whittington, P., and Wilkinson, S. L. (2022). Saturated hydraulic conductivity in northern peats inferred from other measurements. *Water Resources Research*, 58(11):e2022WR033181.

Moukalled, F., Mangani, L., and Darwish, M. (2016). *The Finite Volume Method*, pages 103–135. Springer International Publishing, Cham.

Munir, T. M., Perkins, M., Kaing, E., and Strack, M. (2015). Carbon dioxide flux and net primary production of a boreal treed bog: Responses to warming and water-table-lowering simulations of climate change. *Biogeosciences*, 12(4):1091–1111.

Nelson, K., Thompson, D., Hopkinson, C., Petrone, R., and Chasmer, L. (2021). Peatland-fire interactions: A review of wildland fire feedbacks and interactions in canadian boreal peatlands. *Science of The Total Environment*, 769:145212.

Nichols, J. and Peteet, D. (2019). Rapid expansion of northern peatlands and doubled estimate of carbon storage. *Nature Geoscience*, 12:917–921.

Nijp, J. J., Metselaar, K., Limpens, J., Teutschbein, C., Peichl, M., Nilsson, M. B., Berendse, F., and van der Zee, S. E. A. T. M. (2017). Including hydrological self-regulating processes in peatland models: Effects on peatmoss drought projections. *Science of The Total Environment*, 580:1389–1400.

Oborny, B., Meszéna, G., and Szabó, G. (2005). Dynamics of populations on the verge of extinction. *Oikos*, 109(2):291–296.

Ohkubo, S., Hirano, T., and Kusin, K. (2021). Influence of fire and drainage on evapotranspiration in a degraded peat swamp forest in central kalimantan, indonesia. *Journal of Hydrology*, 603:126906.

O'Kelly, B. C. (2013). Effects of decomposition on the compressibility of fibrous peat — a review. *Geomechanics and Geoengineering*, 8(4):286–296.

O'Kelly, B. C. (2015). *Case studies of Vacuum Consolidation Ground Improvement in Peat Deposits*, pages 315–345. Butterworth-Heinemann.

O'Kelly, B. C. (2017). Measurement, interpretation and recommended use of laboratory strength properties of fibrous peat. *Geotechnical Research*, 4(3):136–171.

Parry, L. E., Charman, D. J., and Noades, J. P. W. (2012). A method for modelling peat depth in blanket peatlands. *Soil Use and Management*, 28(4):614–624.

Pauling, A., Luterbacher, J., Casty, C., and Wanner, H. (2006). Five hundred years of gridded high-resolution precipitation reconstructions over europe and the connection to large-scale circulation. *Climate Dynamics*, 26(4):387–405.

Peltoniemi, K., Laiho, R., Juottonen, H., Bodrossy, L., Kell, D. K., Minkkinen, K., Mäkiranta, P., Mehtätalo, L., Penttilä, T., Siljanen, H. M. P., Tuittila, E.-S., Tuomivirta, T., and Fritze, H. (2016). Responses of methanogenic and methanotrophic communities to warming in varying moisture regimes of two boreal fens. *Soil Biology and Biochemistry*, 97:144–156.

Persson, P.-O. and Strang, G. (2004). A simple mesh generator in matlab. *SIAM Review*, 46(2):329–345.

Phillips, P. J. and Wheeler, M. F. (2007). A coupling of mixed and continuous galerkin finite element methods for poroelasticity 1: the continuous in time case. *Computational Geosciences*, 11(2):131–144.

Phoon, K.-K., Cao, Z.-J., Ji, J., Leung, Y. F., Najjar, S., Shuku, T., Tang, C., Yin, Z.-Y., Ikumasa, Y., and Ching, J. (2022). Geotechnical uncertainty, modeling, and decision making. *Soils and Foundations*, 62(5):101189.

Price, Heathwaite, and Baird (2003). Hydrological processes in abandoned and restored peatlands: An overview of management approaches. *Wetlands Ecology and Management*, 11:65–83.

Price, J. S. (2003). Role and character of seasonal peat soil deformation on the hydrology of undisturbed and cutover peatlands. *Water Resources Research*, 39(9).

Price, J. S., Cagampan, J., and Kellner, E. (2005). Assessment of peat compressibility: is there an easy way? *Hydrological Processes*, 19(17):3469–3475.

Price, J. S. and Schlotzhauer, S. M. (1999). Importance of shrinkage and compression in determining water storage changes in peat: the case of a mined peatland. *Hydrological Processes*, 13(16):2591–2601.

Puzrin, A. M., Alonso, E. E., and (Author), N. M. P. (2014). *Geomechanics of Failure*. Springer.

Quinton, W. L., Gray, D. M., and Marsh, P. (2000). Subsurface drainage from hummock-covered hillslopes in the arctic tundra. *Journal of Hydrology*, 237(1):113–125.

Quinton, W. L., Hayashi, M., and Carey, S. K. (2008). Peat hydraulic conductivity in cold regions and its relation to pore size and geometry. *Hydrological Processes*, 22(15):2829–2837.

Ramirez, J. A., Peleg, N., Baird, A. J., Young, D. M., Morris, P. J., Larocque, M., and Garneau, M. (2023). Modelling peatland development in high-boreal quebec, canada, with digibog_boreal. *Ecological Modelling*, 478:110298.

Rana, P. and Tolvanen, A. (2021). Transferability of 34 red-listed peatland plant species models across boreal vegetation zone. *Ecological Indicators*, 129:107950.

Reeve, A. S., Evensen, R., Glaser, P. H., Siegel, D. I., and Rosenberry, D. (2006). Flow path oscillations in transient ground-water simulations of large peatland systems. *Journal of Hydrology*, 316(1):313–324.

Reeve, A. S., Glaser, P. H., and Rosenberry, D. O. (2013). Seasonal changes in peatland surface elevation recorded at gps stations in the red lake peatlands, northern minnesota, usa. *Journal of Geophysical Research: Biogeosciences*, 118(4):1616–1626.

Regan, S., Flynn, R., Gill, L., Naughton, O., and Johnston, P. (2019). Impacts of groundwater drainage on peatland subsidence and its ecological implications on an atlantic raised bog. *Water Resources Research*, 55(7):6153–6168.

Reynolds, W. D., Brown, D. A., Mathur, S. P., and Overend, R. P. (1992). Effect of in-situ gas accumulation on the hydraulic conductivity of peat. *Soil Science*, 153(5):397–408.

Rezanezhad, F., Price, J. S., Quinton, W. L., Lennartz, B., Milojevic, T., and Van Cappellen, P. (2016). Structure of peat soils and implica-

tions for water storage, flow and solute transport: A review update for geochemists. *Chemical Geology*, 429:75–84.

Rezanezhad, F., Quinton, W. L., Price, J. S., Elliot, T. R., Elrick, D., and Shook, K. R. (2010). Influence of pore size and geometry on peat unsaturated hydraulic conductivity computed from 3d computed tomography image analysis. *Hydrological Processes*, 24(21):2983–2994.

Rydin, H. and Jeglum, J. (2006). *The Biology of Peatlands*. Oxford University Press, Oxford.

Scheffer, M., Bascompte, J., Brock, W. A., Brovkin, V., Carpenter, S. R., Dakos, V., Held, H., van Nes, E. H., Rietkerk, M., and Sugihara, G. (2009). Early-warning signals for critical transitions. *Nature*, 461(7260):53–59.

Scheffer, M. and Carpenter, S. R. (2003). Catastrophic regime shifts in ecosystems: linking theory to observation. *Trends in Ecology and Evolution*, 18(12):648–656.

Schlotzhauer, S. M. and Price, J. S. (1999). Soil water flow dynamics in a managed cutover peat field, quebec: Field and laboratory investigations. *Water Resources Research*, 35(12):3675–3683.

Schouten, M. G. C. (2002). *Conservation and restoration of raised bogs: Geological, hydrological, and ecological studies*. The Government Stationary Office.

Shantz, M. and Price, J. (2006). Hydrological changes following restoration of the bois-des-bel peatland, quebec, 1999–2002. *Journal of Hydrology*, 331(3):543–553.

Shewchuk, J. R. (2002). Delaunay refinement algorithms for triangular mesh generation. *Computational Geometry*, 22(1):21–74.

Siegel, D. I., Reeve, A. S., Glaser, P. H., and Romanowicz, E. A. (1995). Climate-driven flushing of pore water in peatlands. *Nature*, 374(6522):531–533.

Silins, U. and Rothwell, R. L. (1998). Forest peatland drainage and subsidence affect soil water retention and transport properties in an alberta peatland. *Soil Science Society of America Journal*, 62(4):1048–1056.

Sottocornola, M., Laine, A., Kiely, G., Byrne, K. A., and Tuittila, E.-S. (2009). Vegetation and environmental variation in an atlantic blanket bog in south-western ireland. *Plant Ecology*, 203(1):69–81.

Speller, J. L. and Forbes, V. (2022). On the role of peat bogs as components of indigenous cultural landscapes in northern north america. *Arctic, Antarctic, and Alpine Research*, 54:96 – 110.

Strack, O. D. L. (1984). Three-dimensional streamlines in dupuit-forchheimer models. *Water Resources Research*, 20(7):812–822.

Surridge, B. W. J., Baird, A. J., and Heathwaite, A. L. (2005). Evaluating the quality of hydraulic conductivity estimates from piezometer slug tests in peat. *Hydrological Processes*, 19(6):1227–1244.

Swindles, G. T., Morris, P. J., Baird, A. J., Blaauw, M., and Plunkett, G. (2012). Ecohydrological feedbacks confound peat-based climate reconstructions. *Geophysical Research Letters*, 39(11).

Swinnen, W., Broothaerts, N., and Verstraeten, G. (2019). Modelling long-term blanket peatland development in eastern scotland. *Biogeosciences*, 16(20):3977–3996.

Tarvainen, O., Hökkä, H., Kumpula, J., and Tolvanen, A. (2022). Bringing back reindeer pastures in cutaway peatlands. *Restoration Ecology*, 30(8):e13661.

Terzaghi, K. (1925). *Erdbaumechanik auf bodenphysikalischer Grundlage*. Deuticke, Wien.

Terzaghi, K. (1943). *Theoretical soil mechanics*. John Wiley and Sons, Inc, New York.

Tezduyar, T. (2001). Finite element methods for flow problems with moving boundaries and interfaces. *Archives of Computational Methods in Engineering*, 8:83–130.

Tipping, R. (2008). Blanket peat in the scottish highlands: timing, cause, spread and the myth of environmental determinism. *Biodiversity and Conservation*, 17:2097–2113.

Treat, C. C., Jones, M. C., Alder, J., Sannel, A. B. K., Camill, P., and Frolking, S. (2021). Predicted vulnerability of carbon in permafrost peatlands with future climate change and permafrost thaw in western canada. *Journal of Geophysical Research: Biogeosciences*, 126(5):e2020JG005872.

Treat, C. C., Jones, M. C., Camill, P., Gallego-Sala, A., Garneau, M., Harden, J. W., Hugelius, G., Klein, E. S., Kokfelt, U., Kuhry, P., Loisel, J., Mathijssen, P. J. H., O'Donnell, J. A., Oksanen, P. O., Ronkainen, T. M., Sannel, A. B. K., Talbot, J., Tarnocai, C., and Väliranta, M. (2016). Effects of permafrost aggradation on peat properties as determined from a pan-arctic synthesis of plant macrofossils. *Journal of Geophysical Research: Biogeosciences*, 121(1):78–94.

Treat, C. C., Wisser, D., Marchenko, S., and Frolking, S. (2013). Modelling the effects of climate change and disturbance on permafrost stability in northern organic soil. *Mires and Peat*, 12.

Turunen, J., Tomppo, E., Tolonen, K., and Reinikainen, A. (2002).

Estimating carbon accumulation rates of undrained mires in finland–application to boreal and subarctic regions. *The Holocene*, 12(1):69–80.

Tuukkanen, T., Marttila, H., and Kløve, B. (2017). Predicting organic matter, nitrogen, and phosphorus concentrations in runoff from peat extraction sites using partial least squares regression. *Water Resources Research*, 53(7):5860–5876.

van der Velde, Y., Temme, A. J. A. M., Nijp, J. J., Braakhekke, M. C., van Voorn, G. A. K., Dekker, S. C., Dolman, A. J., Wallinga, J., Devito, K. J., Kettridge, N., Mendoza, C. A., Kooistra, L., Soons, M. B., and Teuling, A. J. (2021). Emerging forest–peatland bistability and resilience of european peatland carbon stores. *Proceedings of the National Academy of Sciences*, 118(38):e2101742118.

van Duijn, C. J. and Mikelic, A. (2021). Mathematical proof of the mandel–cryer effect in poroelasticity. *Multiscale Modeling & Simulation*, 19(1):550–567.

van Nes, E. H. and Scheffer, M. (2003). Alternative attractors may boost uncertainty and sensitivity in ecological models. *Ecological Modelling*, 159(2):117–124.

Verruijt, A. (2018). Numerical and analytical solutions of poroelastic problems. *Geotechnical Research*, 5(1):39–50.

Waddington, J. M., Kellner, E., Strack, M., and Price, J. S. (2010). Differential peat deformation, compressibility, and water storage between peatland microforms: Implications for ecosystem function and development. *Water Resources Research*, 46(7).

Waddington, J. M., Morris, P. J., Kettridge, N., Granath, G., Thompson,

D. K., and Moore, P. A. (2015). Hydrological feedbacks in northern peatlands. *Ecohydrology*, 8(1):113–127.

Waddington, J. M. and Roulet, N. T. (1996). Atmosphere-wetland carbon exchanges: Scale dependency of co2 and ch4 exchange on the developmental topography of a peatland. *Global Biogeochemical Cycles*, 10:233–245.

Waddington, J. M. and Roulet, N. T. (1997). Groundwater flow and dissolved carbon movement in a boreal peatland. *Journal of Hydrology*, 191(1):122–138.

Wagner, S. T., Isnard, S., Rowe, N. P., Samain, M.-S., Neinhuis, C., and Wanke, S. (2012). Escaping the lianoid habit: Evolution of shrub-like growth forms in aristolochia subgenus isotrema (aristolochiaceae). *American Journal of Botany*, 99(10):1609–1629.

Wallèn, B. (1987). Growth pattern and distribution of biomass of calluna vulgaris on an ombrotrophic peat bog. *Holarctic Ecology*, 10(1):73–79.

Wallén, B. (1986). Above and below ground dry mass of the three main vascular plants on hummocks on a subarctic peat bog. *Oikos*, 46(1):51–56.

Wallén, B., Falkengren-Grerup, U., and Malmer, N. (1988). Biomass, productivity and relative rate of photosynthesis of sphagnum at different water levels on a south swedish peat bog. *Holarctic Ecology*, 11(1):70–76.

Wang, D. and Li, Z. (2023). Shear behaviour of peat at different stress levels. *Proceedings of the Institution of Civil Engineers - Geotechnical Engineering*, pages 1–14.

Wang, H. F. (2000). *Theory of linear poroelasticity with applications to geomechanics and hydrogeology*. Princeton University Press, Princeton, NJ, USA.

Warburton, J., Higgitt, D., and Mills, A. (2003). Anatomy of a pennine peat slide, northern england. *Earth Surface Processes and Landforms*, 28(5):457–473.

Warburton, J., Holden, J., and Mills, A. J. (2004). Hydrological controls of surficial mass movements in peat. *Earth-Science Reviews*, 67(1):139–156.

Whittington, P., Strack, M., Haarlem, R. v., Kaufman, S., Stoesser, P., Maltez, J., Price, J., and Stone, M. (2007). The influence of peat volume change and vegetation on the hydrology of a kettle-hole wetland in southern ontario, canada. *Mires and Peat*, 2.

Whittington, P. N. and Price, J. S. (2006). The effects of water table drawdown (as a surrogate for climate change) on the hydrology of a fen peatland, canada. *Hydrological Processes*, 20(17):3589–3600.

Wierda, A., Fresco, L. F. M., Grootjans, A. P., and van Diggelen, R. (1997). Numerical assessment of plant species as indicators of the groundwater regime. *Journal of Vegetation Science*, 8(5):707–716.

Wilford, G. E. (1966). A peat landslide in Sarawak, Malaysia, and its significance in relation to washouts in coal seams. *Journal of Sedimentary Research*, 36(1):244–247.

Williams, J. W., Grimm, E. C., Blois, J. L., Charles, D. F., Davis, E. B., Goring, S. J., Graham, R. W., Smith, A. J., Anderson, M., Arroyo-Cabrales, J., and et al. (2018). The neotoma paleoecology database, a

multiproxy, international, community-curated data resource. *Quaternary Research*, 89(1):156–177.

Wilson, P. and Hegarty, C. (1993). Morphology and causes of recent peat slides on skerry hill, co. antrim, northern ireland. *Earth Surface Processes and Landforms*, 18(7):593–601.

Winston, R. B. (1994). Models of the geomorphology, hydrology, and development of domed peat bodies. *GSA Bulletin*, 106(12):1594–1604.

Winter, T. C. (2001). The concept of hydrologic landscapes. *Journal of the American Water Resources Association*, 37(2):335–349.

Word, C. S., McLaughlin, D. L., Strahm, B. D., Stewart, R. D., Varner, J. M., Wurster, F. C., Amestoy, T. J., and Link, N. T. (2022). Peatland drainage alters soil structure and water retention properties: Implications for ecosystem function and management. *Hydrological Processes*, 36(3):e14533.

Wust, R. A., Bustin, R., and Lavkulich, L. M. (2003). New classification systems for tropical organic-rich deposits based on studies of the tasek bera basin, malaysia. *CATENA*, 53(2):133–163.

Xu, J., Morris, P. J., Liu, J., and Holden, J. (2018). Peatmap: Refining estimates of global peatland distribution based on a meta-analysis. *CATENA*, 160:134–140.

Xu, X., Lu, K., Wang, Z., Wang, M., and Wang, S. (2021). Effects of drainage on dissolved organic carbon (doc) characteristics of surface water from a mountain peatland. *Science of The Total Environment*, 789:147848.

Yang, J. and Dykes, A. (2006). The liquid limit of peat and its appli-

cation to the understanding of irish blanket bog failures. *Landslides*, 3:205–216.

Young, D. M., Baird, A. J., Charman, D. J., Evans, C. D., Gallego-Sala, A. V., Gill, P. J., Hughes, P. D. M., Morris, P. J., and Swindles, G. T. (2019). Misinterpreting carbon accumulation rates in records from near-surface peat. *Scientific Reports*, 9(1):17939.

Young, D. M., Baird, A. J., Gallego-Sala, A. V., and Loisel, J. (2021). A cautionary tale about using the apparent carbon accumulation rate (acar) obtained from peat cores. *Scientific Reports*, 11(1):9547.

Young, D. M., Baird, A. J., Morris, P. J., Dargie, G. C., Mampouya Wenina, Y. E., Mbemba, M., Boom, A., Cook, P., Betts, R., Burke, E., Bocko, Y. E., Chadburn, S., Crabtree, D. E., Crezee, B., Ewango, C. E. N., Garcin, Y., Georgiou, S., Girkin, N. T., Gulliver, P., Hawthorne, D., Ifo, S. A., Lawson, I. T., Page, S. E., Jovani-Sancho, A. J., Schefuß, E., Sciumbata, M., Sjögersten, S., and Lewis, S. L. (2023). Simulating carbon accumulation and loss in the central congo peatlands. *Global Change Biology*, 29(23):6812–6827.

Young, D. M., Baird, A. J., Morris, P. J., and Holden, J. (2017). Simulating the long-term impacts of drainage and restoration on the ecohydrology of peatlands. *Water Resources Research*, 53(8):6510–6522.

Yu, Z., Beilman, D. W., and Jones, M. C. (2009). *Sensitivity of Northern Peatland Carbon Dynamics to Holocene Climate Change*, pages 55–69. American Geophysical Union (AGU).

Yu, Z., Campbell, I. D., Vitt, D. H., and Apps, M. J. (2001). Modelling long-term peatland dynamics. i. concepts, review, and proposed design. *Ecological Modelling*, 145(2):197–210.

Yu, Z., Loisel, J., Brosseau, D. P., Beilman, D. W., and Hunt, S. J. (2010). Global peatland dynamics since the last glacial maximum. *Geophysical Research Letters*, 37(13).

Zhu, J., Wang, Y., Wang, Y., Mao, Z., and Langendoen, E. J. (2020). How does root biodegradation after plant felling change root reinforcement to soil? *Plant and Soil*, 446(1):211–227.

Zhu, X., Wang, Y., Zan, J., and Li, C. (2006). Application of fractal theory in generation and refinement of finite element mesh. *Applied Mathematics and Computation*, 175(2):1039–1045.

Zienkiewicz, O. C., Taylor, R. L., and Zhu, J. Z. (2013). *The finite element method: its basis and fundamentals*. Elsevier, 7th edition.